

**Insulin receptor, AMPK and CPT-2:
Crystallization experiments and structural characterization
of three proteins relevant to diabetes mellitus**

Inaugural-Dissertation

zur

**Erlangung des Doktorgrades
der Mathematisch-Naturwissenschaftlichen Fakultät
der Universität zu Köln**

vorgelegt von

**Dipl. Biol.
Arne Christian Rufer
aus Hamm/ Westfalen**

Köln, 2005

Die vorliegende Arbeit wurde im Zeitraum März 2002 bis November 2005 in der Abteilung Molecular Structure and Design innerhalb der F. Hoffmann-La Roche AG, Basel, CH, und dem Institut für Biochemie der Universität zu Köln unter der Anleitung von Priv.-Doz. M. Hennig und Prof. H-W. Klein angefertigt.

1. Berichterstatter: Prof. H-W. Klein, Universität zu Köln
2. Berichterstatter: Priv.-Doz. K. Niefind, Universität zu Köln
3. Berichterstatter: Priv.-Doz. M. Hennig, F. Hoffmann-La Roche AG, Basel, CH

Tag der mündlichen Prüfung: 6. Februar 2006

Meiner Familie

Contents

1	Abstract.....	1
2	Introduction.....	2
2.1	Type 2 diabetes mellitus: an increasing health burden.....	2
2.2	Pharmacological treatment of diabetes mellitus.....	4
2.3	Molecular aspects of IR and AMPK signaling.....	6
2.4	Specific aims.....	10
3	Results.....	11
3.1	Characterization and crystallization of IR and IGF-1R constructs.....	11
3.1.1	Summary of literature data.....	11
3.1.2	Crystallization experiments on dimeric IR and IGF-1R constructs.....	12
3.1.3	Interaction of IRTK with small-molecule agonists.....	18
3.2	Characterization and crystallization of AMPK.....	25
3.2.1	Summary of literature and Roche data.....	25
3.2.2	Characterization and crystallization of AMPK_α2 constructs.....	28
3.2.2.1	Biacore.....	31
3.2.2.2	Thermofluor®.....	33
3.2.2.3	Generation of the triple mutant AMPK_α2_1-339_D56A/R171E/T172D..	36
3.2.2.4	Crystallization of AMPK_α2_1-339_D56A/R171E/T172D.....	39
3.2.2.5	Refolding.....	43
3.2.2.6	Free Mounting™ system.....	44
3.2.2.7	Truncated triple (D56A/R171E/T172D) mutants.....	47
3.2.2.8	Crystallization of the AMPK heterotrimer.....	53
3.2.2.9	Crystallization of the AMPK regulatory domains.....	55
3.2.2.10	Interaction of the AMPK heterotrimer with the ligand binding domain of PPARα.....	56
3.2.2.11	Small angle X-ray scattering (SAXS) studies of AMPK.....	57
3.3	Crystallization and structure determination of carnitine palmitoyl- transferase 2 (CPT-2).....	60
3.3.1	The CPT-system: a candidate drug target for T2D.....	60

3.3.2	Biophysical characterization of CPT-2.....	62
3.3.3	Crystallization and overall structure of CPT-2.....	65
3.3.4	Binding mode of ST1326.....	68
3.3.5	Membrane association.....	71
3.3.6	CPT-2 deficiency.....	73
4	Discussion.....	76
4.1	Insulin receptor.....	76
4.2	AMPK.....	79
4.3	CPT-2.....	80
5	Material and Methods.....	82
5.1	Materials.....	82
5.1.1	Chemicals.....	82
5.1.2	Enzymes.....	82
5.1.3	Kits.....	82
5.1.4	Specialty chemicals.....	82
5.1.5	Bacterial strains (chemically competent <i>E. coli</i>).....	83
5.1.6	Consumable supplies and hardware.....	83
5.2	Methods.....	84
5.2.1	Molecular biology methods.....	84
5.2.1.1	Transformation of chemically competent <i>E. coli</i>	84
5.2.1.2	PCR for sequencing.....	84
5.2.1.3	Cloning of AMPK point mutations.....	85
5.2.2	Expression and purification of GST-fusion proteins.....	87
5.2.3	Expression and purification of AMPK constructs.....	88
5.2.3.1	Expression.....	88
5.2.3.2	Cell lysis.....	88
5.2.3.3	Chromatography.....	89
5.2.4	Expression, purification and activity test of rat CPT-2.....	91
5.2.5	Thermofluor® assay.....	92
5.2.6	Phosphorylation assay.....	94

5.2.6.1	Autophosphorylation.....	94
5.2.6.2	Substrate phosphorylation.....	95
5.2.6.3	Quantitation of [γ ³² P]-incorporation.....	95
5.2.7	Limited proteolysis.....	95
5.2.8	Analytical ultracentrifugation (AUC).....	96
5.2.9	Mass spectrometry (MS).....	96
5.2.9.1	Nanoelectrospray ionization (Nano-ESI) MS of intact proteins.....	90
5.2.9.2	Characterization of in-gel digested proteins.....	97
5.2.10	Biacore.....	98
5.2.11	Small angle X-ray scattering (SAXS).....	98
5.2.12	Crystallographic methods (CPT-2).....	100
5.2.12.1	Protein crystallization.....	100
5.2.12.2	Data collection and processing.....	100
5.2.12.3	Structure solution and refinement.....	101
6	References.....	102
7	Appendix.....	120
7.1	GST publication and poster.....	121
7.2	AMPK_α2_1-339_D56A/R171E/T172D diffraction images.....	125
7.3	Sequence and primer data for rat AMPK_α2.....	127
7.4	Abbreviations.....	132
	Zusammenfassung.....	135
	Danksagung.....	137
	Erklärung.....	138
	Teilpublikationen dieser Arbeit.....	139
	Lebenslauf.....	140

1 Abstract

Impaired insulin signaling due to peripheral insulin resistance and failure of pancreatic insulin secretion is a key factor for the onset and manifestation of type 2 diabetes mellitus (T2D). Insulin receptor (IR) agonists are being developed to restore insulin signaling via direct activation of the cytoplasmic insulin receptor tyrosine kinase activity. Two classes of such compounds have been developed by the pharmaceutical companies Merck & Co., Inc., and Telik, Inc., but in patents and literature there is no data as to how these compounds activate the IR kinase activity.

Attempts to solve the crystal structures of dimeric human IR kinase domains and complexes of these with IR agonists within this thesis failed. However, biophysical characterization of the full-length intracellular part of the IR containing the kinase domain demonstrated an intrinsic ability to dimerize independently of the enzyme-substrate type of interaction seen in IR autophosphorylation. This dimer formation was found to be enhanced in the presence of a distinct IR agonist.

Crystals of various constructs and isoforms of the key antidiabetic target AMP-activated protein kinase (AMPK) were obtained. Despite substantial optimization trials these crystals were not sufficient for solving the structure of AMPK.

However, the crystal structure of carnitine palmitoyltransferase 2 (CPT-2), a protein downstream of the metabolite signaling initiated by AMPK, was solved. CPT-1 and -2 facilitate the import of long-chain fatty acids into mitochondria. Modulation of the catalytic activity of the CPT system is currently under investigation for the development of novel drugs against diabetes mellitus. The crystal structure of the full-length mitochondrial membrane protein CPT-2 was solved at a resolution of 1.6 Å. The structure of CPT-2 in complex with the generic CPT-inhibitor ST1326 [(R)-N-tetradecylcarbamoyl-aminocarnitine], a substrate analog mimicking palmitoylcarnitine and currently in clinical trials for T2D treatment, was solved at 2.5 Å resolution. These structures of CPT-2 provide insight into the function of residues involved in substrate binding and determination of substrate specificity, thereby facilitating the rational design of novel antidiabetic drugs. A sequence insertion uniquely found in CPT-2 was identified that mediates membrane localization. Mapping of mutations described for CPT-2 deficiency, a hereditary disorder of lipid metabolism, implies effects on substrate recognition and structural integrity of CPT-2.

2 Introduction

2.1 Type 2 diabetes mellitus: an increasing health burden

The peptide hormone insulin released from the β -cells of the pancreas is a major regulator of glucose homeostasis and responsible for the uptake of glucose from blood plasma into cells. Type 2 diabetes mellitus (T2D) is a metabolic disorder characterized by resistance of peripheral target tissues, especially skeletal muscle, adipose tissue and liver, to insulin and concomitant relative insulin deficiency. More than 90 % of the diabetics worldwide have the T2D form of the disease as opposed to app. 5 % type 1 (T1D) diabetics, where an absolute insulin deficiency is elicited by destruction of pancreatic β -cells due to autoimmune processes. These two major presentations of diabetes were historically differentiated as non-insulin-dependent vs. insulin-dependent diabetes mellitus (NIDDM and IDDM, respectively). However, according to the recommendations of the Expert Committee on the Diagnosis and Classification of Diabetes Mellitus of the American Diabetes Association (ADA, 2003) this terminology should now be regarded as obsolete. T2D patients may eventually become dependent on insulin supplementation due to β -cell failure as a consequence of prolonged compensation stress. The remaining < 5% of diabetes cases can be attributed to gestational (BUCHANAN and XIANG, 2005) and mitochondrial (MAASSEN *et al.*, 2004) diabetes mellitus as well as rare monogenic presentations such as maturity-onset diabetes of the young (MODY; SHIH and STOFFEL, 2002). In addition, various endocrinopathies (*e.g.*, Cushing's syndrome) and genetic syndromes (*e.g.*, Down's syndrome, Friedreich's ataxia) may be associated with diabetes mellitus depending on the severity of the symptomology (ADA, 2003).

The diverse metabolic aberrations underlying T2D are of multifactorial etiology and render T2D a clinically heterogenous disease (O'RAHILLY *et al.*, 2005). The common symptoms relevant for the diagnosis of diabetes mellitus are casual peaks in the plasma glucose concentration above 200 mg/dl (11.1 mM) combined with polyuria, polydipsia and weight loss. Alternatively, diabetes mellitus is diagnosed if the fasting plasma glucose concentration is raised to more than 126 mg/dl (7 mM) or when an impaired glucose clearance from plasma is detected during an oral glucose tolerance test [*i.e.*, plasma glucose levels above 200 mg/dl (11.1 mM) 2 h after oral administration of 75 g

glucose dissolved in water; ADA, 2003]. The increasingly impaired fasting glucose and glucose tolerance precede the manifestation of overt diabetes mellitus (STUMVOLL *et al.*, 2005) and are frequently accompanied by visceral obesity, dyslipidemia (*i.e.*, hypertriglyceridemia and decreased plasma high density lipoprotein) and hypertension. This constellation of risk factors is referred to as the metabolic syndrome (syndrome X; ALBERTI *et al.*, 2005). The highest prevalence of the metabolic syndrome is found in the US population (app. 39 %; FORD, 2005), but affects an increasing part of the population worldwide. As an effect of this, the number of T2D patients is expected to raise from currently app. 190 million to more than 300 million worldwide within the next 20 years (Figure 2.1-1).

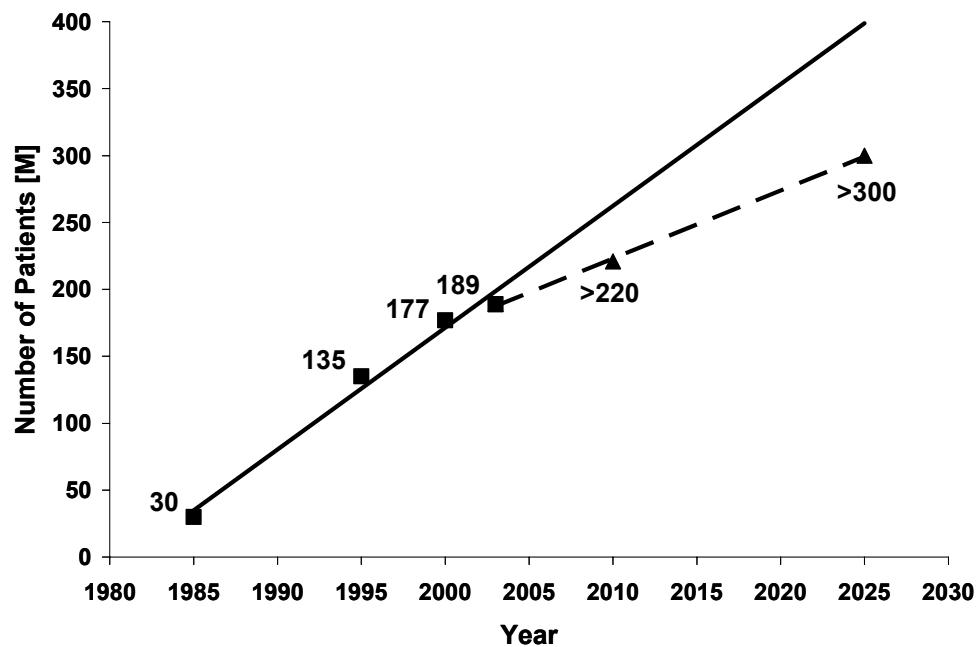


Figure 2.1-1: Number of type 2 diabetics worldwide, in millions. The increase in patient number since 1985 (squares, continuous line) is linearly extrapolated to the year 2025 in order to visualize a "prognosis cone" together with the prospective least patient numbers in 2010 and 2025 (triangles, dashed line; data compiled from KING *et al.*, 1998; ZIMMET *et al.*, 2001; RONDINONE, 2005; STUMVOLL *et al.*, 2005; http://www.who.int/topics/diabetes_mellitus/en/).

Therefore, diabetes mellitus represents a growing health burden as its occurrence is highly correlated with an increased risk of cardiovascular disease (atherosclerosis, heart disease, diabetic retinopathy), neuropathy (sensory loss, diabetic foot disease), and nephropathy (kidney failure rendering patients dependent on hemodialysis). These complications emerge due to chronic hyperglycemia which causes tissue damage by nonenzymatic glycation of proteins, lipids and DNA (ADA, 2003).

2.2 Pharmacological treatment of diabetes mellitus

The vastly growing incidence of T2D worldwide (diabetes epidemic; ZIMMET *et al.*, 2001) and its severe health consequences have to be met by pharmacologic intervention. The lack of endogenous insulin in T1D can be effectively treated by application of the proper insulin preparations (VAJO and DUCKWORTH, 2000). For T2D, several treatments are established today that are applied depending on disease progression and severity of symptoms. Clinically mild presentations of T2D can be treated by established antidiabetic drugs such as insulin secretagogues, insulin sensitizing thiazolidinediones (TZDs), which are agonists of the nuclear hormone receptor PPAR γ , and metformin (reviewed in WAGMAN and NUSS, 2001). Advanced T2D requires administration of exogenous insulin. The mechanism of action of insulin is well established and has been extensively reviewed (KAHN and PESSIN, 2002; WHITE, 2003).

Several members of the TZD class of compounds were approved for the treatment of T2D. However, some TZDs had to be withdrawn from clinical development and the use of approved substances had to be restricted due to hepatotoxicity issues (WAGMAN and NUSS, 2001).

The possibility to mimic the insulin-mediated activation of the insulin receptor (IR) by orally available pharmaceutical substances was confirmed by the discovery of small-molecules that either directly activate the IR (ZHANG *et al.*, 1999) or do so synergistically with insulin (insulin enhancer; MANCHEM *et al.*, 2001). To our knowledge, none of these small-molecule IR agonists has entered the clinical phase of development, and results of this thesis demonstrate why this may be the case.

Metformin decreases plasma glucose levels by inhibition of hepatic gluconeogenesis and increasing glucose consumption in peripheral tissues. This effect can at least partially be attributed to (indirect) activation of the 5'-AMP-activated protein kinase (AMPK), which is physiologically activated upon an increase in the [AMP]/[ATP] ratio due to exercise, hypoxia or hormonal stimuli (reviewed in HARDIE and HAWLEY, 2001; CARLING, 2004; KAHN *et al.*, 2005; Figure 2.3-1). Metformin fails to directly activate purified AMPK *in vitro*, even in the presence of AMP (U. Riek, ETH Zurich, personal communication), but, like TZDs, stimulates AMPK kinase activity in isolated hepatocytes and cultures muscle cells (ZHOU *et al.*, 2001; FRYER *et al.*, 2002; SAHA *et al.*, 2004).

Although metformin was shown to inhibit complex 1 of the respiratory chain, thereby increasing the [AMP]/[ATP] ratio, the metformin-mediated activation of AMPK can proceed in both adenine nucleotide-dependent and -independent manner (FRYER *et al.*, 2002; HAWLEY *et al.*, 2002; ZOU *et al.*, 2004).

However, there is strong experimental evidence that the controlled direct pharmacological activation of AMPK could prevent the progression from a pre-diabetic state with impaired glucose tolerance to the manifestation of overt T2D and would also ameliorate the key symptoms of T2D (HARDIE and HAWLEY, 2001). The adenine nucleotide analog 5-aminoimidazole-4-carboxamide-1- β -D-ribofuranoside (AICAR) is converted into its 5'-monophosphorylated form, ZMP, by adenosine kinase upon entering cells. ZMP mimics AMP and is an allosteric activator of AMPK both *in vitro* and *in vivo*. Impaired insulin sensitivity was found to be highly correlated with reduced enzymatic activity of AMPK and ZMP was shown to effectively improve the glucose tolerance, hyperglycemia and dyslipidemia in animal models of insulin resistance and diabetes (HARDIE and HAWLEY, 2001; YE *et al.*, 2005). These effects of AMPK activation are due to the normalization of substrate flux into catabolic, energy-generating metabolic pathways with simultaneous down-regulation of anabolic pathways. AMPK phosphorylates and inactivates acetyl-CoA carboxylase (ACC) which catalyzes the committed step of fatty acid (FA) synthesis, the formation of malonyl-CoA from acetyl-CoA (CARLING *et al.*, 2003; Figure 2.3-1). The production of FA and triglycerides in lipogenic tissues and ectopic lipid disposal in skeletal muscle, both of which are causative for peripheral insulin resistance and impaired glucose tolerance (lipotoxicity), are decreased by AMPK (CARLING *et al.*, 2003; SCHINNER *et al.*, 2005). Thus, activation of AMPK reduces the FA-dependent serine phosphorylation of insulin receptor substrate 1 (IRS-1) by various PKC isoforms which impairs the insulin-dependent glucose uptake by the glucose transporter GLUT4 (ZICK, 2003 and 2005). Malonyl-CoA is an inhibitor of carnitine palmitoyltransferase 1 (CPT-1) and diminishing malonyl-CoA levels upon AMPK activation allow an increased import of FA into mitochondria via CPT-1 which supports the mobilization of excess lipid depots in skeletal muscle and adipocytes. In the liver the acetyl-CoA derived from β -oxidation is a potent allosteric activator of pyruvate carboxylase (PC, Figure 2.3-1), which initiates

gluconeogenesis (JITRAPAKDEE and WALACE, 1999), but here AMPK inhibits substrate flux into hepatic gluconeogenesis (HARDIE *et al.*, 2003).

Therefore, both the pharmacologic activation of (muscle) AMPK and the inhibition of liver CPT-1 are rational, novel means for reestablishing normoglycemia in T2D patients, by reversing peripheral insulin resistance and normalization of the hepatic gluconeogenesis rate, respectively.

2.3 Molecular aspects of IR and AMPK signaling

Insulin elicits its effects on metabolism via the insulin receptor (IR, Figure 2.3-1). The IR is a type II receptor tyrosine kinase with additional intrinsic dual kinase activity (TENNAGELS *et al.*, 2001) and is expressed in liver, muscle, adipose tissue and neurons, among other tissues. Insulin binds to the extracellular α -subunits of the $(\alpha\beta)_2$ -heterotetrameric IR, thereby inducing a change in conformation of and activating the intracellular kinase domain of the transmembrane β -subunits of (VAN OBBERGHEN *et al.*, 2001; DE MEYTS and WHITTAKER, 2002; DE MEYTS, 2004).

Two isoforms of the IR have been described (SEINO and BELL, 1989). The α -subunit of IR-A lacks 12 amino acids at the carboxy-terminus compared to isoform IR-B as a result of alternative splicing of exon 11. Thus, two nomenclature conventions exist: 1. IR-A, ULLRICH *et al.* (1985) and 2. IR-B, EBINA *et al.* (1985), which was adopted in this thesis in accordance with the residue numbering used for the structure of IR core kinase domain (HUBBARD *et al.*, 1994).

It has been demonstrated that the two isoforms have different properties with regard to insulin affinity, receptor endocytosis and recycling as well as expression patterns (YAMAGUCHI *et al.*, 1993, and references therein). A change in expression rate and isoform-ratio has been implicated in the compensatory mechanism during insulin resistance, but it has not been conclusively shown whether this process is involved in the pathogenesis of T2D or might be exploited for the treatment of diabetic patients (HARING *et al.*, 1994; DE MEYTS and WHITTAKER, 2002).

Several lines of evidence demonstrated the existence of hybrid receptors consisting of an IR $(\alpha\beta)$ -protomer covalently linked to an $(\alpha\beta)$ -protomer of the insulin-like growth factor 1 receptor (IGF-1R). Depending on the isoform of the IR protomer, these hybrid receptors have different affinity for insulin and IGF-1 as well as distinct signaling

properties (PANDINI *et al.*, 2002). The physiological functions in health and disease of the hybrid receptors and that of the insulin-receptor-related receptor (IRR; KLAMMT *et al.*, 2005) remain to be established.

The subunits of the IR are transcribed from a single gene and translation yields a pre-pro-receptor, which is processed to the functional, glycosylated IR in the endoplasmatic reticulum and Golgi-compartment (WILLIAMS *et al.*, 1990). The IR associates with multiple adaptor, substrate and effector proteins that modulate its catalytic activity and signaling properties (KAHN and PESSIN, 2002; PIROLA, 2004).

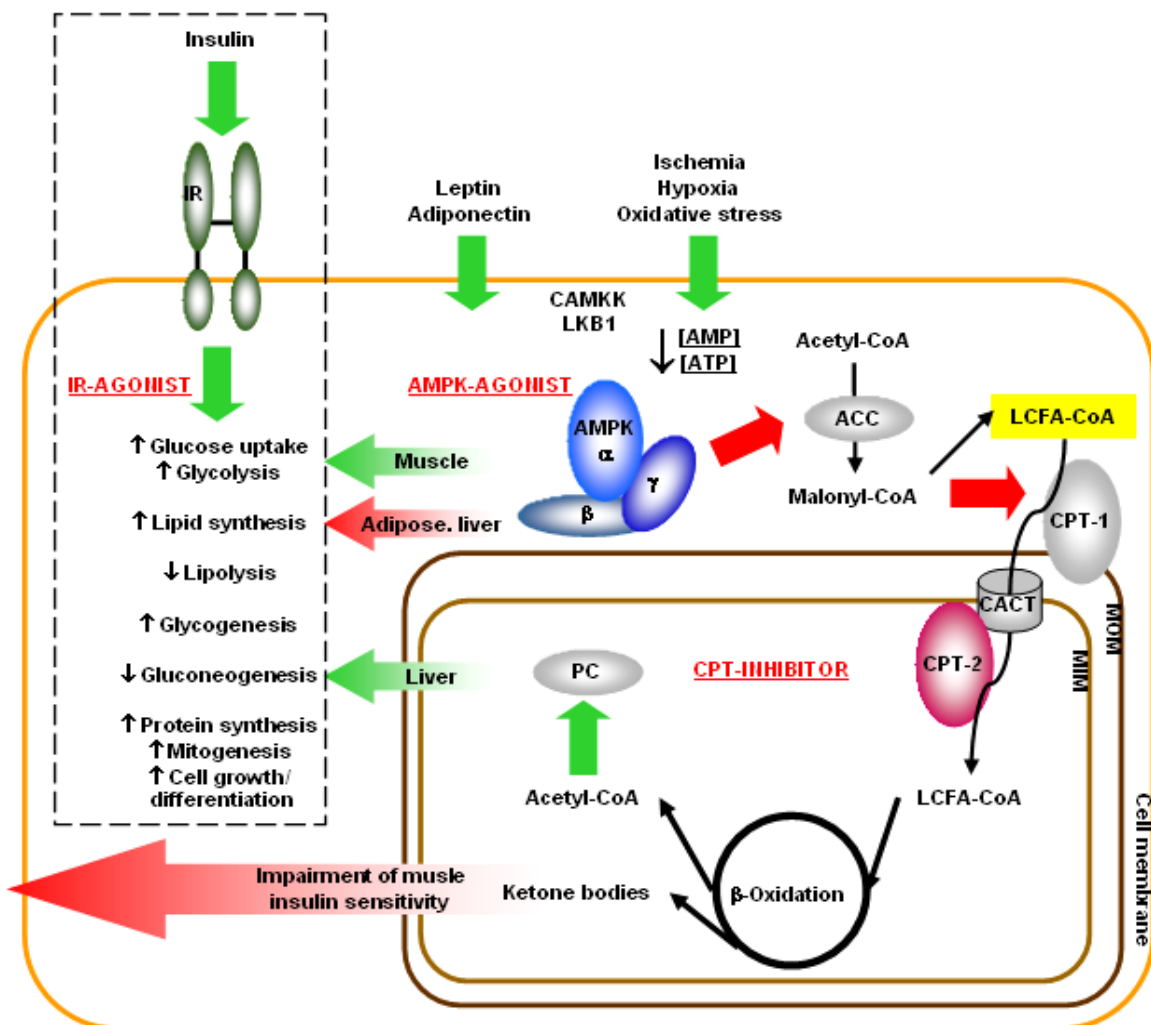


Figure 2.3-1: The interrelation of the insulin signaling response (dashed box) with two key regulators of glucose homeostasis and fatty acid metabolism, AMPK and the CPT-system. Abbreviations as outlined in the text, CACT = carnitine/acylcarnitine translocase. Enzymes examined in this thesis are the IR (green), AMPK (blue) and CPT-2 (magenta). Green arrows indicate activation, red arrows denote inhibition.

For the experiments documented in this thesis the focus was put on the intracellular tyrosine kinase domain of the insulin receptor (IRTK; HERRERA *et al.*, 1988) as well as fusion proteins of IRTK or the core kinase of the IR (IRK; HUBBARD *et al.*, 1994) with the constitutively dimeric glutathione S-transferase from *Schistosoma japonicum* (GST; BAER *et al.*, 2001).

As the concerted regulation of IR effector proteins is abrogated in insulin resistance and diabetes and no clinically save small-molecule IR-agonists exist to date, AMPK and the CPT system have been identified as candidate drug targets for restoring glucose homeostasis.

AMPK is a heterotrimeric protein, consisting of a catalytic α - subunit (two isoforms) and two regulatory β - and γ -subunits (two and three isoforms, respectively). The 12 isoforms combinations can be further modified by alternative promoter usage, splicing, tissue specific expression and post-translational modification, including multiple phosphorylation (α - and β -subunits) and myristoylation (β -subunit; FRYER and CARLING, 2003; CARLING, 2004). The physiological allosteric activator AMP binds to the CBS-domains of the γ -subunit (SCOTT *et al.*, 2004; KEMP *et al.*, 2003) which renders the activation-loop of the α -subunit a better substrate for the upstream kinases LKB1 and Ca^{2+} /calmodulin-activated protein kinase kinase (CAMKK; WOODS *et al.*, 2003 and 2005). The β -subunit tethers the α - and γ -subunits and also contains a glycogen binding domain which might serve to target AMPK to substrates associated with glycogen-particles (POLEKHINA *et al.*, 2005B). This is in-line with the finding that AMPK phosphorylates and inactivates glycogen synthase, thereby inhibiting glycogenesis (HARDIE *et al.*, 2003). As AMPK also inhibits lipid synthesis its effects may seem to partially oppose those of insulin. While this is indeed the case in a healthy metabolic setting (AMPK is considered a fuel-gauge that senses and counteracts nutrient shortfall, while insulin regulates post-prandial nutrient storage), the enzymatic activity of AMPK is suppressed as an effect of excess dietary calory intake, obesity and physical inactivity (YE *et al.*, 2005). In patients with metabolic syndrome and/or T2D the activation of AMPK would allow dissipation of excess energy stores and plasma glucose. This is emphasized by the observation that AMPK promotes the translocation of GLUT4 from intracellular compartments to the cell surface in an IRS-1 dependent

manner (JAKOBSEN *et al.*, 2001), which provides a point of convergence with signaling of the IR.

In the liver an increased substrate flux via the CPT-system results in substantial upregulation of gluconeogenesis due to prevailing glucagonergic effects and via stimulation of pyruvate carboxylase by acetyl-CoA. In T2D patients, whose insulin-sensitive tissues are deprived of glucose, lipogenesis in the adipose tissue and β -oxidation in the liver is highly upregulated, which further suppresses glycolysis. The forced formation of ketone bodies from FA aggravates the diabetic state because these metabolites promote the insulin resistance in skeletal muscle. If not treated properly this metabolic imbalance can eventually lead to diabetic ketoacidosis.

It should be emphasized that the metabolic regulation and potential pharmaceutical approaches described so far are restricted to peripheral tissues. However, the IR, AMPK as well as CPT enzymes are also expressed in the central nervous system (CNS) with high abundance in the hypothalamus (ISGANAITIS and LUSTIG, 2005; KAHN *et al.*, 2005; PLUM *et al.*, 2005; OBICI *et al.*, 2003). Here these proteins regulate systemically food intake and energy homeostasis via the efferent pathways of the autonomous nervous system (sympathetic and parasympathetic signals).

The peripheral tissues signal to the hypothalamus by means of the release of peptide hormones (insulin, adipokines, gut hormones) into the blood. Interestingly, the AMPK and the CPT-system are reciprocally regulated in the hypothalamus vs. periphery. Insulin and leptin dependent inhibition of hypothalamic AMPK activity constitutes an anorexigenic signal in experimental animal models (KAHN *et al.*, 2005). Food intake is also diminished by pharmacological inhibition of the CPT-system in the CNS, either directly by administration of the competitive pseudosubstrate ST1326 (OBICI *et al.*, 2003) or indirectly by inhibition of fatty acid synthase by the compound C75 (KIM *et al.*, 2004). The latter results in accumulation of the allosteric CPT-1 inhibitor malonyl-CoA.

In addition, defects in insulin as well as IGF-1 signaling have been implicated in the progression of central neurodegenerative diseases (especially Alzheimer's disease; PLUM *et al.*, 2005) which suggests a neuroprotective function of these peptide hormones.

2.4 Specific aims

During the course of this thesis three projects were followed up with the purpose to

- 1) assess the crystallizability and to solve the crystal structure of a GST-dimerized IR (or alternatively IGF-1R) construct and to evaluate its interaction with published agonists.
- 2) assess the crystallizability of and to solve the crystal structure of AMPK or truncated constructs thereof.
- 3) assess the crystallizability and to solve the crystal structure of CPT-2.

Projects 1 and 2 were terminated because no crystals suitable for solving the crystal structures were obtained and the published IR agonists had adverse effects on the integrity of the intracellular part of the IR *in vitro*. The aim of project 3 was successfully accomplished.

3 Results

3.1 Characterization and crystallization of IR and IGF-1R constructs

3.1.1 Summary of literature data

The kinase domain of the IR was the first tyrosine kinase whose structure was solved by X-ray crystallography (HUBBARD *et al.*, 1994). Since then a number of mechanistic studies on the enzymology of the IR and IGF-1R kinase activities were accompanied by crystallographic examinations of intrinsically monomeric kinase domains (Table 3.1.1-1).

Receptor	PDB code	Author (Publication)	Comment
IR	1irk	HUBBARD <i>et al.</i> , 1994	apo, 0-P
	1ir3	HUBBARD <i>et al.</i> , 1997	AMP-PNP, 3-P
	1gag	Parang <i>et al.</i> , 2001	bisubstrate inhibitor
	1i44	Till <i>et al.</i> , 2001	Asp1161Ala in A-loop
	1p14	Li <i>et al.</i> , 2003	role of Tyr984 in JM
	1rqq	Hu <i>et al.</i> , 2003	complex with SH2 of APS
IGF-1R	1k3a	FAVELYUKIS <i>et al.</i> 2001	AMP-PCP, 3-P
	1jqh	PAUTSCH <i>et al.</i> , 2001	AMP-PNP, 2-P
	1m7n	MUNSHI <i>et al.</i> , 2002	apo, 0-P, dimer?
	1p4o	MUNSHI <i>et al.</i> , 2003	apo, 0-P, hinge mutant, dimer?

Table 3.1.1-1: Compilation of IR and IGF-1R related entries in the PDB. No PDB entry has been released for a study by ABLOOGLU *et al.*, 2000, where peptide substrates containing a fluorinated tyrosine residue were used to investigate the mechanism of phosphotransfer.

Despite the low resolution structure of the IR with bound insulin determined by electron microscopy (LUO *et al.*, 1999), only in the two crystal structures of the unphosphorylated kinase domain of the highly homologous IGF-1R (PDB codes 1m7n and 1p4o) the formation of dimers can be observed. In both structures the contents of the asymmetric unit consists of a dimer with the active sites facing each other, while a second dimer with the α D-helices as interface is generated via crystallographic symmetry (MUNSHI *et al.*, 2003).

However, from these structures it cannot be inferred how autophosphorylation occurs. The activation loop (A-loop) adopts a similar conformation as seen in the structure of the unphosphorylated IRK (PDB code 1irk) with Tyr1135 forming a tight hydrogen bond (2.57 Å in chain A) with the catalytic Asp1105. This conformation of the A-loop does not allow the simultaneous binding of ATP and autophosphorylation. Here it should be noted that the conformation of the A-loop in the structures of the unphosphorylated IRK

and IGFK is not a means of autoinhibition because physiological concentrations of ATP or dimerization can readily displace the A-loop (MADDUX and GOLDFINE, 1991; FRANKEL *et al.*, 1999 and 2001; BAER *et al.*, 2001).

Moreover, the A-loop of IRK was classified as non-gated (ADAMS, 2003), *i.e.*, phosphorylation of A-loop tyrosines enhances the phosphoryl transfer step but not substrate (ATP and peptide) binding. The amino-terminal peptide of one monomer of IGFK (including the autophosphorylation site Tyr950) is reciprocally situated in the active site cleft of the second monomer in the asymmetric unit of the high resolution structure of IGFK (PDB code 1p4o). This conformation is also not compatible with autophosphorylation. The hydroxy group of Tyr950 (chain B) is 5.38 Å away from the nearest side chain oxygen of the catalytic residue ASP1105 of chain A.

Therefore, these residues are not positioned within hydrogen-bonding distance, which is a prerequisite for the phosphotransfer reaction to occur (ADAMS, 2001). Moreover, the amino-terminus of IGFK occupies the space taken by the A-loop in the active conformation of IGFK (PDB code 1k3a) and phosphorylation of the juxtamembrane has been shown to occur in *cis*, *i.e.*, in an intramolecular reaction, for the highly homologous IR (CANN and KOHANSKI, 1997).

3.1.2 Crystallization experiments on dimeric IR and IGF-1R constructs

In order to elucidate the crystal structures of functional dimeric IR and IGF-1R kinase domains the full-length intracellular domains or truncated kinase domains of these receptors were expressed as fusion proteins with the constitutively dimeric protein GST (by K. Baer, M. Gompert, L. Thiebach; Table 3.1.2-1; BAER *et al.*, 2001). This thesis assignment comprised purification of these constructs (Figure 3.1.2-1) and subjection to crystallization trials.

Construct	AA	Source	Comment
His ₆ _IRTK	R953- S1355	Sf9, in-house, H-J. Schönfeld	monomer
GST-IRTK	R953- S1355	Sf9, lysate & cells, Klein group	dimer
GST-IRTK_D1120A	R953 - 1355	Sf9, lysate & cells, Klein group	dimer, inactive
GST-IRTK_ΔNT/CT (GST-IRK)	V978 - K1283	Sf9, lysate & cells, Klein group	dimer, NT and CT deletion
GST-IGFK_ΔNT/CT	V986 - K1286	Sf9, lysate & cells, Klein group	dimer, NT and CT deletion

Table 3.1.2-1: Constructs of human IR and IGF-1R used for characterization and crystallization. The monomeric hexahistidine-tagged construct His₆_IRTK was used for the investigation of the effect of IR-agonists on dimerization (see 3.1.3). AA = amino acids of IR or IGF-1 fused to GST.

The GST-tag and purification by GST affinity chromatography increased the stability and yield of the tagged vs. untagged kinase domains, respectively. In addition to GST-mediated dimerization, these constructs also allowed the exploitation of carrier protein (*i.e.*, GST) driven crystallization (CARTER *et al.*, 1994; LIM *et al.*, 1994; MCTIGUE *et al.*, 1995A and 1995B; KUGE *et al.*, 1997; TANG *et al.*, 1998; HAN *et al.*, 2001; ZHAN *et al.*, 2001; SMYTH *et al.*, 2003).

A two step purification protocol [1. GSH-sepharose affinity chromatography, 2. size exclusion chromatography (SEC)] yielded 10 - 15 mg of purified fusion protein from app. 10^9 Sf9 cells. While the solubilization and the affinity chromatography were performed with DTT as reducing agent, tris-(2-carboxyethyl)phosphine (TCEP, GETZ *et al.*, 1999) was used during the final SEC in order to avoid any covalent modification on cysteine residues of the enzyme by DTT or glutathione, which was used for elution from the GST-affinity column. The post-translational modification of proteins, including the IR, with thiol-reactive compounds is now recognized as a reversible means of regulating their activity in response to oxidative stress (SCHMID *et al.*, 1998; O'BRIEN and CHU, 2005). As a change in activity is generally accompanied by a change in conformation, any heterogeneity with respect to redox-modifications was sought to be avoided during preparation and crystallization of the GST-tagged IR and IGF-1R constructs.

Physiological as well as exogenous redox reagents had been described to alter the activity of the holo-IR (SCHMID *et al.*, 1998 and 1999A/B; SWEET *et al.* 1986; WILDEN *et al.*, 1986; WILDEN and PESSIN, 1987; ENGL *et al.* 1994; HOTZ-WAGENBLATT and DROGE, 2002). While redox reagents could have multiple effects on the IR in cellular assays or the purified IR (*e.g.*, modification of phosphatase activity, reviewed by TONKS, 2005; IR quaternary structure or insulin binding), SCHMITT *et al.* (2005) observed a modulation of the enzymatic activity of purified GST-IRTK_ΔNT/CT (GST-IRK) by changes in the redox status. Glutathione, which was used in millimolar quantities for the elution of the fusion proteins from the affinity column, could exert modification of the IR (SCHMITT *et al.*, 2005). Covalent modification and regulation of kinase activity by S-glutathionylation was also shown for PKA (HUMPHRIES *et al.*, 2002 and 2005).

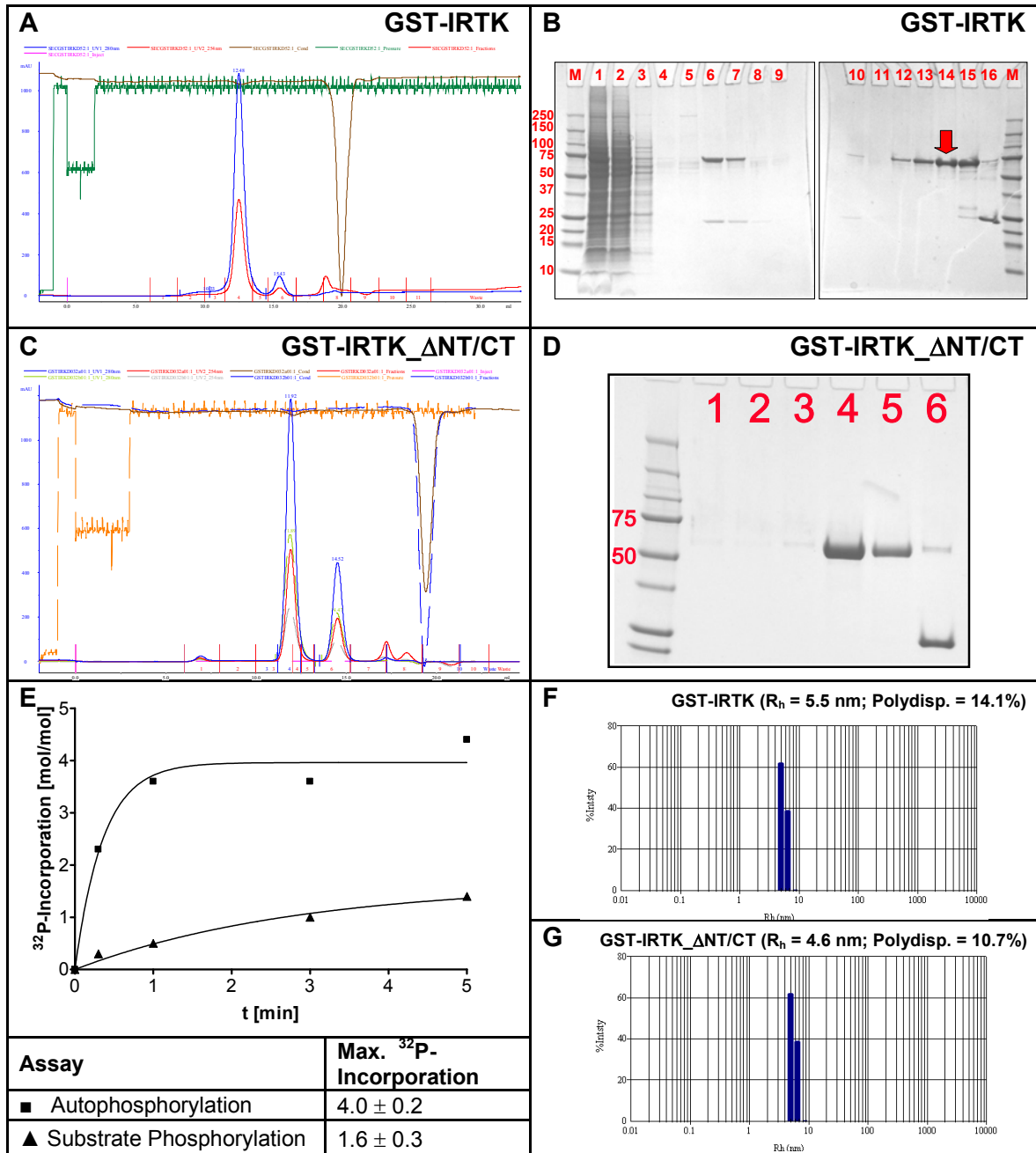


Figure 3.1.2-1: Purification and characterization of GST-tagged kinase domains of the IR and IGF-1R as exemplified by GST-IRTK and GST-IRTK_ΔNT/CT (GST-IRK). **A**, SEC elution profile and **B**, SDS-PAGE of GST-IRTK (theoretical MW = 72 kDa, the red arrow indicates the peak fraction of A used for characterization and crystallization). **C**, SEC elution profile and **D**, SDS-PAGE of GST-IRTK_ΔNT/CT (theoretical MW = 61 kDa, lane 4 depicts the peak fraction of C). The sizes of molecular weight marker proteins are indicated for C and D. The minor peaks in the SEC profiles are residual free GST, which could be completely separated from the fusion proteins. **E**, activity assay, *i.e.*, time course of autophosphorylation (squares) and substrate (GST_IRS-1_p30) phosphorylation (triangles), of GST-IRTK in the presence of 2 mM TCEP. The data from a single experiment were fit to a monophasic exponential association curve. The values for the maximal phosphate incorporation are in-line with those determined for preparations containing DTT (BAER *et al.*, 2001). The results from DLS indicate monodisperse preparations for the concentrated samples (10 mg/ml of peak fraction from A and C, respectively) of **F**, GST-IRTK and **G**, GST-IRTK_ΔNT/CT.

Along these lines, non-modifying protease inhibitors (Roche Complete) instead of phenylmethylsulphonylfluoride (PMSF), which is generally known to covalently modify serine residues, were used. GST-IRTK retained full activity when purified in the presence of the reducing agent TCEP and was found to be devoid of any covalent modifications as determined by mass spectrometry. This also confirmed the absence of phosphorylation, which might interfere with crystallization. All preparations of GST-tagged IR and IGF-1R kinase domains were found to be monodisperse when examined by dynamic light scattering (DLS; Figure 3.1.2-1).

The purified GST-fusion proteins were subjected to crystallization trials using the modified microbatch method (D'ARCY *et al.*, 2003 and 2004) with various sets of screening solutions. Crystals were obtained from assays containing GST-IRTK or GST-IRTK_ΔNT/CT (GST-IRK), but not with GST-IGFK or GST-IGFK_ΔNT/CT (Figure 3.1.2-2).

Construct	Condition		Crystal	
GST-IRTK	H01 (in-house)	25 % (w/v) PEG 1500 -no diffraction		
	PEG/Ion Screen™ (Hampton Research)	# 2 0.2 M KF, 20 % PEG 3350, pH 7.2 - no diffraction	#2 	#14 
		# 14 0.2 M KSCN, 20 % PEG 3350, pH 7.0 - no diffraction		
		# 21 0.2 M NaCHO2, 20 % PEG 3350, pH 7.2 - no diffraction	#21 	#27 
		# 27 0.2 M NaOAc, 20 % PEG 3350, 7.9 - no diffraction		
# 31 0.2 M Li2SO4, 20 % PEG 3350, pH 6.4 - complete dataset collected (2.5 Å resolution) *	#31 	#45 		
# 45 0.2 M tri-Li citrate, 20 % PEG 3350, pH 8.1 - no diffraction				
GST-IRKD ΔNT/CT (GST-IRK)	Index Screen™ (Hampton Research) # 42 0.1 M BisTris pH 5.5, 25 % PEG 3350 Stura Footprint Screen 2 (Molecular Dimensions) #20 0.1 M NaOAc, pH5.5, 36 % PEG MME 5000 Fragment (GST) crystallized and structure solved (Rufer <i>et al.</i> , 2005; see Appendix 7.1)		no picture	

Figure 3.1.2-2: Crystallization hits from assays containing GST-IRTK or GST-IRTK_ΔNT/CT (GST-IRK).
* Data statistics are summarized in Table 3.1.2-2.

Preincubation of the GST-fusion proteins with the generic kinase inhibitor staurosporine (FUJITA-YAMAGUCHI and KATHURIA, 1988; RUEGG and BURGESS, 1989) or the IGF-1R-specific inhibitors genistein or tyrphostin AG1024 did not improve the crystallization behavior.

A dataset could be collected from a single crystal grown from an assay containing GST-IRKD (10 mg/ml) with condition 31 of the PEG/Ion Screen™, Hampton Research, as precipitant (Table 3.1.2-1).

Data Collection			
		Program	
		XDS / XSCALE	DENZO / SCALEPACK
Space group		I222 (or I2 ₁ 2 ₁ 2 ₁) [§]	I222 (or I2 ₁ 2 ₁ 2 ₁) [§]
Cell dimensions			
a, b, c [Å]		93.6, 98.8, 102.4	93.6, 98.8, 102.4
α, β, γ [°]		90.0, 90.0, 90.0	90.0, 90.0, 90.0
Resolution [Å] *		70.0 - 2.5 (2.65 - 2.50)	70.0 - 2.5 (2.61 - 2.50)
R _{sym} [%]		11.6 (29.0)	9.1 (18.2)
I/ σ		16.9 (7.8)	13.8 (6.0)
Completeness [%]		98.9 (94.1)	94.4 (92.5)
Redundancy		4.4 (4.4)	4.0 (4.0)
Matthews' Parameter Calculation			
MW [kDa]	Nmol / AU	Matthew's Coefficient	Solvent Content
72 (GST-IRTK)	1	1.6	24.6
46 (IRTK)	1	2.6	51.8
	2	1.3	3.7
26 (GST)	1	4.6	72.8
	2	2.3	45.6
	3	1.5	18.3

Table 3.1.2-2: Data collection (SLS, 110 K) statistics of the crystal obtained from an assay containing GST-IRTK and PEG/Ion Screen™ solution number 31. The Matthews' parameter (V_M) calculation (MATTHEWS, 1968) suggests that solely a fragment of GST-IRTK was crystallized as the solvent content of a theoretical crystal packing consisting of closely packed spheres is app. 26 % (KANTARDJEFF and RUPP, 2003). However, GST-IRTK is not necessarily spherical and trypsin crystals (P3₁21 cell) were reported with a solvent content between 11 % and 18 % (C. Vonrhein, Global Phasing, personal communication). The good resolution (2.5 Å) of the diffraction data collected from the tiny crystal indicates a high protein content and dense crystal packing. According to the TRUNCATE statistics, twinning of the crystal and concomitant underestimation of V_M due to apparent higher symmetry could be ruled out (a 50 % twinning fraction with a diad twin symmetry would result in an V_M reduced by factor 2). Calculation of self-rotation functions (MolRep, AMoRe) did not resolve the ambiguity of the asymmetric unit contents.

* Values in parentheses are for the highest resolution shell. Processing of the data with DENZO/SCALEPACK produced a decreased value for R_{merge} , but the number of rejected reflections was higher with a concomitant decrease in completeness. § The orthorhombic body-centered space groups cannot be distinguished based on systematic absences. Therefore, the molecular replacement trials were performed in both I222 and I2₁2₁2₁. Processing the data in P1 and search for higher symmetry with the program XPREP (SHELXTL package) confirmed the choice of these space groups.

The data were processed and scaled with XDS/XSCALE as well as DENZO/SCALEPACK yielding similar results. Subsequent phasing trials were conducted with various molecular replacement programs (AMoRe, MOLREP, BEAST,

PHASER). Multiple structures of kinase domains from the PDB as well as all publically available GST structures were used as search models. However, none of the molecular replacement calculations gave an indication for a correct solution with respect to correlation coefficients of observed and calculated amplitudes, R-factors, results of packing functions or maximum likelihood scores.

Fragmentation of GST-IRTK in the crystallization trials seemed likely based on the Matthews' parameter analysis for the dataset. This was also found to be the case for the truncated construct GST-IRTK_ΔNT/CT (GST-IRK; Figure 3.1.2-3).

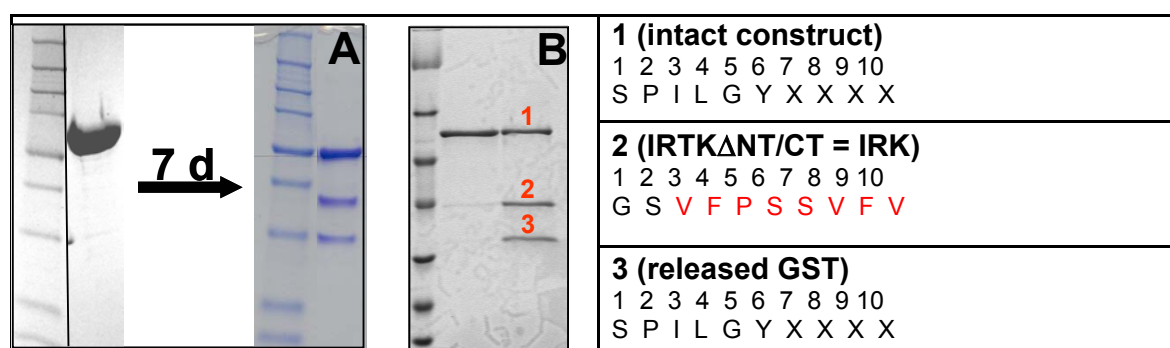


Figure 3.1.2-3: Spontaneous fragmentation of GST-IRTK_ΔNT/CT (GST-IRK). Essentially homogeneous preparations were not stable during storage in 50 mM Tris/HCl pH 7.5, 150 mM NaCl, 2mM TCEP (**A**) or 2 mM DTT (**B**, purified with an alternative protocol by K. Baer, University of Cologne) for 7 days at 4°C. The right panel shows the results of the amino-terminal (Edman) sequencing of the blotted fragments. The data clearly demonstrated that the construct GST-IRTK_ΔNT/CT (GST-IRK) was cleaved in the linker (thrombin cleavage site) of the fusion protein, yielding fragment 2 (IRTK_ΔNT/CT = IRK, red, plus two additional amino terminal residues from the linker) and fragment 3 (free GST plus six additional carboxy-terminal residues from the linker).

No contaminating protease activity could be detected using a sensitive spectroscopic assay with resorufin-labeled casein als generic protease substrate. Supplementing the storage buffer with diisopropyl fluorophosphate (5 mM f.c.) and Roche Complete protease inhibitor (2 Tbs/l f.c.) did not prevent the decomposition of the GST-IRTK_ΔNT/CT (GST-IRK). Therefore, it was concluded that spontaneous autocatalytic cleavage as described for nucleolin and myelin basic protein (CHEN *et al.*, 1991; D'SOUZA *et al.*, 2005), which also undergo degradation independent of both endogeneous and exogeneous protease activity, could be the reason for the instability of the GST-IRTK_ΔNT/CT (GST-IRK; RUFER *et al.*, 2005; Appendix 7.1). Analysis by mass spectrometry combined with amino-terminal sequencing of the fragments revealed that the cleavage occurred in the linker of the fusion protein (Figure 3.1.2-3).

Replacement of the linker between GST and IRTK_ΔNT/CT (IRK) was not pursued because the introduction of a (Gly-Ala)₅ linker resulted in significant loss of activity in autophosphorylation assays indicating suboptimal alignment of the kinase domains (A. KLOSE, 2000, Diploma thesis, University of Cologne).

3.1.3 Interaction of IRTK with small-molecule agonists

Non-peptidic small-molecule compounds that directly activate the kinase activity of the isolated kinase domain of the IR *in vitro* or elicit an insulin-sensitizing activity had been described by the pharmaceutical companies Merck & Co., Inc., and Telik, Inc., (Table & Figure 3.1.3-1; AIR *et al.*, 2002; GURA, 1999; ZHANG *et al.*, 1999; LIU *et al.*, 2000; QURESHI *et al.*, 2000; WEBER *et al.*, 2000; WOOD *et al.*, 2000; ZHANG and MOLLER, 2000; BALASUBRAMANYAM and MOHAN, 2001; LI *et al.*, 2001 and 2002; MANCHEM *et al.*, 2001; SALITURO *et al.*, 2001; DING *et al.*, 2002; LABORDE and MANCHEM, 2002; PENDER *et al.*, 2002; PERSAUD *et al.*, 2002; PIRRUNG *et al.*, 2002; WEBSTER *et al.*, 2003; CHENG *et al.*, 2004; STROWSKI *et al.*, 2004; reviewed in DE MEYTS and WHITTAKER, 2002).

The parent compound of the asterriquinone series pursued by Merck & Co., Inc., (Table 3.1.3-1) was initially isolated from the fungus *Pseudomassaria spec.* This compound was highly potent as it could stimulate *in vitro* the activity of GST-IRTK, which is a constitutive dimer with elevated intrinsic activity (ZHANG *et al.*, 1999; BAER *et al.*, 2001). 2,4-Dihydroxylation rendered the quinoid compounds insensitive to redox-reactions and, therefore, a redox-priming type of activation of purified IR *in vitro* (SCHMID *et al.*, 1998) or modification of other cellular components in cell-based assays could be excluded. Three related bioactive asterriquinones from *Aspergillus sp.* were described by ONO *et al.*, 1991, ALVI *et al.*, 1999 and WIJERATNE *et al.*, 2003. These compounds were found to elicit diverse effects including inhibition of HIV-reverse transcriptase, disruption of binding of the Grb-2 SH2 domain to the phosphorylated epidermal growth factor receptor (EGFR) and inhibition of cell cycle progression in tumor cell lines, respectively.

The insulin-sensitizing Telik1 compound (Table 3.1.3-1) was identified by screening a compound library for insulin receptor agonist activity in an affinity fingerprint assay (KAUVAR *et al.*, 1995; MANCHEM *et al.*, 2001). Two successor compounds with

decreased molecular weights and enhanced, direct agonistic potency with respect to activation of the IR kinase activity both *in vitro* and *in vivo* were developed by Telik.

Interestingly, the recently identified adipokine visfatin also binds directly to the IR and activates the kinase activity of the IR without competing with insulin binding. The discovery of this physiologic insulin-mimetic emphasizes the feasibility of heterologous activation of the IR, albeit further characterization of the exact binding mode of visfatin is needed (FUKUHARA *et al.*, 2005; HUG and LODISH, 2005).

Initial incubation and co-crystallization experiments of His₆-IRTK (purified by H-J. Schönfeld and B. Pöschl, Roche Basel) and the GST-tagged constructs with the Merck1/2 and Telik3 compounds showed that the compounds tended to aggregate the protein as judged from analysis by DLS and increased precipitation in crystallization screens. In order to characterize the protein ligand interactions and the physico-chemical properties of the compounds, limited proteolysis and analytical ultracentrifugation (AUC) were performed. The tryptic cleavage pattern of His₆-IRTK (0.5 mg/ml \approx 10 μ M) after incubation with Merck1 (RO0716631) was changed such that the A-loop was protected from tryptic cleavage (Figure 3.1.3-1). Whereas the presence of the Merck1 compound provoked the release of a distinct 30 kDa fragment, the formation of this fragment was less pronounced with the compounds Merck2 and Telik3 (all 20 mM). AMP-PCP (100 mM), a non hydrolyzable analog of the kinase co-substrate ATP, rendered the activation loop highly susceptible for tryptic cleavage.

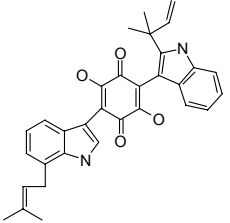
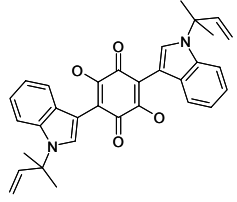
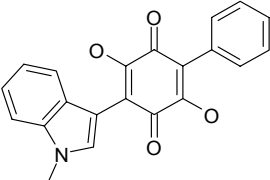
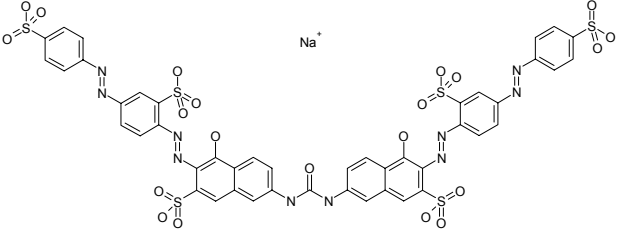
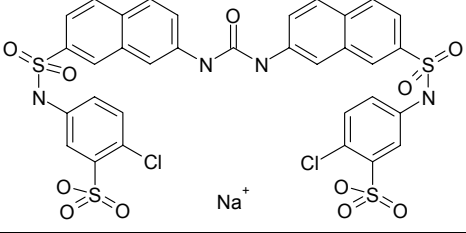
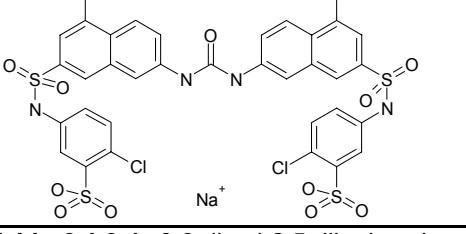
Compound		Comment
	Prototype asterriquinone 	Merck1 (RO0716631) L-783,281 Demethylasterriquinone B1 <i>Pseudomassaria</i> sp. activates GST-IRTK <i>in vitro</i> MW = 506.6 EC ₅₀ = 5 μM ZHANG <i>et al.</i> , 1999
		Merck2 (RO0721705) 2,5-Dihydroxy-3-(1-methylindol-3-yl)-3-phenyl-1,4-benzoquinone synthesized as derivative of Merck1 MW = 345.4 EC ₅₀ = 0.3 μM LIU <i>et al.</i> , 2000
		Telik1 TLK16998 MW = 1241.2 (free acid) EC ₅₀ = 1 μM MANCHEM <i>et al.</i> , 2001
		Telik2 (RO4590422) TLK19780 MW = 851.7 (free acid) EC ₅₀ = 0.1 μM PENDER <i>et al.</i> , 2002
		Telik3 (RO0731502) TLK19781 MW = 883.7 (free acid) EC ₅₀ = 0.1 μM CHENG <i>et al.</i> , 2004

Table 3.1.3-1: 3,6-diaryl-2,5-dihydroxybenzoquinones (MERCK compounds; the generic asterriquinone, 2,5-bis-[1-(1,1-dimethyl-2-propenyl)-indol-3-yl]-3,6-dihydroxy-1,4-benzoquinone, is shown as reference) and the symmetrical urea-derivatives (TELIK compounds) that were found to stimulate the tyrosine kinase activity of the IR *in vitro*. The app. *in vitro* EC 50 values are indicated.

This suggested that the A-loop might be buried in a dimer interface, *i.e.*, the Merck1 compound promotes the formation of productive dimers primed for autophosphorylation. The formation of His₆-IRTK dimers mediated by Merck1 was verified by AUC. However, the AUC data also clearly showed that the Merck1 compound leads to aggregation and sedimentation loss of His₆-IRTK in a concentration dependent manner (Figure 3.1.3-1B).

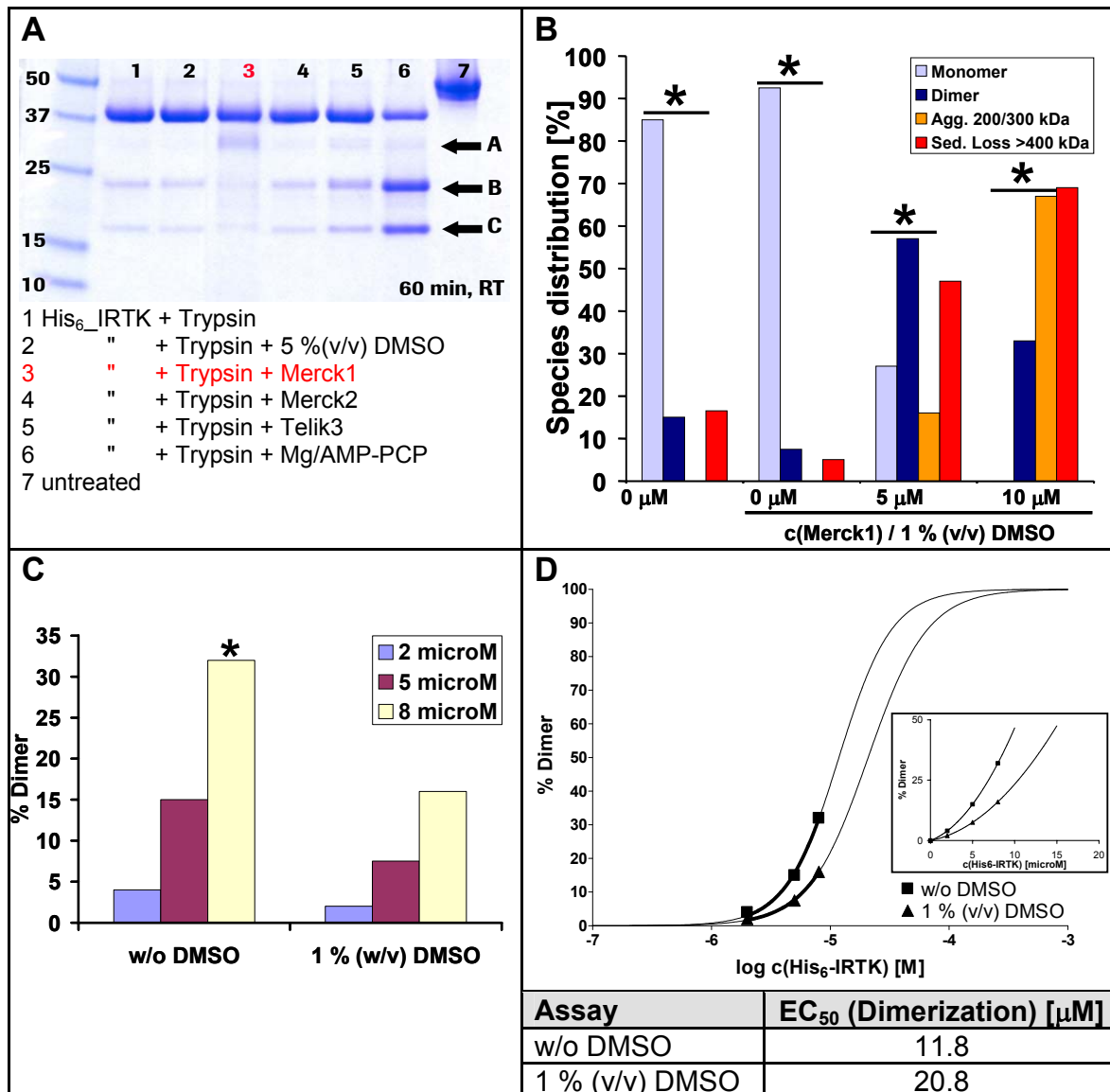
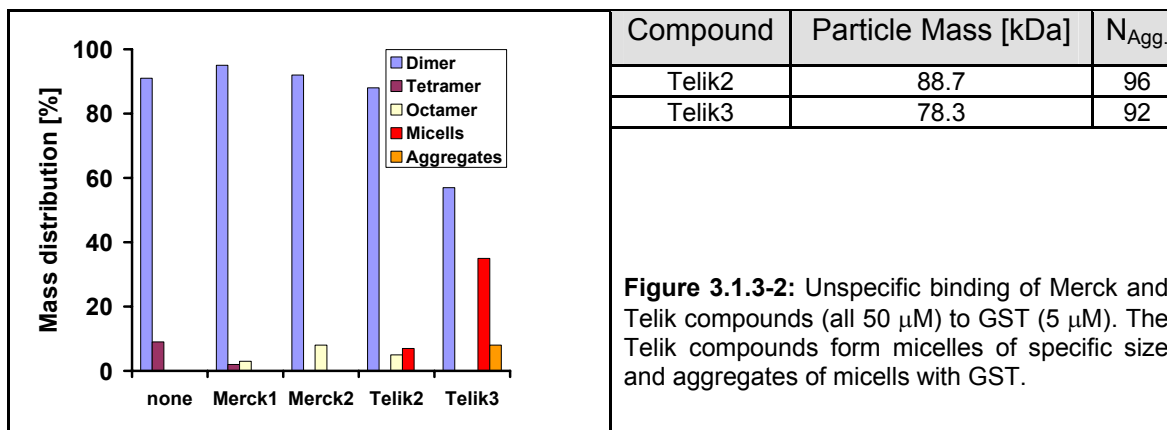


Figure 3.1.3-1: Characterization of the effect of small-molecule IR agonists (and DMSO control) on the quaternary structure/ oligomerization of His₆_IRTK. All characterizations were performed in 50 mM HEPES/ NaOH pH 7.7, 100 mM NaCl supplemented with DMSO as indicated. **A**, limited tryptic proteolysis of His₆_IRTK (0.5 mg/ml + 0.006 mg/ml trypsin) in the absence (lane 1, lane 2 is DMSO control) or presence (lanes 3-5) of agonists. The non-hydrolyzable nucleotide-analog AMP-PCP (lane 6) was used as positive control for triggering the gate-open conformation of His₆_IRTK. Lane 7 shows the untreated enzyme. Three fragments are released upon cleavage by trypsin [A (30 kDa) cleaved after Lys1030 of ATP binding site; B (24 kDa) cleaved at activation loop and C (16 kDa) cleaved at carboxy-terminus; ZHANG *et al.*, 1999; SALITURO *et al.*, 2001; BAER *et al.*, 2001). **B**, results from analytical ultracentrifugation of His₆_IRTK (5 μM) in absence (0 μM, plus DMSO control) or presence of 5 μM (*i.e.*, equimolar) and 10 μM Merck1 compound. The asterisk indicates 100 % supernatant at equilibrium speed. **C**, effect of concentration and DMSO on the quaternary structure of His₆_IRTK (the asterisk indicates an extrapolated value), as determined by AUC. Concentrations higher than 8 μM His₆_IRTK could not be investigated because of the limited dynamic range in absorption spectroscopy during AUC. **D**, based on the AUC data (bold curves, measured data) the EC₅₀ for the association of His₆_IRTK during dimer formation was calculated with a sigmoidal fit (thin curves, simulated; Prism 3.0, GraphPad Software). The inset shows the second order polynomial fit of the AUC data (up to the inflection point of the association curve) that was used for determining appropriate initial values for the sigmoidal fit.

Another important result of the AUC studies was the finding that the intrinsically monomeric His₆_IRTK (unphosphorylated apo enzyme) forms dimers in a concentration dependent manner with an EC₅₀ = 11.8 μM. The concentration for half-maximal dimer formation was shifted to EC₅₀ = 20.8 μM in the presence of 1 % (v/v) f.c. DMSO, which was essential for solubilizing the hydrophobic agonists. Therefore, the DMSO interfered with dimer formation (Figure 3.1.3-1C), while it was simultaneously used as vehicle for dimerization inducing compounds in published and in-house *in vitro* kinase assays. Extrapolation of the simulated association curves (Figure 3.1.3-1) revealed that theoretically 100 % dimerization was reached at app. 550 μM, independent of the presence of DMSO. At the His₆_IRTK concentration of 10 mg/ml ≈ 200 μM which was used for crystallization experiments, still ≥ 95 % of the protein could be expected to be in its dimeric form.

In order to characterize the specificity of the Merck1, Telik1 and Telik2 compounds regarding their agonist activity, DLS and AUC analyses with the free compounds or in the presence of GST were performed. This also served as pilot study for the evaluation of the effect of these compounds on GST-IRTK. According to a DLS screen, the Merck1 and Telik2/3 compounds formed particles of app. 50 - 150 nm. Surprisingly, AUC runs in absence of protein with free Telik2 and its derivative Telik3 in the GST-IRTK storage buffer (20 mM TRIS/HCl, pH7.5, 150 mM NaCl, 2 mM TCEP, 0.02 % NaN₃, 1 % v/v DMSO) showed that these compounds formed micelles with aggregation numbers of 96 and 92, respectively (Figure 3.1.3-2). Moreover, the compounds had an effect on the oligomerization state of GST which indicated unspecific protein binding.



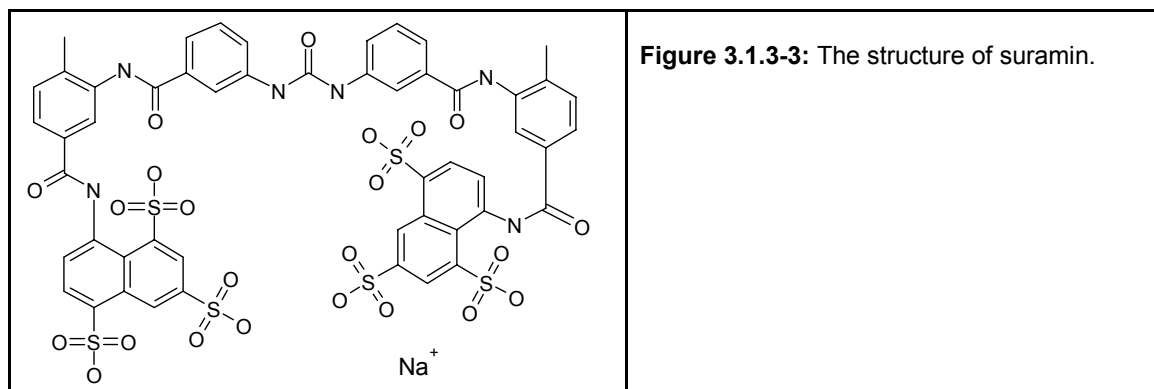
The formation of particles and micelles of defined size was described for screening hits and drug-like compounds of unrelated structure (MCGOVERN *et al.*, 2002 and 2003; SEIDLER *et al.*, 2003). Regarding the experimental results and literature data it seems reasonable to argue that the *in vitro* agonistic potential of the published IRTK enhancers can be largely attributed to adsorption of IRTK molecules to particle or micelle surfaces. Thereby, the local concentration of the enzyme is increased, which then promotes autophosphorylation. The formation of aggregates by adsorption and/or absorption of IRTK by particles of agonist molecules also explains the sedimentation loss observed with increasing agonist concentrations.

However, when administered to animal models of T2D (db/db, ob/ob and streptozotocin/high fat diet treated mice), both the Merck (p.o.) and the Telik (i.p.) compounds do possess *in vivo* efficacy (ZHANG *et al.*, 1999; MANCHEM *et al.*, 2001). As the Merck1 compound was also found to dimerize and activate the BDNF/neurotrophin receptors TrkA/B/C in cellular assays by binding to the intracellular kinase domains (WILKIE *et al.*, 2001; POLLACK and HARPER, 2002A and B), the compound seems to possess an unspecific agonistic activity on several receptor tyrosine kinase domains. Interestingly, the Trk receptors display significant sequence similarity (app. 60 %) and identity (app. 45 %) to the IR based on an alignment of 270 amino acids of their core kinases. The highest similarity (app. 80 %) and identity (app. 70 %) is seen in the 30 amino acids of the activation loops, where both IR and Trk receptors have three autophosphorylation sites. This could imply a similar mode of activation for these receptors, despite the fact that the quaternary structure of the native IR provides

endogenous dimerization of its two kinase domains as opposed to the monomeric Trk receptors.

The establishment of a preliminary structure activity relationship for the Merck compounds (WOOD *et al.*, 2000) suggested that the astringinone series could be amenable to optimization with regard to its specificity and physico-chemical properties. Nevertheless, a cytotoxicity issue remains because the Merck1 compound and astringinones in general have been shown to intercalate into genomic DNA, thereby causing cell death (WILKIE *et al.*, 2001; KAJI *et al.*, 1997).

The specificity of the Telik compound is also questionable because the highly related compound suramin (Figure 3.1.3-3) was identified as a direct activator of Trk receptors as well (GILL and WINDEBANK, 1998; POLLACK and HARPER, 2002A and B), besides having diverse effects on multiple other enzymes (EICHHORST *et al.*, 2004, and references therein).



3.2 Characterization and crystallization of AMPK

3.2.1 Summary of literature and Roche data

The initial focus of AMPK crystallization was put on the catalytic α -subunit for reasons of better biochemical tractability as opposed to the regulatory β - and γ -subunits or the heterotrimeric holoenzyme. Two soluble GST-fusion constructs of the rat α 1-subunit, comprising amino acids 1-312 and 1-392, respectively, had been described by CRUTE *et al.* (1998; see also HAMILTON *et al.*, 2002). The lengths of these constructs had been determined based on their biochemical properties. Truncation of the α 1-subunit at amino acid 392 yielded an inactive enzyme and fully abolished binding to the regulatory subunits. In contrast, CRUTE *et al.* (1998) found the AMPK_ α 2_1-312 construct to be constitutively active in the absence of the allosteric activator AMP when phosphorylated on T172 in the activation loop. These results implied the presence of an autoinhibitory sequence in amino acids 312-392 of the AMPK α 1-subunit.

The corresponding constructs of the rat α 2 isoform were cloned in-house, yielded stable proteins without GST-fusion and were subjected to crystallization trials. The entire work on the α -subunit in our laboratory was focused on constructs of the rat α 2 isoform, which is almost identical to the clinically relevant human α 2 isoform (Table 3.2.1-1).

	Species					
	rat	mouse		human		
	α 1	α 1	α 2	α 1 isoform1	α 1 isoform 2	α 2
rat α 2 NP_076481	86.4 (94.1) P54645	86.1 (93.8) AAW79567	99.1 (99.7) NP_835279	85.3 (93.0) Q13131	82.0 (89.3) NP_996790	99.1 (99.7) P54646

Table 3.2.1-1: Percent identity (in parentheses: similarity; calculated with Needle, EMBOSS, RICE *et al.*, 2000) of amino acid sequences for residues 1-339 of catalytic AMPK α -subunits in comparison to the rat α 2-subunit used in-house (EC2.7.1.-, with accession codes). Isoform 2 of human AMPK α 1 is a splice variant and has a 15 amino acid insert which is predicted to localize between helices α D and α E close to the hinge region and the lobe interface. The function of this insert had not been characterized.

In addition, the activation loop mutants T172D were prepared for both the published constructs in order to mimic the regulatory phosphorylation by an upstream kinase and, thereby, populate a distinct conformation. STEIN *et al.* (2000) reported that introduction of the T172D mutation into heterotrimeric AMPK is sufficient for stimulating approximately 50 % of the wild-type activity. Conflicting data had been published regarding the activity of the construct AMPK_ α 2_1-312_T172D, which was described

to be constitutively active by TSUBOI *et al.* (2003), whereas CRUTE *et al.* (1998) detected no activity. Therefore, it was not clear whether the T172D mutation was sufficient for mimicking phosphorylation. Further truncation of the enzyme (AMPK_α2_1-301) was found to destabilize the protein which could be partially compensated by addition of 20 mM imidazole and 10 % (v/v) glycerol during purification. As screening of these constructs with commercial and in-house sets of precipitants (developed based on the publication by JANCARIK and KIM, 1991) and mutants did not yield crystals, a limited proteolytic digest of apo AMPK_α2_1-392 was performed in order to identify the actual domain boundary. Cleavage with subtilisin yielded a stable fragment, AMPK_α2_1-339, as identified by mass spectrometry (no post-translational modification found) and amino-terminal sequencing (Edman microsequencing from blotted sample according to MATSUDAIRA, 1989) of an excised gel band (Figure 3.2.1-1).

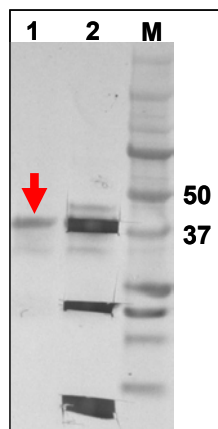


Figure 3.2.1-1: Limited proteolysis of apo AMPK_α2_1-392 with subtilisin. Lane 1: incubation for 24 h on ice. Lane 2: incubation for 8 h at 21°C. Three major bands were excised for analysis. M: marker, molecular weight [kDa] is indicated. In both reactions the same main fragment (AMPK_α2_1-339, red arrow) was produced.

This construct was found to be enzymatically inactive (M. Andjelkovic, Roche Basel), albeit the effect of phosphorylation of T172 in the activation loop by an upstream AMPKK preparation (HAMILTON *et al.*, 2002), CAMKKβ (HAMILTON *et al.*, 2002; HAWLEY *et al.*, 2005; HURLEY *et al.*, 2005; WOODS *et al.*, 2005) or purified LKB1 (HAWLEY *et al.* 2003; LIZCANO *et al.*, 2004) was not investigated.

Crystallization trials of AMPK_α2_1-339 ($c = 10$ mg/ml, in 20 mM Tris/HCl pH 7.8, 150 mM NaCl, 2 mM MgCl₂, 2 mM TCEP) resulted in reproducible crystals with 5 % (w/v) PEG 8000, 0.1 M NH₄OAc, 0.02 M MgCl₂ and 0.1 M HEPES pH 7.0 (Natrix Screen™ # 39, Hampton Research) as precipitant. After refinement of the crystallization conditions to 2-3 % (w/v) PEG 8000, 0.4-0.5 M NH₄OAc, 2-10 mM MgCl₂ and 0.1 M HEPES/NaOH

pH 7.0-7.4 (depending on drop ratio), the crystals diffracted to a resolution of 6.5 Å at the SLS synchrotron. The space group symmetry could not be assigned due to the limited diffraction quality of the crystals. AMPK_α2_1-339 crystallized under similar conditions with and without amino-terminal His₆-tag (from pET-15b expression vector). Amino-terminal truncation (AMPK_α2_8-339) or introduction of the activation loop mutant (AMPK_α2_1-339_T172D) resulted in additional crystallization conditions but did not improve the diffraction quality of the crystals. An AMPK homology model based on the structure of PKA (BOSSEMEYER *et al.*, 1993, PDB code 1cdk) was built (B. Kuhn, Roche Basel) in order to allow selection of flexible surface residues which could be mutated in order to facilitate crystallization by improving crystal contacts (reviewed in DALE *et al.*, 2003 and DEREWENDA, 2004; see PATEL *et al.*, 2004, for example on p38α kinase). None of the constructs with surface mutants (K12A, R239A and K255A for AMPK_α2_1-312_D172D; K107A, Y237R and Y292A for AMPK_α2_1-339) crystallized.

Addition of the nucleoside analog 5-aminoimidazole-4-carboxamide-1-β-D-ribofuranoside (AICAR) or its phosphoric acid derivative 5'-AICAR monophosphate (ZMP) produced weakly diffracting crystals with AMPK_α2_1-339 and AMPK_α2_1-339_T172D, respectively. The presence of the generic kinase inhibitor staurosporine (RUEGG and BURGESS, 1989) completely prevented crystallization. This could most likely be attributed to a pronounced change in the conformation of the AMPK catalytic domain, similar to that observed upon binding of staurosporine to PKA (PRADE *et al.*, 1997). The change from conventional protein concentration via microconcentrators to step elution from a 1ml anion-exchange column greatly improved the quality of the protein preparation in terms of avoiding aggregation. Despite purification of homogeneous and monodisperse proteins and various crystallization conditions, all the crystals had the same morphology and diffracted X-rays poorly (max. 6.5 Å resolution).

A collaboration with the group of Prof. T. Wallimann, Institute of Cell Biology, ETH Zurich, was established which granted access to lysates from *E. coli* expressing heterotrimeric rat AMPK_α1β1γ1 and AMPK_α2β2γ1 expressed from a tricistronic vector (NEUMANN *et al.*, 2003). Crystallization trials with the latter yielded needle-

shaped crystals with 1 M Li_2SO_4 , 0.01 M NiCl_2 and 0.1 M Tris/HCl pH 8.5 (Jena Bioscience screen 10/B1) as precipitant. As crystals of AMPK_α2_1-339 were obtained under identical conditions and both the α2-subunit constructs as well as the trimeric AMPK were found to bind to Ni-NTA-resin even after cleavage of the His₆-tag, NiCl_2 was tested as additive. However, addition of NiCl_2 during purification did not improve the quality of the protein and crystals thereof.

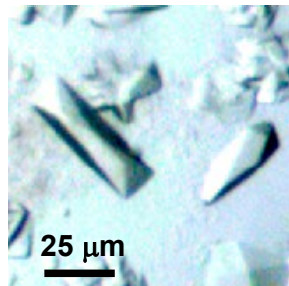
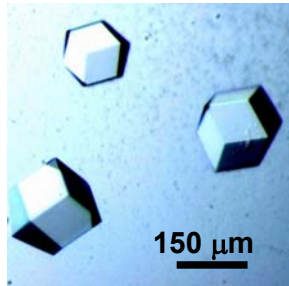
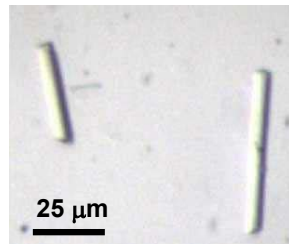
3.2.2 Crystallization and characterization of AMPK_α2 constructs

All the following experiments were performed as part of this thesis. AMPK_α2_1-339 (wild-type) was selected from the existing constructs of the α-subunit for further optimization because the purification protocol and crystallization was more reproducible compared to other constructs. In addition, this was the only construct for which initial crystallization conditions were available. For subsequent protein preparations the final storage buffer was changed to HEPES (instead of Tris) because AMPK_α2_1-339 crystallized repeatedly from HEPES-buffered conditions.

Rescreening the crystallization properties of this construct at 15°C instead of the established 21°C using the modified microbatch method (D'ARCY *et al.*, 2003 and 2004) with 25 % (v/v) silicone oil/ 75 % (v/v) paraffin oil as opposed to standard 50 % (v/v) silicone oil/ 50 % (v/v) paraffin oil (Al's Oil) as evaporation barrier provoked a slower nucleation and extended crystallization phase (CHAYEN, 1997 and 2004). This change in the progress along the trajectory through the crystallization phase diagram caused AMPK_α2-1-339 to crystallize from 15 % (v/v) Tacsimate*, 2 % (w/v) PEG 3350 and 0.1 M HEPES pH 7.0 (Hampton Research Index Screen™ # 36). After exchanging the PEG 3350 to 3 % (w/v) PEG 8000 large, single orthorhombic crystals were obtained with 6 % (w/v) dextran sulfate as additive, whereas crystals with a hexagonal habitus grew under the exact same conditions with 9 mM hexamine-Co(III)-chloride as additive (Table 3.2.2-1).¹

* Tacsimate is a specially formulated, proprietary salt mixture composed of neutralized organic acids including but not limited to malonic acid, succinic acid, and malic acid. Sam Patel, Hampton Research

Table 3.2.2-1: In-house preparations of AMPK that were subjected to crystallization during the course of this thesis. Numbers in parentheses indicate drop ratios for setting up crystallization trials from stock solutions [μ l, protein + precipitant (+ additive, where applicable)].

Construct		Crystals/ Comment	
AMPK_α2_1-339_wt *			apo, 30 mg/ml (2+2+1) Diffraction to 6.5 Å orthorhombic 15 % Tacsimate pH 7.0 0.1 M HEPES pH 7.0 3 % PEG 8000 6 % Dextran Sulfate 5000 - optimized from Hampton Research Index # 36 Additive Screen 3.8
			
AMPK_α2_1-339_T172D *		no crystals	
AMPK_α2_8-339_wt *		no crystals	
D56A/R171E/T172D	AMPK_α2_1-339		Staurosporine (5+2) Diffraction to 7.5 Å cubic 0.2 M tri-Na-Citrate 20 % PEG 3350 0.16 mM n-Decyl-β-D-maltopyranside (1X CMC) - optimized from Hampton Research Index # 94 Detergent Screen 1.9
	AMPK_α2_1-301	minute crystals, no optimization	
	AMPK_α2_1-312	minute crystals, no optimization	
	AMPK_α2_1-249	insoluble in expression test	
	AMPK_α2_1-262	insoluble in expression test	
	AMPK_α2_1-263	insoluble in expression test	
	AMPK_α2_1-264	insoluble in expression test	
	AMPK_α2_1-326	no crystals	
AMPK_β1γ1(Δ1-67) *		no crystals	
AMPK_β1γ1(Δ1-185) *		no crystals	
His ₆ _AMPK_α1β1γ1_wt §		apo, 10 mg/ml (2+1) orthorhombic Diffraction to 7.5 Å 0.2 M MgCl ₂ 0.1 M TRIS/HCl pH 8.5 25 % PEG 3350 - optimized from Hampton Research Index # 85	

* cloned by D. Burger, R. Thoma. § purified in-house by H-J. Schönfeld and B. Pöschl from *E. coli* cell lysate provided by Wallimann group, ETH Zurich.

These crystals diffracted X-rays to 6.5 Å and 7.5 Å at the SLS, respectively (see Appendix 7.2 for diffraction images). Indexing of the orthorhombic crystals revealed a very large unit cell with $a = 132.1$ Å, $b = 157.9$ Å and $c = 379.4$ Å with a C centered Bravais lattice. In a recent survey by KANTARDJIEFF and RUPP, 2003, a median Matthews' coefficient (MATTHEWS, 1968) of 2.52 Å³/Da for 10,471 protein crystal structures in the PDB was reported. A Matthews' coefficient of 2.5 Å³/Da could be calculated for the orthorhombic AMPK_α2-1-339 crystals assuming 10 molecules per AU (51 % solvent, point group 222). If this was the true value for this crystal form, the solution of the structure would have been very difficult. However, if the true Matthews' coefficient was higher, *i.e.*, there were fewer molecules in the asymmetric unit and the solvent content was higher, this could have accounted for the limited diffraction quality of the orthorhombic crystals.

For the hexagonal crystals the unit cell parameters were $a = b = 143.4$ Å and $c = 203.4$ Å, which would correspond to a Matthews' coefficient of 2.6 Å³/Da (assuming 3 molecules per AU for point group 622 or 6 molecules per AU for point group 6; 52 % solvent). However, the indexing of both the orthorhombic and hexagonal crystal forms was not unequivocal due to limited diffraction quality, *i.e.*, resolution limit, small number and limited profile quality of indexed spots.

The usage of 25 % (v/v) silicone oil/ 75 % (v/v) paraffin oil also allowed the identification of crystallization conditions containing volatile ingredients like Matrix Screen™ # 20 (0.1 M ammonium acetate, 0.015 M magnesium acetate, 10 % (v/v) i-propanol and 0.05 M sodium cacodylate pH 6.5), among others. A screen with the precipitant synergy screen (MAJEED *et al.*, 2003) that had been designed to rationally combine mechanistically distinct precipitants, yielded small crystals with 1 M ammonium sulfate, 15 % (v/v) i-propanol and 0.1 M Tris/HCl pH 8.5. This emphasized the tendency of AMPK_α2_1-339 to crystallize from conditions containing combinations of salts of organic acids and small organic compounds. With these a gradual increase of the ionic strength and a simultaneous decrease of the dielectricity constant in the buffer could be achieved during drop equilibration in order to drive salting-out and crystallization. Generally, salts of carbonic acids are ideally suited for obtaining high ionic strength without the formation of salt crystals. However, this rational way of optimizing the crystallization of AMPK_α2_1-339 did not result in diffraction quality crystals.

3.2.2.1 Biacore

Part of the putative autoinhibitory sequence (amino acids 313-392) of the catalytic α -subunit was contained in the construct AMPK_ α 2_1-339. The actual mechanism of inhibition had not been elucidated for AMPK_ α 2_1-392. Therefore, it was not known whether the autoinhibitory sequence would function as a pseudosubstrate (CRUTE *et al.*, 1998; for review see KEMP *et al.*, 1994) or by imposing conformational control on AMPK activity (reviewed in ADAMS, 2001; ENGH and BOSSEMEYER, 2002; HUSE and KURIYAN, 2002; NOLEN *et al.*, 2004).

In order to explore the accessibility of the active site and the possibility to improve the crystal quality by co-crystallization of active site ligands, surface plasmon resonance (Biacore; COOPER, 2003; HOMOLA, 2003) measurements were performed (in collaboration with W. Huber, Roche Basel). These measurements clearly demonstrated that ATP-analogs and compound C (ZHOU *et al.*, 2001; synthesized by P. Hebeisen, Roche Basel) could bind to the active site of (unphosphorylated) AMPK_ α 2_1-339 (Figure 3.2.2.1-1) despite the presence of part of the autoinhibitory sequence.

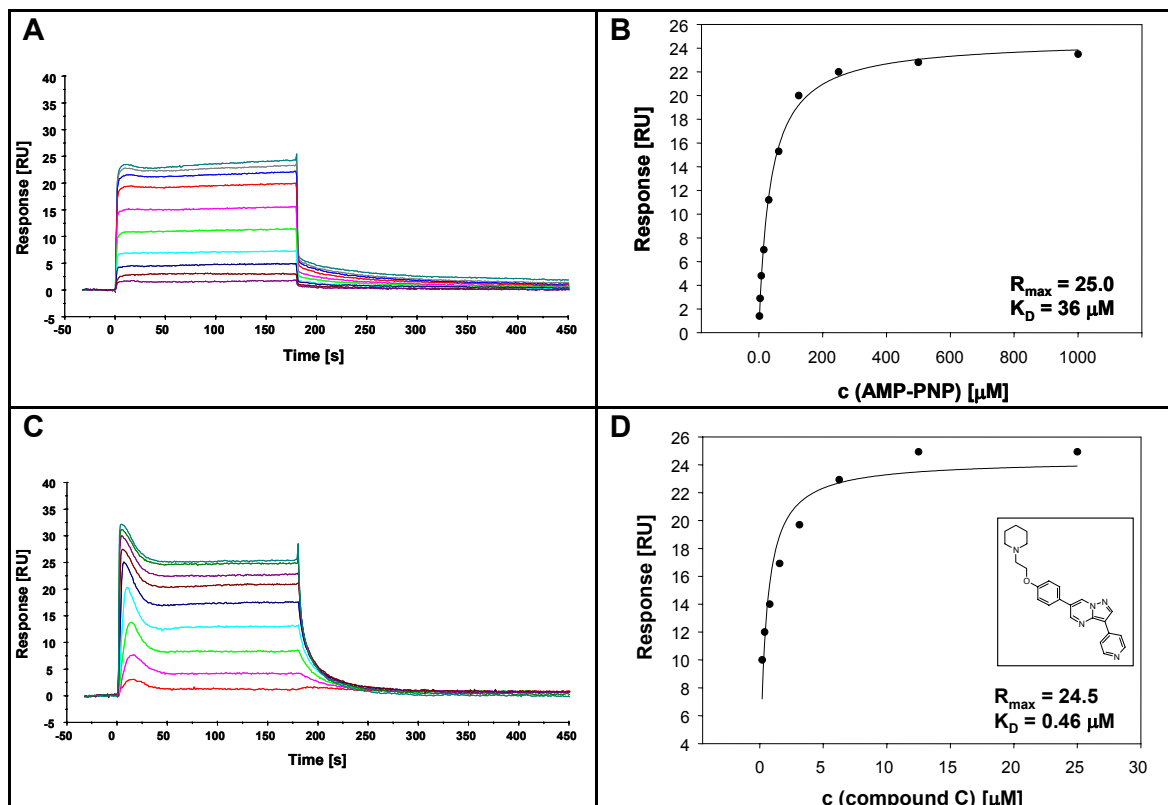


Figure 3.2.2.1-1: Results of surface plasmon resonance measurements that proved the accessibility of the active site of AMPK $_{\alpha 2}$ _1-339 for the non-hydrolyzable ATP-analog AMP-PNP and the inhibitor compound C. All measurements were performed in crystallization buffer, *i.e.*, 20 mM HEPES/NaOH pH 7.8, 2 mM MgCl₂, 2 mM TCEP and 250 mM NaCl. Data were analyzed by non-linear regression assuming a single class of binding site in a stoichiometric 1:1 complex. **A**, sensorgram and **B**, Langmuir adsorption isotherm (20°C) of AMP-PNP. **C**, sensorgram and **D**, Langmuir adsorption isotherm of compound C (20°C, structure depicted in inset). Other ATP-analogs bound to AMPK $_{\alpha 2}$ _1-339 with a K_D in the mid to high micromolar range (data not shown).

Interestingly, the $K_D = 460$ nM for the binding of compound C to AMPK $_{\alpha 2}$ _1-339 was in the range of the K_i of this compound for the inhibition of a partially purified preparation of the AMPK heterotrimer equilibrated with ATP ($K_i = 109 \pm 16$ nM, ZHOU *et al.*, 2001). Although the dynamic light scattering profile was greatly improved by preincubation of AMPK $_{\alpha 2}$ _1-339 with AMP-PCP, AMP-PNP or compound C, the addition of these compounds fully abolished crystallization indicating an effect of complex formation on conformation (Figure 3.2.2.1-2).

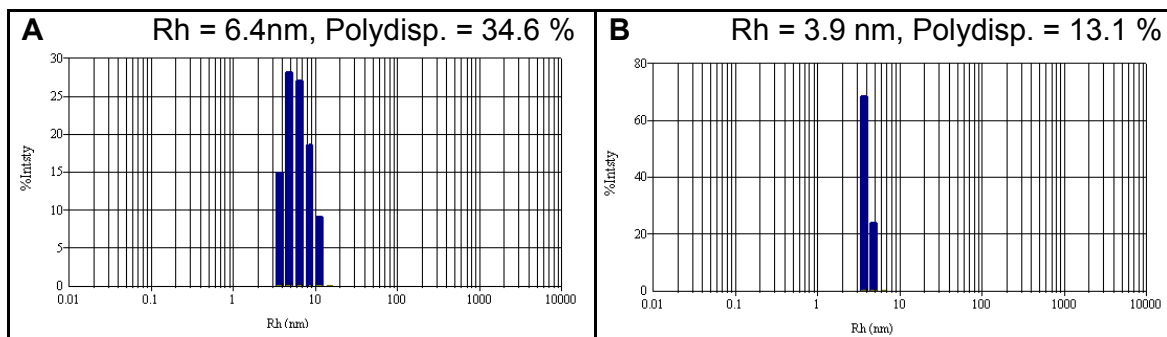


Figure 3.2.2.1-2: Dynamic light scattering (20°C) of concentrated (20 mg/ml) **A**, apo AMPK_{α2_1-339} and **B**, material from the same preparation after overnight incubation at 4°C with a 10-fold molar excess of compound C. Both samples were centrifuged for 30 min at 20,000 g and 4°C prior to the measurement. Similar results were obtained with nucleotide analogs (data not shown).

A Biacore assay was also conducted with the intact AMPK_{α1β1γ1} heterotrimer as well as the β1γ1-dimer of regulatory subunits and the AMPK_{α2_1-339} kinase domain construct immobilized in parallel on a three-channel chip. These experiments clearly showed that the physiological ligands of AMPK, AMP and ATP (the non-hydrolyzable analogs AMP-PNP and AMP-PCP were used), can bind to both the allosteric and catalytic sites (data not shown). This emphasizes the difficulties to design a robust assay for AMPK activity because the allosteric activator outcompetes the co-substrate ATP from the active site (and *vice versa*) in a concentration dependent manner.

3.2.2.2 Thermofluor®

Pre-incubation with staurosporine completely abolished crystallization of AMPK_{α2_1-339} under all conditions investigated, which implied a pronounced effect of staurosporine on the conformation. Since staurosporine is too adhesive for Biacore measurements the Thermofluor® technique was chosen to characterize the complex formation. This method allows analysis of the stability of protein-ligand complexes based on their thermal unfolding curves (PANTOLIANO *et al.*, 2001; LO *et al.*, 2004; CARVER *et al.*, 2005, MATULIS *et al.*, 2005; PARKS *et al.*, 2005). For monitoring of the unfolding process the fluorescence probe SYPRO orange was added to the protein or protein ligand complexes. This dye only emits fluorescence upon binding to the hydrophobic core of proteins which becomes exposed to the solvent during the process of unfolding. The thermal stability of AMPK_{α2_1-339} was examined with the apo enzyme and with enzyme pre-incubated with the non-hydrolyzable nucleotide analogs

AMP-PNP, AMP-PCP as well as staurosporine (Figure 3.2.2.2-1). These measurements were also performed with AMPK α 2_1-392 in order to elucidate the effect of the putative autoinhibitory domain on the stability of this construct.

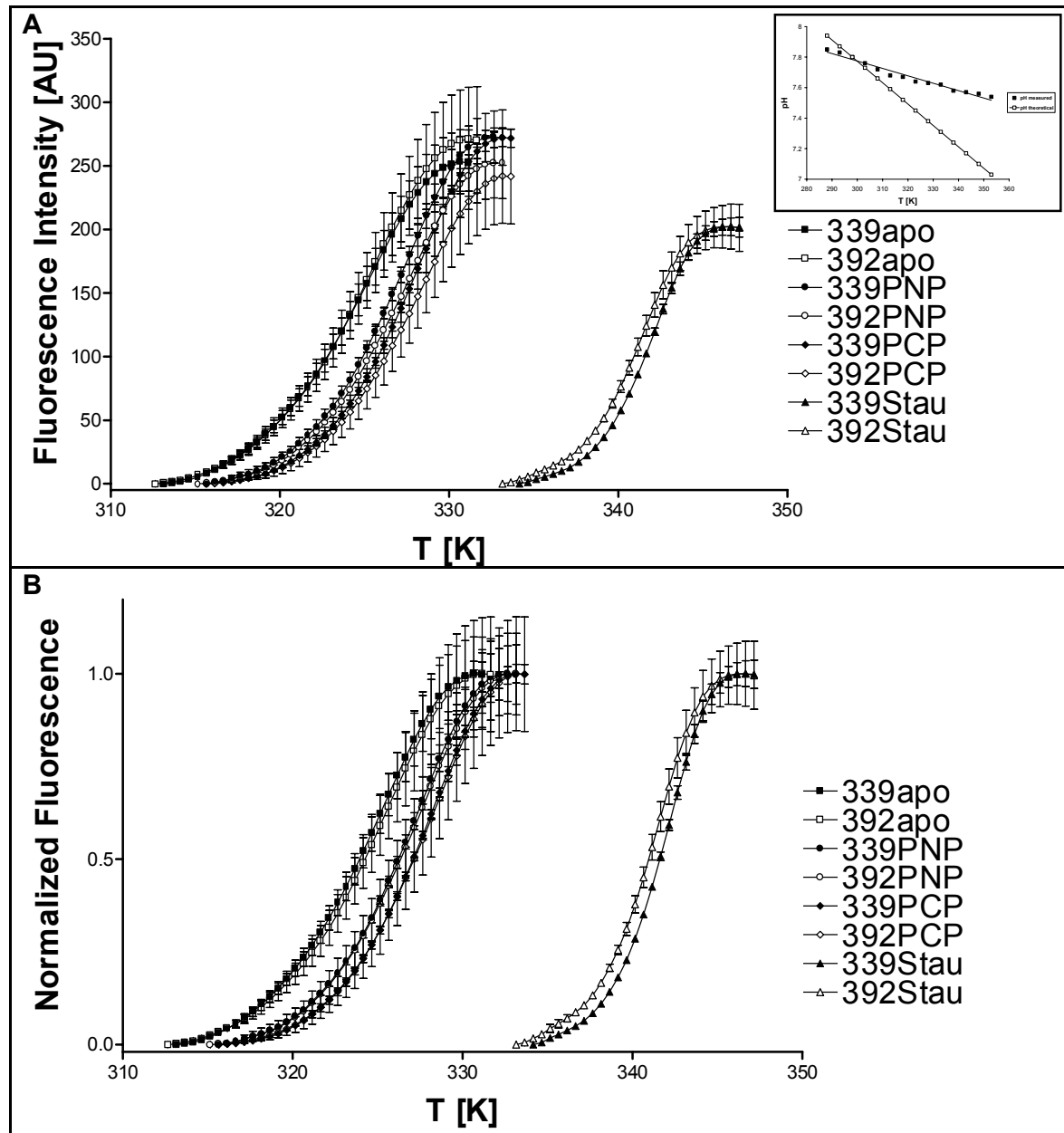


Figure 3.2.2.2-1: A, melting curves of AMPK α 2_1-339 and AMPK α 2_1-392 in the presence or absence of the active site inhibitors AMP-PNP (PNP), AMP-PCP (PCP) or staurosporine (Stau). Means \pm SEM of two (PNP, Stau) or three (apo, PCP) independent experiments are presented. The base line of the raw data was corrected for photobleaching and thermal disintegration of the fluorescence probe SYPRO orange. The **inset** shows the pH dependency of the buffer used for the ThermoFluor[®] assays. **B**, Normalized data of A which emphasize the clustering of the melting curves in four discrete bins. See Material and Methods for details of data processing.

The data fully supported the results of surface plasmon resonance measurements (3.2.2.1) regarding the accessibility of the active site of the AMPK constructs. The melting curves of both AMPK $_{\alpha 2}$ _1-339 and AMPK $_{\alpha 2}$ _1-392 clearly showed that the presence of an active site inhibitor enhances the thermal stability of these constructs. The construct length had no significant effect on the respective melting points, which implied that the autoinhibitory sequence (here aa 340-392) of AMPK does not bind with high affinity to the catalytic core. Whereas AMP-PCP was found to be slightly more effective than AMP-PNP in increasing the melting points, the presence of staurosporine caused a pronounced shift of the melting points to higher temperatures for both examined constructs (Table 3.2.2.1-1). The melting point temperatures for the complexes of AMPK constructs with ATP analogs were found to be in the range of those reported for PKA equilibrated with 1 mM ATP (HERBERG *et al.*, 1999).

Construct	Ligand	Melting Point ± SEM [K]	K _D [μM]	95 % conf. int. [μM]
AMPK $_{\alpha 2}$ _1-339	apo	323.7 ± 0.6	n/a	n/a
	AMPPNP	326.0 ± 0.3	442 (36)	237-663
	AMPPCP	326.9 ± 0.2	311	171-490
	Staurosporine	341.5 ± 0.2	0.0005	6E-12 - 2.8E-8
AMPK $_{\alpha 2}$ _1-392	apo	324.1 ± 0.4	n/a	n/a
	AMPPNP	326.1 ± 0.2	480	322-641
	AMPPCP	327.0 ± 0.2	336	214-495
	Staurosporine	340.8 ± 0.2	0.0009	2.8E-11 - 1.7E-8

Table 3.2.2.1-1: Melting points and dissociation constants (value in parantheses was determined by Biacore measurements), plus values for the 95 % confidence interval, of AMPK $_{\alpha 2}$ _1-339 and AMPK $_{\alpha 2}$ _1-392. The values were determined from the melting curves by non-linear regression using the equations described in Materials and Methods.

The dissociation constant of the AMPK $_{\alpha 2}$ _1-339•AMP-PNP complex (K_D = 442 μM) which was determined by the ThermoFluor® assay was found to be one order of magnitude larger in comparison to the value measured by Biacore (K_D = 36 μM). This could be due to interference of the fluorescence probe SYPRO orange with ligand binding to AMPK $_{\alpha 2}$ _1-339 by, *e.g.*, altering the conformation or accessibility of the nucleotide binding site. The 95 % confidence intervals for the dissociation constants of staurosporine are wide in comparison to those of AMP-PNP or AMP-PCP. This can be explained by the fact that the concentration of enzyme cannot be neglected during calculation of the K_D values for the staurosporine complexes. A 1:4 molar enzyme to ligand ratio had to be used because of the limited solubility of staurosporine in aqueous

buffer. However, the order of the numeric values of the dissociation constants reflects well their effect on the stability of the AMPK constructs. The K_D values determined for staurosporine (app. 1 nM) are in-line with those reported by EISINGER *et al.* (2003) for the AMPK heterotrimer.

The pH of the buffer used in the Thermofluor® assays (20 mM HEPES/NaOH pH 7.8, 2 mM $MgCl_2$, 150 mM NaCl and 2 mM TCEP) was found to decrease by less than 0.3 pH units (pH = 7.8 at 298 K / 25 °C; pH = 7.54 at 353 K / 80 °C) over the temperature range of the experiment. The actual change in pH is likely to be even smaller because of the buffer capacity of the protein, which is a polyampholyte. The pH range of the experiment was well above the isoelectric points and, therefore, the solubility boundary of AMPK_α2_1-339 (pI = 6.56) and AMPK_α2_1-392 (pI = 6.65). As HEPES has a pK_a = 7.5 the change in ionic strength of the buffer was negligible. From these observations it seems reasonable that the melting behavior is entirely dependent on the increase in temperature and the stability of the apo proteins or the protein-ligand complexes.

The Thermofluor® experiments showed that the binding of staurosporine to AMPK_α2_1-339 and AMPK_α2_1-392 markedly increased the thermal stability of these enzymes. This effect on stability could be exploited for improving the crystallization of an activation loop mutant of AMPK_α2_1-339 (see below).

3.2.2.3 Generation of the triple mutant AMPK_α2_1-339_D56A/R171E/T172D

As the crystals of the wild type construct, *i.e.*, the enzyme in its inactive conformation, were of poor diffraction quality it was anticipated that populating the active conformation might facilitate better crystallization. Since AMPK does not undergo autophosphorylation on the activation loop and the upstream kinase was not known at the time of the study, a site-directed mutagenesis approach was chosen. Inspection of the homology model of the α-subunit suggested that in addition to the T172D mutation, a R171E and a D56A mutation could be introduced in order to improve the interaction of the activation loop with the amino-terminal lobe of AMPK (Figure 3.2.2.3-1).

The crystal structure of PKA in its active conformation (PDB code 1cdk; BOSSEMEYER *et al.*, 1993) reveals a tight salt bridge (2.64 Å) of a phosphoryl-oxygen of pT193 in the activation loop with the guanidinium group of the conserved R165 of the catalytic loop. The respective residues in the catalytic α-subunit of AMPK are T172 and R138,

respectively. If a T172D mutation in AMPK_α2_1-339 was to mimic phosphorylation of this residue, the neighbouring R171 might compensate the single negative charge, thereby obstructing the interaction with R138. Therefore, a R171E mutation was introduced, which could support lobe closure by electrostatic interaction with K60 or R63 in helix αC. In order to stabilize these interactions D56 at the amino-terminal end of helix αC was mutated to alanine (see Appendix 7.3 for sequence data).

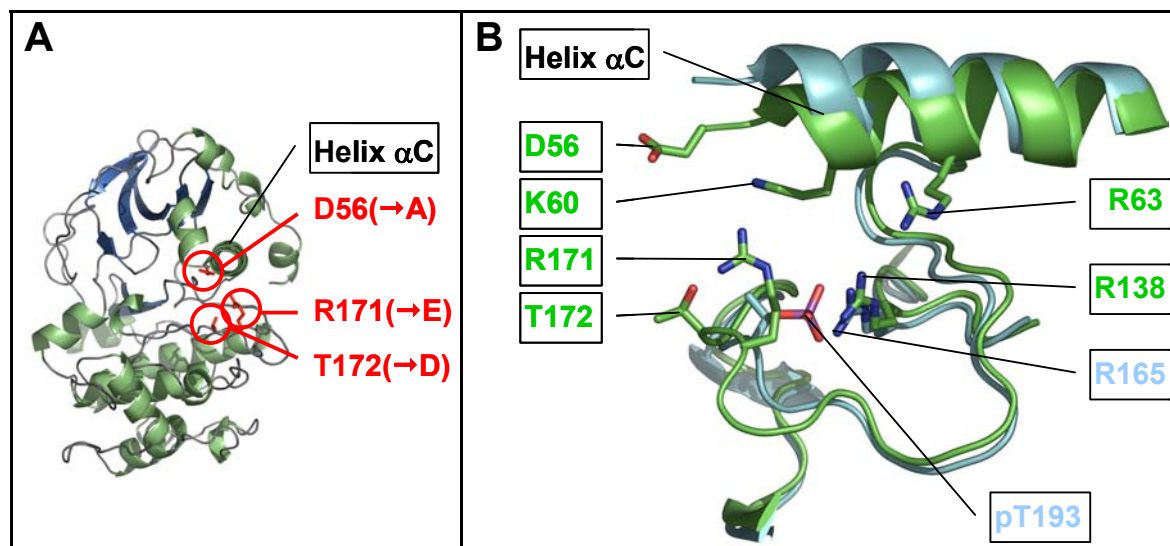
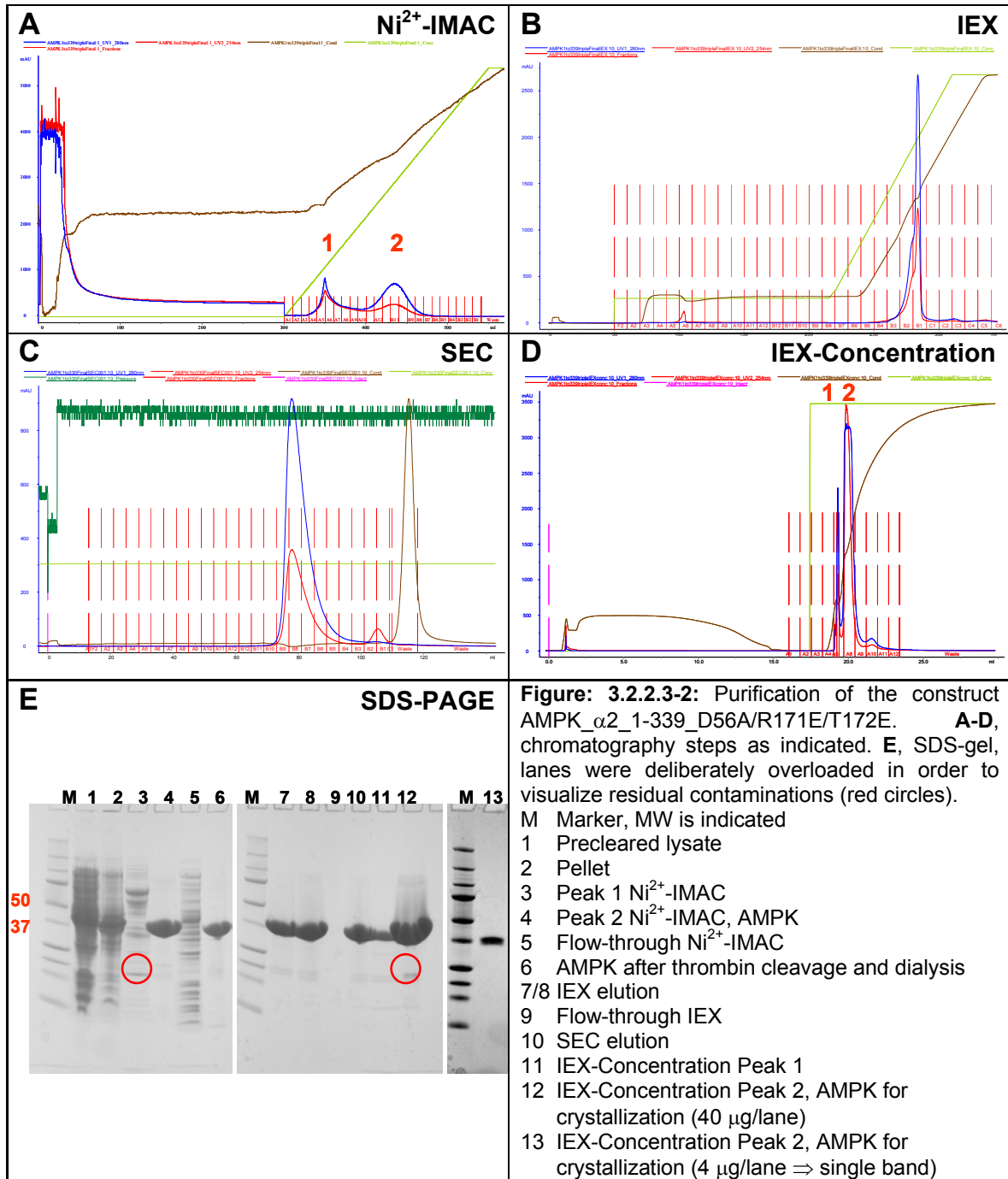


Figure 3.2.2.3-1: **A**, Homology model of AMPK_α2_1-339 in the standard orientation, *i.e.*, looking down helix αC (amino- to carboxy terminus). The residues that were mutated are highlighted. The model is colored according to secondary structure (α-helices: green; β-sheets: blue). **B**, close-up of a superimposition of the activation segment of AMPK_α2_1-339 (homology model, green) and PKA (cyan, PDB code 1cdk), in an orientation rotated 90° to the left with respect to the view in A.

A pET-15b vector with the coding sequence of AMPK_α2_1-339_T172D was used as a template to generate the triple mutant, AMPK_α2_1-339_D56A/R171E/T172D, by means of site directed mutagenesis. The Quick Change® Multi site directed mutagenesis kit (Stratagene) was used according to the manufacturers specifications (primers listed in Appendix 7.3). Introduction of the mutants and integrity of the construct was verified by fluorescence-based DNA sequencing after PCR amplification (sequencing primers listed in Appendix 7.3). The identity of the expressed protein was confirmed by mass spectrometry (no post-translational modification found). The resulting protein was in the soluble fraction when expressed in *E. coli*. and could be purified by Ni²⁺-IMAC, IEX chromatography and final SEC (Figure 3.2.2.3-2; see also Material and Methods).



AMPK_{α2}_1-339_D56A/R171E/T172D could be purified to homogeneity, despite traces of an uncharacterized ~17 kDa contamination. This contamination was most likely a protein from the *E. coli* host cells because it was shown to co-elute with AMPK constructs of different lengths and no signs for proteolytic degradation could be detected (data not shown). Most of this protein was separated by Ni²⁺-IMAC (Peak 1).

The typical yield of 40 mg AMPK_α2_1-339_D56A/R171E/T172D per liter bacterial culture after scale up of the expression was 10-50 % higher compared to the previous constructs. Assuming unchanged mRNA and protein half-life this suggested improved protein stability compared to the wild-type construct. No enzymatic activity could be detected in a preliminary gel-shift assay with a commercial GST-tagged substrate. Nevertheless, the introduction of the D56A and R171E mutants had a pronounced effect on conformation as implied by the totally different crystallization behavior of AMPK_α2_1-339_D56A/R171E/T172D in comparison to the wild-type construct (see below).

3.2.2.4 Crystallization of AMPK_α2_1-339_D56A/R171E/T172D

Using dynamic light scattering the mutant AMPK_α2_1-339_D56A/R171E/T172D was found to be monodisperse and monomeric as apo protein and in complex with active site inhibitors (Figure 3.2.2.4-1).

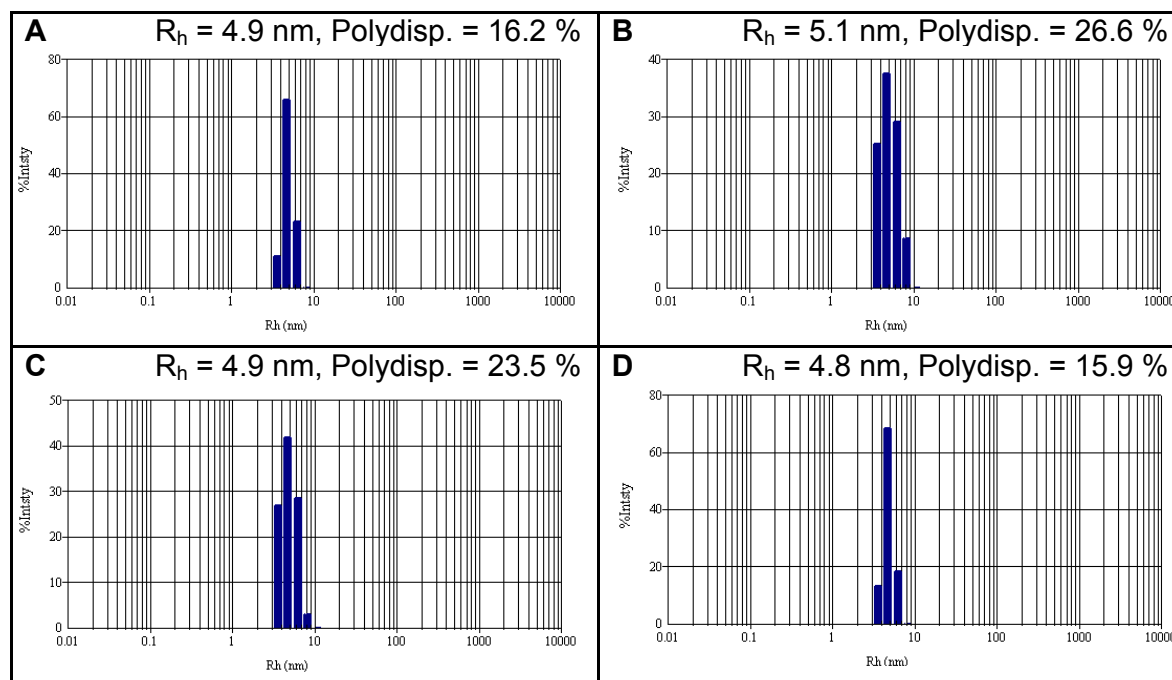


Figure 3.2.2.4-1: Dynamic light scattering (DLS) profiles of AMPK_α2_1-339_D56A/R171E/T172D. DLS was used as quality check on the concentrated protein samples (20 mg/ml) and protein-ligand complexes after overnight incubation at 4°C prior to setting up the crystallization drops. All samples were measured in identical buffer (20 mM HEPES/NaOH pH 7.8, 2 mM MgCl₂, 2 mM TCEP and 250 mM NaCl) at 20°C after centrifugation at 20,000 g for 30 min. The determined hydrodynamic radii (Rh) and the percent polydispersity (% polydisp.) are indicated. **A**, apo enzyme. **B**, complex with staurosporine (1.5 X molar excess). **C**, complex with AMP-PCP (10 mM) and **D**, complex with AMP-PNP (10 mM). No difference in the affinity and association/dissociation kinetics for small molecule active site binders was detected for the wild-type vs. the triple mutant enzyme (collaboration with Biacore, Uppsala, Sweden). This indicated unhindered access of the ligands to the active site.

A positive correlation of low (generally $\leq 20\%$) polydispersity of a given protein sample and the tendency to crystallize had been described (ZULAUF and D'ARCY, 1992; D'ARCY, 1994). Despite high purity and the absence of aggregation, initial screens with apo AMPK $_{\alpha 2}$ _1-339_D56A/R171E/T172D did not result in crystals as opposed to the wild-type construct. Staurosporine was reported to be a strong inhibitor of full-length AMPK with an IC_{50} of approximately 1 nM (EISINGER *et al.*, 2003) and markedly stabilized the AMPK $_{\alpha 2}$ _1-339 construct in the Thermofluor® assay (3.2.2.2). In order to stabilize AMPK $_{\alpha 2}$ _1-339_D56A/R171E/T172D for crystallization, a 20 (-30) mg/ml preparation of the protein was incubated with a 1.5 molar excess of staurosporine overnight at 4°C. In contrast to the wild type construct and the mutant apo protein, the complex of the triple mutant with staurosporine crystallized from various conditions (Table 3.2.2.4-1, no crystals were obtained from AMP-PCP or AMP-PNP complexes).

Crystallization Screen	Condition	
	#	precipitant solution
Index Screen TM ₁	63	5 % (v/v) Tacsimate, 10 % (w/v) PEGMME 5000, 0.1 M HEPES pH 7.0
	74	0.2 M LiSO ₄ , 25 % (w/v) PEG 3350, 0.1 M Bis-Tris pH 6.5
	75	0.2 M LiSO ₄ , 25 % (w/v) PEG 3350, 0.1 M HEPES pH 7.5
	76	0.2 M LiSO ₄ , 25 % (w/v) PEG 3350, 0.1 M Tris pH 8.5
	86	0.2 M Na/K-tartrate, 20 % (w/v) PEG 3350
	87	0.2 M Na-malonate pH 7.0, 20 % (w/v) PEG 3350
	94	0.2 M Na/K-citrate, 20 % (w/v) PEG 3350
Wizard TM I + II ₂	10	20 % (w/v) PEGMME 2000, Tris pH 7.0
	15	0.2 M LiSO ₄ , 10 % (w/v) PEG 3000, 0.1 M imidazole pH 8.0
Structure Screen TM ₃	1/26	0.8 M Na/K-tartrate, 0.1 M HEPES pH 7.5
	2/3	2 % (w/v) dioxane, 10 % (w/v) PEG 20000, 0.1 M Bicine pH 9.0
Precipitant Synergy Screen ₄	31	0.5 M NaCl, 30 % MPD, 8 % (w/v) PEG 8000, 0.1 M Tris pH 8.5

Table 3.2.2.4-1: Compilation of screening solutions from which crystals of the AMPK $_{\alpha 2}$ _1-339_D56A/R171E/T172D • staurosporine complex were obtained (1: Hampton Research; 2: Emerald Biostructures/ deCode genetics; 3: Molecular Dimensions Ltd.; 4: MAJEED *et al.*, 2003).

All crystals of the triple mutant had identical crystal morphology (Table 3.2.2-1) and unit cell parameters. The diffraction pattern indicated that the crystals had an I-centered cubic Bravais lattice with unit cell dimensions $a = b = c = 177.7 \text{ \AA}$. With a calculated MW of 38,942 Da for the AMPK $_{\alpha 2}$ _1-339_D56A/R171E/T172D construct the Matthews' coefficient was determined to be $3.0 \text{ \AA}^3/\text{Da}$ (assuming 2 molecules per AU for point group 23 or 1 molecule per AU for point group 432), which corresponds to a solvent content of 59 %).

Despite extensive optimization trials using grids of 24 conditions around the initial crystallization conditions of the screening hits and exploitation of four different crystallization methods (free interface diffusion in the Fluidigm® system, HANSEN *et al.*, 2002, modified microbatch with hydrophobic and hydrophilic plate surfaces, sitting and hanging drop) all these crystals diffracted merely to 7 Å at the SLS. The diffraction images recorded in-house also had a resolution limit of app. 7 Å indicating that not crystal size but rather dynamic disorder limited diffraction.

As AMPK_α2_1-339_D56A/R171E/T172D recurrently crystallized under conditions containing salts of carboxylic acids, which had been described to improve crystal quality (especially sodium malonate, MC PHERSON, 2001; HOLYOAK *et al.*, 2003; XING and XU, 2003), a range of salts of organic acids in combination with 20 % (w/v) PEG 3350 were tested as precipitants. This yielded crystals with the sodium salts (unbuffered and solutions buffered with HEPES/NaOH pH 7-8) of acetate, malate, malonate, maleinate, succinate, oxalate, benzoate as well as ammonium citrate, but not with formate and had no effect on diffraction quality. Interestingly, large crystals could also be obtained from unbuffered 1 M sodium acetate alone. With acetate the counterions Mg²⁺, Ca²⁺, Zn²⁺ and NH₄⁺ (all 1 M f.c.) abolished crystallization.

The addition of arginine, which is commonly used in refolding protocols as stabilizing agent, or other amino acid (salts of proline, aspartic acid, glutamic acid) as sole precipitants were ineffective with regard to improving diffraction quality. Attempts to optimize the crystallization of AMPK_α2_1-339_D56A/R171E/T172D by using various redox-agents [dithiothreitol (DTT) and reduced glutathione (GSH) which might covalently modify the enzyme as described for PKA (HUMPHRIES *et al.*, 2002), β-mercaptoethanol (β-ME), L-cysteine, and tris-(carboxyethyl)-phosphine (TCEP); GETZ *et al.*, 1999; BURNS *et al.*, 1991), detergents or other additives (Hampton Research Detergent/ Additive Screens), heavy atom derivatives as additives for co-crystallization (Hampton Research Hg and Pt heavy atom kits) and in-gel crystallization in hanging drops (DONG *et al.*, 1999; MORENO *et al.*, 2002) yielded crystals under several conditions but did not improve diffraction quality.

The effect of different cryo-protocols was also investigated with regard to the choice of cryo-protectant and the way of cooling the crystals to the cryogenic temperature of liquid nitrogen for synchrotron measurements. Incubating the crystals of AMPK $_{\alpha 2}$ _1-339_D56A/R171E/T172D for 30 s in mother liquor supplemented with 20 % (v/v) ethylene prior to direct mounting in the cryo-stream at 110 K was found to be a proper cryo-protocol. Crystals measured at room temperature (see 3.2.2.6) did not diffract X-rays better than the cryo-cooled specimens.

Analysis of buffer-dependent protein solubility according to JANCARIK *et al.* (2004) revealed discrete solubility optima for AMPK $_{\alpha 2}$ _1-339_D56A/R171E/T172D (Figure 3.2.2.4-1).

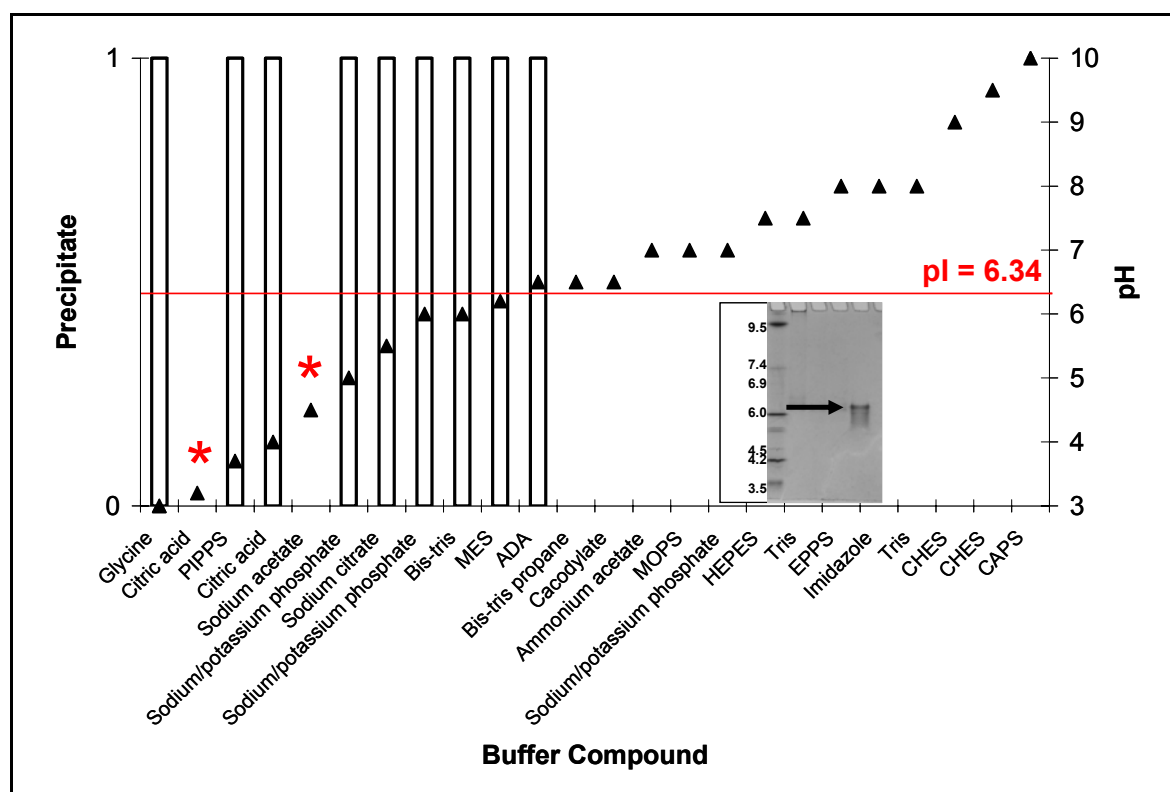


Figure 3.2.2.4-1: Plot of the solubility (bars, 1= insoluble precipitate, 0 = clear drop) of the triple mutant AMPK $_{\alpha 2}$ _D56A/R171E/T172D as a function of pH (triangles) and various buffer compounds (all 100 mM). Citrate and acetate apparently stabilize the protein (red asterisks) as implied by the results of crystallization. Independent of the buffer compound the triple mutant remained soluble above its isoelectric point (calculated pI = 6.34). Solutions of different buffer species were not corrected for ionic strength. The inset shows the experimental determination of the pI of the triple mutant via isoelectric focusing (IEF), the pI values of marker proteins are indicated. The smeared band is probably due to the presence of TCEP, which is known to cause artifacts in IEF (Invitrogen product information).

The lack of precipitate with 100 mM citric acid at pH 3.2 and 100 mM sodium acetate at pH 4.5 emphasizes the stabilizing effect of these organic acids (salts) on AMPK $_{\alpha 2}$ _1-339_D56A/R171E/T172D. However, optimization of pH against the concentrations sodium citrate or sodium acetate did not result in crystals in the the pH range close to the respective pK_a values. This might reflect the observation that acidic proteins generally tend to crystallize 0-2.5 pH units above their pI (KANTARDJEFF and RUPP, 2004).

3.2.2.5 Refolding

In order to investigate the possibility that AMPK $_{\alpha 2}$ _1-339_D56A/R171E/T172D might be misfolded due to the heterologous expression in a prokaryotic system or that micro-impurities (e.g., small molecule contaminations or residual *E. coli* host proteins) might interfere with crystallization, it was decided to produce the protein by refolding. For this AMPK $_{\alpha 2}$ _1-339_D56A/R171E/T172D was expressed in *E. coli* using a fermenter at 37°C, which resulted in a high yield of inclusion bodies (**Figure 3.2.2.5-1**).

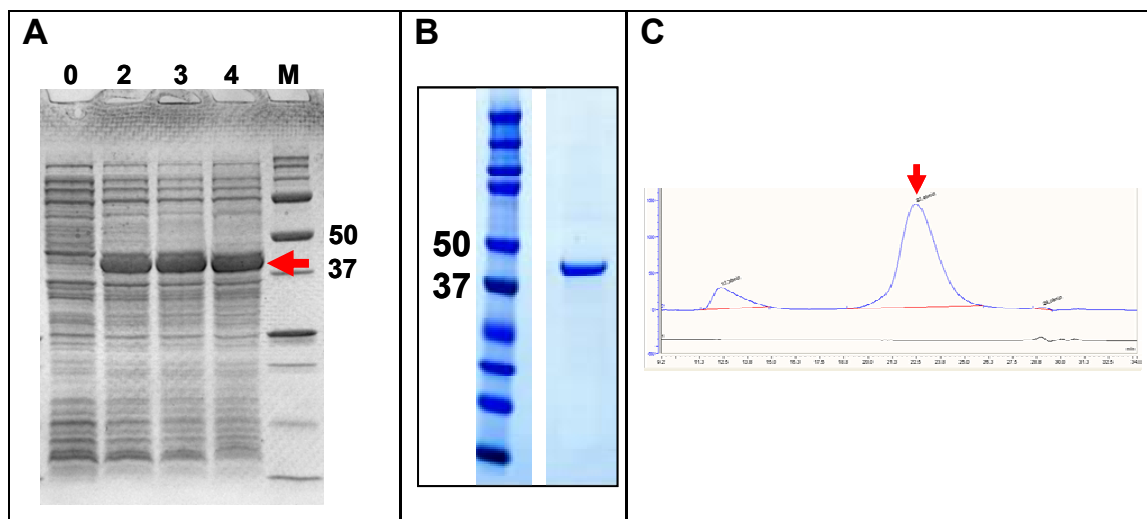


Figure 3.2.2.5-1: **A**, SDS-PAGE of the expression profile of the inclusion body production of AMPK $_{\alpha 2}$ _1-339_D56A/R171E/T172D (red arrow indicates product, lane 0: before induction, lanes 2-4: hours of expression). After cell disruption and centrifugation the insoluble fraction was dissolved in 8 M urea, 100 mM Tris pH 8.5, 4% (w/v) SDS and 7 mM β -mercaptoethanol. **B**, SDS-PAGE showing the electrophoretic homogeneity of refolded AMPK $_{\alpha 2}$ _1-339_D56A/R171E/T172D. **C**, elution profile from final size exclusion chromatography of refolded AMPK $_{\alpha 2}$ _1-339_D56A/R171E/T172D in 50 mM Tris/HCl pH 7.5, 500 mM NaCl, 3 mM CHAPS, 10 % (v/v) glycerol and 2 mM TCEP. The arrow indicates the monomeric main species.

The inclusion bodies were subjected to a generic kinase refolding protocol, and electrophoretically pure, monomeric protein was obtained (M. Dangl, Roche Penzberg; FIGURE 3.2.2.5-1). Despite the His₆-tag the preparative Ni²⁺-IMAC step was omitted, thereby excluding the possibility of oxidative modification by undergoing a redox-reaction with Ni²⁺-ions of AMPK_α2_1-339_D56A/R171E/T172D on the column. The refolded enzyme crystallized under identical conditions as the conventionally purified material but resolution was still limited to app. 7 Å. The metabolic status of the *E.coli* host cells during expression at 37°C was likely to differ from that at the established expression temperature of 20°C and, therefore, a different contamination profile was to be expected. Taken together, these results indicated that not contaminations but intrinsic properties (e.g., loop flexibility) of AMPK caused the observed crystallization behavior. This conclusion is supported by the observation that the crystal structure of the core kinase domain of yeast AMPK (app. 60 % amino acid identity and 75 % similarity) shows a high degree of disorder (RUDOLPH *et al.*, 2005).

3.2.2.6 Free Mounting™ system

Since attempts to optimize the crystallization of AMPK_α2_1-339_D56A/R171E/T172D by conventional, chemical means were unsuccessful, the impact of physical modification of the crystals was investigated. Desiccation of protein crystals had been described to improve crystal packing and diffraction (ABERGEL, 2004). The Free Mounting™ system (KIEFERSAUER *et al.*, 2000) allows capillary-free mounting of protein crystals at room temperature. The advantage of this technique is the gentle mounting of crystals directly from the mother liquor, *i.e.*, mechanical forces and soaking in cryo buffer that might destroy crystal quality are avoided. Gradients of controlled humidity can be applied after mounting in order to dehydrate the crystal, which potentially improves their diffraction quality by rearrangement of the crystal lattice. For this the dew point of the mother liquor is determined by mounting a drop from the mother liquor without crystal and adjusting a stream of humidified air hitting the loop until the volume (as determined by integration of the contour area) remains constant over time. X-ray still images are taken during the gradient program to follow the effect on diffraction quality as a function of relative humidity.

Cubic crystals of AMPK_α2_1-339_D56A/R171E/T172D in complex with staurosporine grown from 0.2 M sodium/potassium tartrate or 0.2 M sodium citrate and 20 % (w/v) PEG 3350 (Index Screen™ 86 or 96 from Hampton Research, respectively) in hanging drops were subjected to optimization trials with the free mounting system (Figure 3.2.2.6-1).

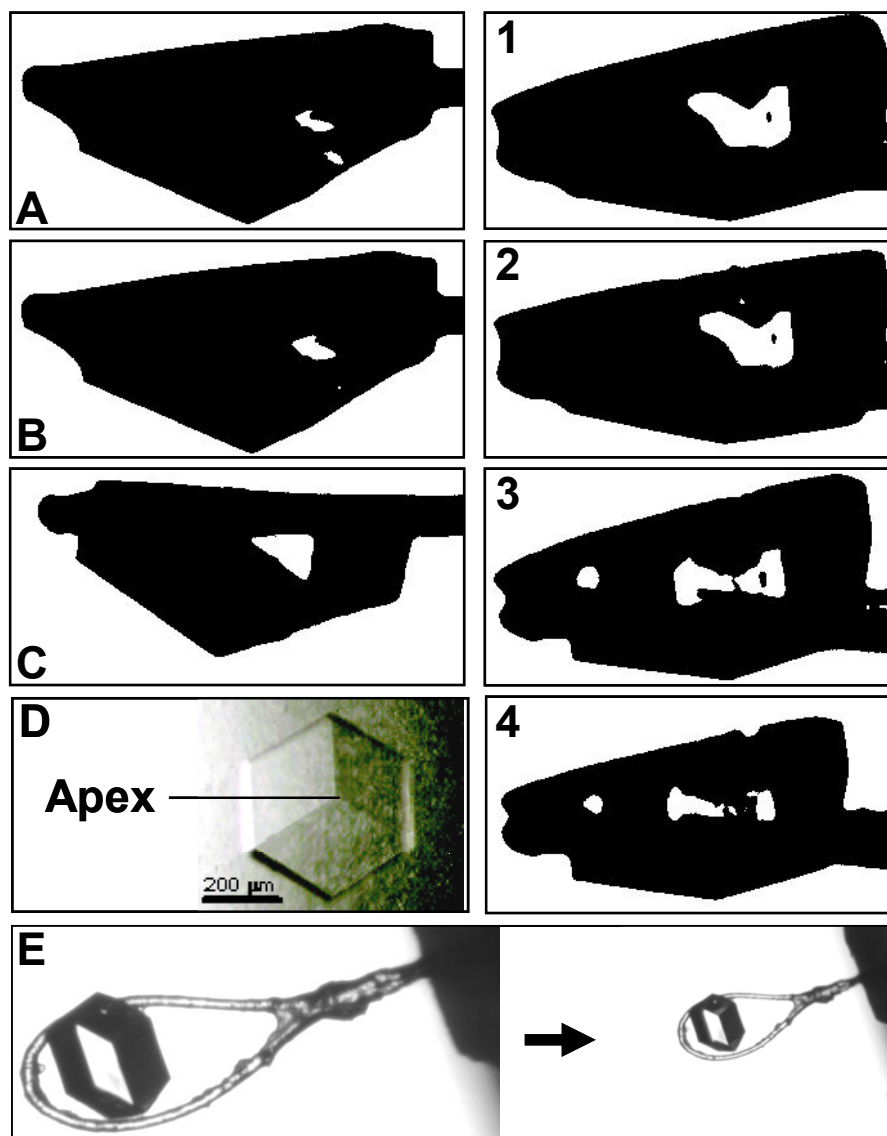


Figure 3.2.2.6-1: A-C and 1-4 depict the contour area images of the gradual dehydration of two AMPK_α2_1-339_D56A/R171E/T172D crystals. Both the crystals have a similar orientation with their apex (D) pointing down. The change in volume is recorded by integrating the pixel number of the crystal profiles. The bottom panel (E) shows another crystal (mounted in a 0.4 -0.5 mm cryo-loop) during the process of dehydration. Any residual mother liquor had been completely withdrawn and the crystal remains attached to the loop by only one side.

The crystals were mounted at 96 % of the relative humidity that corresponded to the saturated vapor pressure of the mother liquor (at 21°C and atmospheric pressure) in order to avoid condensation of water on the loop, which might dissolve the crystal. The relative humidity generated close to the crystal can be calculated by the empirical Magnus formula (KIEFERSAUER *et al.*, 2000).

Analyses of the contour area during dehydration revealed that the AMPK_α2_1-339_D56A/R171E/T172D crystals changed their size in a pronounced step at a relative humidity between app. 91 % and 88 % (Figure 3.2.2.6-2). The differences in the curves can be ascribed to direction-dependent, *i.e.*, non-isotropic, lattice forces (KIEFERSAUER *et al.*, 2000). The dehydration process was fully reversible (Appendix 7.2).

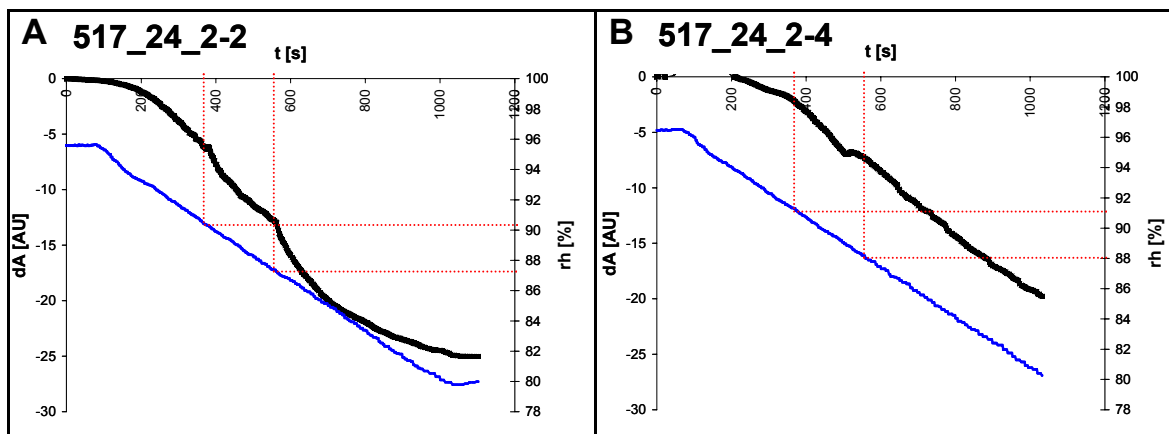


Figure 3.2.2.6-2: Plots of the change in contour area (black curves) and relative humidity (blue curves) over time for two separate crystals (**A** and **B**) harvested from the same hanging drop.

Despite various dehydration protocols (steepness of gradients, initial relative humidity), there was no significant improvement in the diffraction quality of the AMPK_α2_1-339_D56A/R171E/T172D crystals. In retrospective, the dehydration procedure with the Free Mounting™ system according to KIEFERSAUER *et al.* (2000) had a success rate of 15 % with crystals of app. 100 different protein crystallization projects (H. Brandstetter, personal communication). However, the important information that was gained from these experiments was that the limited quality of the crystals tested in-house and at the SLS was not due to adverse effects of freezing and data collection at cryogenic temperatures.

3.2.2.7 Truncated triple (D56A/R171E/T172D) mutants

The triple mutant AMPK_α2_1-339_D56A/R171E/T172D showed strongly improved crystallization when compared to the corresponding wild-type construct, yet the diffraction limit was not sufficient for solving the structure. For this reason the effect on protein stability and crystallization of the introduction of the three point mutations into the short constructs AMPK_α2_1-301 and AMPK_α2_1-312 was investigated. Cloning of these mutants was performed by excising the coding region for amino acids 1 to 268 (comprising the three point mutations) by *NdeI/PmeI* restriction of a pET-15b-AMPK_α2_1-339_D56A/R171E/T172D vector and subsequent introduction of this fragment into vectors coding for the AMPK_α2_1-301 and AMPK_α2_1-312 constructs (Figure 3.2.2.7-1).

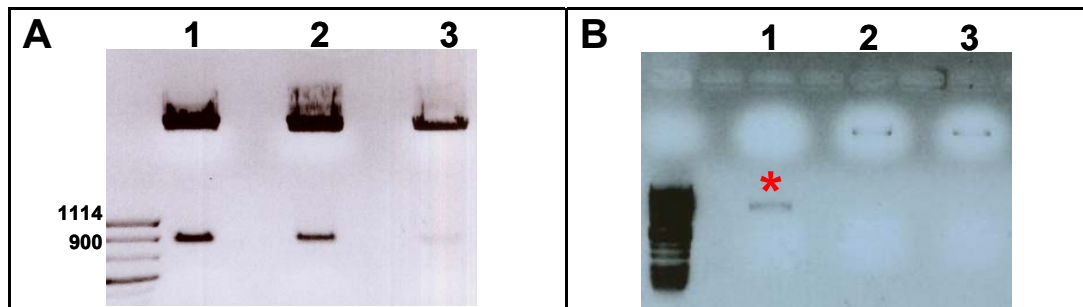
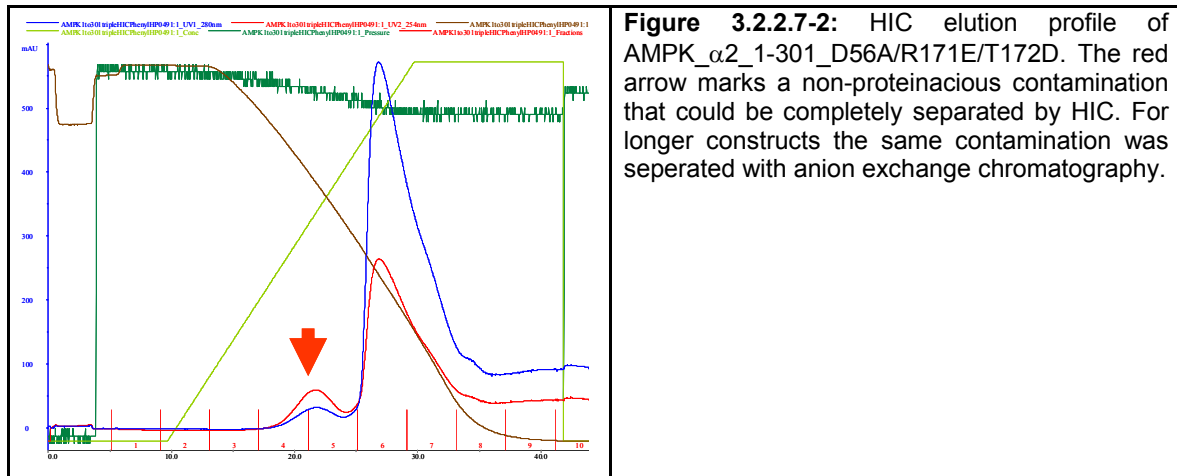


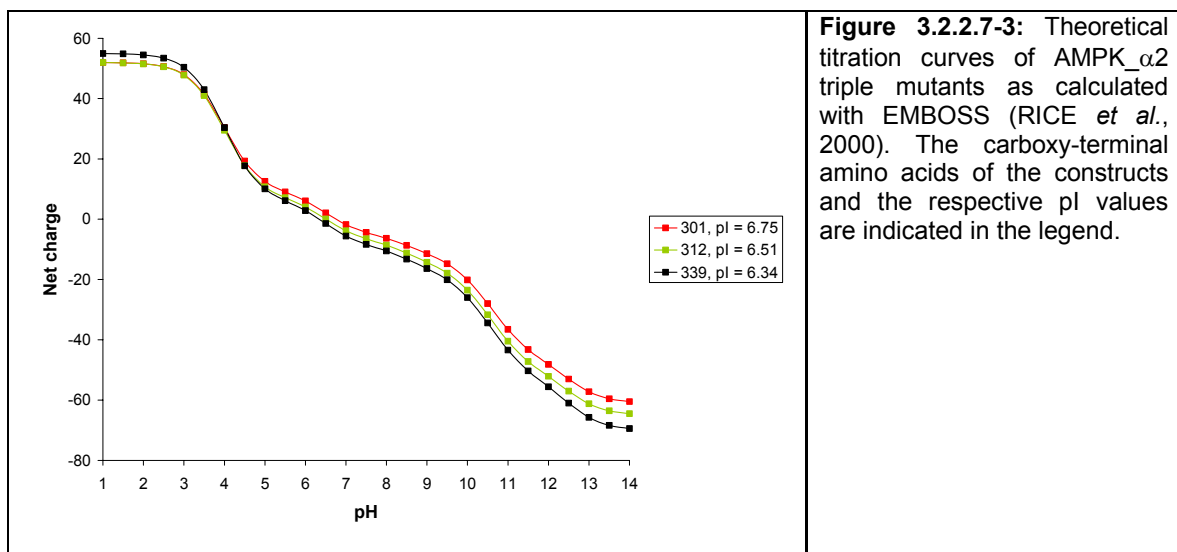
Figure 3.2.2.7-1: **A**, analytical agarose gel of the *NdeI/PmeI* restriction of pET-15b vectors carrying the coding sequence for 1, AMPK_α2_1-339_D56A/R171E/T172D, 2, AMPK_α2_1-301_wt and 3, AMPK_α2_1-312_wt. The three excised 805 bp fragments showed slightly increased apparent molecular weight. **B**, analytical gel of the extracted and purified excised fragment (1, *), which was ligated as insert into the cut vectors (2, 3) from the gel shown in **A**. The integrity of the resulting vectors was confirmed by nucleotide sequencing and the correct identity of the resulting proteins was confirmed by mass spectrometry (no post-translational modification found).

AMPK_α2_1-301_D56A/R171E/T172D exhibited very low recovery from the preparative Resource Q anion exchange column that had been used in the second step of purification of previous constructs and mutants. Running this purification step at decreased pH (7.0-7.4) in order to weaken the interaction of the target protein with the IEX resin was not sufficient to improve the yield. Therefore, a hydrophobic interaction chromatography (HIC) protocol was established (see Material and Methods). A 1 ml phenyl sepharose high performance (34 μm bead matrix) column with a ligand density of 25 μmol/ml was found to be optimal in terms of purification, recovery and resolution of the elution peak profile (Figure 3.2.2.7-2).



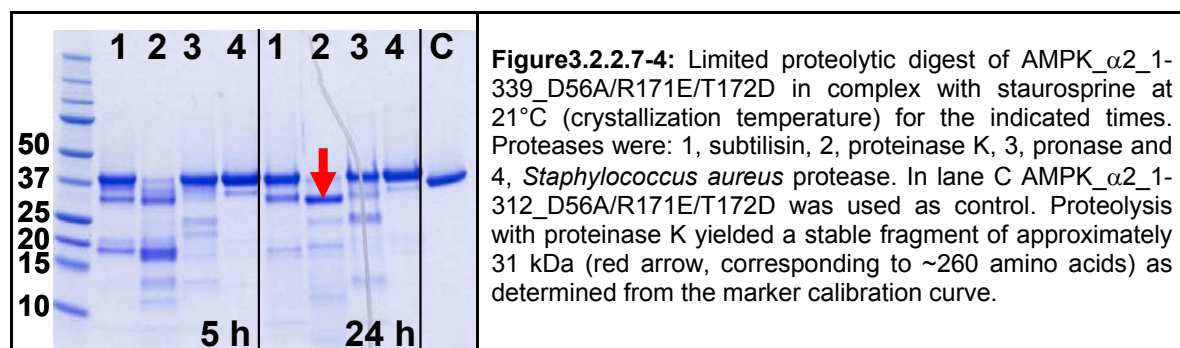
The AMPK_α2_1-312_D56A/R171E/T172D construct also did not elute completely during the preparative anion exchange chromatography but here a decrease of the pH to 7.4 was sufficient for optimization of the elution. This suggested that part of the pronounced retention of this construct could be due to the Donnan effect, which causes an increase in the pH of the microenvironment of the anion exchanger surface (SCOPEs, 1993; SHEN and FREY, 2004).

Since the shorter triple mutant constructs have a higher pI (Figure 3.2.2.7-3) and altered surface properties compared to AMPK_α2_1-339_D56A/R171E/T172D, the behavior during elution from the IEX column could be attributed to protein-protein interaction and possibly aggregation on the IEX column rather than increased interaction with the resin.



After optimization of the purification protocols both the truncated triple mutant constructs could be prepared in substantially higher yields compared to the wild-type constructs. Tiny needle-shaped crystals of AMPK $_{\alpha 2}$ _1-312_D56A/R171E/T172D in complex with staurosporine were obtained with 10 % (w/v) PEG 3000 or 8000, 0.2 M NaCl and 0.1 M CHES/ NaOH pH 9.5 (Emerald Wizard Screen 1, conditions 26 or 29, respectively). The further truncated construct AMPK $_{\alpha 2}$ _1-301_D56A/R171E/T172D also crystallized as tiny needles from these conditions. However, optimization trials around these conditions did not improve crystal size.

The results of the crystallization trials indicated that the carboxy-terminal construct boundary seemed to determine crystallization behavior and crystal size. A limited proteolytic digest of AMPK $_{\alpha 2}$ _1-339_D56A/R171E/T172D in complex with staurosporine was performed in order to define stable truncated constructs derived from the complex that crystallized best (Figure 3.2.2.7-4).



The results of the limited proteolysis suggested that the preparation of stable core kinase constructs might be feasible, especially because no precipitate of insoluble fragments became visible. However, a given protease could cut a target protein into two (insoluble) fragments which remain associated in a stable (and soluble) complex and are only separated upon denaturing electrophoresis. Here, interpretation of the results was unambiguous because from previous experiments it was known that the amino-terminus of the soluble constructs of the α -subunit of AMPK was resistant to proteolysis under the conditions employed as opposed to the presumably flexible carboxy-terminus. Based on the homology model of AMPK $_{\alpha 2}$ _1-339 four truncation points (*i.e.*, after amino acid 249 and 262/3/4, Figure 3.2.2.7-5) were selected for generating the core kinase constructs by mutating the consecutive codons to stop codons by site directed

mutagenesis. The three constructs with carboxy-terminal residues 262/3/4 were made in order to exploit the effect of a positively or negatively charged or an uncharged carboxy-terminus on the biochemical properties of these constructs.

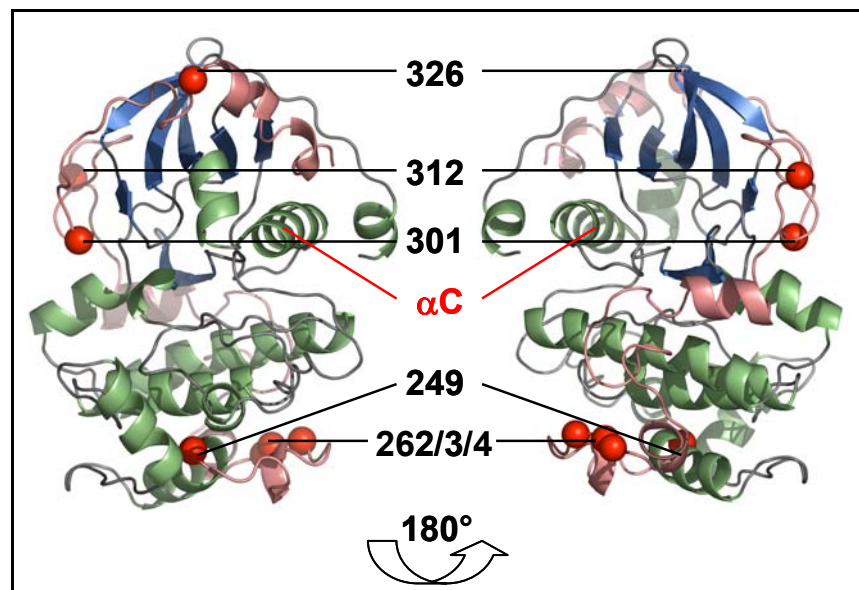


Figure 3.2.2.7-5: Standard orientation (left) and view rotated by 180° (right) of the homology model of AMPK $_{\alpha 2}$ _1-339. The position of helix α C is indicated for clarity, α -helices green, β -sheets blue, despite amino acids 249 to 339 of the carboxy-terminus which are colored light red. The red spheres represent the carboxy-terminal amino-acids of the truncated constructs.

These construct boundaries could be verified by the FoldIndex© prediction tool (Figure 3.2.2.7-6; PRILUSKY *et al.*, 2005). For a given protein sequence this program examines the correlation of the mean hydrophobicity (according to KYTE and DOLITTLE, 1982) to the mean net charge, as described by UVERSKY *et al.* (2000). Generally, natively unfolded proteins and amino acid sequences without secondary structure are found to possess a relatively high net charge together with low mean hydrophobicity. This interferes with the mechanisms proposed to underlie protein folding, *i.e.*, gradual formation of local secondary structure with subsequent formation of tertiary structure, hydrophobic collapse or a nucleation-condensation driven process because of the repulsion of homonymous charges and the lack of formation of a hydrophobic core (NÖLTING and ANDERT, 2000).

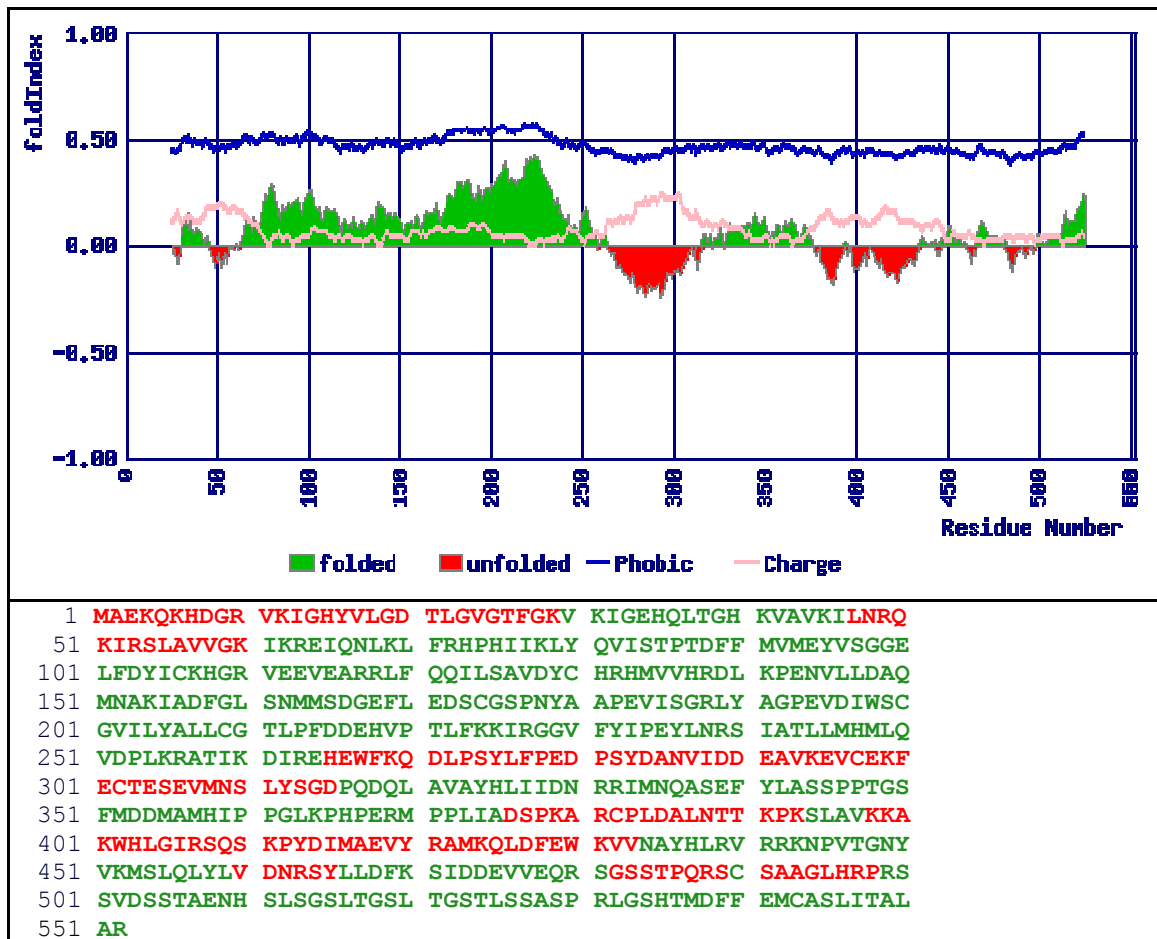


Figure 3.2.2.7-6: Output from the analysis of the full-length AMPK_{α2}_1-552 (D56A/R171E/T172D) by the FoldIndex© prediction tool. **Top panel**, plot of the distribution of hydrophobicity (blue) and net charge (pink). Sections of the sequence with predicted folded domains are shown in green, whereas sections with relatively low hydrophobicity and high net charge are predicted to be unfolded (red). **Bottom panel**, amino acid sequence colored according to sections predicted to be structurally ordered (green) and disordered (red). The data from this analysis imply a domain/construct boundary for the core kinase at amino acid E251. Similar results were obtained with the DisEMBL algorithm (LINDING *et al.*, 2003; data not shown).

None of the core kinase constructs was found to yield soluble protein in expression tests in *E. coli*. This together with previous observations suggested that the sequence comprising amino acids 250 to 312 had a substantial effect on protein stability. This led to the decision to determine a carboxy-terminal construct boundary based on constructs used for the crystallization of a homologous kinase.

Although AMPK has not been shown to be directly regulated by Ca²⁺/calmodulin it is a member of the family of Ca²⁺/calmodulin-dependent protein kinases (CAMK; MANNING *et al.*, 2002). The sequences of rat AMPK_{α2}_1-339 and the construct of rat CAMK-1

whose structure had been solved (GOLDBERG *et al.*, 1996, PDB code 1a06) possess 31.3 % identity and 44.6 % similarity (Figure 3.2.2.7-7).

AMPK_α2	1	maekqkhdgrvkighyvlgdtlgvgtfgkvkigehqtlghkva	43
CAMK_1a06	1	MPGAVEGPRWKQAEDIR---DIYDFRDVLGTGAFSEVILAEDKRTQKLVA	47
AMPK_α2	44	vkilnrqkirsLavvgkikreiqnklfrhphiiklyqvistptdffmvm	93
CAMK_1a06	48	IKCIAKKALEGKE--GSMENEI AVLHKIKHPNIVALDDIYESGGHLYLIM	95
AMPK_α2	94	eyvsggelfdyickhgrveearrlfqqlsavdychrhmvvhrdlkpe	143
CAMK_1a06	96	QLVSGGELFDRIVEKGFYTERDASRLIFQVLDAVKYLHDLGIVHRDLKPE	145
AMPK_α2	144	nvl---ldaqmnaKiadfglnmmsdgefledscgspnyaapevisgrly	190
CAMK_1a06	146	NLLYYSLDEDSKIMISDFGLSKMEDPGSVLSTACGTPGYVAPEVLAQKPY	195
AMPK_α2	191	agpevdiwscgvilyallcgtlpfddehvptlfkkirggvfypiey----	236
CAMK_1a06	196	S-KAVDCWSIGVIAYILLCGYPPFYDENDAKLFEQILKA-----EYEFDS	239
AMPK_α2	237	-----lnrsiatllmhmLqvdplkratikdirehewfkqdlpsylfpedp	281
CAMK_1a06	240	PYWDDISDSAKDFIRHLM EK DPEKRFTCEQALQHPW-----IAGDT	280
AMPK_α2	282	sydanviddeavkevcek-----fectesevmnslYsgdpqqla	321
CAMK_1a06	281	ALDKNI--HQSVSEQIKKNFAKSKWKQAFNAT-----A	311
AMPK_α2	322	vayhliidnrirmnqase	339
CAMK_1a06	312	VVRHM-----RKLQLGHQPGGTGDS	332

Figure 3.2.2.7-7: Sequence alignment (Needle, EMBOSS, RICE *et al.*, 2000) of rat AMPK_α2_1-339_D56A/R171E/T172E and rat CAMK-1_1-332 as deposited in PDB entry 1a06 (CAMK_1a06). The carboxy-terminal residues of truncated constructs are labeled red.

Alignment of the sequences emphasized that residue 326 of the α2-subunit of AMPK precedes a discontinuity in homology. It should be noted that CAMK-1 and AMPK_α2 show a good overall alignment for the relevant constructs but only limited homology in the amino acid sequence spanning the transition from the kinase to the regulatory domains. However, sequence analysis with other isoforms and programs (data not shown) confirmed a break in local homology at position 326 in AMPK_α2. Therefore, the construct AMPK_α2_1-326_D56A/R171E/T172D was generated, purified to homogeneity and subjected to crystallization trials, but no crystals were obtained.

3.2.2.8 Crystallization of the AMPK heterotrimer

In addition to efforts to crystallize the catalytic domain of AMPK the option of crystallizing the holo-trimer was pursued. For this a collaboration with the group of Prof. T. Wallimann, ETH Zurich, had been established which granted access to cell lysates and purified protein of rat isoform combinations expressed from a tricistronic vector in *E. coli* (NEUMANN *et al.*, 2003). The His₆-tagged $\alpha\beta\gamma$ 1 isoform combination was purified by H-J. Schönfeld and B. Pöschl, Roche Basel, from cell lysate provided by the Wallimann group. The purified protein was concentrated to 10 mg/ml in 25 mM HEPES/NaOH pH 7.8, 1 mM MgCl₂, 200 mM NaCl, 1 mM DTT and subjected to commercial crystallization screens as apo enzyme and in combination with a range of nucleotide analogs as well as the active-site inhibitors compound C (ZHOU *et al.*, 2001) and indirubin-5-sulphonate (synthesized by U. Riek, ETH Zurich; HOESSEL *et al.*, 1999; DAVIES *et al.*, 2001). Crystals of the apo enzyme could be obtained from 24 out of 48 conditions of the PEG/Ion Screen™ (Hampton Research) using the free interface diffusion and modified microbatch methods. This demonstrated for the first time the feasibility to crystallize the heterotrimeric holoenzyme of AMPK. Optimization of the initial crystallization conditions proved difficult as the protein exhibited a substantial batch-to-batch variability with regard to its capability to crystallize, although the preparations were of high quality in terms of elution profiles during chromatography as well as final electrophoretic purity and monodispersity in dynamic light scattering (Figure 3.2.2.8-1).

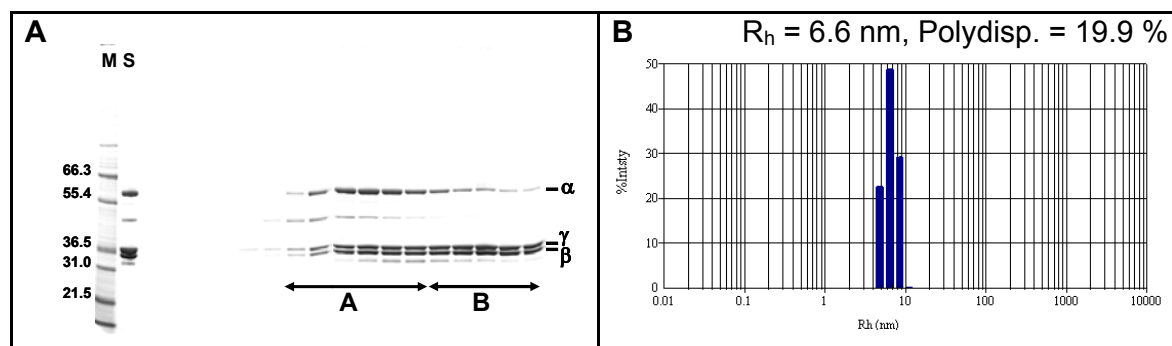


Figure 3.2.2.8-1: **A**, SDS_PAGE of a preparative SEC of His₆-AMPK_α1β1γ1, with marker (lane M, MW is indicated), sample (lane S, before SEC) and fractions. Pools A and B were subjected to crystallization trials. **B**, DLS signal of His₆-AMPK_α1β1γ1 (10 mg/ml).

Assuming a spherical protein the hydrodynamic radius of 6.6 nm corresponds to a molecular weight of 280 kDa. Despite the fact that a concentrated (presumably non-ideal) sample solution was measured this demonstrated the formation of dimers of AMPK heterotrimers in solution, which was later confirmed by small angle X-ray scattering (SAXS; see 3.2.2.11). The best crystals of AMPK $_{\alpha 1\beta 1\gamma 1}$ were grown with the hanging drop technique in optimized conditions of the Index Screen™ (Hampton Research) and diffracted X-rays to 7 Å (Table 3.2.2-1, page 29).

From the purified AMPK heterotrimers delivered by the Wallimann group the isoform combinations $\alpha 2\beta 1\gamma 1$ and $\alpha 2\beta 2\gamma 1$ crystallized reproducibly (Table 3.2.2.8-1).

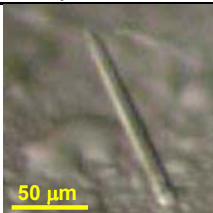
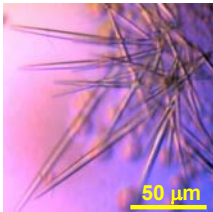
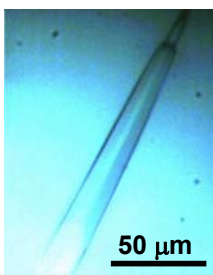
Isoform/ Mutant	Crystals/ Conditions	
His ₆ -(TEV)-AMPK $_{\alpha 1\beta 1\gamma 1}$	no crystals	
AMPK $_{\alpha 1\beta 1\gamma 1}$	no crystals	
AMPK $_{\alpha 1\beta 1\gamma 1}$ _D157A	no crystals	
AMPK $_{\alpha 1\beta 2\gamma 1}$ _wt	no crystals	
AMPK $_{\alpha 2\beta 1\gamma 1}$ _wt		19 % PEGMME 2000, 0.2 M NaCl, 0.1 M Bis-Tris pH 6.5 (optimized from NHR-LB Screen Extension Kit, MDL)
		12.5 % PEGMME2000, 0.4 M NaCl, 0.1 M Bis-Tris pH 6.5 (optimized from NHR-LB Screen Extension Kit, MDL)
		10 % PEGMME2000, 0.2 M NaCl 0.1 M Bis-Tris pH 6.5 (optimized from NHR-LB Screen Extension Kit, MDL)
AMPK $_{\alpha 2\beta 2\gamma 1}$ _wt	needle-shaped crystals similar to AMPK $_{\alpha 2\beta 1\gamma 1}$ _wt	

Table 3.2.2.8-1: Crystallization conditions of AMPK heterotrimer isoforms obtained from Wallimann group, ETH Zurich.

As observed with AMPK $_{\alpha 1\beta 1\gamma 1}$ purified in-house, the variability of the crystallization behavior between different batches precluded extensive optimization trials. No crystals were obtained of AMPK $_{\alpha 1\beta 1\gamma 1}$ or a derived trimer with a point mutation of catalytic

base (AMPK $\alpha 1\beta 1\gamma 1_{D157A}$), as opposed to the AMPK_ $\alpha 1\beta 1\gamma 1$ purified in-house. This discrepancy emphasized the sensitivity of the trimer to minute changes in the construct and purification conditions (all preparations of AMPK_ $\alpha 1\beta 1\gamma 1$ were performed with cell paste from the same fermentation).

3.2.2.9 Crystallization of the AMPK regulatory subunits

The crystals of various $\alpha 2$ -subunit constructs, which were flawless in regard to visual inspection, and those of various isoform combinations of the heterotrimer were of limited diffraction quality. This suggested that the α -subunit might be responsible for the disorder of the crystals. Therefore, two constructs comprising the regulatory β - and γ -subunits were cloned, expressed in *E. coli* and purified (R. Thoma, Roche Basel). These were AMPK_ $\beta 1_{\Delta 1-67} \cdot \gamma 1$ and AMPK_ $\beta 1_{\Delta 1-185} \cdot \gamma 1$, *i.e.*, two amino-terminally truncated constructs of the $\beta 1$ -subunit in complex with the full-length $\gamma 1$ -subunits, respectively (Figure 3.2.2.9-1).

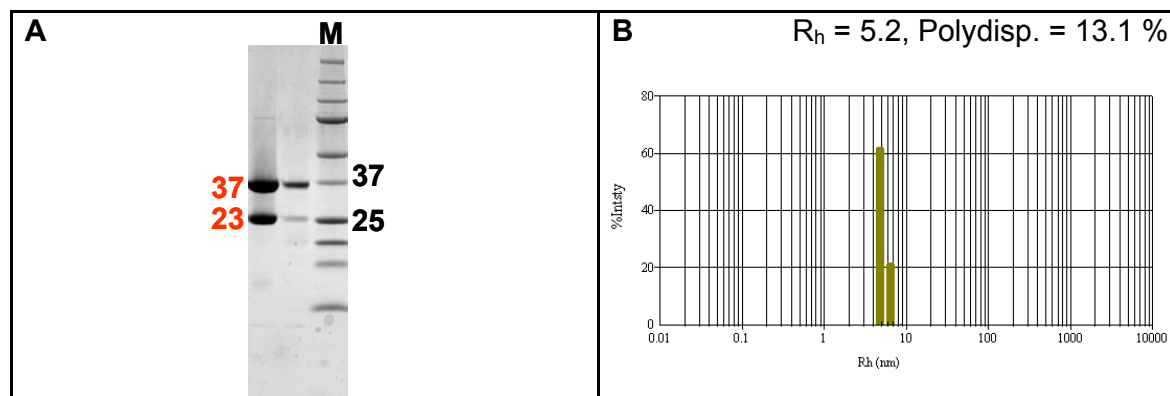


Figure 3.2.2.9-1: **A**, SDS-Page (red, calculated MW; M, marker with MW) and **B**, DLS of purified AMPK_ $\beta 1_{\Delta 1-67} \cdot \gamma 1$.

The amino-terminal construct boundaries for the $\beta 1$ -subunit had been chosen according to the analyses performed by POLEKHINA *et al.* (2003; reviewed in KEMP *et al.*, 2003) who had shown that residues 68 to 163 of AMPK_ $\beta 1$ form a functional glycogen binding domain (GBD). In fact, this GBD is the only domain of mammalian AMPK for which experimental structural information is available (POLEKHINA *et al.*, 2005A and B). Neither of the purified heterodimers of the regulatory $\beta 1$ -subunit (in presence or absence of the GBD \pm β -cyclodextrin) in complex with the $\gamma 1$ -subunit crystallized.

Preliminary results of limited proteolysis experiments with AMPK $_{\alpha 2\beta 2\gamma 1}$ (Figure 3.2.2.9-2) suggested that further preparation of truncated AMPK constructs should be included in the optimization scheme. Trypsin, pronase and *Staphylococcus aureus* protease cut preferentially the catalytic α -subunit, while the regulatory β - and γ -subunits showed partial resistance to cleavage by these proteases. A future construct optimization scheme should include the analysis of the cleavage products by analytical SEC and native PAGE followed by SDS-PAGE and MS. This will allow the separation and identification of those fragments that can still form stable complexes.

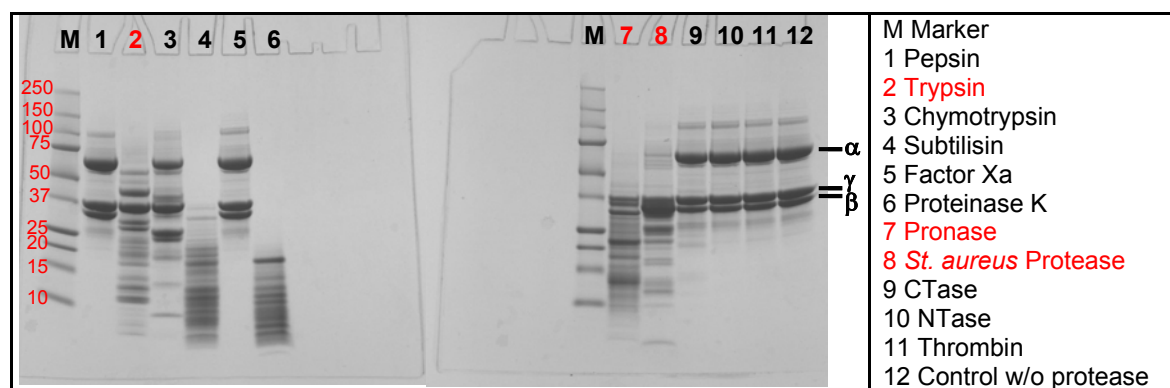


Figure 3.2.2.9-2: Limited proteolysis of AMPK $_{\alpha 2\beta 2\gamma 1}$. The reaction was performed with a 1:10,000 (w/w) ratio of protease to AMPK trimer for 5 h at 21°C in 50 mM HEPES/NaOH pH 8, 200 mM NaCl, 2 mM MgCl₂ and 2 mM TCEP.

3.2.2.10 Interaction of the AMPK heterotrimer with the ligand binding domain of PPAR α

BRONNER *et al.* (2004) showed that the $\alpha 2$ -subunit of (human) AMPK physically interacts with the ligand binding domain (LBD) of the (murine) nuclear hormone receptor PPAR α *in vitro*. Nuclear localization and direct phosphorylation of proteins involved in gene transcription were demonstrated for the AMPK- $\alpha 2$ subunit (SALT *et al.*, 1998; LEFF, 2003). In order to assess whether this complex formation could enhance the crystallization of the heterotrimer, AMPK $_{\alpha 2\beta 2\gamma 1}$ was incubated with an equimolar amount of (human) PPAR α . The PPAR α was a preparation of an in-house construct, which was 42 amino-acids shorter than that used in the study by BRONNER *et al.* (2004). Despite using a buffer system as published, no interaction of AMPK $_{\alpha 2\beta 2\gamma 1}$ with the LBD of PPAR α could be detected using analytical size exclusion chromatography and only a very weak interaction could be demonstrated by Biacore

(data not shown) and this strategy for crystallization was not pursued. However, these results could indicate that the 42 amino acids at the amino-terminus of LBD missing in the in-house PPAR α constructs are essential for the interaction with AMPK α 2.

3.2.2.11 Small angle X-ray-scattering (SAXS) studies of AMPK

As the AMPK crystals were not suitable for solving the structure, SAXS studies were performed in order to elucidate the low resolution (app. 15-20 Å) solution structures of wild-type AMPK α 2 $_1$ -392 and the AMPK α 2 β 2 γ 1 heterotrimer. The SAXS measurements and data analyses were done in collaboration with D. Svergun and P. Konarev, EMBL, Hamburg outstation. In order to visualize the shape of AMPK α 2 $_1$ -392 an *ab initio* bead model was generated based on the scattering data (Figure 3.2.2.11-1). In a second approach the AMPK α 2 $_1$ -339 homology model was used as input and the missing residues (aa 340-392) were modeled by minimizing the discrepancy of the scattering intensity calculated from the input data and the experimental scattering intensity (Figure 3.2.2.11-1). While these models cannot be fully superimposed, the elongated shapes of the models clearly accentuate that the putative autoinhibitory domain does not bind to the catalytic core with high affinity. This result is in full agreement with the Thermofluor[®] data (3.2.2.2).

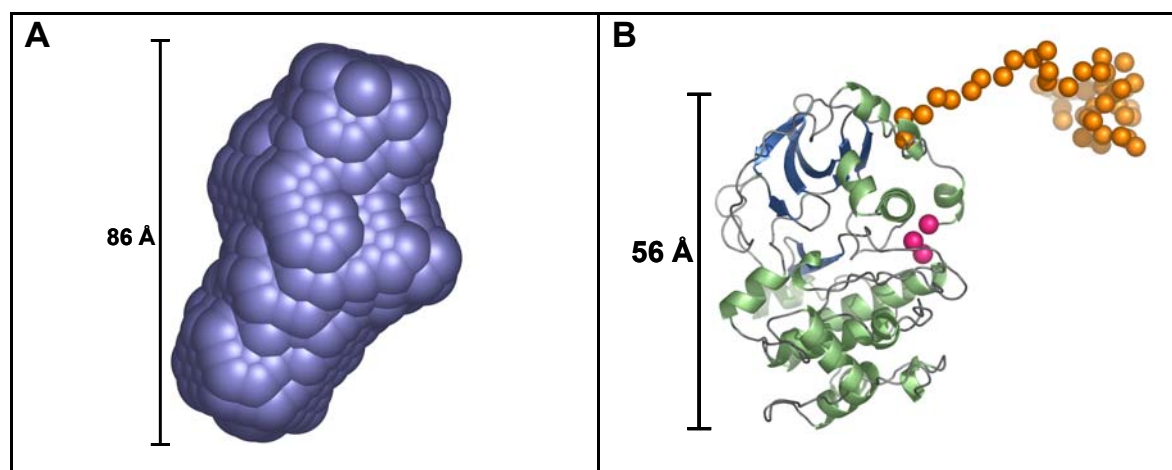


Figure 3.2.2.11-1: SAXS analysis of AMPK α 2 $_1$ -392 (5.4 mg/ml). **A**, *ab initio* bead model generated with the program DAMMIN. **B**, homology model of AMPK α 2 $_1$ -339 (ribbon representation, green: α -helices, blue: β -strands) with the model of the missing part of the putative autoinhibitory domain (aa 340-392, orange spheres), as calculated with the programs CRYSOLO and CREDO (PETOUKHOV *et al.*, 2002). Each sphere represents one added residue, the three residues at the amino-terminus (pink spheres) are derived from the thrombin cleavage site of the His₆-tag.

The scattering curves of full-length heterotrimeric AMPK $_{\alpha 1\beta 1\gamma 1}$ and AMPK $_{\alpha 2\beta 2\gamma 1}$ at concentrations that were used for crystallization trials (1.3-18 mg/ml) indicated that trimeric AMPK has a tendency to oligomerize and aggregate. Dilution of the protein to lower concentrations with the stabilizing buffer (50 mM HEPES/NaOH pH 8.0, 2 mM MgCl $_2$, 200 mM NaCl and 2 mM TCEP) resulted in an decreased signal to noise ratio (electron density contrast), which rendered the data uninterpretable. For AMPK $_{\alpha 2\beta 2\gamma 1}$ (1.3 mg/ml) the program DAMMIN was run with P1 symmetry but produced a model with an approximate two-fold symmetry (Figure 3.2.2.11-2). This result indicated the formation of dimers of heterotrimers because the AMPK heterotrimer has certainly no internal two-fold symmetry. The model has a volume of $3.214 \cdot 10^5 \text{ \AA}^3$, which corresponds to a MW of 160 kDa (assuming a partial specific volume of 0.741 ml/g). As the MW determined by SAXS was between the theoretical MW of the AMPK $_{\alpha 2\beta 2\gamma 1}$ trimer (130 kDa) and that of a dimer of such a heterotrimer, the data suggested that AMPK $_{\alpha 2\beta 2\gamma 1}$ has a tendency to form higher order assemblies. Analyzing the scattering of AMPK $_{\alpha 2\beta 2\gamma 1}$ at 13 mg/ml with a P2 symmetry restriction yielded a model of $6.497 \cdot 10^5 \text{ \AA}^3$ (320 kDa, Figure 3.2.2.11-2).

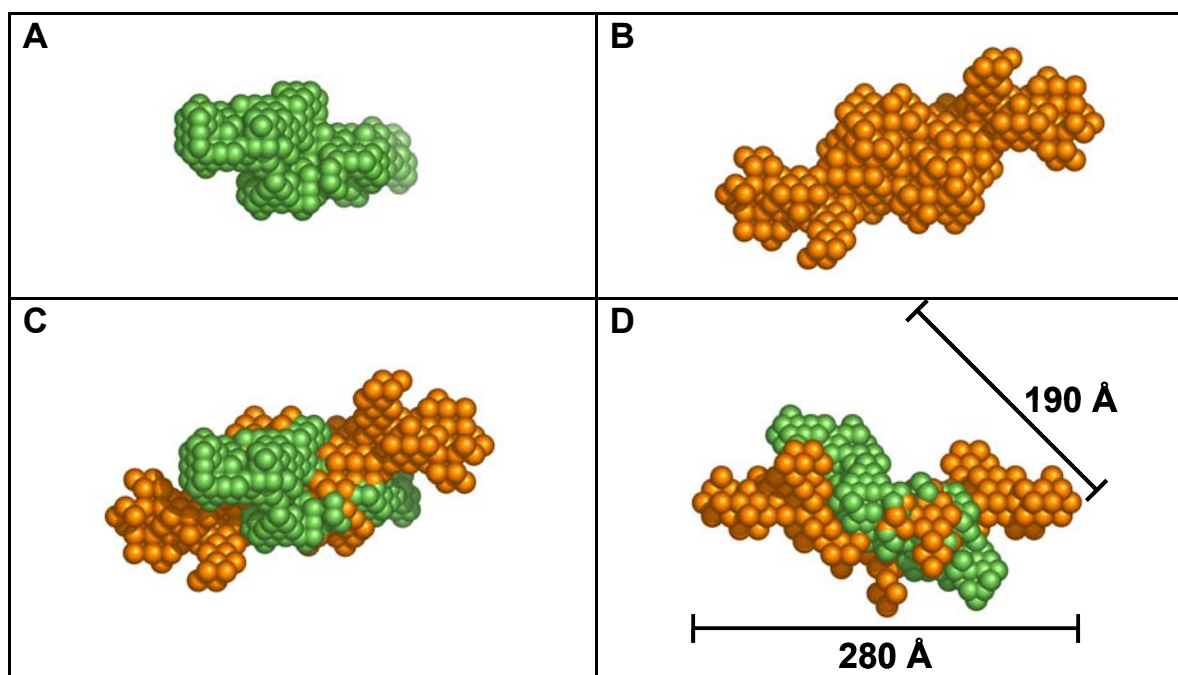


Figure 3.2.2.11-2: *Ab initio* bead models of the AMPK $_{\alpha 2\beta 2\gamma 1}$ heterotrimer. **A**, AMPK $_{\alpha 2\beta 2\gamma 1}$ at 1.3 mg/ml. **B**, AMPK $_{\alpha 2\beta 2\gamma 1}$ at 13 mg/ml. **C**, superimposition of A and B. **D**, same as C but rotated 90° to the back. The maximal particle size (D_{\max} , [Å]) is indicated by the scale bars.

The AMPK $_{\alpha 2\beta 2\gamma 1}$ models calculated from the SAXS data have radii of gyration, *i.e.*, root-mean square distances for all electrons in the model from their center of gravity, of 5.43 nm for the low and 7.26 nm for the high concentration sample. This corresponds very well to the hydrodynamic radii $R_h = 6.29$ nm (13 mg/ml, 32.7 % polydispersity) and $R_h = 6.6$ nm (10 mg/ml, 19.9 % polydispersity) measured by DLS for AMPK $_{\alpha 2\beta 2\gamma 1}$ and AMPK $_{\alpha 1\beta 1\gamma 1}$ (3.2.2.8), respectively. Thus, the formation of oligomeric species in a concentration-dependent manner is likely to be a property of the AMPK heterotrimer and probably interferes with crystallization. Preliminary SAXS experiments with AMPK $_{\alpha 1\beta 1\gamma 1}$ and AMPK $_{\alpha 2\beta 2\gamma 1}$ equilibrated with an 1 mM excess of active (AMP-PNP) and allosteric (AMP) site ligands, revealed that under these conditions the radii of gyration are decreased. This was interpreted as a ligand-dependent shift of the association equilibria towards monomeric $\alpha\beta\gamma$ -trimers, and has to be verified by measuring dilution series of ligand against different protein concentrations.

3.3 Crystallization and structure determination of carnitine palmitoyltransferase 2 (CPT-2)

3.3.1 The CPT-system: a candidate drug target for T2D

The carnitine palmitoyltransferase (CPT) system imports long chain fatty acids (LCFA) into mitochondria, where they are metabolized by β -oxidation (reviewed in MCGARRY & BROWN, 1997; RAMSEY *et al.*, 2001; BONNEFONT *et al.*, 2004). The rate-limiting step of LCFA import is the transesterification of acyl-CoA to acyl-carnitine by CPT-1 (RONNETT *et al.*, 2005), which is integrated into the mitochondrial outer membrane (MOM). Several mechanisms for the delivery of acyl-carnitine esters from the cytosol into the mitochondrial intermembrane space have been proposed (BEBERNITZ and SCHUSTER, 2002). The acyl-carnitine esters are translocated through the mitochondrial inner membrane (MIM) via the carnitine/acyl-carnitine transporter (CACT). CPT-2, which is localized at the matrix side of the MIM, transforms the imported acyl-carnitine back to acyl-CoA.

The muscle isoform of CPT-1 (M-CPT-1), and to a lesser extent the liver isoform (L-CPT-1), are inhibited by malonyl-CoA (ZAMMIT, 1999A), the product of the committed step of fatty acid synthesis. In contrast, the activity of the ubiquitously expressed CPT-2 is not known to be directly regulated by malonyl-CoA or other intermediates of metabolism (MCGARRY and BROWN, 1997; NIC A'BHAIRD *et al.*, 1993) which could be exploited for pharmacological modulation of CPT-2 activity.

Pharmacological inhibition of the CPT system by the glycidic acid derivative etomoxir, an irreversible and non-isoform-specific active site inhibitor of CPTs, has been demonstrated to reduce fasting blood glucose in an animal model of type 2 diabetes mellitus (T2D; BARNETT *et al.*, 1992). Oral administration of etomoxir decreased fasting glucose and ketone body levels in obese T2D patients (RATHEISER *et al.*, 1991), and insulin-mediated glucose uptake was observed to be increased in another study with T2D patients (HUBINGER *et al.*, 1992). However, specific inhibition of L-CPT-1 would be desirable, as this would utilize the glucose-fatty acid (Randle) cycle for restoring glucose homeostasis without affecting mobilization of ectopic lipid depots in skeletal muscle of adipose T2D patients (reviewed in ANDERSON, 1998; RANDLE, 1998; FRAYN, 2003; DULLOO *et al.*, 2004).

The identification of L-CPT-1 as a target for the treatment of T2D is further supported by the finding that inhibition of L-CPT-1 has been shown to reduce gluconeogenesis (WOLF and ENGEL, 1985; KASHIWAGI, 1995; WAGMAN and NUSS, 2001). Inhibition of L-CPT-1 results in depletion of mitochondrial acetyl-CoA which is an allosteric activator of the gluconeogenic enzyme pyruvate carboxylase.

In addition to etomoxir, various series of compounds have been designed that are competitive with substrate binding to CPT-1 (BEBERNITZ and SCHUSTER, 2002). These include the aminocarnitine-related family of emericidins isolated from the ascomycete fungus *Emericella quadrilineata* (SHINAGAWA *et al.*, 1987), which were further developed into more L-CPT-1-specific ureidic acyl-aminocarnitine derivatives (GIANNESI *et al.*, 2001 and 2003). A representative of the latter, (R)-N-(tetradecylcarbamoyl)-aminocarnitine (ST1326) is an analog of palmitoylcarnitine, the product of CPT-1 and substrate of CPT-2. The compound ST1326 is currently in clinical trials at Sigma-Tau Pharmaceuticals. ST1326 was shown to inhibit L-CPT-1 in isolated rat mitochondria with marked specificity over M-CPT-1 (GIANNESI *et al.*, 2003).

Moreover, ST1326 caused a pronounced reduction of serum glucose levels when administered orally to db/db mice (GIANNESI *et al.*, 2003) and was shown to elicit an anorexic effect, as well as to inhibit endogenous glucose production after central administration to rats (OBICI *et al.*, 2003). These features render ST1326 a model compound for L-CPT-1 inhibition in the treatment of diabetes mellitus.

In order to support the discovery of novel anti-diabetic drugs that inhibit the CPT-system, the function and structure of CPT-2 was investigated in this thesis. Full length CPT-2 from rat was expressed in *E. coli*, solubilization and purification of membrane bound CPT-2 with detergent yielded homogeneous and active enzyme. Characterization of the activity of CPT-2 revealed inhibition of CPT-2 *in vitro* by ST1326, which had previously been reported to be a specific inhibitor of L-CPT-1 (GIANNESI *et al.*, 2003). The binding mode of ST1326 was elucidated by solving the crystal structure of full-length rat CPT-2 in complex with ST1326 at 2.5 Å resolution. The structure of the uninhibited enzyme of rat CPT-2 was solved at 1.6 Å and 2.0 Å in two different space groups. The amino acid sequence of CPT-2 revealed a 30 amino acid insert uniquely found in CPT-2 as compared to CPT-1 isoforms, carnitine acetyltransferase (CrAT) and

carnitine octanoyltransferase (CrOT). Based on the crystal structure of CPT-2 a model for membrane attachment of CPT-2 mediated by this insert could be proposed.

The crystal structure of CPT-2 in complex with the substrate analog ST1326 revealed an extensive hydrogen network involving residues highly conserved between CPT-1 and CPT-2 that tightly interact with the hydrophilic aminocarnitine headgroup of ST1326. Furthermore, clear electron density for the hydrophobic tail of ST1326 accommodated in the acyl binding-site was visible. The structure of CPT-2 in complex with ST1326 shows for the first time the substrate binding mode of LCFA-specific carnitine acyltransferases, which are indispensable for the import of substrates for β -oxidation into mitochondria. The CPT-2 structure also allows the correlation of structure and function of amino acids mutated in CPT-2 deficiency, a hereditary disorder of lipid metabolism.

3.3.2 Biophysical characterization of CPT-2

Rat CPT-2 was solubilized in detergent micells and purified to homogeneity by a two step purification protocol. CPT-2 was chosen as a surrogate system because of markedly increased solubility (MURTHY and PANDE, 1987; WOELTJE *et al.*, 1990) and crystallizability when compared to the integral membrane protein CPT-1. Human L-CPT-1 and rat CPT-2 share 27 % identity and 43 % similarity in the amino acid sequence of their catalytic cores and the catalytically important residues are fully conserved (Figure 3.3.2-1).

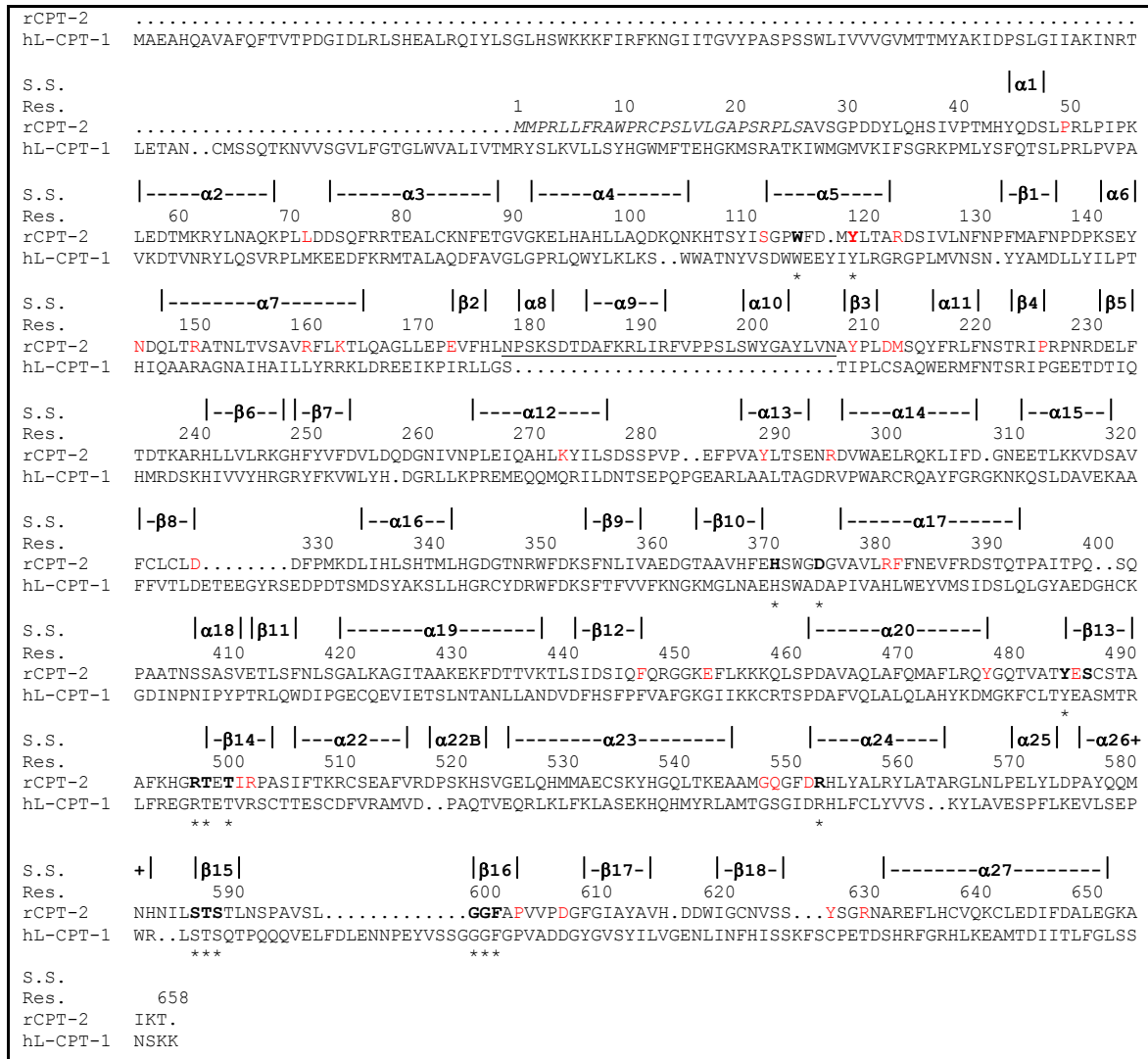


Figure 3.3.2-1: Amino acid sequence alignment (ClustalW, EMBOSS; RICE *et al.*, 2000) of rat CPT-2 (rCPT-2) and human L-CPT-1 (hL-CPT-1). Secondary structure elements (S.S.) are indicated. The residue numbering corresponds to the rCPT-2 precursor and its mitochondrial import sequence is italicized. The CPT-2 specific insert (amino acids 179-208) is underlined. Key residues of the acylcarnitine binding site of rCPT-2 are in bold letters and are labeled with an asterisk when fully conserved in hCPT-1. Residues are printed in red when mutations in CPT-2 deficiency have been reported.

In the final preparative size-exclusion chromatography rat CPT-2 ($c \approx 14$ mg/ml in pooled peak fractions) behaved as a monomer and no aggregates could be detected. In the presence of 1 % (w/v) n-octyl- β -D-glucopyranoside (β OG; app. 1.5-fold CMC concentration), but not in preparations with detergents at CMC-concentration (β OG; n-dodecyl- β -D-maltoside; CHAPS), rat CPT-2 was found to be monomeric and monodisperse as determined by analytical ultracentrifugation (Figure 3.3.2-2).

The purified enzyme was active as monomer and its activity could be inhibited in a concentration dependent manner by ST1326 with an $IC_{50} = 0.24 \mu\text{M}$ (Figure 3.3.2-2).

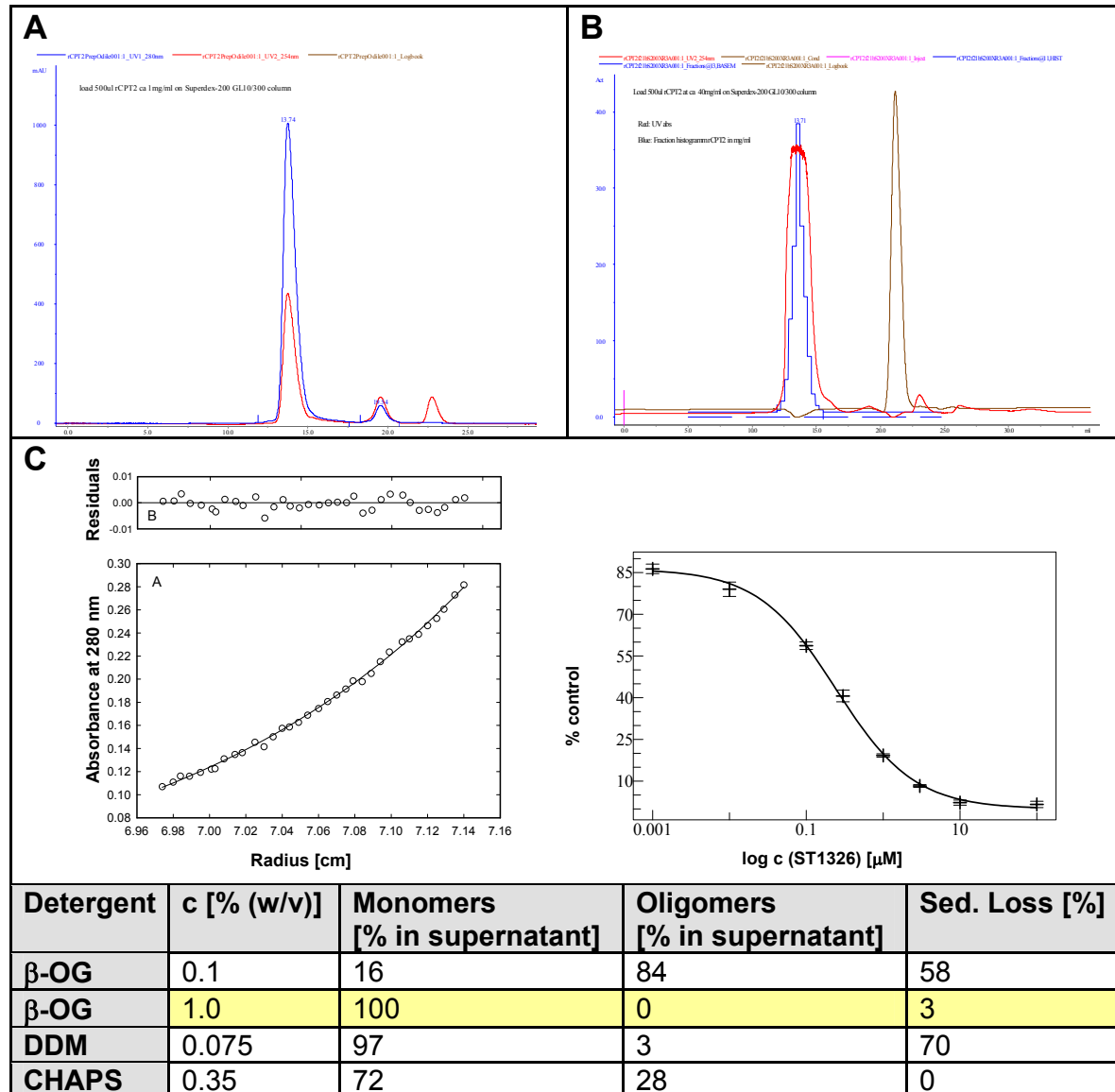


Figure 3.3.2-2: Characterization of rCPT-2. The SEC elution profiles at **A**, app. 1 mg/ml in peak fraction and **B**, app. 40 mg/ml show that rCPT-2 eluted as a single, monomeric species in the presence of 1 % (w/v) βOG . **C**, the left panel shows the sedimentation equilibrium of rat CPT-2 in 1% βOG at 20°C and 12,000 rpm. The absorbance at 280 nm (\circ) is plotted vs. radial distance. The solid line (—) shows the fit corresponding to an apparent single species of 73,471 Da (the theoretical MW of the construct is 73,470.82 Da) with a partial specific volume $\bar{v} = 0.760 \text{ ml/g}$ and a solvent density $\rho = 1.092 \text{ g/ml}$. Residuals of the fitted curve are shown in the top panel. The right panel depicts the inhibition \pm SD of purified rCPT-2 activity by ST1326 ($IC_{50} = 0.24 \mu\text{M}$). The 100 % activity control was determined in the absence of ST1326. The table at the bottom summarizes the AUC data with different detergent conditions. 1 % (w/v) βOG is required for stabilization of rCPT-2.

3.3.3 Crystallization and overall structure of CPT-2

Rat CPT-2 crystallized in complex with the inhibitor ST1326 and as uninhibited enzyme within seven days after setting up the crystallization trials (Figure 3.3.3-1). The term "uninhibited" as opposed to "apo" is used for the structures determined in the absence of ST1326 because in the 1.6 Å high resolution structure significant electron density for a fortuitous ligand bound to the active site was visible (see 3.3.4). While the crystals of the complex from the initial screen were sufficient for determining the structure, the crystals of the uninhibited enzyme had to be optimized by microseeding.

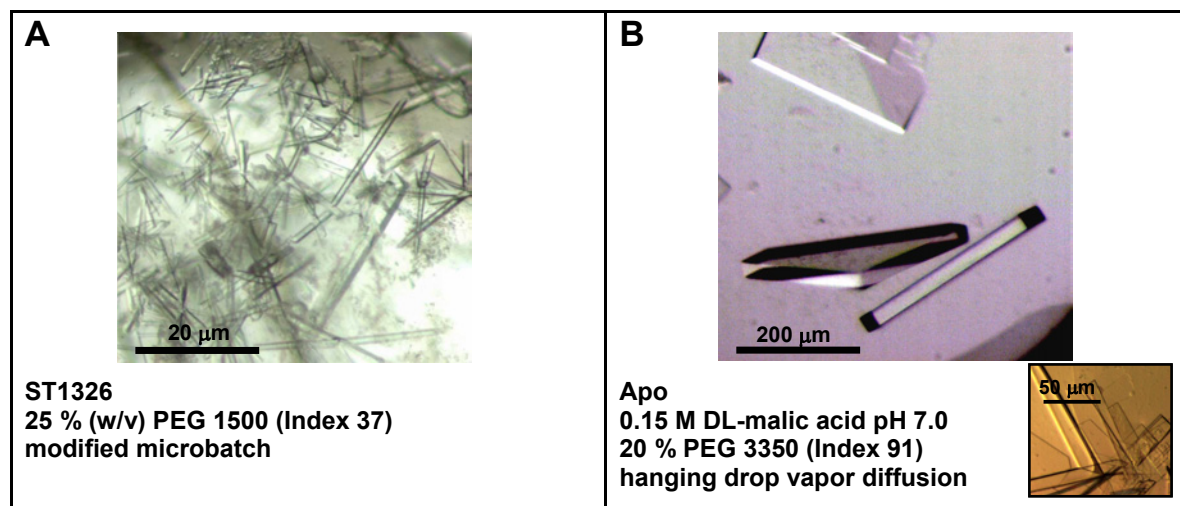


Figure 3.3.3-1: **A**, orthorhombic crystals of the rCPT-2 • ST1326 complex. **B**, tetragonal crystals of apo rCPT-2. Microseeding with a diluted seed stock containing vortexed preliminary crystals (inset) was essential for obtaining large, single diffraction quality crystals of the uninhibited enzyme.

The structure of rCPT-2 was determined by molecular replacement and refined to a resolution of 1.6 Å ($C222_1$) and 2.0 Å ($P4_32_12$) for the uninhibited enzyme and 2.5 Å ($P2_12_12_1$) for the ST1326 complex (see Table 3.3.3-1 for data statistics). The first 31 amino-terminal amino acids, comprising the His₆-tag and five residues of the actual rCPT-2 sequence, are disordered in all three structures. The full carboxy-terminus (Thr 658) is visible in chain A of the uninhibited enzyme in space group $C222_1$, while the last residues with interpretable electron density at the carboxy-termini are Ile 656 and Lys 654 in the tetragonal uninhibited and the complex crystals, respectively.

	uninhibited 1, high resolution	uninhibited 2	CPT-2 / ST1316
Data collection			
Space group	C222 ₁	P4 ₃ 2 ₁ 2	P2 ₁ 2 ₁ 2 ₁
Cell dimensions			
<i>a</i> , <i>b</i> , <i>c</i> (Å)	95.2, 97.3, 310.4	67.6, 67.6, 307.3	85.8, 96.2, 124.3
α, β, γ (°)	90.0, 90.0, 90.0	90.0, 90.0, 90.0	90.0, 90.0, 90.0
Resolution (Å) ^a	23.0 - 1.6 (1.69 - 1.60)	23.0 - 2.0 (2.12 - 2.00)	50.0 - 2.24 (2.38 - 2.24)
<i>R</i> _{sym} ^b	6.2 (21.2)	3.1 (7.4)	16.7 (41.1)
<i>I</i> / σ <i>I</i>	14.04 (7.24)	28.04 (14.80)	9.57 (3.20)
Completeness (%)	99.7 (99.8)	99.9 (100)	92.9 (81.8)
Redundancy	6.7 (5.8)	21.8 (18.5)	6.9 (6.2)
Refinement			
Resolution (Å)	23.0 - 1.6	23.0 - 2.0	15.0 - 2.5
No. reflections	179022	46957	32831
<i>R</i> _{work} / <i>R</i> _{free} ^c	16.5 / 19.4	17.9 / 23.5	24.1 / 29.6
No. atoms (all)	11449	5502	5143
Protein	10085	4977	4963
Ligand/ion	n/a ^d	n/a	28
Water	1364	525	152
<i>B</i> -factors (overall)	20.1	21.9	41.0
Protein	18.7	21.0	41.4
Ligand/ion	n/a ^d	n/a	27.6
Water	30.1	30.7	31.6
R.m.s. deviations			
Bond lengths (Å)	0.014	0.01	0.013
Bond angles (°)	1.225	1.161	1.502

Table 3.3.3-1: Data collection and refinement statistics of the rCPT-2 crystals.

^a Values in parentheses are for highest resolution shells.

^b $R_{\text{sym}} = \sum(I - \langle I \rangle) / \sum(I)$

^c $R = \sum | |F_{\text{obs}}| - |F_{\text{calc}}| | / \sum |F_{\text{obs}}|$; *R*_{free} was calculated using randomly selected 5 % of reflections.

^d The βOG detergent molecule (mean *B* = 54.9 Å²), the two C16 alkyl-moieties (mean *B* = 23.3 Å²) and the two residual, unspecifically bound CoA molecules (mean *B* = 37.7 Å²) were not included in the statistic.

The rCPT-2 secondary structure contains 27 α-helices and 18 β-strands. Amino-terminal (residues 111-440) and carboxy-terminal (residues 441-658, plus 32-110) domains can be assigned to rCPT-2. These domains consist of a six-stranded central anti-parallel β-sheet and surrounding α-helices (Figures 3.3.2-1 and 3.3.3-1). Two of these β-strands (β1, β16) mediate the major domain contact.

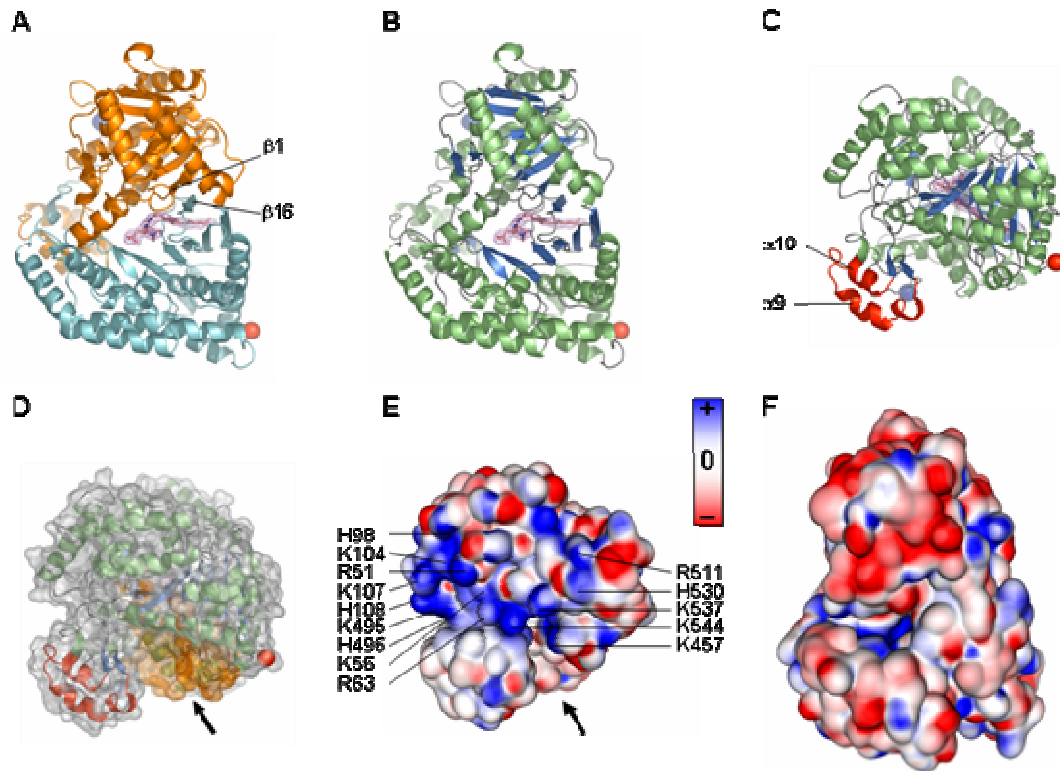


Figure 3.3.3-1: Structure of rCPT-2 with ST1326 bound to its active site. ST1326 and its surrounding *fofc* simulated annealing omit electron density map (1000 K; 2σ contour level) are depicted in pink, the amino- and carboxy-termini are labeled with blue and red spheres, respectively, in **A** through **C**. **A**, ST1326 binds at the interface of the amino-terminal (cyan) and carboxy-terminal (orange) domains of rat rCPT-2. Strands $\beta 1$ and $\beta 16$ mediate the major domain contact by forming an antiparallel sheet. **B**, the central β -strands (blue) are surrounded by α -helices (green). **C**, same as **B** but rotated 90° to the back. The CPT-2-specific insert (red) consisting mainly of helices $\alpha 9$ and $\alpha 10$ protrudes from the amino-terminal domain. **D**, surface representation of **C** that shows the entry (orange) to the active site tunnel close to the insert. **E**, surface in orientation of **C** colored according to electrostatic potential, charges (blue: positive, red: negative; white: neutral) were calculated at neutral pH (MOE). Key basic residues are indicated. **F**, electrostatic potential representation identical to that in **E** with orientation of **B**. An excess of positive charges is found on the surface close to the insert. The arrows indicate the entrance to the CoA-tunnel of the active site.

The loop connecting helices 22 and 23 adopts a helical conformation in the uninhibited structures and is, therefore, designated helix 22B. The corresponding region of the ST1326 complex structure is located close to a crystal contact, which may interfere with secondary structure formation. A 30 amino acid insert (comprising helices α 8-10) uniquely found in CPT-2 when compared to other carnitine acyltransferases (29 amino acids when compared to L-CPT-1, Figures 3.3.2-1 and 3.3.3-1) protrudes from the amino-terminal domain. Despite this insert the overall topology of rat CPT-2 resembles the two domain architecture found in human and mouse CrAT [PDB codes 1s5o (WU *et al.*, 2003; GOVINDASAMY *et al.*, 2004) and 1ndb (JOGL and TONG, 2003), 1t7n (HSIAO *et al.*, 2003)] as well as CrOT [PDB code 1xl7 (JOGL *et al.*, 2005)]. These members of the family of carnitine acyltransferases show approximately 30 % identity and 47 % similarity in the amino acid sequence of their catalytic core.

Uninhibited rCPT-2 and the ST1326 complex crystallized in different crystal forms, but the structures have similar conformations as indicated by a r.m.s. distance of 0.38 Å between all equivalent C α atoms. In all three structures the active site residue Arg 498 is in the generously allowed region of the Ramachandran plot and Leu 129 as well as Asn 230 do not comply with favored geometry of the Ramachandran plot, as indicated by well defined electron density for these residues. Leu 129 is the second residue in a type II reverse turn (equivalent to Ile 116 in mouse CrAT, PDB code 1t7n), whereas Asn 230 is located in a β -turn whose geometry is distorted due to interaction with neighboring Asp 297 and Arg 124. Mutation of Arg 124 is associated with inherited CPT-2 deficiency (see below).

3.3.4 Binding mode of ST1326

The active site of CPT-2 is located in a Y-shaped tunnel at the domain interface (Figures 3.3.3-1 and 3.3.4-1). The tripartite (NIC A'BHAIRD *et al.*, 1993) tunnel consists of binding sites for the acyl-, carnitine- and CoA moieties. In contrast to CrAT and CrOT the acyl-tunnel opens to the surface in rCPT-2. ST1326 is a non-cleavable analog of palmitoyl-carnitine, the physiological substrate of CPT-2. The acyl- and carnitine tunnels of the active site of CPT-2 are occupied by ST1326, whereas the CoA-tunnel can be assigned by homology modeling based on the complex structure of CrAT with CoA (PDB code 1t7q, Figure 3.3.4-1).

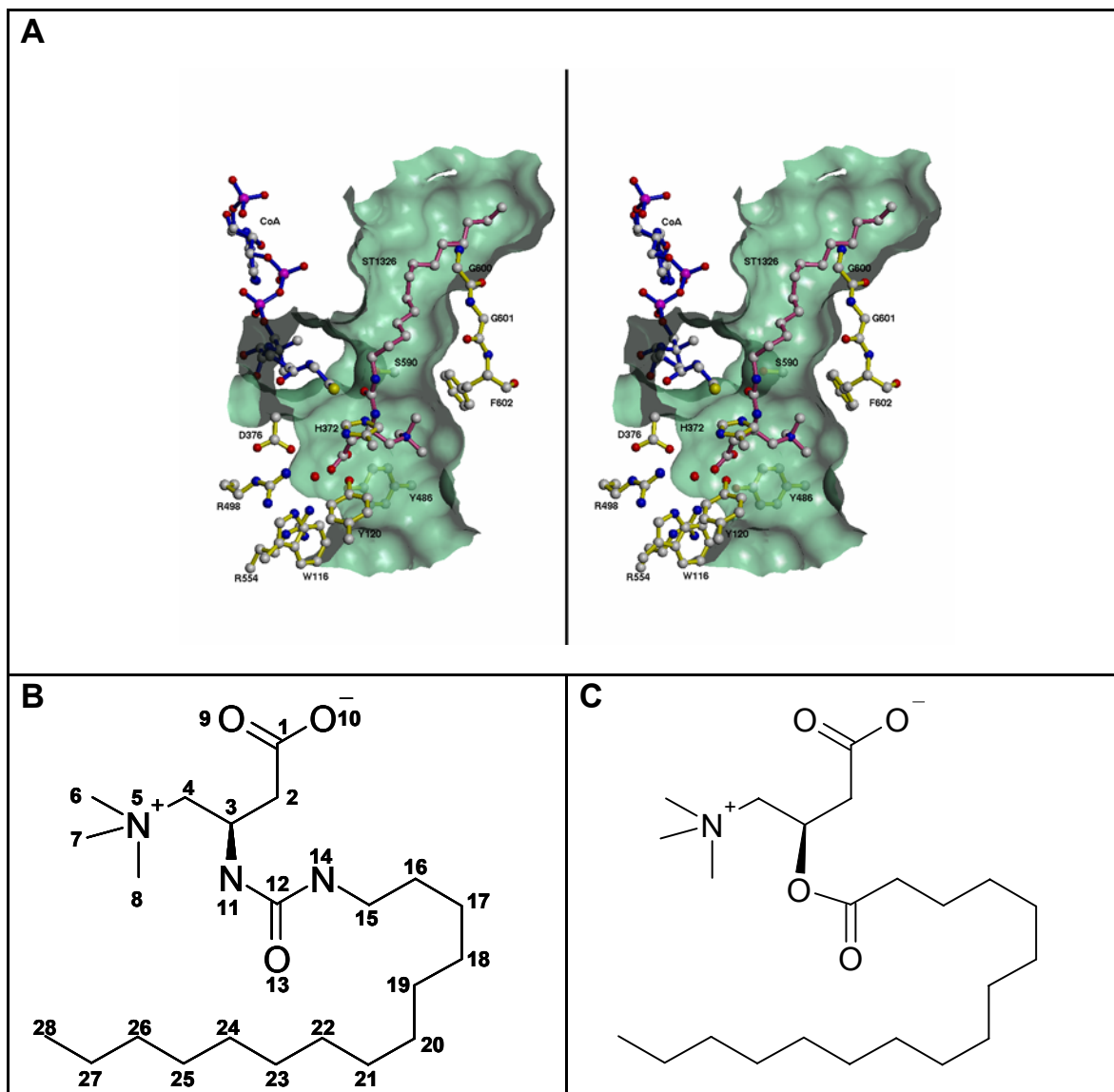


Figure 3.3.4-1: **A**, stereo figure (generated with MOLOC; GERBER, 1992) of the tripartite active site tunnel with bound ST1326 viewed perpendicular to the domain interface. Key active site residues are depicted in yellow. The co-crystallized ST1326 is shown in pink, a CoA molecule (blue) was modeled based on the CoA coordinates from the CrAT-CoA complex structure (PDB code 1t7q). **B**, Fischer projection of ST1326 with atom numbering as used in the text. **C**, Fischer projection of palmitoyl carnitine, the natural substrate of CPT-2.

The hydrophilic aminocarnitine head group of ST1326 is tightly bound in a hydrogen-bond network. The catalytic base His 372 forms a hydrogen bond with the amino-nitrogen (N11) of ST1326, which substitutes the ester oxygen of the native ligand palmitoylcarnitine.

Ser 590 of the Ser-Thr-Ser (STS) motif conserved among carnitine acyltransferases makes a hydrogen bond to the carbamoyl-oxygen (O13) of the ST1326, which confirms the role of this motif in positioning the substrate for catalysis to occur. Tyr 486, Ser 488 and Thr 499 of the carboxy-terminal domain are directly hydrogen-bonded to the carboxyl oxygens (O9 and O10) of ST1326. Hydrogen bonds to the guanidinium group of Arg 554 further stabilize the orientation of Tyr 486 and Thr 499. Residues Trp 116, Tyr 120 and Asp 376 of the amino-terminal domain fix a conserved water molecule that interacts with the carboxy group of ST1326 (Figure 3.3.4-1). Arg 498 forms a strong hydrogen bond with the side chain of Asp 376 and its guanidinium group interacts with the main chain carbonyl oxygen of Ser 373 in the catalytic loop, thereby positioning the active site residues in a position ideal for catalysis. The positively charged tertiary amine of ST1326 is stabilized by cation- π interactions with the conserved Phe 602.

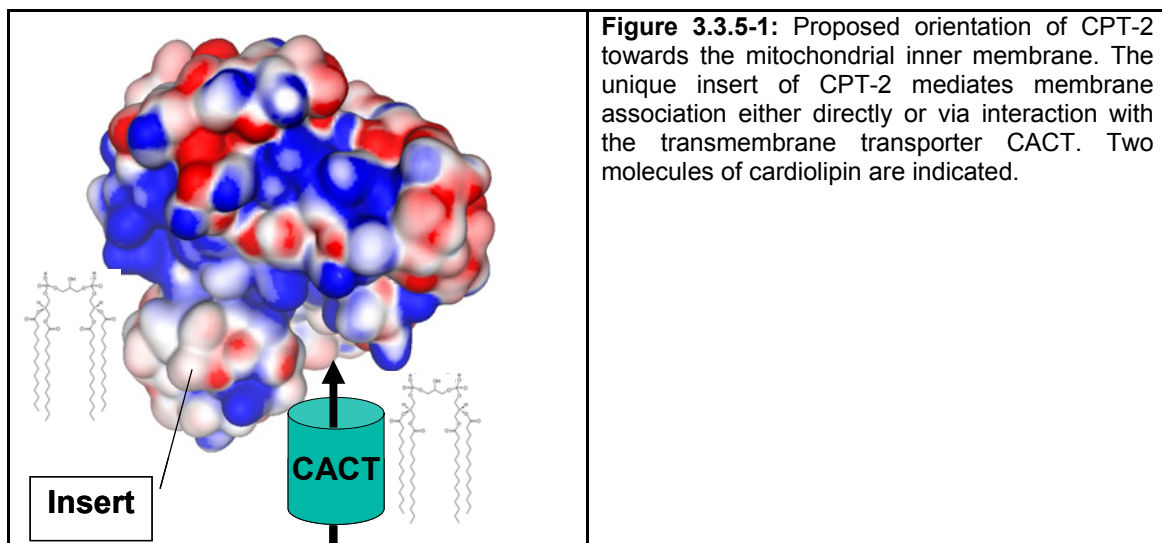
The hydrophobic tunnel that accommodates the aliphatic tetradecanoyl tail of ST1326 is lined by residues of β -strands 1 and 16, which form an anti-parallel β -sheet at the domain interface, and the two carboxy-terminal β -strands 17 and 18. A simulated annealing *fofc* omit map contoured at 2σ shows clear continuous electron density for the ligand ST1326 bound to the active site (Figure 3.3.3-1). The β -strands forming the hydrophobic acyl-tunnel are moved apart in order to make room for the extended hydrophobic tail of the substrate analog ST1326 compared to the closed arrangement in CrAT and CrOT (PDB codes 1ndb, 1t7n and 1xl8). The glycine residue Gly 600, at a position where bulkier residues are found in CrAT (Met 564) and CrOT (Gln 552), allows binding of LCFA carnitine-derivatives in CPT-2, thereby determining substrate specificity. Glu 487 and Glu 500 of CPT-2, which are conserved throughout the carnitine acyltransferases, have been implicated in substrate binding and catalysis by means of mutational analysis (ZHENG *et al.*, 2002). The crystal structure of CPT-2 reveals that Glu 487 is indeed located in the part of the active site tunnel that accommodates the (modeled) CoA. Glu 487 and the highly conserved Asp 464 form a negatively charged patch that is probably required for guiding substrates to the active site. The side chain of Glu 500 interacts with the main chain of conserved Arg 554, which is a crucial component of the hydrogen bond network required for binding the carnitine moiety of acyltransferase substrates.

The side chains of Tyr 120 and the catalytic His 372 have very weak electron density in both the uninhibited structures, but are both well defined in the structure of the ST1326 complex. Significant electron density in the final *fofc* map of the 1.6 Å high resolution apo structure indicated the presence of a fortuitous ligand in the acyl-tunnel of both rCPT-2 molecules in the asymmetric unit (data not shown). This ligand shows the same binding mode as the alkyl-moiety of ST1326 and was interpreted as a C16 aliphatic chain which may be part of a palmitate molecule from the bacterial host metabolism. Those residues in the active site that interact with the hydrophilic aminocarnitine head group of ST1326, as well as Ser 590, are moved slightly away from the ligand binding site in the uninhibited structures, but the overall shape of the active site tunnel is preformed in the uninhibited enzyme.

3.3.5 Membrane association

After cleavage of the amino-terminal mitochondrial targeting sequence, the mature CPT-2 protein is localized to the matrix site of the mitochondrial inner membrane (MIM; RAMSEY *et al.*, 2001). A model for membrane association of CPT-2 had been proposed (WIESER *et al.*, 2003) that predicts an α -helix (Asp 464 to Y479) inserted into the MIM inner leaf. The secondary structure has been predicted correctly (α 21) but the crystal structure of rCPT-2 shows this helix to be an integral component of the carboxy-terminal domain that is not exposed to the surface to be accessible for membrane binding. Structural alignment of the amino acid sequence of rCPT-2 with other acyltransferases clearly accentuates the presence of a unique 30 amino acid insert in rCPT-2 comprising residues Asn 179 to Asn 208 (Figure 3.3.2-1). These residues form a pair of anti-parallel helices (α 9 and α 10) that protrude from the catalytic core in the vicinity of both the amino terminus and the CoA-tunnel leading to the center of the active site (Figure 3.3.3-1). Helix α 9 is clearly amphipathic. It carries two large hydrophobic residues, Phe 188 and Phe 194, opposed to the three positively charged residues Lys 189, Arg 190 and Arg 194. Helix α 10 is predominantly hydrophobic. As CrAT and CrOT lack the insert and are soluble proteins, the insert most likely confers the membrane association of CPT-2. This notion is supported by electron density that indicates the presence of a β OG detergent molecule interacting with Val 195, Leu 199 and Tyr 202 of helix α 10 in chain B of the high (1.6Å) resolution rat CPT-2 structure (data not shown).

A second means for membrane localization by the insert could be the recruitment of CPT-2 to the membrane by direct interaction with CACT. A representation of the charge distribution on the surface of rCPT-2 reveals an excess of positive charges in the vicinity of the largely apolar insert and the entry of the CoA-tunnel (Figure 3.3.3-1). Like other integral membrane proteins, CACT is known to require the negatively charged mitochondrial lipid cardiolipin for activity (reviewed in RUBIO-GOZALBO *et al.*, 2004; PALSDOTTIR and HUNTE, 2004). The positively charged and oblate surface of CPT-2 facing the membrane would be ideally suited for interaction with cardiolipin molecules that surround CACT. With the insert bound to CACT the CoA-tunnel would be oriented perpendicular to the membrane, which would allow direct channeling of acylcarnitine substrates from CACT into the active site of CPT-2. As the acyl-tunnel does not open to the surface in CrAT and CrOT it seems reasonable that the substrates of carnitine palmitoyltransferases enter the active site via the CoA-tunnel. This mechanism for membrane recruitment of CPT-2 fully supports the observation that acylcarnitine esters transported into the mitochondrial matrix by CACT do not equilibrate with the bulk acylcarnitine pool in the mitochondrial matrix (MURTHY and PANDE, 1987; reviewed in ZAMMIT, 1999B). Physical association of CACT and CPT-2 would allow the carnitine released by CPT-2 to be transported back into the cytosol by CACT, whereas the newly formed acyl-CoA esters are directed towards β -oxidation. CPT-2 has been copurified with enzymes of the β -oxidation (KERNER and BIEBER, 1990). Therefore, CACT and CPT-2 form a microenvironment for efficient substrate channeling (Figure 3.3.5-1).



The alpha carbon of Asp 32, the first ordered amino-terminal residue of the CPT-2 structure, is situated in the vicinity of helix α 10 of the insert. His 44 of the amino-terminus directly interacts with the main chain carbonyl oxygens of Ile 192 and Val 195. Therefore, the amino-terminus of rCPT-2 is situated in proximity to the insert. These observations also argue for the insert mediating membrane localization, because all CPT-1 isoforms have an amino-terminal domain with two transmembrane segments (MCGARRY and BROWN, 1997; RAMSEY *et al.*, 2001; PRICE *et al.*, 2002).

3.3.6 CPT-2 deficiency

The clinically heterogeneous disease CPT-2 deficiency is caused by various mutations in the CPT-2 gene and is inherited in an autosomal recessive manner (BONNEFONT *et al.*, 1999 and 2004). Two different manifestations of the disorder can be distinguished based on the time of onset, *i.e.*, the early onset (neonatal or infantile) and the more frequent adult form of CPT-2 deficiency. The early onset form is characterized by a severe symptomatology including cardiomyopathy and hypoketotic hypoglycemia and has been linked to acute liver failure in sudden infant death syndrome (DEMAUGRE *et al.*, 1991). Clinical signs of adult CPT-2 deficiency are recurrent myalgia and myoglobinuria in response to fasting and exercise.

More than 30 point mutations in the coding region for CPT-2 leading to single amino acid exchanges in the enzyme have been identified (Table 3.3.6-1 and Figure 3.3.6-1; BONNEFONT *et al.*, 1999; THUILLIER *et al.*, 2003), in addition to deletions/ insertions causing frame shifts or truncation of the protein.

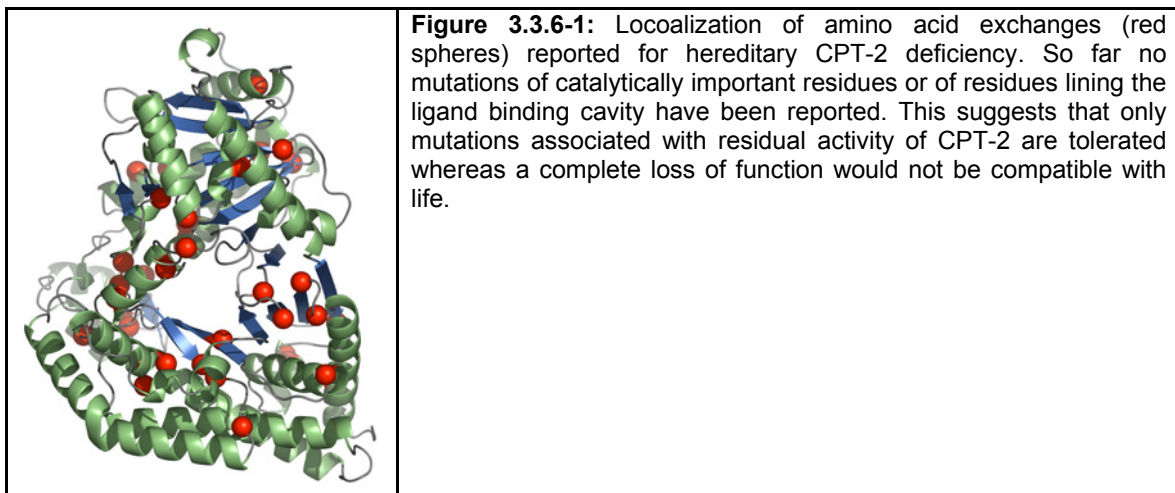
Whereas deletions/ insertions in the CPT-2 gene inevitably lead to a severe neonatal presentation of CPT-2 deficiency by loss of CPT-2 function, a graduated correlation of genotype and severity of clinical phenotype becomes obvious for those missense mutations that have been described in a homozygous state (Table 3.3.6-1). An exception to this correlation is the mutation of Arg 631 to cysteine, which has been identified in homozygous patients both with the adult as well as with the infantile form of CPT-2 deficiency. The crystal structure of rCPT-2 allows mapping and interpretation of the effects of the described mutations (summarized in Table 3.3.6-1). Most (60 %) cases of adult CPT-2 deficiency are associated with a mutation Ser 113 to leucine (TARONI *et al.*, 1993). Ser 113 is located at the amino-terminus of helix α 5 close to the

domain interface. Mutation of Ser 113 residue to a larger, hydrophobic Leu alters the interaction with the neighboring Phe 117. This changes the position and environment of the catalytically important residues Trp 116 and Arg 498, rendering the enzyme less active.

Category	Mutation	Clinical phenotype	Conservation		
			CPT-1	CrAT	CrOT
Substrate binding	S113L	A			
	Y120C				
	E174K	A			
	E454X			D	
	E487K				
I502T			V		V
Structure/ domain contact of amino-terminus residues D32 to S110	P50H	A			
	L72F		(M/B)		
	R161W	A			
	K164X		R or H		
Amino-terminal domain	R124Q/R124X				
	N146T				
	R151Q	I			
	P227L	I			
	K274M				
	Y290X				
	R296Q/R296X				
	D328G	I			
	R382K	I		E	E
F383Y	I		H		
Domain interface	D213G				
	M214T				
	P604S				
	Y628S	I			
Carboxy-terminal domain	F448L				
	Y479F				
	R503C				
	G549D				
	Q550R				
	D553N				
	D608H				
	R631C	I/A		(B)	
			(L/M)		
Insert	Y210D				
Internal salt bridges affected by mutations (bold face) described for CPT-2 deficiency					
R124 - D232			R382 - E174		
R161 - D390			R503 - D553		
R296 - D353			R631 - D608		
R350 - D328			D608 - H584		

Table 3.3.6-1: Residues mutated in human CPT-2 deficiency. All the affected residues are conserved between rat and human CPT-2, residue numbering for the human and rat isoforms of CPT-2 are identical. Homozygous mutations labeled A are associated with the late onset, adult form of CPT-2 deficiency, those labeled I with the early onset, infantile phenotype. Residues that are conserved in other carnitine acyltransferases are highlighted by a gray box. B, L or M in parentheses indicate conservation limited to brain, liver or muscle CPT-1, respectively. Conservative amino acid exchanges are indicated with one letter code abbreviations.

Asp 213 and Glu 487 are affected by naturally occurring mutations and have been determined to be important for CPT-2 function by biochemical analyses (ZHENG *et al.*, 2002; LIU *et al.*, 2005). Asp 213 is located in a loop between β 3 and α 10 of rCPT-2 and aligns with a cysteine conserved in all human CPT-1 isoforms. Mutation of this cysteine to Ala fully abolishes enzyme activity in human M-CPT-1, indicating that this position is crucial for structural integrity in all CPT isoforms. In CPT-2 the side chain of Asp 213 makes a strong interaction with the main chain nitrogen of His 496. This is important for the positioning Arg 498 and Arg 499 which are involved in substrate binding. Mutation of Glu 487 in β 13 to aspartic acid leads to an almost complete loss of CPT-2 activity. This mutation could interfere with CoA binding as Glu 487 is part of the CoA-tunnel surface. From the rCPT-2 crystal structure it can be predicted that an aspartic acid at position 487 would form a strong hydrogen bond with the side chain of Thr 589 of the conserved STS motif, thereby distorting the geometry of the active site. A Glu 487 Lys exchange is one of 6 mutations identified in CPT-2 deficiency that cause disruption of internal salt bridges or hydrogen-bond interactions which are fully conserved in CPT-1, CrAT and CrOT (Table 3.3.6-1). A guanidinium nitrogen of Arg 296 makes a strong (2.7 Å) contact with a side chain oxygen of Asp 353, which is conserved in carnitine acyltransferases. The equivalent residue in M-CPT-1, Asp 454, has been proposed to be part of a catalytic triad (LIU *et al.*, 2005), whereas the CPT-2 crystal structure implicates this residue to form a conserved salt bridge. None of the reported mutants identified in CPT-2 deficiency is located in the insert mediating membrane localization, although they are distributed uniformly in the rest of the structure (Figure 3.3.6-1).



4 Discussion

4.1 Insulin receptor

Although the GST-tagged insulin (and IGF-1) receptor kinase domains proved to be valuable tools for the examination of the reaction kinetics of these enzymes (BAER *et al.*, 2001), they were not adequate for solving the structures of the respective dimeric kinase domains. The insufficient crystallization behavior of the constructs containing the entire intracellular domains might be attributed to flexibility of the linker regions as well as to high mobility of the amino- (juxtamembrane domain) and carboxy termini. Based on the results of activity assays, DLS and mass spectrometry analyses, aberrant folding, aggregation or covalent modification could be ruled out as factors that hindered crystallization. The formation of tetramers of GST observed with AUC ($\leq 10\%$ in supernatant mass distribution at $5\ \mu\text{M}$ GST) is apparently negligible as free GST and various fusion proteins were reported to crystallize readily (ZHAN *et al.*, 2001). In the case of the GST-tagged core kinases, instability of these constructs was shown to interfere with proper crystallization (Rufer *et al.*, 2005). Therefore, future attempts to stabilize and crystallize the dimeric kinase domains of IR (and IGF1-R) may comprise the formation of tyrosine phosphorylation-dependent complexes with high affinity effector or regulatory proteins. The structure of the IR core kinase domain in complex with the SH2 domain of APS (HU *et al.*, 2003) as well as two PDB entries awaiting release of coordinates showing complexes with downstream signaling proteins (Table 4.1-1) emphasize in principle the feasibility of this approach.

PDB code	Author	Title
2b4s	LI <i>et al.</i> , 2005	Crystal structure of a complex between PTP1B and the insulin receptor tyrosine kinase
2auh	DEPETRIS <i>et al.</i> , 2005	Crystal structure of the Grb14 BPS region in complex with the insulin receptor tyrosine kinase

Table 4.1-1: Stoichiometric complexes of the IR core kinase domain with effector proteins whose coordinates are deposited but not yet publically available. An α -helix mediated dimer of IRK is visible in the asymmetric unit of IRK • PTP1B structure by LI *et al.* (2005), but the kinase domains are not aligned in an orientation compatible with autophosphorylation.

Direct interaction of the IR with the SH2 domains of the p85 regulatory subunits of PI3K and the PTB domain of IRS-1 has been shown *in vitro* and in cell-based assays (SANCHEZ-MARGALET *et al.*, 1995; BACKER *et al.*, 1997; SUNG *et al.*, 1998, and

references therein). These interactions could potentially be exploited for binding and stabilizing the juxtamembrane and carboxy-terminal domains of GST-IRTK, respectively. Moreover, interaction of the intrinsically dimeric 14-3-3 γ protein with GST-IGFK phosphorylated on its carboxy-terminal serine residues (LIU *et al.*, 1995; XIAO *et al.*, 1995; PARVARESCH *et al.*, 2002), could provide a means to prepare complexes amenable to crystallization. SAXS studies have been successfully used by other groups in order to characterize the linker peptide of GST-fusion proteins and their overall topology (PETOUKHOV *et al.*, 2002). Therefore, optimization of the linker peptide of GST-IRTK Δ NT/CT (GST-IRK) in order to enhance the stability while retaining the enzymatic activity and fitting the existing structures of GST and IRK into low resolution SAXS envelopes could advance the understanding of IRTK dimerization. Exchange of GST with the FK506-binding protein 12, which forms dimers upon binding of the ligand FK1012 (Keenan *et al.*, 1998; ROLLINS *et al.*, 2000; GAZDOIU *et al.*, 2005), would allow to investigate a different dimerization motif. This chemically induced dimerization has been shown to yield active fusion proteins of IR or platelet-derived growth factor receptor (PDGFR) constructs with FK506 (YANG *et al.*, 1998).

Examination of the concentration-dependent sedimentation equilibria of unphosphorylated, apo His₆-IRTK by AUC revealed that the full-length intracellular domain of the IR has an intrinsic capability to form dimers in solution with an EC₅₀ = 11.8 μ M. As the core kinase construct is less active than the full-length intracellular domain of the IR (THIEBACH, 2003, diploma thesis, University of Cologne) and mutual substrate recognition is a prerequisite for trans-autophosphorylation, it is reasonable to argue that the juxtamembrane and carboxy-terminal domains of IRTK are important for productive dimerization. This hypothesis could be verified by performing AUC analyses with the core kinase constructs or constructs lacking either the amino- or carboxy-terminal domain. Dimers of IRTK need not to be symmetrical, *i.e.*, possess an internal two-fold axis, but could consist of one molecule of IRTK in an enzyme conformation and another in a substrate conformation, assuming intra-dimer phosphorylation. Along these lines, the formation of both symmetric and asymmetric dimers have been suggested for the epidermal growth factor receptor (EGFR; GROENEN *et al.*, 1997) and it has been shown for the EGFR that a basic 13 amino acid peptide (aa 645-657) in the juxtamembrane region is crucial for dimerization of its intracellular domain (AIFA *et al.*,

2005). The available crystal structures of the monomeric kinase domain of the EGFR (STAMOS *et al.*, 2002; PDB accession codes 1m14 and 1m17) do not contain this putative dimerization motif. As the IR switches from auto- to substrate phosphorylation under physiological conditions, it would be interesting to investigate if the activity states are correlated with distinct dimers (as implied by LI *et al.*, 2005) or if the kinase domain becomes independent of dimerization upon full activation.

Limited proteolysis and AUC studies with His₆_IRTK and the Merck1 compound (RO0716631, L-783,281) showed for the first time that this compound indeed alters the conformation (as opposed to other IR agonists) and promotes the dimerization of His₆-IRTK. However, the Merck and Telik compounds were also observed to cause aggregation of His₆_IRTK, tend to form particles/micelles and display promiscuous protein binding. This rendered these compounds unusable for attempts to crystallize dimeric IRTK and constitutes a significant disadvantage for the use of these compounds as reference IR activators/sensitizers in the drug discovery process. The use of detergents for solubilizing the holo IR in activity assays or inclusion of other proteinaceous assay components (*e.g.*, BSA, IR substrates) is likely to further complicate the distribution of free, soluble compound vs. compound particles and compound-protein complexes or mixed micelles with detergent molecules. A 50 % decrease in dimer formation of apo His₆_IRTK was observed in the presence of 1 % (w/v) DMSO under the conditions examined by AUC. This effect of DMSO, which was indispensable for solubilization of the Merck and Telik compounds, interferes with dimer-promoting activity of the compounds. AUC analysis accompanied by activity assays would provide a means to identify solvents that are inert with regard to dimerization of His₆_IRTK. Furthermore, examination of the interaction of the Merck and Telik compounds with full-length (IRTK) vs. truncated (IRK) constructs would allow to map the actual site of interaction.

As attempts to crystallize dimeric IRTK (or IGFK) using the established constructs failed, hydrogen/deuterium exchange coupled with mass spectrometry could provide a valuable tool for mapping the interface of the IRTK dimer and planning novel constructs for crystallization (LANMAN and PREVILEGE, 2004; PANTAZATOS *et al.*, 2004). With the same technique conformational changes upon ligand binding and sites on the

surface of IRTK that interact with small-molecule ligands might be identified (GARCIA *et al.*, 2004).

4.2 AMPK

Crystals of constructs comprising the kinase domain of AMPK including various parts of the putative auto-inhibitory sequence as well as the intact heterotrimer were obtained. Despite setting up over 36,000 individual crystallization drops containing 20 different AMPK constructs, isoform combinations and mutants thereof in combination with app. 750 precipitant solutions, these crystals could not be optimized to meet the diffraction quality needed for structure determination by X-ray crystallography. This is entirely in-line with the results communicated by other laboratories (D. Alessi, D. Carling, G. Hardie, B. Kemp; 2nd Annual Upstate Cell Signaling Symposium on "Implications of the LKB1 and AMPK Systems", 2005).

However, in two recent reports by POLEKHINA *et al.* (2005B) and RUDOLPH *et al.* (2005) the feasibility to obtain diffraction quality crystals of distinct domains of the mammalian and yeast AMPK heterotrimer, respectively, was demonstrated. Therefore, future attempts to crystallize AMPK (-constructs) should be expanded to screening alternative isoforms and AMPK orthologs from different species. Exchanges of exposed residues and deletion/ insertion of loops in these orthologs can be understood as complex surface mutations that might support crystallization. This approach can be combined with limited proteolysis of the AMPK heterotrimer in order to identify compact domains. As AMPK is conserved from yeast to man, the in-depth elucidation of the structural details of the allosteric activation for any ortholog is likely to advance the understanding of mammalian (and human) isoforms.

The SAXS studies on full-length, heterotrimeric AMPK clearly demonstrated that an equilibrium of different oligomeric species of the trimer exists. Characterization of conditions effecting this equilibrium and accumulation of a distinct oligomeric state is expected to improve the crystallization behavior.

In addition, chemical modification of the molecular surface by reductive methylation of lysine residues could provide a means to improve the formation of crystal contacts (RAYMENT, 1997; JBS Methylation Kit). This technique was evaluated with the construct AMPK_α2_1-339_D56A/R171E/T172D which crystallized best and most

reproducibly. While the protein was quantitatively precipitated by addition of ammonium sulfate, which is recommended for quenching unreacted alkyl-donor, the amino acids glycine and arginine were found to serve as efficacious substitutes for the quenching ammonium ion without adverse effects on AMPK stability. Therefore, investigation of the effect of reductive methylation on the crystallization behavior of different AMPK constructs can now be included in the optimization strategy.

Despite the phosphorylation of T172 by upstream kinases the effect of post-translational modification, *i.e.*, autophosphorylation and myristoylation of the β -subunit, on AMPK structure and function is so far inadequately defined. All experiments within this thesis assignment were conducted with unmodified protein. Preparation of homogeneously phosphorylated and/or myristoylated AMPK constructs (in combination with appropriate ligands) might allow to accumulate a discrete (active) conformation and, thereby, improve crystallization.

The generation of antibodies against flexible loops (as defined by proteolysis, D/H exchange and available structural information) would also provide a rational means for optimization of AMPK crystals. Co-crystallization with antibody fragments was demonstrated to enhance the crystallization of several proteins (KOVARI *et al.*, 1995).

4.3 CPT-2

The crystal structure of rCPT-2 in complex with ST1326 reveals the molecular details of protein-substrate interactions of a LCFA-specific acylcarnitine transferase. The key residues of the active site that form an extensive hydrogen network with the aminocarnitine-headgroup of ST1326 (or a physiological LCFA-acylcarnitine substrate) are fully conserved between rCPT-2 and the candidate diabetes drug-target L-CPT-1. The sequence alignment of rCPT-2 and human L-CPT-1 shows, that human L-CPT-1 contains an extended loop between β 15 and β 16, which forms part of the acyl tunnel, and human L-CPT-1 has discrete amino acid exchanges in the acyl-tunnel when compared to human and rat CPT-2. Therefore, the structure of rCPT-2 with bound ST1326 is valuable for guiding the development of novel drugs for the treatment of diabetes mellitus in terms of optimizing affinity and isoform specificity of pseudo substrates as inhibitors of human L-CPT-1.

Investigation of the tissue (liver) exposure and distribution of ST1326 as well as its capability to be transported into mitochondria by CACT are needed to elucidate the effect of this compound on inhibition of the ubiquitous CPT-2. Accumulation of ST1326 in hepatocytes or negligible transport via CACT would greatly increase the safety of ST1326.

The complete inhibition of the CPT system could potentially inflict symptoms of CPT-deficiency on diabetic patients. Therefore, it should be emphasized that downregulation rather than complete inhibition of the activity of L-CPT-1 in diabetic patients should be anticipated in order to restore their gluconeogenesis rate to normal levels.

The proposed mode of membrane association of CPT-2 via its unique insertion is in line with the observation that acylcarnitine esters are transported into the mitochondrial matrix by CACT and are directly conveyed to β -oxidation through CPT-2 (reviewed in Zammit, 1999B). Furthermore, the carnitine released from CPT-2 does not equilibrate with the mitochondrial carnitine pool but is transported back into the cytosol by CACT. This also strongly supports the hypothesis that CPT-2 physically interacts with CACT. Docking the crystal structure of rCPT-2 to the molecular model of CACT (TONAZZI *et al.*, 2005) may be useful to verify a possible direct interaction of CPT-2 and CACT.

The crystal structure of CPT-2 allows the precise allocation of mutants identified in CPT-2 deficiency. The absence of mutations of active site residues in CPT-2 deficiency emphasizes the essential function of CPT-2 for fatty acid metabolism as a complete loss of function might not be compatible with life. Determining the correlation of the effect of an amino acid exchange to CPT-2 function (*i.e.*, its residual activity) could provide a means to link a given genotype to the severity of the corresponding clinical phenotype. CPT-2 deficiency can be detected in a newborn-screening. In the case of a positive diagnosis a correlation of structure and function could help to suggest appropriate dietary measures to ameliorate the clinical symptoms.

5 Materials and Methods

5.1 Materials

5.1.1 Chemicals

All chemicals used for the preparation of media, buffers and solutions for expression, purification, characterization and crystallization were of the highest purity grade commercially available and purchased from AppliChem (via Axon Lab AG, Baden-Dättwil, CH), Bio-Rad Laboratories (Reinach, CH), Fluka (Buchs, CH), Calbiochem/Novabiochem/Novagen (Merck Biosciences, via VWR International Life Science, Lucerne, CH), Jena Bioscience (Jena, D), Hampton Research (Aliso Viejo, CA, USA), Molecular Dimensions (Soham, UK), Pierce (Lausanne, CH), Roche Diagnostics (Rotkreuz, CH) Sigma-Aldrich (Buchs, CH) and Upstate (via Biomol, Hamburg, D).

5.1.2 Enzymes

DNase I	Roche Diagnostics, Rotkreuz, CH
Lysozyme	Serva, Heidelberg, D
<i>Pfu</i> DNA-Polymerase	Stratagene, LaJolla, CA, USA
Restriction Enzymes	New England Biolabs, via BioConcept, Allschwil, CH
Shrimp Alkaline Phosphatase	USB, via GE Healthcare, Otelfingen, CH
T4 DNA Ligase	New England Biolabs, via BioConcept, Allschwil, CH
Trypsin (mod. sequencing grade)	Roche Diagnostics, Rotkreuz, CH
Thrombin	GE Healthcare, Otelfingen, CH

5.1.3 Kits

BigDye Terminator Sequencing Kit	Applied Biosystems, Foster City, CA, USA
DyeEx™ 2.0 Spin Kit	Qiagen, Hombrechtikon, CH
HiSpeed® Plasmid Maxi Kit	Qiagen, Hombrechtikon, CH
NucleoSpin® Extract II	Macherey-Nagel, Oensingen, CH
QuickChange® Multi	Stratagene, LaJolla, CA, USA
JBS Methylation	Jena Bioscience, Jena, D
S.N.A.P. MiniPrep Kit	Invitrogen, Basel, CH

5.1.4 Specialty chemicals

[γ - ³² P]-Adenosin-5'-triphosphate, 5000 Ci/mmol	NEN, Zevenem, Belgien
Sypro® Orange, 5000X concentrate in DMSO	Molecular Probes, Eugene, OR, USA

5.1.5 Bacterial strains (chemically competent *E. coli*)

Cloning, plasmid propagation: DH10B (TOP10®)	Invitrogen, Basel, CH
Expression: BI21(DE3) (One Shot®)	Stratagene, La Jolla, CA, USA,
Selenomethionine labelling: B834(DE3)	Novagen (via VWR International Life Science, Lucerne, CH)

5.1.6 Consumable supplies and hardware

AbiPrism™ 310 Genetic Analyzer	Perkin Elmer, Boston, MA, USA
Absorption Chromatography	
- Cary 100 Bio UV-Visible Spectroph.	Varian, Zug, CH
- NanoDrop® ND-1000 Spectroph.	Witec AG, Littau, CH
Alphalmager™ 340	Alpha Innotech, via Witec AG, Littau, CH
Cell disruptor Basic Z Model	Constant Systems, Warwick, UK
Centrifuges	Sorvall/Heracus, via Kendro, Zurich, CH; Kontron Instruments, via Hemotec, Gelterkinden, CH; Eppendorf, via Dr. Vaudeaux AG, Schönenbuch, CH
Chromatography	
- Columns, Resins	GE Healthcare, Otelfingen, CH Qiagen, Hombrechtikon, CH
- Static light scattering	Wyatt, Santa Barbara, CA, USA
Crystallization tools & plates	Hampton Research, Aliso Viejo, CA, USA; Greiner Bio-One, via Huber AG, Reinach, CH
Crystallography	
- Rotating anode FR591	Nonius, via Bruker AXS, Karlsruhe, D
- Confocal Max-Flux Optics™	Osmic, Auburn Hills, MI, USA
- dtb 345 image plate detector	MarResearch, Hamburg, D
Filtration	Millipore, Bedford, MA, USA
Dynamic Light Scattering	DynaPro™ (Protein Solutions™) via Wyatt, Santa Barbara, CA, USA
Incubators	Kühner AG, Birsfelden, CH; Sanyo, via Labtech Services AG, Wohlen, CH
T3000 Thermocycler for PCR	Biometra, Goettingen, D
Precast electrophoresis gels	Invitrogen, Basel, CH
Robotic Crystallization Systems	
- Freedom Evo	Tecan, Zurich, CH
- Impax I-5	Douglas Instruments, Hungerford, UK
- Topaz FID™ Crystallizer	Fluidigm, San Francisco, CA, USA
Scintillation Counter	Beckman-Coulter, Munich
Spectra/Por® Dialysis Membrane	Spectrum Lab., via Socochem, Lausanne, CH

5.2 Methods

5.2.1 Molecular biology methods

5.2.1.1 Transformation of chemically competent *E. coli*

- 100 μ l *E. coli* suspension is thawed on ice
- addition of 1 μ l of plasmid preparation ($c > 1$ ng/ μ l)
- incubation on ice for 20 min
- heat shock at 42°C for 30 s
- incubation on ice for 2 min
- addition of 250 μ l SOC-AMP⁻- media
- incubation in shaker for 1 h at 37°C/ 220 rpm
- aliquots > 5 μ l on LB-Amp⁺-agar
- incubation of plates at 37°C until colonies visible

5.2.1.2 PCR for sequencing

1. PCR:
 - 5 μ l Plasmid stock
 - 5 μ l mod. dNTP BigDye® Terminator v1.1 Cycle Sequencing Kit
 - 1 μ l Sequencing primer (T7P, α 1, α 2, T7T; 4 tubes)
 - + 9 μ l H₂O
 - 20 μ l

Sequencing PCR Programs				
Primer	α 1 / α 2 AMPK		T7Promotor / T7Terminator	
Steps	T [°C]	t [min]	T [°C]	t [min]
1X	95	2	95	2
Cycle 30X	95	0.5	95	0.5
	45	0.5	50	0.5
	60	4	60	4

2. Processing of PCR-samples over EDGE BIO-SYSTEMS Centriflex Gel Filtration Cartridge
 - resuspension of column resin with 400 μ l H₂O
 - centrifugation 2 min/ 700 g
 - discard flow-through
 - centrifugation 2 min/ 700 g
 - column into sterile tube
 - application of 20 μ l PCR-sample
 - centrifugation 2 min/ 700 g
 - flow-through is lyophilized in Speedvac for 15 min/ 60°C
 - addition of 17 μ l Template Suppression Reagent (Applied Biosystems, Foster City, CA, USA)
 - 2 min at 95°C
 - transfer of sample into sequencing tubes

5.2.1.3 Cloning of AMPK point mutations

Starting with the vector pET-15b_AMPK_α2_1-339_T172D the triple mutant AMPK_α2_1-339_D56A/R171E/T172D was generated by site-directed mutagenesis using the QuickChange® Multi kit (Stratagene) according to the manufacturer's specifications. The annealing temperature was chosen app. 5°C below the lowest primer melting point and strand synthesis was performed at 65°C for 3 min/kBp (30 cycles plus a 15 min final completion step at 65°). The three point mutations were introduced into the sequences coding for AMPK_α2_1-301_wt and AMPK_α2_1-312_wt by restriction fragment cloning.

1. Restriction cut of vectors, 4 h at 37°C

20 µl pET-15b- AMPK_α2_1-339_D56A/R171E/T172D
 3 µl 10X restriction enzyme buffer (#4)
 1 µl NdeI (CA/TATG)
 1 µl PmeI (GTTT/AAAC)
+ 5 µl 6X BSA
 30 µl ⇒ Insert

20 µl pET-15b- AMPK_α2_1-301_wt
 3 µl 10X restriction enzyme buffer (#4)
 1 µl NdeI (CA/TATG)
 1 µl PmeI (GTTT/AAAC)
+ 5 µl 6X BSA
 30 µl ⇒ Vector 301

20 µl pET-15b- AMPK_α2_1-312_wt
 3 µl 10X restriction enzyme buffer (#4)
 1 µl NdeI (CA/TATG)
 1 µl PmeI (GTTT/AAAC)
+ 5 µl 6X BSA
 30 µl ⇒ Vector 312

2. Preparative agarose-gel electrophoresis

The fragments released during the restriction cut were separated by electrophoresis of the entire reaction (30 µl) in a 1 % (w/v) agarose-gel, detected under UV-light and isolated by cutting out of the band with a scalpel.

3. Extraction of DNA from agarose-gel with NucleoSpin®Extract II kit (Machery-Nagel)

4. Dephosphorylation of cut and purified vectors with Shrimp Alkaline Phosphatase (SAP)

48 μ l DNA solution (eluate of step 3)
6 μ l 10X SAP-buffer
+ 6 μ l 1:10 SAP (in SAP dilution buffer)
60 μ l, inkubation 1 h at 37°C, thereafter inaktivierung of SAP 15 min at 65°C

5. 10 μ l of the purified and dephosphorylated fragments were quantified via analytical agarose-gel electrophoresis with size and molecular mass markers.

6. Ligation was performed for 1 h at RT followed 14 h at 16°C

9 μ l Insert
3 μ l Vector 1-301
2 μ l 10X T4-buffer
1 μ l T4-ligase
+ 5 μ l H₂O
20 μ l \Rightarrow AMPK_α2_1-301_D56A/R171E/T172D

9 μ l Insert
3 μ l Vector 1-312
2 μ l 10X T4-buffer
1 μ l T4-ligase (NEB)
+ 5 μ l H₂O
20 μ l \Rightarrow AMPK_α2_1-312_D56A/R171E/T172D

3 μ l Vector 1-302
2 μ l 10X T4-buffer
1 μ l T4-ligase (NEB)
+14 μ l H₂O
20 μ l, control

3 μ l Vector 1-312
2 μ l 10X T4-buffer
1 μ l T4-ligase (NEB)
+14 μ l H₂O
20 μ l, control

7. Transformation of 3 μ l of the ligation reaction

5.2.2 Expression and purification of GST-fusion proteins

Pellets and lysates from *Sf9*-cell expression were prepared by M. Gompert and K. Baer (Klein group, University of Cologne; BAER et al., 2001). Pellets were processed according to the following protocol:

- Lysis buffer: 50 mM Tris/HCl pH 7.5
0.25 M Sucrose
4 Tbs./ 100 ml Roche Complete Protease inhibitor (+EDTA)
5 mM DIFP
1 mM DTT
- frozen pellets are thawed, resuspended, homogenized in lysis buffer (10^8 cells/ 10 ml)
- cells disruption with ultrasound 5 X 5 s (interval 0.5 s, 80 % power)
- addition of Triton-X-100 to 1 % (w/v) f.c., solubilization for 30 min at 4°C
- centrifugation for 10 min at 10,000 g/ 4°C
- preparative ultracentrifugation for 1h at 150,000 g/ 4°C

A two step protocol yielded GST-fusion proteins devoid of any covalent modification. DTT was used during binding of the fusion proteins because decreased affinity was observed with TCEP. The GST-affinity chromatography (25 ml GSH-sepharose FF, GE Healthcare) was carried out in the cold room using a peristaltic pump for sample application.

Purification Step	Buffer
GST-affinity chromatography at 4°C	A Equilibration DTT 50 mM Tris/HCl pH 7.5 4 Tbs./l RocheComplete (+EDTA) 2 mM DTT
	B Wash TCEP 50 mM Tris/HCl pH 7.5 4 Tbs./l RocheComplete (+EDTA) 2 mM TCEP
	C Wash High Salt 50 mM Tris/HCl pH 7.5 4 Tbs./l RocheComplete (+EDTA) 2 mM TCEP 1 M NaCl
	C Wash TCEP 50 mM Tris/HCl pH 7.5 4 Tbs./l RocheComplete (+EDTA) 2 mM TCEP
	D Elution GSH / TCEP 50 mM Tris/HCl pH 7.5 4 Tbs./l RocheComplete (+EDTA) 2 mM TCEP 20 mM GSH
SEC at 21°C	20 mM Tris/HCl pH 7.5 2 Tbs./l Roche Complete (+EDTA) 150 mM NaCl 0.02 % (w/v) NaN ₃ 2 mM TCEP

5.2.3 Expression and purification of AMPK constructs

The following constructs were purified with the protocol mentioned below:

- AMPK_α2_1-339_D56A/R171E/T172D and _wt
- AMPK_α2_1-326_D56A/R171E/T172D
- AMPK_α2_1-312_D56A/R171E/T172D
- AMPK_α2_1-301_D56A/R171E/T172D

For simplicity, the mutant combination D56A/R171/T172D is hereafter called „triple“.

Buffer adjustments for short constructs are indicated in red.

5.2.3.1 Expression

- inoculation of 4 X 1 l LB^{amp⁺} with 25 ml each of a over-night culture of *E. coli* BL21DE3 carrying a pET-15b vector with the relevant construct
- incubation at 30°C/ 230 rpm until A₆₀₀ = 0.45, then incubation at 20 °C/ 230 rpm until A₆₀₀ = 0,75
- induction with 0.5 mM f.c. IPTG, incubation at 20°C/ 230 rpm/ 20 h
- harvesting of cells by centrifugation at 5000 g/ 4°C, resuspension/ washing of cells in 5 ml/g buffer Ni-NTA A at 4°C, centrifugation at 5000 g/ 4°C, storage of pellet at -20 °C

5.2.3.2 Cell lysis

- resuspension and homogenization of cells in 3 ml/g buffer Ni-NTA A

Buffer Ni-NTA A		
AMPK_α2_1-339triple & wt AMPK_α2_1-326triple	AMPK_α2_1-312triple	AMPK_α2_1-301triple
50 mM TRIS/HCl pH 7,8 300 mM NaCl 2 mM TCEP 2 mM MgCl ₂	50 mM TRIS/HCl pH 7,8 300 mM NaCl 2 mM TCEP 2 mM MgCl ₂ 20 mM Imidazol 10 % (v/v) Glycerin	50 mM TRIS/HCl pH 7,8 300 mM NaCl 2 mM TCEP 2 mM MgCl ₂ 20 mM Imidazol 10 % (v/v) Glycerin
4 Tbs /100 ml RoComplete- EDTA 3 mg/100ml DNase I 5 mM DIFP	4 Tbs /100 ml RoComplete- EDTA 3 mg/100ml DNase I 5 mM DIFP	4 Tbs /100 ml RoComplete- EDTA 3 mg/100ml DNase I 5 mM DIFP

- cell disruption at 0.6 bar in continuous precessing disruptor
- centrifugation of flow-through at 30,000 g/ 4°C/ 45 min, filtration of supernatant through 0.2 µm Filter

5.2.3.3 Chromatography

IMAC on 25 ml Qiagen Ni²⁺-NTA resin

- Buffer B = Buffer A + 300 mM imidazole, no protease inhibitors
- sample is applied via sample pump at 4 ml/min, washing with buffer A until A₂₈₀ < 10, gradient of 0 % to 100% buffer B over 10 column volumes, 10 ml fractions

Thrombin cleavage of His₆-tag and dialysis

- 10 U Thrombin per 1 mg AMPK, ad 2.5 mM CaCl₂ f.c. from 50 mM stock solution and dialysis 16 h/ 4°C in MWCO 8000 tube in 5 l of:

AMPK_α2_1-339triple & wt AMPK_α2_1-326triple	AMPK_α2_1-312triple	AMPK_α2_1-301triple
18 h 50 mM TRIS/HCl pH 7,8 2 mM TCEP 2 mM MgCl ₂ 2,5 mM CaCl ₂	15 h 50 mM TRIS/HCl pH 7,8 2 mM TCEP 2 mM MgCl ₂ 2,5 mM CaCl ₂ 20 mM Imidazole	18 h 50 mM TRIS/HCl pH 7,8 2 mM TCEP 2 mM MgCl ₂ 2,5 mM CaCl ₂ 20 mM Imidazole
	3 h 50 mM TRIS/HCl pH 7,4 2 mM TCEP 2 mM MgCl ₂ 2,5 mM CaCl ₂ 20 mM Imidazole	

Anion-IEX on Resource Q Superflow (30 ml)

- AMPK_α2_1-339_D56A/R171E/T172D & wt; AMPK_α2_1-326triple
- AMPK_α2_1-312_D56A/R171E/T172D

	AMPK_α2_1-339triple & wt AMPK_α2_1-326triple	AMPK_α2_1-312triple
Puffer A	50 mM TRIS/HCl pH 7,8 2 mM TCEP 2 mM MgCl ₂	50 mM TRIS/HCl pH 7,4 2 mM TCEP 2 mM MgCl ₂
Puffer B	50 mM TRIS/HCl pH 7,8 2 mM TCEP 2 mM MgCl ₂ 500 mM NaCl	50 mM TRIS/HCl pH 7,4 2 mM TCEP 2 mM MgCl ₂ 500 mM NaCl

- application of sample from dialysis at 2.5 ml/min, chromatography at 4 ml/min

1. Wash 1 CV with 0% B
2. Wash 4 CV with 10 % B 120 ml, 30 min
3. Gradient to 50 % Buffer IEX B over 15 SV 450 ml, 115 min
4. Gradient to 100 % Buffer IEX B over 4 SV 140 ml, 35 min

- the united elution fractions are concentrated in Amicon stirring cell (MWCO 10,000)

HIC on Phenylspharose HP (5 ml)

- AMPK_α2_1-301_D56A/R171E/T172D

- adjustment of sample from dialysis to 1 M (NH₄)SO₄ (4 M stock solution)

	AMPK_α2_1-301triple
Puffer A	50 mM TRIS/HCl pH 7,8 2 mM TCEP 2 mM MgCl ₂ 20 mM Imidazol 1 M (NH ₄)SO ₄
Puffer B	50 mM TRIS/HCl pH 7,8 2 mM TCEP 2 mM MgCl ₂ 20 mM Imidazol

Gelfiltration (Biosec)

- centrifugation 20,000 g/ 4°C/ 20 min before injection

AMPK_α2_1-339triple & wt AMPK_α2_1-326triple	AMPK_α2_1-312triple	AMPK_α2_1-301triple
50 mM TRIS/HCl pH 7,8 2 mM TCEP 2 mM MgCl ₂ 50 mM NaCl	50 mM TRIS/HCl pH 7,8 2 mM TCEP 2 mM MgCl ₂ 50 mM NaCl	20 mM HEPES/NaOH pH 7,8 2 mM TCEP 2 mM MgCl ₂ 150 mM NaCl

Concentration

- step gradient elution (100 % Buffer B) from 1ml ResourceQ IEX

	AMPK_α2_1-339triple & wt AMPK_α2_1-326triple	AMPK_α2_1-312triple	AMPK_α2_1-301triple
Puffer A	20 mM HEPES/NaOH pH 7,8 2 mM TCEP 2 mM MgCl ₂	20 mM HEPES/NaOH pH 7,8 2 mM TCEP 2 mM MgCl ₂	Milipore Concentrator
Puffer B	20 mM HEPES/NaOH pH 7,8 2 mM TCEP 2 mM MgCl ₂ 500 mM NaCl	20 mM HEPES/NaOH pH 7,8 2 mM TCEP 2 mM MgCl ₂ 500 mM NaCl	

5.2.4 Expression, purification and activity test of rat CPT-2

The DNA coding for amino acids 27-658 of rat CPT-2 (provided by Prof. V.A. Zammit, Hannah Research Institute, Ayr, Scotland) was amplified by PCR and subcloned into a Novagen pET-28a vector by using *NdeI* and *NotI* (New England Biolabs) restriction sites. This construct was used to express full-length CPT-2 (without the mitochondrial import sequence, amino acids 1-26 of the CPT-2 precursor) in *E. coli* strain BL21(DE3) at 20°C. After cell disruption the lysate (in 50 mM HEPES/ NaOH pH 8, 0.15 M NaCl, 5 mM TCEP, 10 mM MgCl₂, 30 mg/l DNase I, 30 Tbs./l Roche Complete protease inhibitor) was adjusted with 0.1 % (v/v) Triton-X-100 final concentration. Solubilization and centrifugation (30.000 g, 45 min) was followed by immobilized metal affinity chromatography (IMAC) on a HIS-Select™-HC Nickel Affinity Gel. The detergent was exchanged to 1 % (v/v) n-octyl-β-D-glucopyranoside (βOG) on the column. The eluate from the IMAC step was subjected to a size exclusion chromatography column (S200, Amersham Biosciences/GE Healthcare) equilibrated with 25 mM Tris/ HCl pH 8, 0.15 M NaCl, 2 mM TCEP, 1 % (v/v) βOG, 0.02 % (w/v) NaN₃. ESI-MS confirmed the identity of CPT-2 and showed that the protein was modified by amino-terminal α-N6-phosphogluconoylation (Geoghegan *et al.*, 1999, data not shown). The His₆-tag was not cleavable with thrombin. A 10 l fermentation (45 g of biomass) yielded 300 mg of electrophoretically pure, monomeric and monodisperse protein.

The activity of rat CPT-2 expressed in *E. coli* (30 nM enzyme concentration) was measured for the reverse reaction with a spectrophotometric assay using 5,5'-dithio-bis-(2-nitrobenzoic acid), DTNB. The HS-CoA released on the formation of acylcarnitine from carnitine (500 μM) and palmitoyl-CoA (80 μM) reduced DTNB (300 μM). The resulting 5-mercapto-(2-nitrobenzoic acid) absorbs at 410 nm with a molar extinction coefficient of 13,600 M⁻¹cm⁻¹. The assay buffer contained 120 mM KCl, 25 mM Tris/ HCl pH 7.4, 1 mM EDTA and various concentrations of the inhibitor ST1326.

5.2.5 Thermofluor® assay

Assay contents:

Construct	339apo	392apo	339PNP	392PNP	339PCP	392PCP	339Stau.	392Stau.
Protein [μl]	2.8	3.0	2.8	3.0	2.8	3.0	2.8	3.0
SEC buffer [μl]	47.2	47.0	45.2	45.0	45.2	45.0	45.2	45.0
5X Sypro Orange [μl]	50.0	50.0	50.0	50.0	50.0	50.0	50.0	50.0
ligand stock [μl]	n/a	n/a	2.0	2.0	2.0	2.0	2.0	2.0
f.c. ligand [mM]	n/a	n/a	1	1	1	1	0.004	0.004

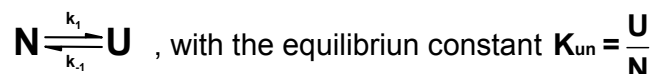
Stock solutions:

- 1) AMPK_α2_1-339wt: 1.44 mg/ml = 36 μM (f.c. = 1 μM)
- 2) AMPK_α2_1-392wt: 1.49 mg/ml = 33 μM (f.c. = 1 μM)
- 3) SEC – Buffer: 20 mM HEPES pH 7.8, 2 mM MgCl₂, 2 mM TCEP, 150 mM NaCl
- 4) Sypro Orange: 5X / SEC – Buffer (f.c. = 2.5X)
- 5) AMP-PNP / SEC – Buffer: 50 mM
- 6) AMP-PCP / SEC – Buffer: 50 mM
- 7) Staurosporine / SEC –Buffer: 200 μM

Blank samples contained all components despite protein.

Derivation of equations for fitting of the Thermofluor® data

Assuming that the temperature-dependent unfolding of a protein is described by the two-state equilibrium (*i.e.*, there is no significant population of intermediate states)



where **N** and **U** are the native and unfolded states, respectively, and **k₁** and **k₋₁** are the apparent rate constants of protein unfolding and folding, the respective mole fractions are given by

$$\mathbf{X}_N = \frac{1}{1+\mathbf{K}_{un}} \text{ and } \mathbf{X}_U = \frac{\mathbf{K}_{un}}{1+\mathbf{K}_{un}}, \text{ with the partition function } \mathbf{Q} = 1+\mathbf{K}_{un}$$

Based on these equations the process of unfolding can be followed and quantified by recording the change in fluorescence upon protein unfolding (EFTINK, 1994; EFTINK and SHASTRY, 1997). If the protein states **N** and **U** have a relative fluorescence of **F_N** and **F_U**, the accumulative temperature-dependent fluorescence signal is given by

$$\begin{aligned}
 F_{(T)} &= \sum X_i F_i = X_N F_N + X_U F_U \\
 &= \frac{F_N}{Q} + \frac{(Q-1)F_U}{Q} \\
 &= \frac{F_N}{Q} + F_U - \frac{F_U}{Q} \\
 &= F_U + \frac{F_N - F_U}{1 + K_{un}}
 \end{aligned}$$

As K_{un} is the temperature dependent equilibrium constant with

$$\Delta G_{(T)} = -RT \ln K_{un} \Leftrightarrow K_{un} = \exp -\frac{\Delta G_{(T)}}{RT}$$

the increase in fluorescence upon binding of the probe Sypro® Orange to a protein undergoing thermal unfolding is described by

$$F_{(T)} = F_U + \frac{F_N - F_U}{1 + \exp -\frac{\Delta G_{(T)}}{RT}} \text{ (Equation 1).}$$

The change in the Gibbs free energy ($\Delta G_{(T)}$) for a two-state thermal unfolding process is also dependent on the differences of the enthalpy (ΔH_{un}) and heat capacity ($\Delta C_{p,un}$) of the native and the unfolded protein states as well as the melting point (T_m , midpoint of the unfolding process), as described by the Gibbs-Helmholtz equation

$$\begin{aligned}
 \Delta G_{(T)} &= \Delta H_{un} \left(1 - \frac{T}{T_m} \right) - \Delta C_{p,un} \left(T_m - T + T \ln \frac{T}{T_m} \right) \\
 \Rightarrow -RT \ln K_{un} &= \Delta H_{un} \left(1 - \frac{T}{T_m} \right) - \Delta C_{p,un} \left(T_m - T + T \ln \frac{T}{T_m} \right) \\
 \Leftrightarrow \ln K_{un} &= -\frac{\Delta H_{un}}{R} \left(\frac{1}{T} - \frac{1}{T_m} \right) + \frac{\Delta C_{p,un}}{R} \left(\ln \frac{T}{T_m} + \frac{T_m}{T} - 1 \right) \text{ (Equation 2).}
 \end{aligned}$$

Substitution of equation 2 into equation 1 yields the formula which was used for fitting the ThermoFluor® data by non-linear regression (Levenberg-Marquardt algorithm, Prism 3.0, GraphPad Software) in order to determine the protein melting points:

$$\begin{aligned}
 F_{(T)} &= F_U + \frac{F_N - F_U}{1 + \exp \left[-\frac{\Delta H_{un}}{R} \left(\frac{1}{T} - \frac{1}{T_m} \right) + \frac{\Delta C_{p,un}}{R} \left(\ln \frac{T}{T_m} + \frac{T_m}{T} - 1 \right) \right]} \\
 \Rightarrow F_{(T_m)} &= \frac{F_U + F_N}{2}, \text{ with } [N] = [U]; K_{un} = 1.
 \end{aligned}$$

The fluorescence signal was recorded on a Bio-Rad iCycler iQ™ Real Time PCR machine with an excitation wavelength of 490 nm and an emission wavelength of 530

nm (the absorption and emission maxima of Sypro® Orange are 470 nm and 570 nm, respectively). The heating rate was 1°C/min which was found to be sufficiently slow to allow complete equilibration of dye adsorption to denatured protein. As opposed to published studies (PANTOLIANO *et al.*, 2001; LO *et al.*, 2004; MATULIS *et al.*, 2005; CARVER *et al.*, 2005) the fluorescence signal was corrected for baseline drift due to thermal disintegration and photo bleaching of the fluorescence probe. The excellent fit of the derived curves to the measured data ($R > 99\%$; $p < 0.0001$) confirmed that the above mentioned assumption (two-state unfolding process) is valid to describe the thermal unfolding of AMPK_α2_1-339 and AMPK_α2_1-392.

The ligand concentration (L_{T_m}) dependent shift of the protein melting point to higher temperature was used to calculate the ligand binding constant $K_{L(T_m)}$ at T_m (LO *et al.*, 2004, based on BRANDTS *et al.*, 1989)

$$K_{L(T_m)} = \frac{\exp\left[-\frac{\Delta H_{un}^{T_0}}{R}\left(\frac{1}{T} - \frac{1}{T_m}\right) + \frac{\Delta C_{p,un}^{T_0}}{R}\left(\ln\frac{T}{T_m} + \frac{T_m}{T} - 1\right)\right]}{L_{T_m}},$$

with $T_m = T_0$, $\Delta H_{un} = \Delta H_{un}^{T_0}$ and $\Delta C_{p,un} = \Delta C_{p,un}^{T_0}$ in the absence of ligand (reference curve). Finally, the ligand binding constant $K_{L(T)}$ at the crystallization temperature (294 K) was calculated according to LO *et al.* (2004):

$$K_{L(T)} = K_{L(T_m)} \exp\left[-\frac{\Delta H_{L(T)}}{R}\left(\frac{1}{T} - \frac{1}{T_m}\right)\right],$$

using the approximation of $\Delta H_{L(T)} \approx -60$ kJ/mol for the ligand binding enthalpy (PANTOLIANO *et al.*, 2001).

5.2.6 Phosphorylation assay

Auto- and substrate phosphorylation of GST-IRTK was examined in order to exclude any detrimental effects on enzymatic activity by the strong reducing agent TCEP, which was used for purification and characterization instead of the established DTT. The SI unit for radioactive decay is Becquerel (Bq [s^{-1}]), whereas the unit generally used in the literature is Curie [Ci [s^{-1}]; 1 Ci = $3.7 \cdot 10^{10}$ Bq].

5.2.6.1 Autophosphorylation

[$\gamma^{32}P$]-ATP with a specific activity of app. 250 cpm/pmol was used as co-substrate for the autophosphorylation reaction of 1 μ M GST-IRTK. The reaction was initiated by

addition of 10X phosphorylation buffer. Aliquots of 10 μ l (10 pmol GST-IRTK; 2 μ Ci) were withdrawn at indicated time points and the reaction was stopped with SDS-PAGE buffer.

10X phosphorylation buffer:

5 μ l	1 M MgCl ₂
50 μ l	0.1 M MnCl ₂
10 μ l	100 mM ATP
20 μ l	50 mM TCEP, 0.5 mM Tris/HCl pH 7.5
10 μ l	1 mg/ml BSA
+ 5 μ l	MQ H ₂ O
100 μ l	

5.2.6.2 Substrate phosphorylation

The substrate GST-IRS-1_p30 (6 μ M f.c.) was mixed with [γ ³²P]-ATP (250 cpm/pmol specific activity) in phosphorylation buffer. The reaction was initiated by addition of 0.3 μ M f.c. GST-IRTK, which had been autophosphorylated for 3 min. Aliquots (10 μ l, with 60 pmol GST-IRS-1_p30; 2 μ Ci) were withdrawn at indicated time points and the reaction was stopped with SDS-PAGE buffer.

5.2.6.3 Quantitation of [γ ³²P]-incorporation

After the phosphorylation reaction kinase, substrate and excess [γ ³²P]-ATP were separated by SDS-PAGE. The gel was fixed for 15 min in destain solution [50 % (v/v) methanol, 7 % (v/v) acetic acid], dried and used for autoradiography. [γ ³²P]-incorporation was determined by measuring the Cerenkov radiation of excised gel bands in a scintillation counter. The data of the time course of phosphorylation were fit to an equation describing a one phase exponential association with pseudo-first order kinetics as implemented in the program Prism 3.0 (GraphPad Software):

$Y_{(t)} = Y_{\max}[1 - \exp(-kt)]$; where k is the association rate constant in [s⁻¹], t is the time [s] and Y is the [γ ³²P]-incorporation [mol/mol].

5.2.7 Limited Proteolysis

The proteases subtilisin, *Staphylococcus aureus* protease, amino-peptidase, carboxy-peptidase, proteinase K, pronase, factor Xa, thrombin, trypsin and chymotrypsin were stored at -20°C in buffers recommended by the manufacturer and supplemented with 50 % (v/v) glycerol. The concentrations of target protein and protease were determined based on the cleavage kinetics with initial screens

containing a 1:80 - 1:10,000 mass ratio in target protein storage buffer at 21°C. The conditions for the cleavage of His₆-IRTK were adapted from BAER *et al.* (2001).

5.2.8 Analytical ultracentrifugation (AUC)

The AUC measurements were performed in collaboration with F. Mueller and E. Kuszniir (Roche, Basel). The partial specific volume of the protein to be analyzed was determined as the arithmetic mean of the value derived from the amino acid sequence (EDSALL, 1943; EMBOSS program suite, Rice *et al.*, 2000) and the value for a hydrated protein (RICKWOOD and CHAMBERS, 1984). The buffer density was measured by the mechanical oscillator technique (ELDER, 1979) on an Anton Paar DMA 4500/RXA density meter. The results from AUC runs on Optima XL-A/I centrifuges (Beckman-Coulter) were analyzed by the program DISCREEQ (SCHUCK, 1994) implemented in the Beckman-Coulter AUC software package. Curve simulation for the determination of the association constants of His₆-IRTK was accomplished with Prism 3.0 (GraphPad Software).

5.2.9 Mass spectrometry (MS)

MS measurements and accompanying Edman microsequencing of peptides (see MATSUDAIRA, 1989, for methodology) were performed by A. Friedlein (Roche Center of Medical Genomics, Basel).

5.2.9.1 Nanoelectrospray ionization (Nano-ESI) MS of intact proteins

The electrospray ionisation approach was used for determining the molecular mass of full-length protein molecules. Comparison of the determined mass and the calculated mass deduced from the amino acid sequence allows the detection of covalent modifications. The protein samples were desalted and, if necessary, concentrated on a pulled capillary containing app. 100 nl POROS R1 reverse phase material (Perseptive Biosystems, Framingham, MA) and eluted with 1 µl of aqueous 50 % (v/v) acetonitrile/ 5% (v/v) formic acid directly into the nanoelectrospray needle (WILM and MANN, 1996). Electrospray mass spectra were acquired on a QSTAR Pulsar i quadrupole TOF tandem mass spectrometer (Applied Biosystems/MDS-Sciex, Toronto, Canada) equipped with a nano electrospray ion source as described by WILM and MANN (1996). All data were acquired with a mass range from 600 to 1600 (m/z, amu). The average molecular masses of the proteins were calculated

from the m/z peaks in the charge distribution profiles of the multiply charged ions. The reconstructed molecular mass profiles were obtained by using a deconvolution algorithm (MDS Sciex).

5.2.9.2 Characterization of in-gel digested proteins

A) Analysis of tryptic peptides by matrix-assisted laser desorption-ionization time of flight (MALDI-TOF) MS

MALDI MS achieves a direct desorption of gas-phase ions from the target by pulse-laser irradiation of a sample. Ions are all formed at the same time and placed in the ion source and then accelerated through a fixed potential into the TOF drift tube. The reflectron compensates for the differences in the velocities of ions with the same m/z and, therefore, increases the resolution of TOF spectrometry.

The in-gel digestion of Coomassie Brilliant Blue-stained protein bands with trypsin was performed according to FOUNTOULAKIS and LANGEN (1997). Following overnight digestion app. 1 μ l sample was mixed with 1 μ l of the saturated matrix [α -cyano cinnamic acid in aqueous 50 % (v/v) acetonitrile/ 0.1 % (v/v) trifluoroacetic acid] and applied to the MALDI-target. The samples were analyzed with a Bruker Daltonics (Bremen, Germany) Ultraflex TOF/TOF mass spectrometer. An acceleration voltage of 25 kV was used. Calibration was internal to the samples with the peptides des-Arg-bradykinin and ACTH(18-38) purchased from Sigma.

B) Analysis of tryptic peptides by nano-ESI tandem MS

For this approach the peptides obtained after tryptic digestion were desalted and concentrated on a pulled capillary column containing approximately 100 nl POROS R2 reverse phase material (Applied Biosystems, Foster City, CA). The peptides were eluted with app. 1 μ l of aqueous 60 % (v/v) acetonitrile/ 5 % (v/v) formic acid directly into a nanoelectrospray capillary needle. Mass spectra were acquired on a QSTAR Pulsar i quadrupole TOF tandem mass spectrometer (Applied Biosystems/MDS-Sciex, Toronto, Canada) equipped with a nano electrospray ion source (Proxeon, Odense, Denmark). Fragmentation by tandem MS yields a stretch of amino acid sequence together with its location in the peptide (sequence tag). With this sequence tag information appropriate databases (Swissprot) were searched using MASCOT Search software (Matrix Science, London, UK).

5.2.10 Biacore

The Biacore (surface plasmon resonance) measurements were conducted in collaboration with W. Huber and J. Kohler (Roche, Basel). Stock solutions of the constructs AMPK_α2_1-339_wt, AMPK_α2_1-339_D56A/R171E/T172D and AMPK_α2_1-392_wt with concentrations of 1 mg/ml in 20 mM HEPES/NaOH pH 7.8, 250 mM NaCl, 10 mM MgCl₂ and 2mM TCEP were diluted to 40 µg/ml in 10 mM NaOAc/AcOH pH 5.0, 10 mM MgCl₂ and 200 µM Merck compound C (RO4499487) shortly prior to immobilization. Incubation with the ligand compound C was indispensable for stabilization of the AMPK constructs during immobilization by amine coupling on Biacore CM5 sensors. The coupling was carried out according to the manufacturer's instructions (Amine Coupling Kit, Biacore). The integrity of the immobilized AMPK constructs (app. 6000 RU, or 6 ng/mm²) were tested by recurrent injection of the active site binder AMP-PNP and comparing the corresponding sensor responses. All measurements were performed on Biacore 2000 and 3000 instruments. K_D values were determined by plotting the steady-state equilibrium binding response units, *i.e.*, the signal obtained when no net association or dissociation of ligand is observed over time, against the respective ligand concentration. The binding curves were calculated by fitting the sensorgram data to an equation describing a Langmuir adsorption isotherm (Biaevaluation software, Biacore). For this fitting procedure one-class of independent binding sites, *i.e.*, absence of lateral protein-protein interactions, in a 1:1 stoichiometry of protein to ligand was assumed.

5.2.11 Small angle X-ray scattering (SAXS)

For a dilute and monodisperse protein solution the X-ray scattering intensity is proportional to the spherically averaged single-particle scattering, *i.e.*, the scattering of randomly oriented protein molecules. The average electron density of a typical biopolymer sample is only 30 % higher than that of the buffer system. Therefore, care must be taken with regard to the choice of buffer system (< 0.5 M salt or glycerol) in order to maximize the electron density contrast. The scattering data is plotted as the logarithm of the scattering intensity against the square of the momentum transfer, $s^2 = [(4\pi/\lambda)\sin\theta]^2$ (Guinier plot), where λ is the X-ray wavelength [Å] and 2θ the scattering angle. From this linearized representation the molecular weight and the radius of gyration R_G of a particle in solution can be determined. At a given

concentration the scattering intensity at zero angle (extrapolation to y-intercept) is proportional to the molecular mass of the scatterer, while the slope is inversely proportional to the square of R_G . Deviation from linearity in the Guinier plot indicates solution non-ideality or significant deviation from globular shape of the scatterer, *i.e.*, polydispersity due to interparticle interference (oligomerization or aggregation). As the signal of intensity vs. s decays rapidly the maximal resolution of SAXS is limited to $s = (4\pi/\lambda)\sin\theta = 2\pi/d$, where $d \approx 15 \text{ \AA}$ (reviewed in SVERGUN and KOCH, 2002 and 2003).

The SAXS measurements were performed in collaboration with the group of D. Svergun, EMBL Hamburg outstation, on beamline X33 in the HASYLAB (DORIS III storage ring at DESY). A temperature controlled (21°C) mica flat cell ($V = 100\mu\text{l}$) was used as sample cuvette. The X-ray wavelength was 1.5 Å and data were collected on a conventional Mar345 image plate detector (data range $0.012 < s < 0.45 \text{ \AA}^{-1}$) with a 2.7 m sample-detector distance. A 5 mg/ml BSA standard (66 kDa monomer) in 50 mM HEPES pH 7.5 was measured before and after the set of AMPK samples for calibration purposes. Standard and sample protein concentrations were measured in denaturing buffer in order to obtain exact values for the normalization of dilution series. As the X-ray beam intensity at the DORIS III synchrotron decays in between of injection cycles, AMPK storage buffer was measured immediately before and after each protein sample in order to allow precise baseline subtraction. The PRIMUS program package (KONAREV *et al.*, 2003) was used for raw data reduction and processing.

The shape of AMPK_α2_1-339 and trimeric AMPK_2α2β1γ was calculated with the program DAMMIN (P. Konarev, EMBL Hamburg Outstation; SVERGUN, 1999). This program constructs a sphere of densely packed dummy atoms encompassing the full protein volume and its maximal diameter. Each of the dummy atoms is assigned to either protein or solvent. The DAMMIN *ab initio* algorithm then selects a continuous and compact set of dummy atoms that fits the scattering data by minimizing the discrepancy of calculated and measured scattering curves. The resulting structure is optimized by simulated annealing.

5.2.12 Crystallographic methods (CPT-2)

5.2.12.1 Protein crystallization

Crystals of uninhibited rCPT-2 and (R)-*N*-tetradecylcarbamoyl-aminocarnitine (ST1326, IUPAC: (3R)-3-[(tetradecylaminocarbonylamino]-4-(trimethylazaniumyl) butanoate, synthesized in-house by Med. Chem. Dept.) complex were obtained at a protein concentration of 10-20 mg/ml and 21°C using hanging drops with 0.15 M DL-malic acid pH 7.0, 20 % (w/v) PEG 3350 or the modified microbatch (D'ARCY *et al.*, 2003) method with 25 % (w/v) PEG 1500, respectively (Index 91 and 37, Hampton Research). For complex formation rCPT-2 was incubated with an 3-fold molar excess of the inhibitor ST1326 for 3 h on ice prior to crystallization. The crystals were flash frozen in liquid nitrogen after 30 s soaks in mother liquor supplemented with 25 % (w/v) PEG 200 (uninhibited) or exchanging excess mother liquor and Al's oil against 100 % (v/v) paraffin oil (ST1326).

5.2.12.2 Data collection and processing

Datasets for uninhibited rCPT-2 and the ST1326 complex were collected on beam line X10SA at SLS, Villigen, Switzerland. The measurements were performed at 100 K with $\lambda = 0.97853 \text{ \AA}$ (uninhibited tetragonal, Se peak wavelength), $\lambda = 0.97899 \text{ \AA}$ (uninhibited orthorhombic) and $\lambda = 1.008 \text{ \AA}$ (ST1326). The datasets were processed and scaled with XDS (KABSCH, 1993). The space groups were determined as $P4_32_12$ (uninhibited tetragonal; $a = b = 67.6 \text{ \AA}$, $c = 307.3 \text{ \AA}$; $\alpha = \beta = \gamma = 90^\circ$; Matthew's Coeff. = 2.4 (Matthews, 1986); 1 mol/AU), $C222_1$ (uninhibited orthorhombic; $a = 95.2 \text{ \AA}$, $b = 97.3 \text{ \AA}$, $c = 310.4 \text{ \AA}$; Matthew's Coeff. = 2.4; 2 mol/AU) and $P2_12_12_1$ (ST1326; $a = 85.8 \text{ \AA}$, $b = 96.2 \text{ \AA}$, $c = 124.3 \text{ \AA}$; $\alpha = \beta = \gamma = 90^\circ$; Matthew's Coeff. = 3.5; 1mol/AU). The diffraction of first crystals of uninhibited rCPT-2 from conventional bacterial expression was not sufficient for structure determination. In contrast, apo crystals obtained from material that was seleno-methionine labeled by standard procedures (CHENE *et al.*, 1995) were of superior diffraction quality, which could be attributed to improved protein quality due to the different media composition and bacterial host protein expression profile during labeling. When the $P4_32_12$ crystals were soaked in mother liquor containing CoA the space group was changed to the maximal non-isomorphic subgroup $C222_1$. In the resulting high resolution structure one partial molecule of CoA per molecule rCPT-2 could be assigned to

electron density at a crystal contact distant from the physiological CoA binding site. The XDS rejection statistics report merely 0.26 % rejected misfits which fully supports the choice of $P2_12_12_1$ as the correct space group for the complex crystal despite the rather high value for R_{merge} of 16.7% .

5.2.12.3 Structure solution and refinement

Molecular replacement was performed using AMoRe in the CCP4 interface (NAVAZA, 1992; Collaborative Computational Project, Number 4, 1994). For the ST1326 complex a rCPT-2 homology model built with XSAE (C. Broger, Roche, Basel) based on mouse CrAT (JOGL and TONG, 2003; PDB code 1t7n) served as search model. The solution was refined by simulated annealing with CNS (BRÜNGER, 1992). The final model was built using iterative cycles of model building in MOLOC (GERBER, 1992), solvent building in autoBUSTER (ROVERSI *et al.*, 2000) and refinement in Refmac (MURSHUDOV *et al.*, 1999). Despite Se-labeling the structures of the uninhibited enzyme were also solved by molecular replacement using the refined complex structure as search model, followed by automated model building with Arp/wArp (PERRAKIS *et al.*, 1999) and iterative Refmac and MOLOC cycles. For the orthorhombic (tetragonal) uninhibited structure 94.0 % (92.7 %) of the residues lie in the most favored and 5.4 % (6.8 %) in the additionally allowed regions of the Ramachandran plot. For the ST1326 complex structure these values are 88.2 % and 11.3 %, respectively. Arg 498 (generously allowed region) and Leu 129 as well as Asn 230 (Ramachandran outliers) account for the differences to 100 %. PyMOL (DELANO, 2002) was used for preparing structure representations. Calculation of the electrostatic potential surface of rCPT- 2 was performed with MOE (Chemical Computing Group, Inc.).

6 References

- Abergel, C (2004) Spectacular improvement of X-ray diffraction through fast desiccation of protein crystals. *Acta Crystallogr D Biol Crystallogr*, **60**: 1413-1416
- Ablooglu AJ, Till JH, Kim K, Parang K, Cole PA, Hubbard SR, Kohanski RA (2000) Probing the catalytic mechanism of the insulin receptor kinase with a tetrafluorotyrosine-containing peptide substrate. *J Biol Chem*, **275**: 30394-30398
- ADA (2003) Report of the Expert Committee on the Diagnosis and Classification of Diabetes Mellitus. *Diabetes Care*, **26**: S 5-20
- Adams JA (2001) Kinetic and catalytic mechanisms of protein kinases. *Chem Rev*, **101**: 2271-2290
- Adams JA (2003) Activation loop phosphorylation and catalysis in protein kinases: is there functional evidence for the autoinhibitor model? *Biochemistry*, **42**: 601-607
- Aifa S, Aydin J, Nordvall G, Lundstrom I, Svensson SP, Hermanson O (2005) A basic peptide within the juxtamembrane region is required for EGF receptor dimerization. *Exp Cell Res*, **302**: 108-114
- Air EL, Strowski MZ, Benoit SC, Conarello SL, Salituro GM, Guan XM, Liu K, Woods SC, Zhang BB (2002) Small molecule insulin mimetics reduce food intake and body weight and prevent development of obesity. *Nat Med*, **8**: 179-183
- Alberti KG, Zimmet P, Shaw J; IDF Epidemiology Task Force Consensus Group (2005) The metabolic syndrome-a new worldwide definition. *Lancet*, **366**: 1059-1062
- Alvi KA, Pu H, Luche M, Rice A, App H, McMahon G, Dare H, Margolis B (1999) Asterriquinones produced by *Aspergillus candidus* inhibit binding of the Grb-2 adapter to phosphorylated EGF receptor tyrosine kinase. *J Antibiot (Tokyo)*, **52**: 215-223
- Anderson RC (1998) Carnitine palmitoyltransferase: a viable target for the treatment of NIDDM? *Curr Pharm Des*, **4**: 1-16
- Backer JM, Wjasow C, Zhang Y (1997) In vitro binding and phosphorylation of insulin receptor substrate 1 by the insulin receptor. Role of interactions mediated by the phosphotyrosine-binding domain and the pleckstrin-homology domain. *Eur J Biochem*, **245**: 91-96
- Baer K, Al-Hasani H, Parvaresh S, Corona T, Rufer A, Nolle V, Bergschneider E, Klein HW (2001) Dimerization-induced activation of soluble insulin/IGF-1 receptor kinases: an alternative mechanism of activation. *Biochemistry*, **40**: 14268-14278
- Balasubramanyam M, Mohan V (2001) Orally active insulin mimics: where do we stand now? *J Biosc*, **26**: 383-390
- Barnett M, Collier GR, O'Dea K (1992) The longitudinal effect of inhibiting fatty acid oxidation in diabetic rats fed a high fat diet. *Horm. Metab Res*, **24**: 360-362
- Bebornitz GR, Schuster HF (2002) The impact of fatty acid oxidation on energy utilization: targets and therapy. *Curr Pharm Des*, **8**: 1199-1227
- Bell IM, Stirdivant SM, Ahern J, Culberson JC, Darke PL, Dinsmore CJ, Drakas RA, Gallicchio SN, Graham SL, Heimbrook DC, Hall DL, Hua J, Kett NR, Kim AS, Kornienko M, Kuo LC, Munshi SK, Quigley AG, Reid JC, Trotter BW, Waxman LH, Williams TM, Zartman CB (2005) Biochemical and structural characterization of a novel class of inhibitors of the type 1 insulin-like growth factor and insulin receptor kinases. *Biochemistry*, **44**: 9430-9440

- Bonnefont JP, Demaugre F, Prip-Buus C, Saudubray JM, Brivet M, Abadi N, Thuillier L (1999) Carnitine palmitoyltransferase deficiencies. *Mol Genet Metab*, **68**: 424-440
- Bonnefont JP, Djouadi F, Prip-Buus C, Gobin S, Munnich A, Bastin J. (2004) Carnitine palmitoyltransferases 1 and 2: biochemical, molecular and medical aspects. *Mol Aspects Med*, **25**: 495-520
- Bossemeyer D, Engh, RA, Kinzel, V, Ponstingl, H, Huber, R (1993) Phosphotransferase and substrate binding mechanism of the cAMP-dependent protein kinase catalytic subunit from porcine heart as deduced from the 2.0 Å structure of the complex with Mn²⁺ adenylyl imidodiphosphate and inhibitor peptide PKI(5-24). *EMBO J*, **12**: 849-859
- Brandts JF, Hu CQ, Lin LN, Mos MT (1989) A simple model for proteins with interacting domains. Applications to scanning calorimetry data. *Biochemistry*, **28**: 8588-96
- Breitenlechner C, Engh RA, Huber R, Kinzel V, Bossemeyer D, Gassel M (2004) The typically disordered N-terminus of PKA can fold as a helix and project the myristoylation site into solution. *Biochemistry*, **43**: 7743-7749
- Bronner M, Hertz R, Bar-Tana J (2004) Kinase-independent transcriptional co-activation of peroxisome proliferator-activated receptor alpha by AMP-activated protein kinase. *Biochem J*, **384**: 295-305
- Brünger AT (1992) X-PLOR Manual Version 3.1. *Yale University Press, New Haven, CT, USA*
- Buchanan TA, Xiang AH (2005) Gestational diabetes mellitus. *J Clin Invest*, **115**: 485-491
- Burns JA, Butler, JC, Moran J, Whitesides GM (1991) Selective reduction of disulfides by Tris-(2-carboxyethyl)-phosphine. *J Org Chem*, **56**: 2648-2650
- Cann AD, Kohanski RA (1997) Cis-autophosphorylation of juxtamembrane tyrosines in the insulin receptor kinase domain. *Biochemistry*, **36**: 7681-7689
- Carling D, Fryer LG, Woods A, Daniel T, Jarvie SL, Whitrow H (2003) Bypassing the glucose/fatty acid cycle: AMP-activated protein kinase. *Biochem Soc Trans*, **31**: 1157-1160
- Carling D (2004) The AMP-activated protein kinase cascade - a unifying system for energy control. *Trends Biochem Sci*, **29**: 18-24
- Carter DC, Rüker F, Ho JX, Lim K, Keeling K, Gilliland G, Ji X (1994) Fusion proteins as alternative crystallization paths to difficult structure problems. *Prot Pept Lett*, **1**: 175-178
- Carver TE, Bordeau B, Cummings MD, Petrella EC, Pucci MJ, Zawadzke LE, Dougherty BA, Tredup JA, Bryson JW, Yanchunas J Jr, Doyle ML, Witmer MR, Nelen MI, DesJarlais RL, Jaeger EP, Devine H, Asel ED, Springer BA, Bone R, Salemme FR, Todd MJ (2005) Decrypting the biochemical function of an essential gene from *Streptococcus pneumoniae* using ThermoFluor technology. *J Biol Chem*, **280**: 11704-11712
- Chayen NE (1997) The role of oil in macromolecular crystallization. *Structure*, **15**: 1269-1274
- Chayen NE (2004) Turning protein crystallisation from an art into a science. *Curr Opin Struct Biol*, **14**: 577-583
- Chen CM, Chiang SY, Yeh NH (1991) Increased stability of nucleolin in proliferating cells by inhibition of its self-cleaving activity. *J Biol Chem*, **266**: 7754-7758
- Chene C, Fountoulakis M, Döbeli H, D'Arcy B, Winkler F, D'Arcy A. (1995) Crystallization of the complex of human IFN-gamma and the extracellular domain of the IFN-gamma receptor. *Proteins*, **23**: 591-594

- Cheng M, Chen S, Schow SR, Mancham VP, Spevak WR, Cristobal CP, Shi S, Macsata RW, Lum RT, Goldfine ID, Keck JG (2004) In vitro and in vivo prevention of HIV protease inhibitor-induced insulin resistance by a novel small molecule insulin receptor activator. *J Cell Biochem*, **92**: 1234-1245
- Collaborative Computational Project, Number 4 (1994) The CCP4 suite: Programs for protein crystallography. *Acta Crystallogr D Biol Crystallogr*, **50**: 760-763
- Cooper MA (2003) Label-free screening of bio-molecular interactions. *Anal Bioanal Chem*, **377**: 834-842
- Crute BE, Seefeld K, Gamble J, Kemp BE, Witters LA (1998) Functional domains of the alpha1 catalytic subunit of the AMP-activated protein kinase. *J Biol Chem*, **273**, 35347-35354
- Dale GE, Oefner C, D'Arcy A (2003) The protein as a variable in protein crystallization. *J Struct Biol*, **142**: 88-97
- D'Arcy A (1994) Crystallizing proteins - a rational approach? *Acta Crystallogr D Biol Crystallogr*, **50**: 469-471
- D'Arcy A, Mac Sweeney A, Stihle M, Haber A (2003) The advantages of using a modified microbatch method for rapid screening of protein crystallization conditions. *Acta Crystallogr D Biol Crystallogr*, **59**: 396-399
- D'Arcy A, Sweeney AM, Haber A (2004) Practical aspects of using the microbatch method in screening conditions for protein crystallization. *Methods*, **34**: 23-328
- Davies TG, Tunnah P, Meijer L, Marko D, Eisenbrand G, Endicott JA, Noble ME (2001) Inhibitor binding to active and inactive CDK2: the crystal structure of CDK2-cyclin A/indirubin-5-sulphonate. *Structure*, **9**: 389-397
- DeLano WL (2002) The PyMOL User's Manual. *DeLano Scientific, San Carlos, CA, USA*
- Demaugre F, Bonnefont JP, Colonna M, Capanec C, Leroux JP, Saudubray JM (1991) Infantile form of carnitine palmitoyltransferase II deficiency with hepatomuscular symptoms and sudden death. Physiopathological approach to carnitine palmitoyltransferase II deficiencies. *J Clin Invest*, **87**: 859-864
- De Meyts P, Whittaker J (2002) Structural biology of insulin and IGF1 receptors: implications for drug design. *Nat Rev Drug Discov*, **1**:769-783
- De Meyts P (2004) Insulin and its receptor: structure, function and evolution. *Bioessays*, **26**: 1351-1362
- Depetris RS, Hu J, Gimpelevich I, Holt LJ, Daly RJ, Hubbard SR (2005) Structural basis for inhibition of the insulin receptor by the adaptor protein grb14. *Mol Cell*, **20**: 325-333
- Derewenda ZS (2004) Rational protein crystallization by mutational surface engineering. *Structure*, **12**: 529-535
- Ding VD, Qureshi SA, Szalkowski D, Li Z, Biazzo-Ashnault DE, Xie D, Liu K, Jones AB, Moller DE, Zhang BB (2002) Regulation of insulin signal transduction pathway by a small-molecule insulin receptor activator. *Biochem J*, **367**: 301-306
- Dong J, Boggon TJ, Chayen NE, Raftery J, Bi RC, Helliwell JR (1999) Bound-solvent structures for microgravity-, ground control-, gel- and microbatch-grown hen egg-white lysozyme crystals at 1.8 Å resolution. *Acta Crystallogr D Biol Crystallogr*, **55**: 745-752
- D'Souza CA, Wood DD, She YM, Moscarello MA (2005) Autocatalytic cleavage of myelin basic protein: an alternative to molecular mimicry. *Biochemistry*, **44**: 12905-12913

- Duhe RJ, Clark EA, Farrar WL (2002) Characterization of the in vitro kinase activity of a partially purified soluble GST/JAK2 fusion protein. *Mol Cell Biochem*, **236**: 23-35
- Dulloo AG, Gubler M, Montani JP, Seydoux J, Solinas G (2004) Substrate cycling between de novo lipogenesis and lipid oxidation: a thermogenic mechanism against skeletal muscle lipotoxicity and glucolipotoxicity. *Int J Obes Relat Metab Disord*, **28**: S29-37
- Ebina Y, Ellis L, Jarnagin K, Edery M, Graf L, Clauser E, Ou JH, Masiarz F, Kan YW, Goldfine ID, *et al.* (1985) The human insulin receptor cDNA: the structural basis for hormone-activated transmembrane signalling. *Cell*, **40**: 747-758
- Edsall JT (1943) Proteins, amino acids and peptides as ions and dipolar ions, *Reinhold, New York, NY, USA*
- Eftink MR (1994) The use of fluorescence methods to monitor unfolding transitions in proteins. *Biophys J*, **66**: 482-501
- Eftink MR, Shastry MC (1997) Fluorescence methods for studying kinetics of protein-folding reactions. *Methods Enzymol*, **278**: 258-86
- Eichhorst ST, Krueger A, Muerkoster S, Fas SC, Golks A, Gruetzner U, Schubert L, Opelz C, Bilzer M, Gerbes AL, Krammer PH (2004) Suramin inhibits death receptor-induced apoptosis in vitro and fulminant apoptotic liver damage in mice. *Nat Med*, **10**: 602-609
- Eisinger, DP, Damour, M, LaMarche, A (2003) Multiplex kinase selectivity assays using Beadlyte. SBS conference poster, http://www.upstate.com/img/pdf/bead_poster_kinase_selectivity.pdf
- Elder JP (1979) Density measurements by the mechanical oscillator. *Methods Enzymol*, **61**: 12-25
- Engl RA, Bossemeyer D (2002) Structural aspects of protein kinase control-role of conformational flexibility. *Pharmacol Ther*, **93**: 99-111
- Engl J, Moule M, Yip CC (1994) Dithiothreitol stimulates insulin receptor autophosphorylation at the juxtamembrane domain. *Biochem Biophys Res Commun*, **201**: 1439-1444
- Favelyukis S, Till JH, Hubbard SR, Miller WT (2001) Structure and autoregulation of the insulin-like growth factor 1 receptor kinase. *Nat Struct Biol*, **8**: 1058-1063
- Ford ES (2005) Prevalence of the metabolic syndrome defined by the international diabetes Federation among adults in the U.S. *Diabetes Care*, **28**: 2745-2749
- Fountoulakis M, Langen H (1997) Identification of Proteins by Matrix-Assisted Laser Desorption-Ionization Mass Spectrometry Following In-Gel Digestion In Low-Salt, Nonvolatile Buffer and Simplified Peptide Recovery. *Anal Biochem*, **250**: 153-156.
- Frankel M, Bishop SM, Ablooglu AJ, Han YP, Kohanski RA (1999) Conformational changes in the activation loop of the insulin receptor's kinase domain. *Protein Sci*, **8**: 2158-2165
- Frankel M, Ablooglu AJ, Leone JW, Rusinova E, Ross JB, Heinrikson RL, Kohanski RA (2001) Intrasteric inhibition of ATP binding is not required to prevent unregulated autophosphorylation or signaling by the insulin receptor. *Mol Cell Biol*, **21**: 4197-4207
- Frayn KN (2003) The glucose-fatty acid cycle: a physiological perspective. *Biochem Soc Trans*, **31**: 1115-1119
- Fryer LG, Parbu-Patel A, Carling D (2002) The Anti-diabetic drugs rosiglitazone and metformin stimulate AMP-activated protein kinase through distinct signaling pathways. *J Biol Chem*, **277**: 25226-25232

- Fryer LG, Carling D (2005) AMP-activated protein kinase and the metabolic syndrome. *Biochem Soc Trans*, **33**: 362-366
- Fujita-Yamaguchi Y, Kathuria S (1988) Characterization of receptor tyrosine-specific protein kinases by the use of inhibitors. Staurosporine is a 100-times more potent inhibitor of insulin receptor than IGF-I receptor. *Biochem Biophys Res Commun*, **157**: 955-962
- Fukuhara A, Matsuda M, Nishizawa M, Segawa K, Tanaka M, Kishimoto K, Matsuki Y, Murakami M, Ichisaka T, Murakami H, Watanabe E, Takagi T, Akiyoshi M, Ohtsubo T, Kihara S, Yamashita S, Makishima M, Funahashi T, Yamanaka S, Hiramatsu R, Matsuzawa Y, Shimomura I (2005) Visfatin: a protein secreted by visceral fat that mimics the effects of insulin. *Science*, **307**: 426-430
- Garcia RA, Pantazatos D, Villarreal FJ (2004) Hydrogen/deuterium exchange mass spectrometry for investigating protein-ligand interactions. *Assay Drug Dev Technol*, **2**: 81-91
- Gazdoui S, Yamoah K, Wu K, Escalante CR, Tappin I, Bermudez V, Aggarwal AK, Hurwitz J, Pan ZQ (2005) Proximity-induced activation of human Cdc34 through heterologous dimerization. *Proc Natl Acad Sci U S A*, **102**: 15053-15058
- Geoghegan KF, Dixon HB, Rosner PJ, Hoth LR, Lanzetti AJ, Borzilleri KA, Marr ES, Pezzullo LH, Martin LB, LeMotte PK, McColl AS, Kamath AV, Stroh JG (1999) Spontaneous alpha-N-6-phosphogluconoylation of a "His tag" in *Escherichia coli*: the cause of extra mass of 258 or 178 Da in fusion proteins. *Anal Biochem*, **267**: 169-184
- Gerber PR (1992) Peptidemechanics: a force field for peptides and proteins working with entire residues as small units. *Biopolymers*, **32**: 1003-1017
- Getz EB, Xiao M, Chakrabarty T, Cooke R, Selvin PR (1999) A comparison between the sulfhydryl reductants tris(2-carboxyethyl)phosphine and dithiothreitol for use in protein biochemistry. *Anal Biochem*, **273**: 73-80
- Giannessi F, Chiodi P, Marzi M, Minetti P, Pessotto P, De Angelis F, Tassoni E, Conti R, Giorgi F, Mabilia M, Dell'Uomo N, Muck S, Tinti MO, Carminati P, Arduini A (2001) Reversible carnitine palmitoyltransferase inhibitors with broad chemical diversity as potential antidiabetic agents. *J Med Chem*, **44**: 2383-2386
- Giannessi F, Pessotto P, Tassoni E, Chiodi P, Conti R, De Angelis F, Dell'Uomo N, Catini R, Deias R, Tinti MO, Carminati P, Arduini A (2003). Discovery of a long-chain carbamoyl aminocarnitine derivative, a reversible carnitine palmitoyltransferase inhibitor with antiketotic and antidiabetic activity. *J Med Chem*, **46**: 303-309
- Gill JS, Windebank AJ (1998) Direct activation of the high-affinity nerve growth factor receptor by a non-peptide symmetrical polyanion. *Neuroscience*, **87**: 855-860
- Gimeno-Alcaniz JV, Sanz P (2003) Glucose and type 2A protein phosphatase regulate the interaction between catalytic and regulatory subunits of AMP-activated protein kinase. *J Mol Biol*, **333**: 201-209
- Goldberg, J., Nairn, A.C., Kuriyan, J. Structural basis for the autoinhibition of calcium/calmodulin-dependent protein kinase I. *Cell*, **84**, 875-887 (1996)
- Govindasamy L, Kukar T, Lian W, Pedersen B, Gu Y, Agbandje-McKenna M, Jin S, McKenna R, Wu D (2004) Structural and mutational characterization of L-carnitine binding to human carnitine acetyltransferase. *J Struct Biol*, **146**: 416-424
- Groenen LC, Walker F, Burgess AW, Treutlein HR (1997) A model for the activation of the epidermal growth factor receptor kinase involvement of an asymmetric dimer? *Biochemistry*, **36**: 3826-3836.
- Gura T (1999) New lead found to a possible "insulin pill". *Science*, **284**: 886

- Hamilton SR, O'Donnell JB Jr, Hammet A, Stapleton D, Habinowski SA, Means AR, Kemp BE, Witters LA (2002) AMP-activated protein kinase: detection with recombinant AMPK alpha1 subunit. *Biochem Biophys Res Commun*, **293**: 892-898
- Han YH, Chung YH, Kim TY, Hong SJ, Choi JD, Chung YJ (2001) Crystallization of *Clonorchis sinensis* 26 kDa glutathione S-transferase and its fusion proteins with peptides of different lengths. *Acta Crystallogr D Biol Crystallogr*, **57**: 579-581
- Hansen CL, Skordalakes E, Berger JM, Quake SR (2002) A robust and scalable microfluidic metering method that allows protein crystal growth by free interface diffusion. *PNAS*, **99**: 16531-16536
- Hardie DG, Hawley SA (2001) AMP-activated protein kinase: the energy charge hypothesis revisited. *Bioessays*, **23**: 1112-1119
- Hardie DG, Scott JW, Pan DA, Hudson ER (2003) Management of cellular energy by the AMP-activated protein kinase system. *FEBS Lett*, **546**: 113-120
- Haring HU, Kellerer M, Mosthaf L (1994) Modulation of insulin signalling in non-insulin-dependent diabetes mellitus: significance of altered receptor isoform patterns and mechanisms of glucose-induced receptor modulation. *Horm Res*, **41** Suppl 2: 87-91; discussion 92
- Hawley SA, Gadalla AE, Olsen GS, Hardie DG (2002) The antidiabetic drug metformin activates the AMP-activated protein kinase cascade via an adenine nucleotide-independent mechanism. *Diabetes*, **51**: 2420-2425
- Hawley SA, Boudeau J, Reid JL, Mustard KJ, Udd L, Makela TP, Alessi DR, Hardie DG (2003) Complexes between the LKB1 tumor suppressor, STRAD alpha/beta and MO25 alpha/beta are upstream kinases in the AMP-activated protein kinase cascade. *J Biol*, **2**: 28
- Hawley SA, Pan DA, Mustard KJ, Ross L, Bain J, Edelman AM, Frenguelli BG, Hardie DG (2005) Calmodulin-dependent protein kinase kinase-beta is an alternative upstream kinase for AMP-activated protein kinase. *Cell Metab*, **2**: 9-19
- Herberg, FW, Doyle, ML, Cox, S, Taylor, SS (1999) Dissection of the nucleotide and metal-phosphate binding sites in cAMP-dependent protein kinase. *Biochemistry*, **38**, 6352-6360
- Herrera R, Lebwohl D, Garcia de Herreros A, Kallen RG, Rosen OM (1988) Synthesis, purification, and characterization of the cytoplasmic domain of the human insulin receptor using a baculovirus expression system. *J Biol Chem*, **263**: 5560-5568
- Hoessel R, Leclerc S, Endicott JA, Nobel ME, Lawrie A, Tunnah P, Leost M, Damiens E, Marie D, Marko D, Niederberger E, Tang W, Eisenbrand G, Meijer L (1999) Indirubin, the active constituent of a Chinese antileukaemia medicine, inhibits cyclin-dependent kinases. *Nat Cell Biol*, **1**: 60-67
- Holyoak T, Fenn TD, Wilson MA, Moulin AG, Ringe D, Petsko GA (2003) Malonate: a versatile cryoprotectant and stabilizing solution for salt-grown macromolecular crystals. *Acta Crystallogr D Biol Crystallogr*, **59**: 2356-2358
- Homann S, Schacher B, Zumstein-Mecker S, Fabbro D, Bold G, Ferrari S (2001) Expression and purification of human recombinant GST-FGF receptor-1. *J Biotechnol*, **86**: 51-58
- Homola J (2003) Present and future of surface plasmon resonance biosensors. *Anal Bioanal Chem.*, **377**: 528-539
- Hotz-Wagenblatt A, Droge W (2002) Redox-mediated functional and structural changes in insulin receptor kinase. *Methods Enzymol*, **348**: 288-296

- Hsiao YS, Jogl G, Tong L (2004) Structural and biochemical studies of the substrate selectivity of carnitine acetyltransferase. *J Biol Chem*, **279**: 31584-31589
- Hu J, Liu J, Ghirlando R, Saltiel AR, Hubbard SR (2003) Structural basis for recruitment of the adaptor protein APS to the activated insulin receptor. *Mol Cell*, **12**: 1379-1389
- Hubbard SR, Wei L, Ellis L, Hendrickson WA (1994) Crystal structure of the tyrosine kinase domain of the human insulin receptor. *Nature*, **372**: 746-754
- Hubbard SR (1997) Crystal structure of the activated insulin receptor tyrosine kinase in complex with peptide substrate and ATP analog. *EMBO J*, **16**: 5572-5581
- Hubinger A, Weikert G, Wolf HP, Gries FA (1992) The effect of etomoxir on insulin sensitivity in type 2 diabetic patients. *Horm Metab Res*, **24**: 115-118
- Hudson ER, Pan DA, James J, Lucocq JM, Hawley SA, Green KA, Baba O, Terashima T, Hardie DG (2003) A novel domain in AMP-activated protein kinase causes glycogen storage bodies similar to those seen in hereditary cardiac arrhythmias. *Curr Biol*, **13**: 861-866
- Hug C, Lodish HF (2005) Visfatin: a new adipokine. *Science*, **307**: 366-367
- Humphries KM, Juliano C, Taylor SS (2002) Regulation of cAMP-dependent protein kinase activity by glutathionylation. *J Biol Chem*, **277**: 43505-43511
- Humphries KM, Deal MS, Taylor SS (2005) Enhanced dephosphorylation of cAMP-dependent protein kinase by oxidation and thiol modification. *J Biol Chem*, **280**: 2750-2758
- Hurley RL, Anderson KA, Franzone JM, Kemp BE, Means AR, Witters LA (2005) The Ca²⁺/calmodulin-dependent protein kinase kinases are AMP-activated protein kinase kinases. *J Biol Chem*, **280**, 29060-29066
- Huse M, Kuriyan J (2002) The conformational plasticity of protein kinases. *Cell*, **109**: 275-282
- Iseli TJ, Walter M, van Denderen BJ, Katsis F, Witters LA, Kemp BE, Michell BJ, Stapleton D (2005) AMP-activated protein kinase beta subunit tethers alpha and gamma subunits via its C-terminal sequence (186-270). *J Biol Chem*, **280**: 13395-13400
- Isganaitis E, Lustig RH (2005) Fast Food, Central Nervous System Insulin Resistance, and Obesity. *Arterioscler Thromb Vasc Biol*, 2005 Sep 15; [Epub ahead of print]
- Jakobsen SN, Hardie DG, Morrice N, Tornqvist HE (2001) 5'-AMP-activated protein kinase phosphorylates IRS-1 on Ser-789 in mouse C2C12 myotubes in response to 5-aminoimidazole-4-carboxamide riboside. *J Biol Chem*, **276**: 46912-46916
- Jancarik J, Kim SH (1991) Sparse matrix sampling: a screening method for crystallization of proteins. *J Appl Cryst*, **24**: 409-411
- Jancarik J, Pufan R, Hong C, Kim SH, Kim R (2004) Optimum solubility (OS) screening: an efficient method to optimize buffer conditions for homogeneity and crystallization of proteins. *Acta Crystallogr D Biol Crystallogr*, **60**: 1670-1673
- Jitrapakdee S, Wallace JC. (1999) Structure, function and regulation of pyruvate carboxylase. *Biochem J*, **340**: 1-16
- Jogl G, Tong L (2003) Crystal structure of carnitine acetyltransferase and implications for the catalytic mechanism and fatty acid transport. *Cell*, **112**: 113-122

- Jogl G, Hsiao YS, Tong L (2005). Crystal structure of mouse carnitine octanoyltransferase and molecular determinants of substrate selectivity. *J Biol Chem*, **280**: 738-744
- Kabsch W (1993) Automatic processing of rotation diffraction data from crystals of initially unknown symmetry and cell constants. *J Appl Cryst*, **26**: 795-800
- Kahn AH, Pessin JE (2002) Insulin regulation of glucose uptake: a complex interplay of intracellular signalling pathways. *Diabetologia*, **45**: 1475-1483
- Kahn BB, Alquier T, Carling D, Hardie DG (2005) AMP-activated protein kinase: ancient energy gauge provides clues to modern understanding of metabolism. *Cell Metab*, **1**: 15-25
- Kaji A, Saito R, Nomura M, Miyamoto K, Kiriya N (1997) Mechanism of the cytotoxicity of asterriquinone, a metabolite of *Aspergillus terreus*. *Anticancer Res*, **17**: 3675-3679
- Kantardjieff KA, Rupp B (2003) Matthews coefficient probabilities: Improved estimates for unit cell contents of proteins, DNA, and protein-nucleic acid complex crystals. *Protein Sci*, **12**: 1865-1871
- Kantardjieff KA, Rupp B (2004) Protein isoelectric point as a predictor for increased crystallization screening efficiency. *Bioinformatics*, **20**: 2162-2168
- Kashiwagi A (1995) Rationale and hurdles of inhibitors of hepatic gluconeogenesis in treatment of diabetes mellitus. *Diabetes Res Clin Pract*, **28**: S195-200
- Kauvar LM, Higgins DL, Villar HO, Sportsman JR, Engqvist-Goldstein A, Bukar R, Bauer KE, Dilley H, Roche DM (1995) Predicting ligand binding to proteins by affinity fingerprinting. *Chem Biol*, **2**: 107-118
- Keenan T, Yaeger DR, Courage NL, Rollins CT, Pavone ME, Rivera VM, Yang W, Guo T, Amara JF, Clackson T, Gilman M, Holt DA (1998) Synthesis and activity of bivalent FKBP12 ligands for the regulated dimerization of proteins. *Bioorg Med Chem*, **6**: 1309-1335
- Kemp BE, Parker MW, Hu S, Tiganis T, House C (1994) Substrate and pseudosubstrate interactions with protein kinases: determinants of specificity. *Trends Biochem Sci*, **19**: 440-444
- Kemp BE, Stapleton D, Campbell DJ, Chen ZP, Murthy S, Walter M, Gupta A, Adams JJ, Katsis F, van Denderen B, Jennings IG, Iseli T, Michell BJ, Witters LA (2003) AMP-activated protein kinase, super metabolic regulator. *Biochem Soc Trans*, **31**: 162-168
- Kemp BE (2004) Bateman domains and adenosine derivatives form a binding contract. *J Clin Invest*, **113**: 182-184
- Kerner J, Bieber L. (1990) Isolation of a malonyl-CoA-sensitive CPT/beta-oxidation enzyme complex from heart mitochondria. *Biochemistry*, **29**: 4326-4334
- Kiefersauer R, Than ME, Dobbek H, Gremer L, Melero M, Strobl S, Dias JM, Soulimane T, Huber R (2000) A novel free-mounting system for protein crystals: transformation and improvement of diffraction power by accurately controlled humidity changes. *J Appl Cryst*, **33**: 1223-1230
- Kim EK, Miller I, Aja S, Landree LE, Pinn M, McFadden J, Kuhajda FP, Moran TH, Ronnett GV (2004) C75, a fatty acid synthase inhibitor, reduces food intake via hypothalamic AMP-activated protein kinase. *J Biol Chem*, **279**: 19970-6
- King H, Aubert RE, Herman WH (1998) Global burden of diabetes, 1995-2025: prevalence, numerical estimates, and projections. *Diabetes Care*, **21**: 1414-1431
- Klammt J, Garten A, Barnikol-Oettler A, Beck-Sickinger AG, Kiess W (2005) Comparative analysis of the signaling capabilities of the insulin receptor-related receptor. *Biochem Biophys Res Commun*, **327**: 557-564

- Koch MH, Vachette P, Svergun DI (2003) Small-angle scattering: a view on the properties, structures and structural changes of biological macromolecules in solution. *Q Rev Biophys*, **36**: 147-227
- Konarev PV, Volkov VV, Sokolova AV, Koch MHJ, Svergun DI (2003) PRIMUS- a Windows-PC based system for small-angle scattering data analysis. *J Appl Crystallogr*, **36**: 1277-1282
- Kovari LC, Momany C, Rossmann MG (1995) The use of antibody fragments for crystallization and structure determinations. *Structure*, **3**: 1291-1293.
- Kuge M, Fujii Y, Shimizu T, Hirose F, Matsukage A, Hakoshima T (1997) Use of a fusion protein to obtain crystals suitable for X-ray analysis: crystallization of a GST-fused protein containing the DNA-binding domain of DNA replication-related element-binding factor, DREF. *Protein Sci*, **6**: 1783-1786
- Kyte J, Doolittle RF (1982) A simple method for displaying the hydrophobic character of a protein. *J Mol Biol*, **157**:105-132
- Laborde E, Manchem VP (2002) Small molecule activators of the insulin receptor: potential new therapeutic agents for the treatment of diabetes mellitus. *Curr Med Chem*, **9**: 2231-2242
- Lanman J, Prevelige PE Jr (2004) High-sensitivity mass spectrometry for imaging subunit interactions: hydrogen/deuterium exchange. *Curr Opin Struct Biol*, **14**: 181-188
- Leff T (2003) AMP-activated protein kinase regulates gene expression by direct phosphorylation of nuclear proteins. *Biochem Soc Trans*, **31**: 224-227
- Li M, Youngren JF, Manchem VP, Kozlowski M, Zhang BB, Maddux BA, Goldfine ID (2001) Small molecule insulin receptor activators potentiate insulin action in insulin-resistant cells. *Diabetes*. **50**: 2323-2328
- Li M, Youngren JF, Dunaif A, Goldfine ID, Maddux BA, Zhang BB, Evans JL (2002) Decreased insulin receptor (IR) autophosphorylation in fibroblasts from patients with PCOS: effects of serine kinase inhibitors and IR activators. *J Clin Endocrinol Metab*, **87**: 4088-4093
- Li S, Covino ND, Stein EG, Till JH, Hubbard SR (2003) Structural and biochemical evidence for an autoinhibitory role for tyrosine 984 in the juxtamembrane region of the insulin receptor. *J Biol Chem*, **278**: 26007-26014
- Li S, Depetris RS, Barford D, Chernoff J, Hubbard SR (2005) Crystal Structure of a Complex between Protein Tyrosine Phosphatase 1B and the Insulin Receptor Tyrosine Kinase. *Structure*, **13**: 1643-1651
- Lim K, Ho JX, Keeling K, Gilliland GL, Ji X, Ruker F, Carter DC (1994) Three-dimensional structure of *Schistosoma japonicum* glutathione S-transferase fused with a six-amino acid conserved neutralizing epitope of gp41 from HIV. *Protein Sci*, **3**: 2233-2244
- Linding R, Jensen LJ, Diella F, Bork P, Gibson TJ, Russell RB (2003) Protein disorder prediction: implications for structural proteomics. *Structure*, **11**: 1453-1459
- Liu D, Bienkowska J, Petosa C, Collier RJ, Fu H, Liddington R (1995) Crystal structure of the zeta isoform of the 14-3-3 protein. *Nature*, **376**: 191-194
- Liu K, Xu L, Szalkowski D, Li Z, Ding V, Kwei G, Huskey S, Moller DE, Heck JV, Zhang BB, Jones AB (2000) Discovery of a potent, highly selective, and orally efficacious small-molecule activator of the insulin receptor. *J Med Chem*, **43**: 3487-3494
- Liu H, Zheng G, Treber M, Dai J, Woldegiorgis G (2005) Cysteine-scanning mutagenesis of muscle carnitine palmitoyltransferase I reveals a single cysteine residue (Cys-305) is important for catalysis. *J Biol Chem*, **280**: 4524-4531

- Lizcano JM, Goransson O, Toth R, Deak M, Morrice NA, Boudeau J, Hawley SA, Udd L, Makela TP, Hardie DG, Alessi DR (2004) LKB1 is a master kinase that activates 13 kinases of the AMPK subfamily, including MARK/PAR-1. *EMBO J*, **23**:833-843
- Llovera M, de Pablo Y, Egea J, Encinas M, Peiro S, Martin-Zanca D, Rocamora N, Comella JX (2004) Trk is a calmodulin-binding protein: implications for receptor processing. *J Neurochem*, **88**: 422-433
- Lo MC, Aulabaugh A, Jin G, Cowling R, Bard J, Malamas M, Ellestad G (2004) Evaluation of fluorescence-based thermal shift assays for hit identification in drug discovery. *Anal Biochem*, **332**:153-159
- Luo RZ, Beniac DR, Fernandes A, Yip CC, Ottensmeyer FP (1999) Quaternary structure of the insulin-insulin receptor complex. *Science*, **285**: 1077-1080
- Maassen JA, 'T Hart LM, Van Essen E, Heine RJ, Nijpels G, Jahangir Tafrechi RS, Raap AK, Janssen GM, Lemkes HH (2004) Mitochondrial diabetes: molecular mechanisms and clinical presentation. *Diabetes*, **53** Suppl 1: S103-109
- Maddux BA, Goldfine ID (1991) Evidence that insulin plus ATP may induce a conformational change in the beta subunit of the insulin receptor without inducing receptor autophosphorylation. *J Biol Chem*, **266**: 6731-6736
- Majeed S, Ofek G, Belachew A, Huang CC, Zhou T, Kwong PD (2003) Enhancing protein crystallization through precipitant synergy. *Structure*, **11**: 1061-1071
- Manchem VP, Goldfine ID, Kohanski RA, Cristobal CP, Lum RT, Schow SR, Shi S, Spevak WR, Laborde E, Toavs DK, Villar HO, Wick MM, Kozlowski MR (2001) A novel small molecule that directly sensitizes the insulin receptor in vitro and in vivo. *Diabetes*, **50**: 824-830
- Manning G, Whyte DB, Martinez R, Hunter T, Sudarsanam S (2002) The protein kinase complement of the human genome. *Science*, **298**: 1912-1934
- Matsudaira PT, editor (1989) A practical guide to protein and peptide purification for microsequencing, *Academic Press, San Diego, USA*
- Matthews BW (1968) Solvent content of protein crystals. *J Mol Biol*, **33**: 491-497
- Matulis D, Kranz JK, Salemme FR, Todd MJ (2005) Thermodynamic stability of carbonic anhydrase: measurements of binding affinity and stoichiometry using ThermoFluor. *Biochemistry*, **44**: 5258-5266
- McGarry JD, Brown NF (1997) The mitochondrial carnitine palmitoyltransferase system. From concept to molecular analysis. *Eur J Biochem*, **244**: 1-14
- McGovern SL, Caselli E, Grigorieff N, Shoichet BK (2002) A common mechanism underlying promiscuous inhibitors from virtual and high-throughput screening. *J Med Chem*, **45**: 1712-1722
- McGovern SL, Helfand BT, Feng B, Shoichet BK (2003) A specific mechanism of nonspecific inhibition. *J Med Chem*, **46**: 4265-4272
- McPherson AA (2001) Comparison of salts for the crystallization of macromolecules. *Protein Sci*, **10**: 418-422
- McTigue MA, Bernstein SL, Williams DR, Tainer JA (1995A) Purification and crystallization of a schistosomal glutathione S-transferase. *Proteins*, **22**: 55-57
- McTigue MA, Williams DR, Tainer JA (1995B) Crystal structures of a schistosomal drug and vaccine target: glutathione S-transferase from *Schistosoma japonica* and its complex with the leading antischistosomal drug praziquantel. *J Mol Biol*, **246**: 21-27

- Mokdad AH, Ford ES, Bowman BA, Dietz WH, Vinicor F, Bales VS, Marks JS (2003) Prevalence of obesity, diabetes, and obesity-related health risk factors, 2001. *JAMA*, **289**: 76-79
- Moreno A, Saridakis E, Chayen NE (2002) Combination of oils and gels for enhancing the growth of protein crystals. *J Appl Cryst*, **35**: 140-142
- Munshi S, Kornienko M, Hall DL, Reid JC, Waxman L, Stirdivant SM, Darke PL, Kuo LC (2002) Crystal structure of the Apo, unactivated insulin-like growth factor-1 receptor kinase. Implication for inhibitor specificity. *J Biol Chem*, **277**: 38797-38802
- Munshi S, Hall DL, Kornienko M, Darke PL, Kuo LC (2003) Structure of apo, unactivated insulin-like growth factor-1 receptor kinase at 1.5 Å resolution. *Acta Crystallogr D Biol Crystallogr*, **D59**: 1725-1730
- Murshudov GN, Vagin AA, Lebedev A, Wilson KS, Dodson EJ (1999) Efficient anisotropic refinement of macromolecular structures using FFT. *Acta Crystallogr D Biol Crystallogr*, **55**: 247-255
- Murthy MS, Pande SV (1985) Microcompartmentation of transported carnitine, acetylcarnitine and ADP occurs in the mitochondrial matrix. Implications for transport measurements and metabolism. *Biochem J*, **230**: 657-663
- Murthy MS, Pande SV (1987) Some differences in the properties of carnitine palmitoyltransferase activities of the mitochondrial outer and inner membranes. *Biochem J*, **248**: 727-733
- Navaza J (1992) AMoRe: a new package for molecular replacement, in Molecular replacement. *Proceedings of the CCP4 Study Weekend, 87-90, Daresbury Laboratory, Warrington, England*
- Neumann D, Woods A, Carling D, Wallimann T, Schlattner U (2003) Mammalian AMP-activated protein kinase: functional, heterotrimeric complexes by co-expression of subunits in Escherichia coli. *Protein Expr Purif*, **30**: 230-237
- Nic a' Bhaird N, Kumaravel G, Gandour RD, Krueger MJ, Ramsay RR (1993) Comparison of the active sites of the purified carnitine acyltransferases from peroxisomes and mitochondria by using a reaction-intermediate analogue. *Biochem J*, **294**, 645-651
- Nölting B, Andert K (2000) Mechanism of protein folding. *Proteins*, **41**: 288-298
- Nolen B, Taylor SS, Ghosh G (2004) Regulation of protein kinases; controlling activity through activation segment conformation. *Mol Cell*, **15**: 661-675
- Obici S, Feng Z, Arduini A, Conti R, Rossetti L. (2003) Inhibition of hypothalamic carnitine palmitoyltransferase-1 decreases food intake and glucose production. *Nat Med*, **6**: 756-761
- O'Brian CA, Chu F (2005) Post-translational disulfide modifications in cell signaling-role of inter-protein, intra-protein, S-glutathionyl, and S-cysteaminy disulfide modifications in signal transmission. *Free Radic Res*, **39**: 471-480
- Ono K, Nakane H, Shimizu S, Koshimura S (1991) Inhibition of HIV-reverse transcriptase activity by asterriquinone and its analogues. *Biochem Biophys Res Commun*, **174**: 56-62
- O'Rahilly S, Barroso I, Wareham NJ (2005) Genetic factors in type 2 diabetes: the end of the beginning? *Science*, **307**: 370-373
- Palsdottir H, Hunte C (2004) Lipids in membrane protein structures. *Biochim. Biophys. Acta*, **1666**: 2-18
- Pandini G, Frasca F, Mineo R, Sciacca L, Vigneri R, Belfiore A (2002) Insulin/insulin-like growth factor I hybrid receptors have different biological characteristics depending on the insulin receptor isoform involved. *J Biol Chem*, **277**: 39684-39695

- Pantazatos D, Kim JS, Klock HE, Stevens RC, Wilson IA, Lesley SA, Woods VL Jr. (2004) Rapid refinement of crystallographic protein construct definition employing enhanced hydrogen/deuterium exchange MS. *Proc Natl Acad Sci U S A*, **101**: 751-756
- Pantoliano MW, Petrella EC, Kwasnoski JD, Lobanov VS, Myslik J, Graf E, Carver T, Asel E, Springer BA, Lane P, Salemme FR (2001) High-density miniaturized thermal shift assays as a general strategy for drug discovery. *J Biomol Screen.*, **6**: 429-440
- Parang K, Till JH, Ablooglu AJ, Kohanski RA, Hubbard SR, Cole PA (2001) Mechanism-based design of a protein kinase inhibitor. *Nat Struct Biol*, **8**: 37-41
- Parks DJ, Lafrance LV, Calvo RR, Milkiewicz KL, Gupta V, Lattanze J, Ramachandren K, Carver TE, Petrella EC, Cummings MD, Maguire D, Grasberger BL, Lu T (2005) 1,4-Benzodiazepine-2,5-diones as small molecule antagonists of the HDM2-p53 interaction: discovery and SAR. *Bioorg Med Chem Lett*, **15**: 765-770
- Parvaresch S, Yesilkaya T, Baer K, Al-Hasani H, Klein HW (2002) 14-3-3 binding to the IGF-1 receptor is mediated by serine autophosphorylation. *FEBS Lett*, **532**: 357-362
- Patel SB, Cameron PM, Frantz-Wattley B, O'Neill E, Becker JW, Scapin G (2004) Lattice stabilization and enhanced diffraction in human p38 alpha crystals by protein engineering. *Biochim Biophys Acta*, **1696**: 67-73
- Pautsch A, Zoepfel A, Ahorn H, Spevak W, Hauptmann R, Nar H (2001) Crystal structure of bisphosphorylated IGF-1 receptor kinase: insight into domain movements upon kinase activation. *Structure*, **9**: 955-965
- Pender C, Goldfine ID, Manchem VP, Evans JL, Spevak WR, Shi S, Rao S, Bajjalieh S, Maddux BA, Youngren JF (2002) Regulation of insulin receptor function by a small molecule insulin receptor activator. *J Biol Chem*, **277**: 43565-43571
- Perrakis A, Morris R, Lamzin VS (1999) Automated protein model building combined with iterative structure refinement. *Nat. Struct. Biol*, **6**: 458-463
- Persaud SJ, Asare-Anane H, Jones PM (2002) Insulin receptor activation inhibits insulin secretion from human islets of Langerhans. *FEBS Lett*, **510**: 225-228
- Petoukhov MV, Eady NA, Brown KA, Svergun DI (2002) Addition of missing loops and domains to protein models by x-ray solution scattering. *Biophys J*, **83**: 3113-3125
- Pirola L, Johnston AM, Van Obberghen E (2004) Modulation of insulin action. *Diabetologia*, **47**: 170-184
- Pirrung MC, Li Z, Park K, Zhu J (2002) Total syntheses of demethylasterriquinone B1, an orally active insulin mimetic, and demethylasterriquinone A1. *J Org Chem*, **67**: 7919-7926
- Plum L, Schubert M, Bruning JC (2005) The role of insulin receptor signaling in the brain. *Trends Endocrinol Metab*, **16**: 59-65
- Pollack SJ, Harper SJ (2002A) Trk Neurotrophin Receptor Activators. *Drug News Perspect*, **15**: 268-277
- Pollack SJ, Harper SJ (2002B) Small molecule Trk receptor agonists and other neurotrophic factor mimetics. *Curr Drug Targets CNS Neurol Disord*, **1**: 59-80
- Polekhina G, Gupta A, Michell BJ, van Denderen B, Murthy S, Feil SC, Jennings IG, Campbell DJ, Witters LA, Parker MW, Kemp BE, Stapleton D (2003) AMPK beta subunit targets metabolic stress sensing to glycogen. *Curr Biol*, **13**: 867-871

- Polekhina G, Feil SC, Gupta A, O'Donnell P, Stapleton D, Parker MW (2005A) Crystallization of the glycogen-binding domain of the AMP-activated protein kinase subunit and preliminary X-ray analysis. *Acta Crystallographica F Struct Biol Cryst Comm*, **61**: 39-42
- Polekhina G, Gupta A, van Denderen BJ, Feil SC, Kemp BE, Stapleton D, Parker MW (2005B) Structural Basis for Glycogen Recognition by AMP-Activated Protein Kinase. *Structure*, **13**: 1453-1462
- Prade L, Engh RA, Girod A, Kinzel V, Huber R, Bossemeyer D (1997) Staurosporine-induced conformational changes of cAMP-dependent protein kinase catalytic subunit explain inhibitory potential. *Structure*, **5**: 1627-1637
- Price N, van der Leij F, Jackson V, Corstorphine C, Thomson R, Sorensen A, Zammit V (2002) A novel brain-expressed protein related to carnitine palmitoyltransferase I. *Genomics*, **80**: 433-442
- Prilusky J, Felder CE, Zeev-Ben-Mordehai T, Rydberg EH, Man O, Beckmann JS, Silman I, Sussman JL (2005) FoldIndex: a simple tool to predict whether a given protein sequence is intrinsically unfolded. *Bioinformatics*, **21**: 3435-3438
- Qureshi SA, Ding V, Li Z, Szalkowski D, Biazzo-Ashnault DE, Xie D, Saperstein R, Brady E, Huskey S, Shen X, Liu K, Xu L, Salituro GM, Heck JV, Moller DE, Jones AB, Zhang BB (2000) Activation of insulin signal transduction pathway and anti-diabetic activity of small molecule insulin receptor activators. *J Biol Chem*, **275**: 36590-36595
- Ramsay RR, Gandour RD, Feike R, van der Leij FR (2001) Molecular enzymology of carnitine transfer and transport. *Biochim Biophys Acta*, **1546**: 21-43
- Randle PJ (1998) Regulatory interactions between lipids and carbohydrates: the glucose fatty acid cycle after 35 years. *Diabetes Metab Rev*, **14**: 263-283
- Ratheiser K, Schneeweiss B, Waldhausl W, Fasching P, Korn A, Nowotny P, Rohac M, Wolf HP (1991). Inhibition by etomoxir of carnitine palmitoyltransferase I reduces hepatic glucose production and plasma lipids in non-insulin-dependent diabetes mellitus. *Metabolism*, **40**: 1185-1190
- Rayment I (1997) Reductive alkylation of lysine residues to alter crystallization properties of proteins. *Methods Enzymol*, **276**: 171-179
- Rice P, Longden I, Bleasby A (2000) EMBOSS: the European Molecular Biology Open Software Suite. *Trends Genet.*, **16**: 276-277
- Rickwood D, Chambers JAA (1984) *Centrifugation, a Practical Approach, 2nd Edition*, IRL Press, Oxford, UK
- Rollins CT, Rivera VM, Woolfson DN, Keenan T, Hatada M, Adams SE, Andrade LJ, Yaeger D, van Schravendijk MR, Holt DA, Gilman M, Clackson T (2000) A ligand-reversible dimerization system for controlling protein-protein interactions. *Proc Natl Acad Sci U S A*, **97**: 7096-7101
- Rondinone CM (2005) Diabetes: the latest developments in inhibitors, insulin sensitisers, new drug targets and novel approaches. October 18-19, 2004, The Hatton, London, UK. *Expert Opin Ther Targets*, **9**: 415-8
- Ronnett GV, Kim EK, Landree LE, Tu Y (2005) Fatty acid metabolism as a target for obesity treatment. *Physiol Behav*, **85**: 25-35
- Roversi P, Blanc E, Vonrhein C, Evans G, Bricogne G (2000) Modelling prior distributions of atoms for macromolecular refinement and completion. *Acta Crystallogr D Biol Crystallogr*, **56**: 1316-1323
- Rubio-Gozalbo ME, Bakker JA, Waterham HR, Wanders RJ (2004) Carnitine-acylcarnitine translocase deficiency, clinical, biochemical and genetic aspects. *Mol Aspects Med*, **25**: 521-532

- Rudolph MJ, Amodeo GA, Bai Y, Tong L (2005) Crystal structure of the protein kinase domain of yeast AMP-activated protein kinase Snf1. *Biochem Biophys Res Commun*, **337**: 1224-1228
- Ruegg UT, Burgess GM (1989) Staurosporine, K-252 and UCN-01: potent but nonspecific inhibitors of protein kinases. *Trends Pharmacol Sci*, **10**: 218-220
- Rufer AC, Thiebach L, Baer K, Klein HW, Hennig M (2005) X-ray structure of glutathione S-transferase from *Schistosoma japonicum* in a new crystal form reveals flexibility of the substrate-binding site. *Acta Crystallographica F Struct Biol Cryst Comm*, **F61**: 263-265
- Saha AK, Avilucea PR, Ye JM, Assifi MM, Kraegen EW, Ruderman NB (2004) Pioglitazone treatment activates AMP-activated protein kinase in rat liver and adipose tissue in vivo. *Biochem Biophys Res Commun*, **314**: 580-585
- Salituro GM, Pelaez F, Zhang BB (2001) Discovery of a small molecule insulin receptor activator. *Recent Prog Horm Res*, **56**: 107-126
- Salt I, Celler JW, Hawley SA, Prescott A, Woods A, Carling D, Hardie DG (1998) AMP-activated protein kinase: greater AMP dependence, and preferential nuclear localization, of complexes containing the alpha2 isoform. *Biochem J*, **334**: 177-187
- Sanchez-Margalet V, Goldfine ID, Truitt K, Imboden J, Sung CK (1995) Role of p85 subunit of phosphatidylinositol-3-kinase as an adaptor molecule linking the insulin receptor to insulin receptor substrate 1. *Mol Endocrinol*, **9**: 435-442
- Schinner S, Scherbaum WA, Bornstein SR, Barthel A (2005) Molecular mechanisms of insulin resistance. *Diabet Med*, **22**: 674-682.
- Schmid E, El Benna J, Galter D, Klein G, Droge W (1998) Redox priming of the insulin receptor beta-chain associated with altered tyrosine kinase activity and insulin responsiveness in the absence of tyrosine autophosphorylation. *FASEB J*, **12**: 863-870
- Schmid E, Hotz-Wagenblatt A, Hacj V, Droge W (1999A) Phosphorylation of the insulin receptor kinase by phosphocreatine in combination with hydrogen peroxide: the structural basis of redox priming. *FASEB J*, **13**: 1491-1500
- Schmid E, Hotz-Wagenblatt A, Droge W (1999B) Inhibition of the insulin receptor kinase phosphorylation by nitric oxide: functional and structural aspects. *Antioxid Redox Signal*, **1**: 45-53
- Schmitt TL, Hotz-Wagenblatt A, Klein H, Droge W (2005) Interdependent regulation of insulin receptor kinase activity by ADP and hydrogen peroxide. *J Biol Chem*, **280**: 3795-37801
- Schuck P (1994) Simultaneous radial and wavelength analysis with the Optima XL-A analytical ultracentrifuge. *Progr Colloid Polym Sc*, **94**: 1-13
- Scopes, RK (1993) Protein purification. Principles and Practice. *Springer Advanced Texts in Chemistry, 3rd edition, New York, NY, USA*
- Scott JW, Hawley SA, Green KA, Anis M, Stewart G, Scullion GA, Norman DG, Hardie DG (2004) CBS domains form energy-sensing modules whose binding of adenosine ligands is disrupted by disease mutations. *J Clin Invest*, **113**: 274-284
- Seidler J, McGovern SL, Doman TN, Shoichet BK (2003) Identification and prediction of promiscuous aggregating inhibitors among known drugs. *J Med Chem*, **46**: 4477-4486
- Seino S, Bell GI (1989) Alternative splicing of human insulin receptor messenger RNA. *Biochem Biophys Res Commun*. **159**: 312-316

- Shen H, Frey DD (2004) Charge regulation in protein ion-exchange chromatography: development and experimental evaluation of a theory based on hydrogen ion Donnan equilibrium. *J Chromatogr A*, **1034**, 55-68
- Shih DQ, Stoffel M (2002) Molecular etiologies of MODY and other early-onset forms of diabetes. *Curr Diab Rep.* **2**: 125-134
- Shinagawa S, Kanamaru T, Harada S, Asai M, Okazaki H (1987) Chemistry and inhibitory activity of long chain fatty acid oxidation of emariamine and its analogues. *J Med Chem*, **30**: 1458-1463
- Smyth DR, Mrozkiewicz MK, McGrath WJ, Listwan P, Kobe B (2003) Crystal structures of fusion proteins with large-affinity tags. *Protein Sci*, **12**: 1313-1322
- Sowadski JM, Ellis CA, Madhusudan (1996) Detergent binding to unmyristylated protein kinase A--structural implications for the role of myristate. *J Bioenerg Biomembr*, **28**: 7-12.
- Stamos J, Sliwkowski MX, Eigenbrot C (2002) Structure of the epidermal growth factor receptor kinase domain alone and in complex with a 4-anilinoquinazoline inhibitor. *J Biol Chem*, **277**: 46265-46272.
- Stein SC, Woods A, Jones NA, Davison MD, Carling D (2000) The regulation of AMP-activated protein kinase by phosphorylation. *Biochem J*, **345**: 437-443
- Strowski MZ, Li Z, Szalkowski D, Shen X, Guan XM, Juttner S, Moller DE, Zhang BB (2004) Small-molecule insulin mimetic reduces hyperglycemia and obesity in a nongenetic mouse model of type 2 diabetes. *Endocrinology*, **145**: 5259-5268
- Stumvoll M, Goldstein BJ, van Haeften TW (2005) Type 2 diabetes: principles of pathogenesis and therapy. *Lancet*, **365**: 1333-1346
- Sung CK, Choi WS, Sanchez-Margalet V (1998) Guanosine triphosphatase-activating protein-associated protein, but not src-associated protein p68 in mitosis, is a part of insulin signaling complexes. *Endocrinology*, **139**: 2392-2398
- Svergun DI (1999) Restoring low resolution structure of biological macromolecules from solution scattering using simulated annealing. *Biophys J*, **76**: 2879-2886
- Svergun DI, Koch MH (2002) Advances in structure analysis using small-angle scattering in solution. *Curr Opin Struct Biol*, **12**: 654-660
- Svergun DI, Koch MH (2003) Small-angle scattering studies of biological macromolecules in solution. *Rep Prog Phys*, **66**: 1735-1782
- Sweet LJ, Wilden PA, Pessin JE (1986) Dithiothreitol activation of the insulin receptor/kinase does not involve subunit dissociation of the native alpha 2 beta 2 insulin receptor subunit complex. *Biochemistry*, **25**: 7068-7074
- Tang L, Guo B, van Wijnen AJ, Lian JB, Stein JL, Stein GS, Zhou GW (1998) Preliminary crystallographic study of glutathione S-transferase fused with the nuclear matrix targeting signal of the transcription factor AML-1/CBF-alpha2. *J Struct Biol*, **123**: 83-85
- Taroni F, Verderio E, Dworzak F, Willems PJ, Cavadini P, DiDonato S (1993) Identification of a common mutation in the carnitine palmitoyltransferase II gene in familial recurrent myoglobinuria patients. *Nat Genet*, **4**: 314-320
- Tennagels N, Telting D, Parvaresh S, Maassen JA, Klein HW (2001) Identification of Ser(1275) and Ser(1309) as autophosphorylation sites of the human insulin receptor in intact cells. *Biochem Biophys Res Commun*, **282**: 387-393

- Thuillier L, Rostane H, Droin V, Demaugre F, Brivet M, Kadhom N, Prip-Buus C, Gobin S, Saudubray JM, Bonnefont JP (2003) Correlation between genotype, metabolic data, and clinical presentation in carnitine palmitoyltransferase 2 (CPT2) deficiency. *Hum Mutat*, **21**: 493-501
- Till JH, Ablooglu AJ, Frankel M, Bishop SM, Kohanski RA, Hubbard SR (2001) Crystallographic and solution studies of an activation loop mutant of the insulin receptor tyrosine kinase: insights into kinase mechanism. *J Biol Chem*, **276**: 10049-10055
- Tonks NK (2005) Redox redux: revisiting PTPs and the control of cell signaling. *Cell*, **121**: 667-670
- Tonazzi A, Giangregorio N, Indiveri C, Palmieri F (2005) Identification by site-directed mutagenesis and chemical modification of three vicinal cysteine residues in rat mitochondrial carnitine/acylcarnitine transporter. *J Biol Chem*, **280**: 19607-19612
- Tsuboi T, da Silva Xavier G, Leclerc I, Rutter GA 5'-AMP-activated protein kinase controls insulin-containing secretory vesicle dynamics (2003) *J Biol Chem*, **278**, 52042-52051
- Ullrich A, Bell JR, Chen EY, Herrera R, Petruzzelli LM, Dull TJ, Gray A, Coussens L, Liao YC, Tsubokawa M, *et al.* (1985) Human insulin receptor and its relationship to the tyrosine kinase family of oncogenes. *Nature*, **313**: 756-761
- Uversky VN, Gillespie JR, Fink AL (2000) Why are "natively unfolded" proteins unstructured under physiologic conditions? *Proteins*, **41**: 415-427
- Vajo Z, Duckworth WC (2000) Genetically engineered insulin analogs: diabetes in the new millenium. *Pharmacol Rev*, **52**: 1-9
- Van Obberghen E, Baron V, Delahaye L, Emanuelli B, Filippa N, Giorgetti-Peraldi S, Lebrun P, Mothe-Satney I, Peraldi P, Rocchi S, Sawka-Verhelle D, Tartare-Deckert S, Giudicelli J (2001) Surfing the insulin signaling web. *Eur J Clin Invest*, **31**: 966-977
- Wagman AS, Nuss JM (2001) Current therapies and emerging targets for the treatment of diabetes. *Curr Pharm Des*, **7**: 417-450
- Warden SM, Richardson C, O'Donnell J Jr, Stapleton D, Kemp BE, Witters LA (2001) Post-translational modifications of the beta-1 subunit of AMP-activated protein kinase affect enzyme activity and cellular localization. *Biochem J*, **354**: 275-283
- Weber MA, Lidor A, Arora S, Salituro GM, Zhang BB, Sidawy AN (2000) A novel insulin mimetic without a proliferative effect on vascular smooth muscle cells. *J Vasc Surg*, **32**: 1118-1126
- Webster NJ, Park K, Pirrung MC (2003) Signaling effects of demethylasterriquinone B1, a selective insulin receptor modulator. *Chembiochem*, **4**: 379-385
- Wei L, Hubbard SR, Hendrickson WA, Ellis L (1995) Expression, characterization, and crystallization of the catalytic core of the human insulin receptor protein-tyrosine kinase domain. *J Biol Chem*, **270**: 8122-8130
- White MF (2003) Insulin signaling in helath and disease. *Science*, **302**: 1710-1711
- Wieser T, Deschauer M, Olek K, Hermann T, Zierz S (2003) Carnitine palmitoyltransferase II deficiency: molecular and biochemical analysis of 32 patients. *Neurology*, **60**: 1351-1353
- Wijeratne EM, Turbyville TJ, Zhang Z, Bigelow D, Pierson LS 3rd, VanEtten HD, Whitesell L, Canfield LM, Gunatilaka AA (2003) Cytotoxic constituents of *Aspergillus terreus* from the rhizosphere of *Opuntia versicolor* of the Sonoran Desert. *J Nat Prod*, **66**: 1567-1573

- Wilden PA, Boyle TR, Swanson ML, Sweet LJ, Pessin JE (1986) Alteration of intramolecular disulfides in insulin receptor/kinase by insulin and dithiothreitol: insulin potentiates the apparent dithiothreitol-dependent subunit reduction of insulin receptor. *Biochemistry*, **25**: 4381-4388
- Wilden PA, Pessin JE (1987) Differential sensitivity of the insulin-receptor kinase to thiol and oxidizing agents in the absence and presence of insulin. *Biochem J*, **245**: 325-331
- Wilkie N, Wingrove PB, Bilsland JG, Young L, Harper SJ, Hefti F, Ellis S, Pollack SJ (2001) The non-peptidyl fungal metabolite L-783,281 activates TRK neurotrophin receptors. *J Neurochem*, **78**: 1135-1145
- Wilkinson DL, Harrison RG (1991) Predicting the solubility of recombinant proteins in *Escherichia coli*. *Biotechnology*, **9**: 443-448
- Williams JF, McClain DA, Dull TJ, Ullrich A, Olefsky JM (1990) Characterization of an insulin receptor mutant lacking the subunit processing site. *J Biol Chem*, **265**: 8463-8469
- Wilm M, Mann M (1996) Analytical Properties of the Nano-electrospray Ion Source. *Anal Chem*, **68**: 1-8
- Woeltje KF, Esser V, Weis BC, Cox WF, Schroeder JG, Liao ST, Foster DW, McGarry JD (1990) Inter-tissue and inter-species characteristics of the mitochondrial carnitine palmitoyltransferase enzyme system. *J Biol Chem*, **265**: 10714-10719
- Wolf HP, Engel DW (1985) Decrease of fatty acid oxidation, ketogenesis and gluconeogenesis in isolated perfused rat liver by phenylalkyl oxirane carboxylate (B 807-27) due to inhibition of CPT I (EC 2.3.1.21). *Eur J Biochem*, **146**: 359-363
- Wood HB Jr, Black R, Salituro G, Szalkowski D, Li Z, Zhang Y, Moller DE, Zhang B, Jones AB (2000) The basal SAR of a novel insulin receptor activator. *Bioorg Med Chem Lett*, **10**: 1189-1192
- Woods A, Johnstone SR, Dickerson K, Leiper FC, Fryer LG, Neumann D, Schlattner U, Wallimann T, Carlson M, Carling D (2003) LKB1 is the upstream kinase in the AMP-activated protein kinase cascade. *Curr Biol*, **13**: 2004-2008
- Woods A, Dickerson K, Heath R, Hong SP, Momcilovic M, Johnstone SR, Carlson M, Carling D (2005) (Ca²⁺)/calmodulin-dependent protein kinase-beta acts upstream of AMP-activated protein kinase in mammalian cells. *Cell Metab*, **2**: 21-33
- Wu D, Govindasamy L, Lian W, Gu Y, Kukar T, Agbandje-McKenna M, McKenna R (2003) Structure of human carnitine acetyltransferase. Molecular basis for fatty acyl transfer. *J Bio Chem*, **278**: 13159-13165
- Xiao B, Smerdon SJ, Jones DH, Dodson GG, Soneji Y, Aitken A, Gamblin SJ (1995) Structure of a 14-3-3 protein and implications for coordination of multiple signalling pathways. *Nature*, **376**: 188-191
- Xing Y, Xu W (2003) Crystallization of the PX domain of cytokine-independent survival kinase (CISK): improvement of crystal quality for X-ray diffraction with sodium malonate. *Acta Crystallogr D Biol Crystallogr*, **59**: 1816-1818
- Yamaguchi Y, Flier JS, Benecke H, Ransil BJ, Moller DE (1993) Ligand-binding properties of the two isoforms of the human insulin receptor. *Endocrinology*, **132**: 1132-1138
- Yang J, Symes K, Mercola M, Schreiber SL (1998) Small-molecule control of insulin and PDGF receptor signaling and the role of membrane attachment. *Curr Biol*, **8**: 11-18
- Ye JM, Ruderman NB, Kraegen EW (2005) AMP-activated protein kinase and malonyl-CoA: targets for treating insulin resistance? *Drug Discovery Today: Therapeutic Strategies*, **2**: 157-163
- Zammit VA (1999A) The malonyl-CoA-long-chain acyl-CoA axis in the maintenance of mammalian cell function. *Biochem J*, **343**: 505-515

- Zammit VA (1999B) Carnitine acyltransferases: functional significance of subcellular distribution and membrane topology. *Prog Lipid Res*, **38**: 199-224
- Zhan Y, Song X, Zhou GW (2001) Structural analysis of regulatory protein domains using GST-fusion proteins. *Gene*, **281**: 1-9
- Zhang B, Salituro G, Szalkowski D, Li Z, Zhang Y, Royo I, Vilella D, Diez MT, Pelaez F, Ruby C, Kendall RL, Mao X, Griffin P, Calaycay J, Zierath JR, Heck JV, Smith RG, Moller DE (1999) Discovery of a small molecule insulin mimetic with antidiabetic activity in mice. *Science*, **284**: 974-977
- Zhang BB, Moller DE (2000) New approaches in the treatment of type 2 diabetes. *Curr Opin Chem Biol*, **4**: 461-467
- Zheng G, Dai J, Woldegiorgis G (2002) Identification by mutagenesis of a conserved glutamate (Glu487) residue important for catalytic activity in rat liver carnitine palmitoyltransferase II. *J Biol Chem*, **277**: 42219-42223
- Zhou G, Myers R, Li Y, Chen Y, Shen X, Fenyk-Melody J, Wu M, Ventre J, Doebber T, Fujii N, Musi N, Hirshman MF, Goodyear LJ, Moller DE (2001) Role of AMP-activated protein kinase in mechanism of metformin action. *J Clin Invest*, **108**: 1167-1174
- Zou MH, Kirkpatrick SS, Davis BJ, Nelson JS, Wiles WG 4th, Schlattner U, Neumann D, Brownlee M, Freeman MB, Goldman MH. (2004) Activation of the AMP-activated protein kinase by the anti-diabetic drug metformin in vivo. Role of mitochondrial reactive nitrogen species. *J Biol Chem*, **279**: 43940-43951
- Zick Y (2003) Role of Ser/Thr kinases in the uncoupling of insulin signaling. *Int J Obes Relat Metab Disord*, **27** Suppl 3: S56-60
- Zick Y (2005) Ser/Thr phosphorylation of IRS proteins: a molecular basis for insulin resistance. *Sci STKE*, **268**: pe4
- Zimmet P, Alberti KG, Shaw J (2001) Global and societal implications of the diabetes epidemic. *Nature*, **414**: 782-787
- Zulauf M, D'Arcy A (1992) Light scattering of proteins as a criterion for crystallization. *J Cryst Growth*, **122**: 102-106

7 Appendix

7.1

Rufer AC, Thiebach L, Baer K, Klein HW, Hennig M (2005) X-ray structure of glutathione S-transferase from *Schistosoma japonicum* in a new crystal form reveals flexibility of the substrate-binding site. *Acta Crystallographica F Struct Biol Cryst Comm*, **F61**: 263-265

Poster presented at DGK Meeting, Cologne, 02/28/2005 - 03/04/2005:

X-ray-structure of glutathione S-transferase from *Schistosoma japonicum* in a new crystal form reveals flexibility of substrate binding site. Rufer AC, Thiebach L, Baer K, Klein HW, Hennig M

7.2

AMPK_α2_1-339_D56A/R171E/T172D diffraction images recorded at Proteros, Munich, on the Free Mounting™ system

7.3

Nucleotide and amino acid sequence of the α2-subunit of rat AMPK; primer

7.4

Abbreviations

Arne Christian Rufer,^{a,b*} Lars
Thiebach,^b Kristin Baer,^b
Helmut W. Klein^b and Michael
Hennig^a^aF. Hoffmann–La Roche AG, Pharma Research
Discovery Chemistry, 4070 Basel, Switzerland,
and ^bUniversity of Cologne, Institute for
Biochemistry, 50674 Cologne, Germany

Correspondence e-mail: arne.rufer@roche.com

Received 22 November 2004
Accepted 11 February 2005
Online 24 February 2005**PDB Reference:** glutathione *S*-transferase, 1y6e,
r1y6esf.

X-ray structure of glutathione *S*-transferase from *Schistosoma japonicum* in a new crystal form reveals flexibility of the substrate-binding site

The crystal structure of the 26 kDa glutathione *S*-transferase from *Schistosoma japonicum* (*Sj*GST) was determined at 3 Å resolution in the new space group $P2_12_12_1$. The structure of orthorhombic *Sj*GST reveals unique features of the ligand-binding site and dimer interface when compared with previously reported structures. *Sj*GST is recognized as the major detoxification enzyme of *S. japonicum*, a pathogenic helminth causing schistosomiasis. As resistance against the established inhibitor of *Sj*GST, praziquantel, has been reported these results might prove to be valuable for the development of novel drugs.

1. Introduction

A fusion protein of the constitutively dimeric 26 kDa glutathione *S*-transferase from *Schistosoma japonicum* (*Sj*GST) with the full-length intracellular domain of the human insulin receptor facilitates investigation of receptor tyrosine kinase activation mediated by dimerization (Baer *et al.*, 2001). As the structures of both the core kinase domain of the human insulin receptor (IRK; Hubbard *et al.*, 1994) and *Sj*GST (McTigue *et al.*, 1995) are known, we attempted to crystallize the corresponding fusion protein, *Sj*GST-IRK, by means of carrier-protein-driven crystallization (Carter *et al.*, 1994; Lim *et al.*, 1994; Zhan *et al.*, 2001; Smyth *et al.*, 2003). The construct *Sj*GST-IRK was shown to be stable during purification and kinase activity was demonstrated in both auto- and substrate-phosphorylation assays (Baer, personal communication).

Crystallization experiments with the fusion protein yielded crystals that were shown to consist of *Sj*GST only. The fusion protein is obviously cleaved under the crystallization conditions and the released *Sj*GST crystallizes in a new crystal form ($P2_12_12_1$), showing distinctively novel features of the dimer interface and ligand-binding site. Coordinates and structure factors have been deposited in the PDB (PDB code 1y6e).

2. Experimental methods

Cloning of the construct GST-IRK will be described elsewhere (Baer *et al.*, manuscript in preparation). A PCR product comprising the coding region of IRK (residues Val966–Lys1271, C969S, Y972F) was cloned into pAc-G2T, resulting in a fusion protein containing a thrombin-cleavage site as a linker between GST and IRK. Expression in Sf9 cells and purification was performed according to Baer *et al.* (2001), with the exception that the crude lysate was incubated for 30 min at 277 K after adding Triton X-100 in order to solubilize *Sj*GST-IRK and Tris-(2-carboxyethyl)-phosphine hydrochloride (TCEP) was used as a reducing agent during purification and subsequent crystallization. 10^9 cells from a 1 l fermentation typically yielded 10 mg of GST-IRK, which was found to be electrophoretically pure (Fig. 1).

Prior to crystallization, GST-IRK was concentrated to 10 mg ml^{-1} in 20 mM Tris-HCl pH 7.5, 150 mM NaCl, 2 mM TCEP in a 30 kDa concentrator (Amicon, Millipore). Crystallization trials were set up directly after purification at 294 K with the modified microbatch method (D'Arcy *et al.*, 2003) and crystals appeared within 7 d with 0.1 M Bis-Tris pH 5.5, 25% (w/v) PEG 3350 (Index Screen condition No. 42; Hampton Research) and 0.1 M sodium acetate pH 5.5,

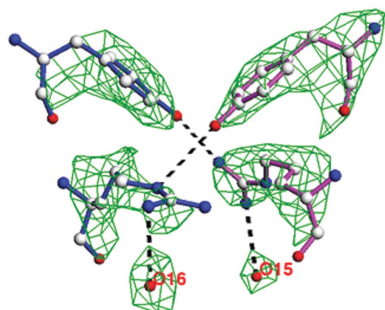


Table 1
Data-collection and refinement statistics.

Values in parentheses are for the highest resolution shell.

Beamline	X06SA, SLS
Wavelength (Å)	0.90006
Resolution (Å)	30.0–3.0 (3.14–3.0)
Space group	$P2_12_12_1$
Unit-cell parameters (Å)	$a = 161.22, b = 50.75, c = 57.50$
V_M † (Å ³ Da ⁻¹)	2.2
Solvent content (%)	44.8
Total reflections	114066
Unique reflections	9910
Average redundancy	11.5 (8.6)
$I/\sigma(I)$	8.1 (5.5)
Completeness (%)	99.6 (99.4)
Wilson B (Å ²)	43.2
$R_{\text{merge}}^{\ddagger}$	12.3 (43.7)
$\langle B \rangle$ (Å ²)	36.7
$\sigma(B)$ (Å ²)	14.8
R_{cryst} (%)	21.1
R_{free} (%)	27.9
R.m.s.d. bond lengths (Å)	0.008
R.m.s.d. bond angles (°)	1.44
Ramachandran plot (%)	
Most preferred regions	85.9
Allowed regions	12.8
Generously allowed regions	1.3
Disallowed regions	0.0

† Matthews (1968). ‡ $R_{\text{merge}} = \sum_{hkl} \sum_i |I_i(hkl) - \langle I(hkl) \rangle| / \sum_{hkl} \sum_i I_i(hkl)$.

36% (w/v) PEG MME 5000 (Stura Footprint Screen 2 condition No. 20; Molecular Dimensions Ltd) as precipitant solutions. Crystals grew to a maximum diameter of 15 μm within 7 d and were flash-frozen in liquid nitrogen directly from the screening plates.

Data were collected at the Swiss Light Source beamline X06SA at 100 K using a 165 mm MAR CCD detector with a 260 mm crystal-to-detector distance and an oscillation range of 1°. 180 frames were collected and processed with *DENZO* and *SCALEPACK* (Otwinowski, 1993). Despite their small size, the crystals diffracted to 3.0 Å resolution and analysis of the systematic absences revealed that they belong to space group $P2_12_12_1$. A noncrystallographic twofold axis generates one GST dimer per asymmetric unit. The crystallographic parameters are summarized in Table 1.

A molecular-replacement solution was found with the program *MOLREP* (Vagin & Teplyakov, 1997; Collaborative Computational Project, Number 4, 1994) using the modified PDB entry 1dug (Ware *et al.*, 1999), *i.e.* an unligated dimer of GST comprising residues 1–217. Following rigid-body refinement in *REFMAC* (Murshudov *et al.*, 1997; Collaborative Computational Project, Number 4, 1994), the structure of orthorhombic GST was refined by iterative conjugate-gradient minimization with subsequent grouped *B*-factor refinement in *CNX* (Brünger, 1992) and manual model building with *MOLOC* (Gerber, 1992; refinement statistics in Table 1). The two carboxy-

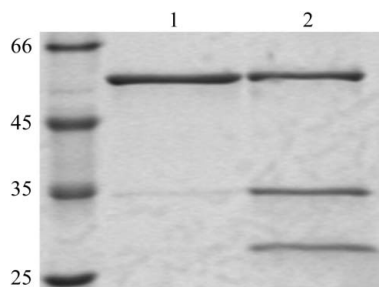


Figure 1
SDS-PAGE. Lane 1 shows the pooled elution fractions of SjGST-IRK from a gel-filtration column. In lane 2 the same preparation is depicted after storage on ice for 10 d. The molecular weights (kDa) of the marker proteins are indicated.

Table 2
26 kDa SjGST (EC 2.5.1.18) structures in PDB.

PDB entry	Space group	Unit-cell parameters			Apo/ligand	Fusion protein
		<i>a</i> (Å)	<i>b</i> (Å)	<i>c</i> (Å)		
1dug	$P4_12_12$	105.78	105.78	137.23	1	Yes
1b8x	$P4_32_12$	93.40	93.40	57.60	a	Yes
1bg5	$P4_32_12$	92.17	92.17	57.57	a	Yes
1gne	$P4_32_12$	94.74	94.74	58.13	1	Yes
1ua5	$P4_32_12$	92.53	92.53	57.66	1	No
1gta	$P6_322$	125.20	125.20	70.20	a	No
1gtb	$P6_322$	123.80	123.80	70.20	1	No
1m99	$P6_322$	115.07	115.07	78.28	1	No
1m9a	$P6_322$	114.99	114.99	78.35	1	No
1m9b	$P6_322$	116.57	116.57	78.75	1	No

terminal amino acids Pro217 and Lys218 have been omitted from refinement because no clear electron density was visible for these residues. Based on the same argument, six residues (*i.e.* SDLVPR) of the linker peptide encoded by pAc-G2T that were still attached at the carboxy-terminus of the SjGST moiety according to mass spectrometry and amino-terminal sequencing (data not shown) were also left out from refinement. Finally, 16 water molecules were added manually based on electron density and hydrogen bonding.

3. Results and discussion

Analysis of the X-ray data resulted in determination of the space group as orthorhombic $P2_12_12_1$, with unit-cell parameters $a = 161.22$, $b = 50.75$, $c = 57.50$ Å. The calculated volume of the asymmetric unit, 117 622.3 Å³, was obviously incompatible with the presence of the intact fusion protein with a molecular weight of 61 kDa. Consequently, we concluded that only a fragment of SjGST-IRK had crystallized. Although the fusion protein had been purified to homogeneity, it was realised that the protein spontaneously degraded to SjGST and IRK during prolonged storage on ice (*i.e.* within 10 d), independent of the purification protocol employed (Fig. 1). Addition of protease inhibitors (RoComplete, Roche; diisopropyl fluorophosphate, Fluka) to the storage buffer did not prevent degradation and no proteases could be detected using a sensitive spectroscopic assay with resorufin-labelled casein as substrate (Universal Protease Substrate assay, Roche). We assume that spontaneous autocatalytic cleavage as described for nucleolin (Chen *et al.*, 1991), which also undergoes degradation independent of both exogenous and endogenous protease activity, could be the reason for the degradation. Replacement of the pAc-G2T linker with a thrombin-cleavage site by a more rigid connection according to Smyth *et al.* (2003) was not pursued as the introduction of a (Gly-Ala)₅ linker resulted in significant loss of activity in autophosphorylation assays indicating suboptimal alignment of the kinase domains.

Molecular-replacement trials with a high-resolution structure of SjGST (PDB code 1dug) were performed which yielded marked peaks for both the rotation and translation functions. Given the crystal packing and electron density, the crystals were determined to consist of SjGST crystallized in space group $P2_12_12_1$ (Table 1). To our knowledge these are the first orthorhombic crystals of SjGST, as exclusively tetragonal and hexagonal crystal forms have been reported so far (Table 2; for a review, see Zhan *et al.*, 2001). For the deposited SjGST structures no correlation exists between space group and crystallization conditions in terms of protein fusion or presence of ligand (Table 2). Inspection of the crystal packing in orthorhombic SjGST leads to the conclusion that the solvent-channel cavity around the carboxy-termini could potentially accommodate covalently linked peptides but no larger protein domain for carrier-

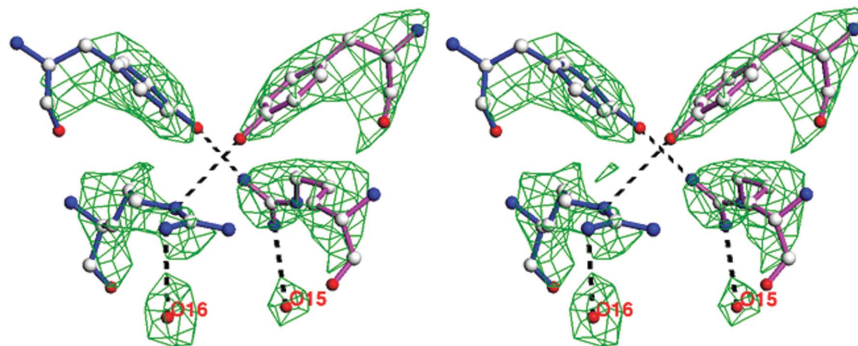


Figure 2

Stereoview of the reciprocal dimer contact between Tyr103 and Arg107 of chains *A* (blue) and *B* (magenta). The distance of the hydroxy O atom of Tyr103A to the terminal amino N atom of Arg107B is 3.3 Å and N^ε of Arg107A is 3.5 Å away from the hydroxy O atom of Tyr103B. Residues Arg107 of chains *A* and *B* each hydrogen bond (3.3 and 3.1 Å distance to W16 and W15, respectively) to water molecules.

protein-driven crystallization. Although the overall structure of orthorhombic *Sj*GST is similar to previously reported *Sj*GST structures solved in different space groups (r.m.s.d.s for main- and side-chain atoms are 0.51 and 1.34 Å for chain *A* and 0.86 and 1.47 Å for chain *B* using residues 1–217 of 1dug as reference), a unique contact in the dimer interface was identified in the present structure.

The $F_o - F_c$ simulated-annealing omit electron-density map contoured at 4σ clearly indicates that the side chains of Tyr103 are rotated by approximately 100° around the $C^\alpha - C^\beta$ bond and the positions of the side chains of Arg107 are considerably different compared with all previously published *Sj*GST structures (Fig. 2). The phenyl hydroxy group of Tyr103 in chain *A* is at a hydrogen-bonding distance from the guanidinium group of Arg107 of chain *B* (and *vice versa*), thereby establishing a reciprocal dimer contact. Interestingly, residue Tyr103 of *Sj*GST is a critical part of the hydrophobic binding site (H-site) for endogenous substrates, xenobiotics and the only effective anti-schistosomal drug praziquantel, which additionally contacts Arg107 (McTigue *et al.*, 1995; Cardoso *et al.*, 2003; Hu *et al.*, 2004). In the structure presented here, Tyr103 partially occupies the praziquantel-binding site. Although the structure of *Sj*GST with bound praziquantel and its corresponding apo-structure (PDB codes 1gtb and 1gta, respectively; McTigue *et al.*, 1995) imply a preformed binding site for the drug, our data reveal a conformational flexibility for the critical residues Tyr103 and Arg107. This, together with the absence of a homologous tyrosine residue in mammalian GSTs (McTigue *et al.*, 1995), might support the design of specific drugs targeting the 26 kDa GST of *Schistosoma* spp., which have already been shown to develop resistance against praziquantel (Hu *et al.*, 2004, and references therein). The need for novel highly potent drugs is also emphasized by the finding that an estimated 250 million people are infected with *Schistosoma* spp.

The authors would like to thank the staff of X06SA at SLS, Villigen, Switzerland for support during data collection, A. Friedlein

(F. Hoffmann–La Roche Ltd, Basel) for MS analysis, M. Gompert (University of Cologne) for maintaining Sf9 cell cultures and Anke Klose (University of Cologne) for constructing the linker mutant.

References

- Baer, K., Al-Hasani, H., Parvaresch, S., Corona, T., Rufer, A., Nolle, V., Bergschneider, E. & Klein, H. W. (2001). *Biochemistry*, **40**, 14268–14278.
- Brünger, A. T. (1992). *X-PLOR Manual Version 3.1*. New Haven, CT, USA: Yale University Press.
- Cardoso, R. M., Daniels, D. S., Bruns, C. M. & Tainer, J. A. (2003). *Proteins*, **51**, 137–146.
- Carter, D. C., Rüker, F., Ho, J. X., Lim, K., Keeling, K., Gilliland, G. & Ji, X. (1994). *Protein Pept. Lett.* **1**, 175–178.
- Chen, C. M., Chiang, S. Y. & Yeh, N. H. (1991). *J. Biol. Chem.* **266**, 7754–7758.
- Collaborative Computational Project, Number 4 (1994). *Acta Cryst.* **D50**, 760–763.
- D'Arcy, A., Mac Sweeney, A., Stihle, M. & Haber, A. (2003). *Acta Cryst.* **D59**, 396–399.
- Gerber, P. R. (1992). *Biopolymers*, **32**, 1003–1017.
- Lim, K., Ho, J. X., Keeling, K., Gilliland, G. L., Ji, X., Rüker, F. & Carter, D. C. (1994). *Protein Sci.* **3**, 2233–2244.
- Hu, W., Brindley, P. J., McManus, D. P., Feng, Z. & Han, Z. G. (2004). *Trends Mol. Med.* **10**, 217–225.
- Hubbard, S. R., Wei, L., Ellis, L. & Hendrickson, W. (1994). *Nature (London)*, **372**, 746–753.
- McTigue, M. A., Williams, D. R. & Tainer, J. A. (1995). *J. Mol. Biol.* **246**, 21–27.
- Matthews, B. W. (1968). *J. Mol. Biol.* **33**, 491–497.
- Murshudov, G. N., Vagin, A. A. & Dodson, E. J. (1997). *Acta Cryst.* **D53**, 240–255.
- Otwinowski, Z. (1993). *Proceedings of the CCP4 Study Weekend. Data Collection and Processing*, edited by L. Sawyer, N. Isaacs & S. Bailey, pp. 56–62. Warrington: Daresbury Laboratory.
- Smyth, D. R., Mrozkiewicz, M. K., McGrath, W. J., Listwan, P. & Kobe, B. (2003). *Protein Sci.* **12**, 1313–1322.
- Vagin, A. & Teplyakov, A. (1997). *J. Appl. Cryst.* **30**, 1022–1025.
- Ware, S., Donahue, J. P., Hawiger, J. & Anderson, W. F. (1999). *Protein Sci.* **12**, 2663–2671.
- Zhan, Y., Song, X. & Zhou, G. W. (2001). *Gene*, **281**, 1–9.

X-ray-structure of glutathione S-transferase from *Schistosoma japonicum* in a new crystal form reveals flexibility of substrate binding site

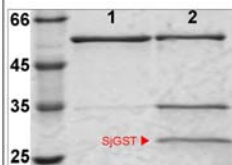
Arne C. Rufer^{1,2}, Lars Thiebach², Kristin Baer², Helmut W. Klein² and Michael Hennig¹

¹ F. Hoffmann-La Roche Ltd., Pharma Research Discovery, 4070 Basel, Switzerland

² University of Cologne, Institute for Biochemistry, 50674 Cologne, Germany

The crystal structure of 26 kDa glutathione S-transferase from *Schistosoma japonicum* (SjGST) was determined at 3 Å resolution in the new space group P2₁2₁2₁. The structure of orthorhombic SjGST reveals unique features of the ligand binding site and dimer interface when compared to previously reported structures. SjGST is recognized as the major detoxification enzyme of *Schistosoma japonicum*, a pathogenic helminth causing schistosomiasis. As resistance against the established inhibitor of SjGST, praziquantel, has been reported our results might prove to be valuable for the development of novel drugs.

Purification, crystallization and structure determination of orthorhombic SjGST



Initially, we sought to solve the structure of a fusion protein by exploiting carrier-driven crystallization. The fusion protein turned out to be unstable independent of the purification protocol employed. However, crystallization trials yielded diffraction quality crystals of SjGST in the unreported space group P2₁2₁2₁.

SDS-PAGE: Lane 1 shows the pooled elution fractions of SjGST-fusion protein from a gel filtration column. In lane 2 the same preparation is depicted after storage for 10 days on ice. Molecular weights (kDa) of marker proteins are indicated.

Crystallization trials were set up directly after purification at 21°C with the modified microbatch method and crystals appeared within 7 days with 0.1 M Bis-Tris pH 5.5, 25% (w/v) PEG 3350 (Index, Hampton Research, condition 42) and 0.1 M sodium acetate pH 5.5, 36% (w/v) PEG MME 5000 (Stura Footprint Screen 2, Molecular Dimensions Limited, condition 20) as precipitant solutions.

Data collection

Beamline	X06SA, SLS
wavelength (Å)	0.90006
resolution (Å)	30.0 - 3.0 (3.14-3.0)
space group	P2 ₁ 2 ₁ 2 ₁
unit cell parameters (Å)	a = 161.22; b = 50.75; c = 57.50
V _m (Å ³ Da ⁻¹) ; solvent (%) ^a	2.2 ; 44.8
total reflections (N)	114066
unique reflections (N)	9910
average redundancy	11.5 (8.6)
R _{int} (I)	8.1 (5.5)
completeness (%)	99.6 (99.4)
Wilson B (Å ²)	43.2
R _{merge} ^b	12.3 (43.7)

Refinement

R _{cryst} (R _{free}) (%)	21.1 (27.9)
(B ₁) ; σ(B) (Å ²)	36.7 ; 14.8
rmsd bond length (Å)	0.008
rmsd bond angles (deg)	1.44
Ramachandran plot (%)	
most preferred	85.9
allowed	12.8
gen. allowed	1.3
disallowed	0.0

Values in parentheses are for the highest resolution shell.

^a Matthews (1968)

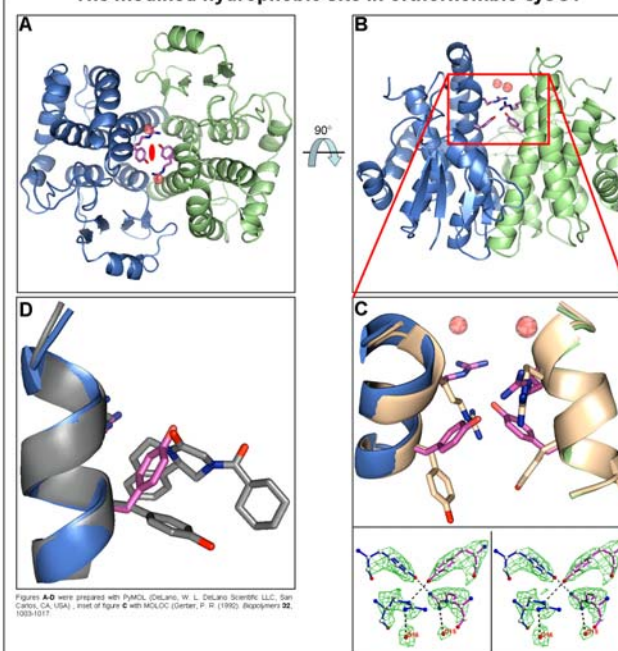
^b $R_{merge} = \sum_{i,j} |I_{ij}(hkl) - \langle I_{ij}(hkl) \rangle| / \sum_{i,j} I_{ij}(hkl)$

Data processing and reduction was performed with Dens and Scaparc (Drenthowski, Z. (1993). Proceedings of the CCP4 Study Weekend, Data Collection and Processing, L. Vignery, A. Isaacs, and D. Bailey, eds., SERC, Daresbury Laboratory, pp. 56-62). Data reduction was performed with X-RED (Drenthowski, Z. (1993). X-RED (Version 3.0) Manual, New Haven, CT: The Howard Hughes Medical Institute and Department of Molecular Biophysics and Biochemistry, Yale University) web used for refinement.

PDB entry	Space group	Unit cell constants	apo/ligand	Fusion protein
1dug	P 4 ₁ 2 ₁ 2	105.78; 105.78; 137.23	l	yes
1b8x	P 4 ₁ 2 ₁ 2	93.40; 93.40; 57.60	a	yes
1bg5	P 4 ₁ 2 ₁ 2	92.17; 92.17; 57.57	a	yes
1gne	P 4 ₁ 2 ₁ 2	94.74; 94.74; 58.13	l	yes
1uas	P 4 ₁ 2 ₁ 2	92.53; 92.53; 57.66	l	no
1gta	P 6 ₁ 2 2	125.20; 125.20; 70.20	a	no
1gtb	P 6 ₁ 2 2	123.80; 123.80; 70.20	l	no
1m99	P 6 ₁ 2 2	115.07; 115.07; 78.28	l	no
1m9a	P 6 ₁ 2 2	114.99; 114.99; 78.35	l	no
1m9b	P 6 ₁ 2 2	116.57; 116.57; 78.75	l	no
1yfe reported here	P 2 ₁ 2 ₁ 2 ₁	161.22; 50.75; 57.50	a	no

Exclusively tetragonal and hexagonal crystal forms of SjGST have been reported so far. For the deposited SjGST structures no correlation exists between space group and crystallization conditions in terms of protein fusion or presence of ligand.

The modified hydrophobic site in orthorhombic SjGST



Figures A-D were prepared with PyMOL (DeLano, W. L. DeLano Scientific LLC, San Carlos, CA, USA). Inset of figure C with MOLSOLO (Gentier, P. P. (1992). Biochimie 92, 1033-1037).

A. View onto a dimer of SjGST along the pseudo-twofold axis (the asymmetric unit contains one dimer, subunit A: blue; subunit B: green). The residues Tyr103 and Arg107 that form the unique dimer contact in orthorhombic SjGST are shown as stick model (magenta). The two water molecules coordinated by the Arg residues are depicted as semitransparent red spheres.

B. Same as A, rotated by 90°.

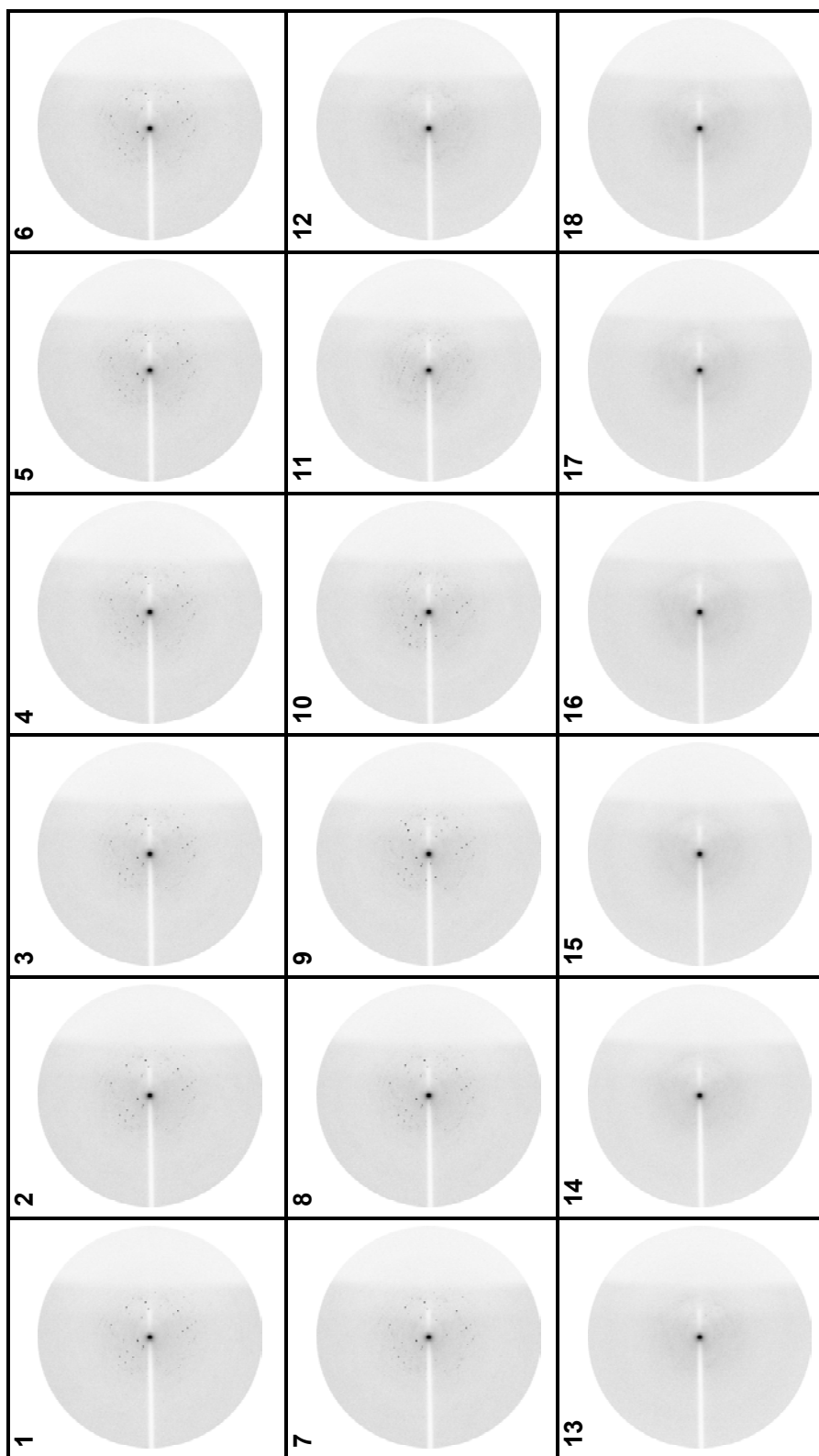
C. Boxed region of B (helix α4) zoomed out. A superposition with the corresponding region of 1dug (light brown, used as search model for molecular replacement) shows that the positions of the sidechains of Tyr103 and Arg107 differ markedly whereas the helices α4 show a good overlay. Inset: Stereo view of the reciprocal dimer contact between Y103 and R107 of chains A (blue) and B (magenta). The distance of the hydroxy oxygen of Y103A to the terminal amino nitrogen of R107B is 3.3 Å and Nε of R107A is 3.5 Å away from the hydroxy oxygen of Y103B. Residues R107 of chains A and B each hydrogen bond (3.3 Å and 3.1 Å distance to W16 and W15, respectively) to water molecules.

D. Superposition of helices α4 of SjGST in complex with the leading anti-schistosomal drug praziquantel (grey, PDB entry 1gtb) and orthorhombic SjGST (blue). The conformation Tyr103 of in the present structure is not compatible with binding of praziquantel.

Conclusion

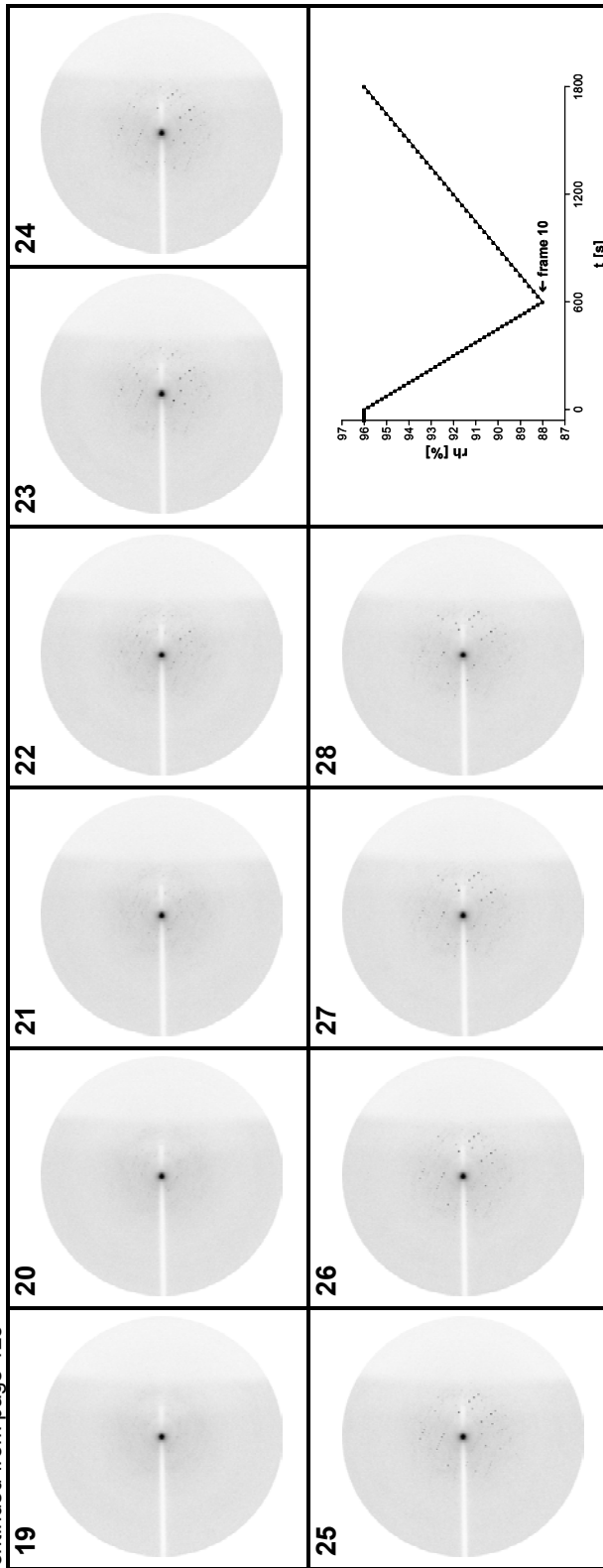
- The sidechains of Y103 and R107 can form a reciprocal dimer contact, thereby distorting the hydrophobic binding site for endogenous substrates of SjGST and xenobiotics.
- Therefore, the binding site for the only effective anti-schistosomal drug, praziquantel, is not preformed in the apo-enzyme as suggested by earlier structures

This work has been accepted for publication in Acta Crystallographica B. Coordinates and structure factors were deposited in the PDB (accession code 1yfe).



X-ray still images (30 sec exposures on Proteros equipment) showing the diffraction of AMPK α_2 D56A/R171E/T172D crystals during dehydration/rehydration. The loss of diffraction after frame 10 (88 % rel. humidity) was fully reversible. Continued on page 126.

Continued from page 125



Sequence of rat AMPK_α2_1-552

▼ *NdeI*

```

catatgggctgagaagcagaagcagcagcgggctgtgaagatcgggacactacgtgctgggggac
      10      20      30      40      50      60
----:----|----:----|----:----|----:----|----:----|----:----|
taccgactcttctgtcttctgtgctgccccgcacacttctagcctgtgatgcacgacccctg
M A E K Q K H D G R V K I G H Y V L G D 20

accctgggctgctggcacccttcggcaaaagtgaagattggagaacatcaattgacagggcat
      70      80      90     100     110     120
----:----|----:----|----:----|----:----|----:----|----:----|
tgggacccgcagccgtggaagccgtttcacttctaacctctttagttaaactgtccggta
T L G V G T F G K V K I G E H Q L T G H 40

aaagtggcagttaagatcttaaataagacagaagattcgcagtttagatggttggtaaaa
      130     140     150     160     170     180
----:----|----:----|----:----|----:----|----:----|----:----|
tttcaccgtcaattctagaatttatctgtcttctaagcgtcaaatctacaacaacctttt
K V A V K I L N R Q K I R S L D V V G K 60
                                gct
                                A
                                56

ataaaacgagaaattcaaaatcttaaactctttcgtcatcctcatattatcaaactctac
      190     200     210     220     230     240
----:----|----:----|----:----|----:----|----:----|----:----|
tattttgctctttaagttttagaatttgagaaagcagtaggagtataatagtttgagatg
I K R E I Q N L K L F R H P H I I K L Y 80

caagtgatcagcactccaacagacttttttatggtaatggaatatgtgtctggaggtgaa
      250     260     270     280     290     300
----:----|----:----|----:----|----:----|----:----|----:----|
gttcactagtcgtgaggttgtctgaaaaaataccattaccttatacacagacctccactt
Q V I S T P T D F F M V M E Y V S G G E 100

      ↪ Primer α1
ttgttcgactacatctgtaaacacgggagggttgaagaggtggaagctcgccggctcttc
      310     320     330     340     350     360
----:----|----:----|----:----|----:----|----:----|----:----|
aacaagctgatgtagacatttgtgccctcccaacttctccaccttcgagcggccgagaag
L F D Y I C K H G R V E E V E A R R L F 120

cagcagattctgtctgcccgtggactactgtcacaggcacatggttgtccacagggacctg
      370     380     390     400     410     420
----:----|----:----|----:----|----:----|----:----|----:----|
gtcgtctaagacagacggcacctgatgacagtgccgtgtaccaacaggtgtccctggac
Q Q I L S A V D Y C H R H M V V H R D L 140

aagccagagaacgtgttctggacgcccagatgaatgctaagatagctgacttcggactc
      430     440     450     460     470     480
----:----|----:----|----:----|----:----|----:----|----:----|
ttcggctctcttgcacaacgacctgcccgtctacttacgattctatcgactgaagcctgag
K P E N V L L D A Q M N A K I A D F G L 160

```

```

tctaataatgatgctcagatggatgaatttctaccgaaactagctgtggatcgccaaattatgca
      490      500      510      520      530      540
-----|-----|-----|-----|-----|-----|-----|-----|
agattatactacagtctaccacttaaagatgcttgatcgacacctagcggtttaatacgt
S N M M S D G E F L R T S C G S P N Y A 180
      gaggat
      E D
      171172

```

↪ Primer α2

```

gcaccggagggtcattctcaggaaggctgtatgggggtcctgaggttgatattctggagctgt
      550      560      570      580      590      600
-----|-----|-----|-----|-----|-----|-----|
cgtggcctccagtagagtccctccgacatacggccaggactccaactatagacctcgaca
A P E V I S G R L Y A G P E V D I W S C 200

gggtgttatcctgtatgcccttctctgtggcaccctccggttcgacgatgagcacgtgcct
      610      620      630      640      650      660
-----|-----|-----|-----|-----|-----|-----|
ccacaataggacatacgggaagagacaccgtgggagggcaagctgctactcgtgcacgga
G V I L Y A L L C G T L P F D D E H V P 220

acgctctttaagaagatccgaggggtgtgttctacatcccgagatctcaaccgttct
      670      680      690      700      710      720
-----|-----|-----|-----|-----|-----|-----|
tgcgagaaattcttctaggtccccccacacaagatgtagggcctcatagagttggcaaga
T L F K K I R G G V F Y I P E Y L N R S 240

attgccactctgctgatgcacatgctgcaggtggtggacccttgaagcgagcaactatcaaa
      730      740      750      760      770      780
-----|-----|-----|-----|-----|-----|-----|
taacgggtgagacgactacgtgtacgacgtccacctggggaacttcgctcgttgatagttt
I A T L L M H M L Q V D P L K R A T I K 260
      tag
      *
      250

```

▼ PmeI

```

gacatacgagagcatgaatggtttaaacaggatttggccagttacctctttcctgaagac
      790      800      810      820      830      840
-----|-----|-----|-----|-----|-----|-----|
ctgtatgctctcgtaacttaccaaatttgtcctaaacgggtcaatggagaaaggacttctg
D I R E H E W F K Q D L P S Y L F P E D 280
      tgatagtag
      * * *
      263264265

```

```

ccctcctatgatgctaacgtcattgatgatgaggctgtgaaagaagtatgtgaaaaattt
      850      860      870      880      890      900
-----|-----|-----|-----|-----|-----|-----|
gggaggatactacgattgcagtaactactactccgacactttcttcatacactttttaa
P S Y D A N V I D D E A V K E V C E K F 300

```

▼ BsrGI

```

gaggtacagaatcagaagtgatgaacagtttatacagtggtggaccctcaagaccagctc
      910      920      930      940      950      960
----:----|----:----|----:----|----:----|----:----|----:----|
ctcacatgtcttagtcttcactacttgtcaaatatgtcaccactgggagttctggtcgag
E C T E S E V M N S L Y S G D P Q D Q L 320
tag tag
* *
302 313

gcagtgggcttatcatctcatcattgacaatcggagaataatgaaccaagccagtggagttc
      970      980      990      1000      1010      1020
----:----|----:----|----:----|----:----|----:----|----:----|
cgtcaccgaatagtagagtagtaactgtagcctcttattacttggtcggtcactcaag
A V A Y H L I I D N R R I M N Q A S E F 340
tag tag
* *
327 340

tacctgcctccagtcctccaacgggttccttcattgacgatatggccatgcacattccc
      1030      1040      1050      1060      1070      1080
----:----|----:----|----:----|----:----|----:----|----:----|
atggagcggaggtcaggaggttgcccaaggaagtacctgctataccggtcacgtgtaaggg
Y L A S S P P T G S F M D D M A M H I P 360

ccggcctgaaaccacatcctgaaaggatgccacctctcatagcagacagcccaagca
      1090      1100      1110      1120      1130      1140
----:----|----:----|----:----|----:----|----:----|----:----|
gggccggactttggtgtaggacttctacggtggagagtagcgtctgtcggggttctgt
P G L K P H P E R M P P L I A D S P K A 380

cgctgtccactggatgcactcaacacaactaagcccaaatctttagctgtgaaaaagcc
      1150      1160      1170      1180      1190      1200
----:----|----:----|----:----|----:----|----:----|----:----|
gcgacaggtgacctacgtgagttgtgtgattcgggtttagaaatcgacactttttctgg
R C P L D A L N T T K P K S L A V K K A 400

aagtgggcaccttgggatccgaagccagagcaaaccatacgacattatggcggaggtgtac
      1210      1220      1230      1240      1250      1260
----:----|----:----|----:----|----:----|----:----|----:----|
ttcaccgtggaaccctaggtctcgtttggtatgctgtaatacgcctccacatg
K W H L G I R S Q S K P Y D I M A E V Y 420

cgagctatgaagcagctggactttgaatggaaggtagtgaatgcataccatcttcgagta
      1270      1280      1290      1300      1310      1320
----:----|----:----|----:----|----:----|----:----|----:----|
gctcgatactctgtcgacctgaacttaccttccatacctacgtaggtagaagctcat
R A M K Q L D F E W K V V N A Y H L R V 440

agaagaaaaaacccagtgactggcaattacgtgaaatgagcttacagctttacctggtt
      1330      1340      1350      1360      1370      1380
----:----|----:----|----:----|----:----|----:----|----:----|
tctcttttttgggtcactgaccgttaatgcacttttactcgaatgtcgaaatggacca
R R K N P V T G N Y V K M S L Q L Y L V 460

gacaatcggagctatcttctagactttaaagcatcgatgatgaggtggtggagcagagg
      1390      1400      1410      1420      1430      1440
----:----|----:----|----:----|----:----|----:----|----:----|
ctgtagcctcgatagaagatctgaaatttctgtagctactactccaccacctcgtctcc
D N R S Y L L D F K S I D D E V V E Q R 480

```

```

tctggttcttcaacacctcagcgctcctggtctgctgccggcctccacagacctcggtca
      1450      1460      1470      1480      1490      1500
----:----|----:----|----:----|----:----|----:----|----:----|
agaccaagaagttgtggagtcgcgaggacaagacgacggccggaggtgtctggagccagt
S  G  S  S  T  P  Q  R  S  C  S  A  A  G  L  H  R  P  R  S  500

agtgtcgattccagcacagccgagaaccattcactgtctggctctctcactggttctttg
      1510      1520      1530      1540      1550      1560
----:----|----:----|----:----|----:----|----:----|----:----|
tcacagctaaggtcgtgtcggctcttggttaagtgacagaccgagagagtgaccaagaaac
S  V  D  S  S  T  A  E  N  H  S  L  S  G  S  L  T  G  S  L  520

actggcagcactttgtcctccgcttccccgcgcctgggcagtcataccatggattttttt
      1570      1580      1590      1600      1610      1620
----:----|----:----|----:----|----:----|----:----|----:----|
tgaccgctcgtgaaacaggagggcgaagggggcgcggaccgctcagtatggtacctaataaaaa
T  G  S  T  L  S  S  A  S  P  R  L  G  S  H  T  M  D  F  F  540

gaaatgtgcgccagtccttatactgctttagcccgttgataa
      1630      1640      1650      1660
----:----|----:----|----:----|----:----|----:----|
ctttacacgcggtcagaatagtgacgaaatcgggcaactatt
E  M  C  A  S  L  I  T  A  L  A  R  *  *  (552)

```

Mutagenesis primers					Energy cost of mismatches [%]
Mutation	Sequence	T _m [°C]	Duplex Energy at 55°C [kcal/mol]		
aa	codon				
D56A	GAT → GCT	5'- GACAGAAGATTTCGCAGTTTAA GC TGTTGTTGGAAAAATAAAACGAG -3'	79.8	-49.1	6.3
R171E	CGA → GAG	5'- GATGTCAGATGGTGAAATTTCTA GAG GATAGCTGTGGATCGCC -3'	78.1	-54.7	10.8
I327*	ATC → TAG	5'- CTCGCAGTGGCTTATCATCTC TAG ATTGACAATCGGAGAATAATGAACC -3'	79.2	-57.7	9.9
H265*	CAT → TAG	5'- CAACTATCAAAGACATACGAGAG TAG GAATGGTTTAAACAGGATTTGC -3'	79.5	-54.5	11.2
E264*	GAG → TAG	5'- GCAACTATCAAAGACATACGA TAG CATGAATGGTTTAAACAGG -3'	78.9	-49.5	7.7
R263*	CGA → TGA	5'- CGAGCAACTATCAAAGACATA TAG AGCATGAATGGTTTAAACAG -3'	79.8	-52.8	5.1
Q250*	CAG → TAG	5'- CTGATGCACATGCTGT AG GTGGACCCCTTG -3'	79.0	-45.2	7.5
Sequencing primers					
α1		5'- gactacatctgtaaacacggg -3'			
α2		5'- ggcctgtatgcgggtcctgagg -3'			

Primers used for introduction of point mutations, generation of truncated constructs and nucleotide sequencing.

Abbreviations

<u>A</u>		cAMP	3'-5'-cyclic adenosine monophosphate
A	Deoxyadenosine monophosphate	CAPS	3-(Cyclohexylamino) -1-propanesulfonic acid
Å	Ångström (10 ⁻¹⁰ m)	cDNA	copyDNA
ACC	Acetyl-CoA Carboxylase	CHAPS	
AcNPV	<i>Autographa californica</i> Nuclear Polyhedrosis Virus	CHES	2-(N-Cyclohexylamino) ethanesulfonic acid
ADA	N-(2-Acetamido)-2-iminodiacetic acid	B/L/M-CPT-1	Brain/ liver/ muscle carnitine palmitoyltransferase 1
ADP	Adenosinediphosphate	CPT-2	Carnitine palmitoyltransferase 2
AMP	Adenosinemonophosphate	CrAT	Carnitine acetyltransferase, also abbreviated as CAT in literature
Amp	Ampicilline	CrOT	Carnitine oktanoyltransferase, also abbreviated as COT in literature
Amp⁻	Ampicilline added	CT	Carboxy-terminus
Amp⁺	Ampicilline not added	<u>D</u>	
AMPK	5'-Adenosinemonophosphate activated protein kinase	Da	Dalton
AMP-PCP	Adenylyl-methylenediphosphonate	DBM	Dodecyl-β-D-maltoside
AMP-PNP	Adenylyl-imidodiphosphate	DLS	Dynamic light scattering
app.	approximately	DNA	Deoxyribonucleic acid
ATP	Adenosinetriphosphate	dNTP	Deoxyribonucleoside triphosphate (N=A; C; G; T)
AU	Arbitrary units	dsDNA	double stranded DNA
AUC	Analytical ultracentrifugation	DTT	Dithiothreitol
<u>B</u>		<u>E</u>	
βOG	Octyl-β-D-glucoside	<i>E.coli</i>	<i>Escherichia coli</i>
Bis-Tris	bis(2-Hydroxyethyl)amino-tris(hydroxymethyl)methane	EDTA	Ethylene diamine tetraacetate
bp	Basepair	EPSP	N-(2-Hydroxyethyl)piperazine-N'-(3-propanesulfonic acid
BPS	between PH and SH2	<i>et al.</i>	et alii
<u>C</u>			
C	Deoxycytidine monophosphate		
CACT	Carnitine/ Acylcarnitine translocase		
CAMKK	Ca ²⁺ /calmodulin dependent kinase kinase		

<u>F</u>		IRK3P	trisphosphorylated IRK (pY1146/50/51)
FPLC	Fast Performance Liquid Chromatography	IRS-1	Insulin receptor substrate 1
		IRTK	Insulin Receptor Tyrosine Kinase (entire intracellular part of IR)
<u>G</u>		<u>J</u>	
g	Gram	JM	Juxtamembrane domain of receptor tyrosine kinases
G	Deoxyguanosine monophosphate	<u>K</u>	
X g	fold gravity acceleration (9,81 m/s ²)	K	Equilibrium constant of mass action
Grb14	growth factor receptor-bound protein 14	K_M	Michaelis-Menten-Konstante
GSH	Glutathione (reduced)	kbp	Kilo basenpairs
GST	Glutathione S-Transferase (from <i>Schistosoma</i> <i>japonicum</i>)	kDa	Kilo dalton
<u>H</u>		<u>L</u>	
h	hour	LB	Luria-Bertani
HEPES	N-(2-Hydroxyethyl)piperazin- N'-2-ethansulfonsäure	LCFA	Long chain fatty acid
HIC	Hydrophobic Interaction Chromatography	<u>M</u>	
<u>I</u>		M	molar, mol/l
IEF	Isoelectric focusing	mA	Miliampere
IEX	Ion Exchange Chromatography	MES	2-(N-Morpholino) ethanesulfonic acid
IGF-1	Insulin-like Growth Factor 1	µg	Mikrogram
IGF-1R	Insulin-like Growth Factor 1 Receptor	µl	Microliter
IGFK	Insulin-like Growth Factor 1 Kinase Domain (entire intracellular part of IGF-1R)	ml	Milliliter
IMAC	Immobilized metal affinity chromatography	MIM	Mitochondrial inner membrane
IPTG	Isopropyl-β-D-thiogalactoside	MOM	Mitochondrial outer membrane
IR	Insulin receptor	MOPS	3-(N-Morpholino)- propansulfonsäure
IRK	Core insulin receptor kinase domain	MW	Molecular weight
		<u>N</u>	
		ng	Nanogramm

NT	Amino-terminus	SLS	Swiss Light Source
NTA	Nitrilo-triacetic acid		(synchrotron)
		STAU	Staurosporine
<u>O</u>			
ori	Origin of replication	<u>I</u>	
		T	Deoxythymidine monophosphate
<u>P</u>			
PBS	Phosphate Buffered Saline	T1D	Type 1 diabetes mellitus
PC	Pyruvate carboxylase	T2D	Type 2 diabetes mellitus
PCR	Polymerase Chain Reaction	TCEP	Tris-(2-carboxyethyl)- phosphine
PDB	Protein Data Bank	TRIS	Tris-(hydroxymethyl)- aminomethan
PEG	Polyethylene glycol	tRNA	transfer RNA
PEG-MME	Polyethylene glycol monomethyl ester		
pH	potentium hydrogenii		
pl	isoelectric point	<u>U</u>	
PIPPS	Piperazine-N,N'-bis(2- propanesulfonic acid	UV	ultraviolett
PKA	protein kinase A (cAMP- dependent proteinkinase, here: catalytic domain of PKA)	<u>V</u>	
		v	Volt; Volume
PMSF	Phenylmethylsulfonylfluoride	v/v	Volume per volume
<u>R</u>			
RNA	Ribonucleinsäure	<u>W</u>	
rpm	Revolutions per minute	wt	Wild-type
RT	Room temperature	w/v	Weight per volume
RTK	Receptor tyrosine kinase		
Amino acids were abbreviated according to the one and three letter codes recommended by IUPAC.			
<u>S</u>			
s	Second		
SAXS	Small angle X-ray scattering		
SEC	Size exclusion chromatography		
SDS	Sodium Dodecyl Sulfate		
SDS-PAGE	SDS-polyacrylamide gel- electrophoresis		
Sf9	<i>Spodoptera frugiperda</i> cell line 9 cell line9		

Zusammenfassung

Eingeschränkte Insulinwirkung aufgrund peripherer Insulinresistenz oder unzureichender pankreatischer Insulinsekretion ist ein entscheidender Faktor für die Entstehung und Manifestation von Typ 2 Diabetes mellitus (T2D). Es befinden sich Insulin Rezeptor (IR) Agonisten in der Entwicklung, welche die cytoplasmatische IR Kinaseaktivität direkt aktivieren. Zwei Klassen solcher Verbindungen wurden von den pharmazeutischen Unternehmen Merck & Co., Inc., und Telik, Inc., entwickelt, aber weder in Patenten noch in der Literatur befinden sich Angaben, wie diese Verbindungen die Kinaseaktivität des IR aktivieren.

Versuche, die Kristallstruktur dimerer IR Kinasedomänen oder von Komplexen derselben mit IR Agonisten innerhalb dieser Dissertation zu lösen, sind fehlgeschlagen. Allerdings zeigte die biophysikalische Charakterisierung des gesamten intrazellulären Abschnitts des IR einschließlich der Kinasedomäne ein intrinsisches Vermögen, unabhängig von den Enzym-Substrat-Wechselwirkungen der Autophosphorylierung zu dimerisieren. Die Ausbildung dieses Dimers wird durch die Anwesenheit eines spezifischen IR Agonisten verstärkt

Kristalle verschiedener Konstrukte und Isoformen der AMP-aktivierten Proteinkinase (AMPK), einem wichtigen Zielmolekül für potentielle antidiabetische Substanzen, konnten gezüchtet werden. Trotz ausgiebiger Optimierungsversuche waren diese Kristalle nicht hinreichend für die Lösung der Kristallstruktur der AMPK.

Die Kristallstruktur der Carnitinpalmitoyltransferase 2 (CPT-2), ein Protein in der durch AMPK ausgelösten Metaboliten-Signalkaskade, konnte dagegen gelöst werden. CPT-1 und -2 importieren langkettige Fettsäuren in Mitochondrien. Die Modulation der katalytischen Aktivität des CPT-Systems wird derzeit für die Entwicklung von neuartigen Medikamenten gegen T2D untersucht. Die Kristallstruktur des vollständigen mitochondrialen Membranproteins CPT-2 konnte mit einer Auflösung von 1.6 Å gelöst werden. Die Struktur von CPT-2 im Komplex mit dem generischen CPT-inhibitor ST1326 [(R)-N-Tetradecylcarbamoylaminocarnitine], einem Palmitoylcarnitinnachahmendes Substratanalogon, derzeit in klinischen Studien für die Behandlung von T2D, wurde mit einer Auflösung von 2.5 Å gelöst. Diese Strukturen gewähren Einsicht in die Funktion von Aminosäuren, die in die Bindung von Substrat und die Determination der Substratspezifität involviert sind, und erlauben somit die Entwicklung neuartiger

antidiabetischer Wirkstoffe. Eine Insertion in der Sequenz der CPT-2 vermittelt die Membranlokalisierung. Die Kartierung der für die CPT-2 Defizienz (eine vererbte Fettstoffwechselstörung) beschriebenen Mutationen impliziert Effekte auf Substraterkennung und strukturelle Integrität der CPT-2.

Danksagung

Mein besonderer Dank gilt Priv.-Doz. M. Hennig und Prof. H. W. Klein für ihr Vertrauen und die Betreuung dieser Dissertation, die fortlaufende Unterstützung und die bereitgestellten Mittel.

D. W. Banner, J. Benz, O. Grassmann, A. Kuglstatter, G. Pappenberger und A. Ruf möchte ich dafür danken, ihren unerschöpflichen kristallographischen Fundus mit mir zu teilen.

R. Thoma, B. D'Arcy, D. Burger und D. Schlatter danke ich für die gute Zusammenarbeit und die hilfreichen Anregungen an der Laborbank.

A. Alker sei gedankt für die Wartung und Pflege der Röntgengeräte.

Vielen Dank auch an B. Gsell für die Unterstützung bei allen Fragen der Chromatographie.

E. DeRoo danke ich für die sehr gute Zusammenarbeit auf dem CPT-2 Projekt.

Für die Präparation von His₆_IRTK und vom AMPK_α1β1γ1 danke ich H-J. Schönfeld und B. Pöschl.

Bei M. Stihle und C. Joseph möchte ich mich für die ergiebige Zusammenarbeit im Kristallisationslabor bedanken.

Vielen Dank auch an R. Meier ich für eine gute Zeit im Kristallisationslabor.

A. Friedlein, W. Huber, J. Kohler, F. Mueller und E. Kuznir danke ich für die Zusammenarbeit bei der MS-Analyse, SPR und AUC.

R. Mehlin danke ich für die prompte und unkomplizierte Unterstützung bei allen administrativen Angelegenheiten.

Mercy bien, A. D'Arcy, pour m'assister rapidement avec ton AI's Oil.

Den Biologie-Projektleitern K. Amrein, M. Andjelkovic und O. Chomienne sowie den Mitgliedern ihrer Arbeitsgruppen danke ich für die inspirierende und spannende Zusammenarbeit.

Den Mitgliedern der CAMM-Gruppe, insbesondere T. Schulz-Gasch, B. Kuhn und M. Stahl, gilt mein Dank für die Bereitstellung und Diskussion der Strukturmodelle.

Den Mitarbeitern der Roche Medizinalchemie danke ich für die Synthese und Bereitstellung von Liganden.

Für die Diskussion von Sequenzdaten danke ich C. Broger und M. Ebeling.

Vielen Dank an H. Biller und R. Gey für die hervorragende IRIX/LINUX-Unterstützung.

D. Held und S. Schwarz danke ich für die gute Arbeitsatmosphäre.

Prof. T. Wallimann und den Mitgliedern seiner Arbeitsgruppe, insbesondere U. Riek, D. Neumann und U. Schlattner danke ich für die Kollaboration und ihren Enthusiasmus in dem AMPK Projekt.

D. Svergun und P. Konarev von der SAXS-Gruppe des EMBL, Hamburg, danke ich für die Unterstützung bei der Datensammlung und -auswertung.

Für die hervorragende Betreuung bei der Datensammlung am SLS danke ich C. Schulze-Briese, E. Pohl, T. Tomizaki und A. Wagner.

Bei meinen Kollegen in Köln, insbesondere K. Baer, S. Parvaresh, M. Gompert und L. Thiebach, möchte ich mich für fortlaufend gute Zusammenarbeit bedanken.

HD Dr. N. Hellmann und Prof. R. Sterner danke ich für anregende Diskussionen.

Ich versichere, daß ich die von mir vorgelegte Dissertation selbständig angefertigt, die benutzten Quellen und Hilfsmittel vollständig angegeben und die Stellen der Arbeit (einschließlich Tabellen, Karten und Abbildungen), die anderen Werken im Wortlaut oder dem Sinn nach entnommen sind, in jedem Einzelfall als Entlehnung kenntlich gemacht habe; daß diese Dissertation noch keiner anderen Fakultät oder Universität zur Prüfung vorgelegen hat; daß sie – abgesehen von den unten angegebenen Teilpublikationen – noch nicht veröffentlicht worden ist, sowie, daß ich eine solche Veröffentlichung vor Abschluss des Promotionsverfahrens nicht vornehmen werde. Die Bestimmungen dieser Promotionsordnung sind mir bekannt. Die von mir vorgelegte Dissertation ist von Prof. Dr. H-W. Klein, Institut für Biochemie, Universität zu Köln und Prov.-Doz. Dr. Michael Hennig, F. Hoffmann-LaRoche AG, Basel, CH, betreut worden.

Arne C. Rufer

Teilpublikationen dieser Arbeit

1. Rufer AC, Thiebach L, Baer K, Klein HW, Hennig M (2005) X-ray structure of glutathione S-transferase from *Schistosoma japonicum* in a new crystal form reveals flexibility of the substrate-binding site. *Acta Crystallographica F Struct Biol Cryst Comm*, **F61**: 263-265
2. Rufer AC, Thoma R, Benz J, Stihle M, Gsell B, De Roo E, Banner DW, Mueller F, Chomienne O, Hennig M. The crystal structure of carnitine palmitoyltransferase 2 and implications for the treatment of diabetes mellitus. *Structure, manuscript accepted*.

Lebenslauf

Name, Vorname Rufer, Arne Christian

Geburtsdatum, -ort 5.8.1974, Hamm/ Westfalen

Staatsangehörigkeit deutsch

Schulbesuch 1981-1985 Grundschule Frechen- Königsdorf
1985-1994 Gymnasium Frechen,
Allgemeine Hochschulreife

Zivildienst 4.7.1994 - 30.09.1995,
St. Katharinen Hospital Frechen
Abteilung für Anästhesie und Intensivmedizin

Studium WS 95/96-WS 01/02
Studiengang Diplom Biologie, Universität zu Köln

- 08.10. 1997
Zeugnis über die Diplom-Vorprüfung im Fach
Biologie

- WS 98/99 + SS 99, Fulbright - Stipendium zum
Gastaufenthalt an der University of New Hampshire
Biochemistry and Molecular Biology Department
Durham, NH, USA

- 29.6.2000 - 29.3.2001 Diplomarbeit am Institut für
Biochemie der Universität zu Köln über das Thema
„Untersuchungen zur katalytischen Effizienz der
Kinase-Domäne des Insulinrezeptors“, unter der
Anleitung von Prof. Dr. H-W. Klein

- 04.10.2001
Zeugnis über die Diplomprüfung im Fach Biologie

Industriepraktikum 4.7.2001 - 28.12.2001 Praktikum bei F. Hoffmann-
La Roche AG, Basel, CH
Abteilung für Proteinkristallographie

Promotion Beginn 01.03.2002, unter der Anleitung von Prof.
Dr. H-W. Klein, Institut für Biochemie der Universität
zu Köln und Priv.-Doz. Dr. M. Hennig, F. Hoffmann-
La Roche AG, Basel, CH, mit dem Ziel der
Promotion an der Universität zu Köln. Disputation
am 06.02.2006 im Fach Biochemie (biol. Richtung).

Unterschrift

Arne Rufer